School of Physics and Astronomy
Queen Mary, University of London

Calculation of the Curvature Perturbation During Non-Canonical Multifield Inflation

John William Ronayne

Supervised by Dr. David J. Mulryne and Dr. Karim A. Malik

Submitted in partial fulfilment of the requirements for the degree of
Doctor of Philosophy

Declaration

I hereby certify that this thesis, which is approximately 40,000 words in length, has been written by me; that it is the record of the work carried out by me at the School of Physics and Astronomy, Queen Mary University of London, and that it has not been submitted in any previous application for a higher degree.
The work in this thesis has been completed in collaboration with Pedro Carrilho, Sebatian Garcia-Saenz, Sébastien Renaux-Petel, David Mulryne and, Tommi Tenkanen, and has been published in the following papers:

- S. Garcia-Saenz, S. Renaux-Petel and J. Ronayne.
  JCAP **07** (2018) 057
- P. Carrilho, D. Mulryne, J. Ronayne, and T. Tenkanen.
  JCAP **06** (2018) 032
- J. W. Ronayne and D. J. Mulryne.
  JCAP **01** (2018) 023
- D. J. Mulryne and J. W. Ronayne.
  JOSS **3(23)** (2018) 494

I have made a major contribution to all the original research presented in this thesis. This work was supported by a studentship jointly funded by Queen Mary University of London and by the Frederick Perren Fund of the University of London.

John William Ronayne

Abstract

In this thesis we study models of inflation with a curved field-space metric. We concern ourselves with the calculation of the statistics of curvature perturbations which is essential for connecting models to observations.

To begin, we review the standard model of cosmology. We then reflect on cosmological perturbation theory and quantization procedures for inflationary fields in a flat field-space. With these tools we inspect how curvature perturbations, seeded from inflation, generate observables.

We then extend this framework so that we can calculate observables from models with a curved field-space metric. To do this we extend the transport method for numerically evaluating the statistics in multifield inflation. This allows us to calculate the power spectrum and bispectrum in multifield inflation in the case of a curved field-space metric. This method naturally accounts for all sub- and super-horizon tree level effects, including those induced by the curvature of the field-space. We present an open source implementation of our equations in an extension of the publicly available `PyTransport` code.

Next we apply our numerical methods to models of inflation with field-space metrics that produce interesting observables. We investigate the attractor behaviour of multi-field models of inflation where the fields are coupled non-minimally to gravity for two theories of gravity, metric and Palatini gravity. It is conjectured that the two formalisms will have different attractor behaviour. We present the results, illustrating this attractor behaviour, using our numerical approach and Monte Carlo methods.

Finally we analyze a class of models that undergo what is called the geometric destabilization of inflation. We study the observable consequences of these models after this instability occurs. In particular we calculate the bispectrum with our numerical approach, finding large non-Gaussianities of equilateral and orthogonal shapes.

Acknowledgements

This thesis would not have been possible without the support, encouragement and guidance of my supervisor David Mulryne. I am deeply indebted to you for your time and patience during my time in the Astronomy Unit. I would also like to thank my supervisor Karim Malik, your balance of brilliant intellect and dry humor never failed to brighten my day. I am honestly so lucky to have had a supervisor so friendly, knowledgeable and handsome. Thank you both so very much.

I would like to thank Shailee, thank you so much for putting up with me and for all the amazing times we have had. Thank you to all the students in the Astronomy unit of the years, Rebeca Carrillo, Sanson Poon, Pedro Carrilho, Jorge Venegas, Viraj Sanghai, Maritza Soto, Clark Baker, Domenico Trotta, Louis Coates, Eline De Weerd, Jessie Durk, Francesco Lovascio, Paul Hallam, Callum Boocock, John Strachan, Kit Gallagher, Jack Skinner, Colin McNally, Usman Gilani and Shaoshan Zeng, Sophia Goldberg, Zachary Kenton, Alexander Leithes, Matthew Mutter, Nick Attree and Gavin Coleman. There are so many wonderful memories I will have from our time together. Thank you all for your friendship and for the fun we have had.

A special thanks to everyone in the astronomy unit, past and present, and in particular, Timothy Clifton, Chris Clarkson, Prina Patel, Alkistis Pourtsidou, Julian Adamek, Bernard Carr, Reza Tavakol, Tommi Tenkanen and Raquel Ribeiro.

A big thank you to my non-physicist friends, too many to enumerate. You have all provided me the counter-productivity necessary during this PhD to enjoy life. I especially want to thank my two closest friends since moving to London, Conor and Lucie. You have always been the best support, the best craic and the best at keeping me grounded.

Last, but by no means least, I want to thank my mom, Cecelia Ronayne. Perhaps no amount words can convey the right admiration for your life long support, but maybe 40,000 might. To that end, I dedicate this thesis to you.

"He felt that his whole life was some kind of dream and he sometimes wondered whose it was and whether they were enjoying it. "

–Douglas Adams, The Hitchhiker's Guide to the Galaxy.

Contents

1. Introduction

Our collective understanding of the universe has advanced with the developments in fundamental theories of physics. The development of the hot Big Bang model began with observations that the expansion of the universe can be traced back in time to a point where it was smaller, denser and hotter. In this early universe, where the conditions are extreme, models constructed from theories of high energy particle physics and theories of gravity aim to illuminate us on our path to understanding the universe's evolution. Processes which have occurred at this time have been verified by observation. Modern observations have also shown that the universe is not only expanding but that the expansion itself is accelerating. Dark energy is the widely accepted hypothesis to explain this acceleration. Moreover, the existence of a form of matter invisible to electromagnetic interactions has been conjectured by measurements of the rotations of galaxies and gravitational lensing. This dark matter has been measured to be 5 times more abundant than the matter we observe today [1]. Together with baryonic matter and radiation, the parameterization of all these phenomena and observations into a consistent theory is called the standard model of Big Bang cosmology (sometimes referred to as ΛCDM, where Λ is the cosmological constant and CDM is cold dark matter) [2].

The ΛCDM model together with the theory of general relativity seems to fit all the data we have collected so far from measurements of the large scale structure (LSS), supernovae luminosities, galaxy clustering, CMB constraints and primordial nucleosynthesis [3].

Despite the great success of the hot big bang model, it remains incomplete. Problems exist such as the flatness, horizon and monopole problem as well as the unexplained origin of structure formation. This motivated the idea that another era of the universe evolution occurred before the hot big bang. The best idea so far is inflation, where the universe expands at an exponential rate. Inflation provides an answer for the flatness of space, the horizon and monopole problem. But more importantly in the inflation model, structure is seeded by the quantum fluctuations of the inflation field driving the expansion [4].

1.1. Summary

This thesis is concerned with making quantitative predictions for complicated models of inflation that can then be compared against constraints from observational data. We structure the thesis as follows. In Ch. (2) we introduce the hot big bang model and ΛCDM outlining the need for inflation. We then review cosmological perturbation theory, a toolkit necessary for us to relate predictions from our models to observations. We also show the quantization procedure that is used to calculate the statistics of inflationary perturbations. The chapter concludes by highlighting the landscape of inflationary scenarios.

In Ch. (3) we review and extend cosmological perturbation theory results for scalar field models, which include a curved field-space metric. We introduce the ADM (Arnowitt, Deser and Misner) metric and perturb it, and define the covariant perturbations of the scalar fields. Together we obtain the equations of motion and constraint equation to second order in perturbation theory. Finally, relating back to results from Ch (2), we obtain the second order curvature perturbations in curved field-space.

In Ch. (4), using the interaction picture approach to calculating expectation values of field perturbations, we derive the statistics of inflationary perturbations for inflationary models with curved field-space metric deep inside the cosmic horizon. Both two- and three-point initial conditions are determined. These are later used as the initial conditions for our approach to calculating these statistics at late times, the transport approach.

In Ch. (5) we review analytical methods to calculate the statistics from models of inflation. We then review numerical methods for calculating those same statistics, highlighting the transport method we employ. The method is then extended to included non-canonical models of inflation.

This method is then built into the `PyTransport` code in Ch. (6). We test the code on models of inflation to illustrate the extent of its use and efficiency.

In Ch. (7) we examine multifield models with non-minimal couplings to gravity. Using `PyTransport` we compare the results for two different models of gravity and find that their predictions exhibit attractor like behaviour.

In Ch. (8) we explore the observable consequences of negative field-space curvature on the power-spectrum and bispectrum. We review the phenomena of geometric destabilization and study what occurs after this effect for a wide range of potentials and two field-space metric.

Finally in Ch. (9) we present our conclusions.

1.2. Notation

In this thesis we use three conventions for indices. Greek indices ($\alpha, \beta, etc.$) run over the four space-time coordinates $\{0, 1, 2, 3\}$, with a space-time metric signature of $(-1, 1, 1, 1)$. Lowercase Roman indices ($i, j, etc.$) run over spatial coordinates $\{1, 2, 3\}$ and uppercase Roman indices ($I, J, etc.$) run over field-space coordinates $\{1, 2, \cdots, N\}$. When considering Fourier space quantities we use bold font indices, $\mathbf{I}, \mathbf{J}, \ldots$ to indicate that the usual summation over fields is accompanied by an integration over Fourier space. For example,

$$A^{\mathbf{I}} B_{\mathbf{I}} = \int \frac{d^3 k_I}{(2\pi)^3} A^I(\mathbf{k}_I) B_I(\mathbf{k}_I) \,, \tag{1.1}$$

where the subscript I on $\mathbf{k}_I$ indicates that this is the wavenumber associated with objects that carry the I index. For a vector labeled with space-time (A^α) or field-space (A^I) indices the partial $\partial_\beta A^\alpha$ and covariant derivatives, $\nabla_\beta A^\alpha$, with respect to space-time or field-space coordinates may be respectively denoted by a comma and semi-colon respectively, such that for vector components A^α

$$A^\alpha_{;\beta} = A^\alpha_{,\beta} + \Gamma^\alpha_{\beta\gamma} A^\gamma \,, \tag{1.2}$$

where $\Gamma^\alpha_{\beta\gamma}$ is the Christoffel symbol compatible with the Levi-Civita connection (implying that the bottom indices are symmetric $\Gamma^\alpha_{\beta\gamma} = \Gamma^\alpha_{\gamma\beta}$) corresponding to the space-time metric $g_{\alpha\beta}$,

$$\Gamma^\alpha_{\beta\gamma} = \frac{1}{2} g^{\alpha\delta} \left(g_{\beta\delta,\gamma} + g_{\gamma\delta,\beta} - g_{\beta\gamma,\delta} \right) . \tag{1.3}$$

The Riemann curvature tensor is defined constructed from Christoffel symbols,

$$R^\alpha_{\beta\gamma\delta} = \Gamma^\alpha_{\beta\gamma,\delta} - \Gamma^\alpha_{\beta\delta,\gamma} + \Gamma^\alpha_{\delta\epsilon}\Gamma^\epsilon_{\beta\gamma} - \Gamma^\alpha_{\gamma\epsilon}\Gamma^\epsilon_{\beta\delta} \,. \tag{1.4}$$

There is also the Ricci tensor, which is symmetric and defined as,

$$R_{\mu\nu} = R^\alpha_{\mu\alpha\nu} \,, \tag{1.5}$$

and it's trace defines a scalar, the Ricci scalar (or scalar curvature),

$$R = g^{\mu\nu} R_{\mu\nu} \,. \tag{1.6}$$

The above definitions also hold for quantities in field-space (indicated by uppercase Roman indices and field-space metric denoted G_{IJ}) as well as space-time coordinates. We also define the three-dimensional Laplacian $\Delta = \delta^{ij}\partial_i\partial_j$ with δ^{ij} as the Kronecker delta.

We also define symmetrization of indices using rounded parenthesis, for a example,

$$R^{\alpha}_{\beta(\gamma\delta)} = R^{\alpha}_{\beta\gamma\delta} + R^{\alpha}_{\beta\delta\gamma}\,. \tag{1.7}$$

A bar | denotes a break in the indices that are symmeterized, i.e. ,

$$R^{\alpha}_{(\beta|\gamma|\delta)} = R^{\alpha}_{\beta\gamma\delta} + R^{\alpha}_{\delta\gamma\beta}\,. \tag{1.8}$$

The anti-symmetrization of indices is denoted by square brackets,

$$R^{\alpha}_{\beta[\gamma\delta]} = R^{\alpha}_{\beta\gamma\delta} - R^{\alpha}_{\beta\delta\gamma}\,. \tag{1.9}$$

We define derivatives of quantities (for example scalars ϕ) with respect to coordinate time t as $\dot{\phi}$ and conformal time τ as ϕ' with,

$$\tau = \int \frac{dt}{a}\,, \tag{1.10}$$

where a is the scale factor which will be discussed in later sections. We can also define the covariant parallel transport in field-space, in particular the intinsic derivatives of the scalar fields ϕ^I with respect to coordinate time, conformal time and e-folds as,

$$D_t = \frac{d\phi^I}{dt}\nabla_I\,, \quad D_\tau = \frac{d\phi^I}{d\tau}\nabla_I\,, \quad D_N = \frac{d\phi^I}{dN}\nabla_I\,, \tag{1.11}$$

where the corrseponding covariant equation satisfies,

$$\nabla_I X^J = \frac{\partial}{\partial\phi^I}X^J + \Gamma^J_{IK}X^K\,, \tag{1.12}$$

for some vector X^J and,

$$\nabla_I X^{JK} = \frac{\partial}{\partial\phi^I}X^{JK} + \Gamma^J_{IL}X^{LK} + \Gamma^K_{IL}X^{JL} \tag{1.13}$$

for some tensor X^{JK}. We use natural units with $c = \hbar = 1$ such that we can define the reduced planck mass as $M_{\rm pl} = (8\pi G)^{-1/2} = 2.4 \times 10^{18}$ GeV.

2. Standard Cosmology

We begin with an overview of the cosmological principle and the history of the window into the early universe, the cosmic microwave background. In Sec. (2.1) we review the ΛCDM model of cosmology and discuss how the theoretical framework is highly motivated by observations. We outline the fundamental principles of inflationary cosmology in Sec. (2.3). We then have a brief interlude as we review cosmological perturbation theory in Sec. (2.4) In Sec (2.5) we review gauge invariant cosmological variables by discussing the choices of gauge, the evolution of these variables and their relation to one another. After that we outline the quantization procedure necessary to obtain the statistics of inflation in Sec. (2.6)–(2.7) After briefly catagorising inflationary models we discuss the end of inflation in Sec. (2.9). Finally in Sec. (2.10) both the observational evidence for inflation and constraints on models of inflation is reviewed.

2.1. The ΛCDM Model

The measurement of astrophysical quantities (e.g. luminosity, redshift[1] etc.) requires us to agree on a model of the universe, a concordance model. The current accepted model, the ΛCDM model, makes a number of assumptions necessary to explain current observations. ΛCDM is defined by a flat, homogeneous and isotropic universe with constraints on the quantities of Λ, cold dark matter (CDM), radiation and baryonic matter as well as the amplitude and scale dependence of the initial spectrum of fluctuations from inflation. It is a model of the whole universe from nucleosynthesis onwards

The first assumption is that on large scales the universe appears isotropic and homogeneous, meaning that the universe exhibits rotational and translational invariance in space. Observational evidence for the isotropic universe can be found directly in the temperature mapping of the CMB.

A method to gauge the level of isotropy (and/or anisotropy) is by a spherical harmonic decomposition of the angular temperature data $\Delta T(\theta)$ of the CMB. The

[1] Redshift is the displacement of spectral lines towards longer wavelengths, as in the Doppler effect, and denoted z. Due to the expansion of the universe greater redshift is observed from sources of increasing distances from Earth.

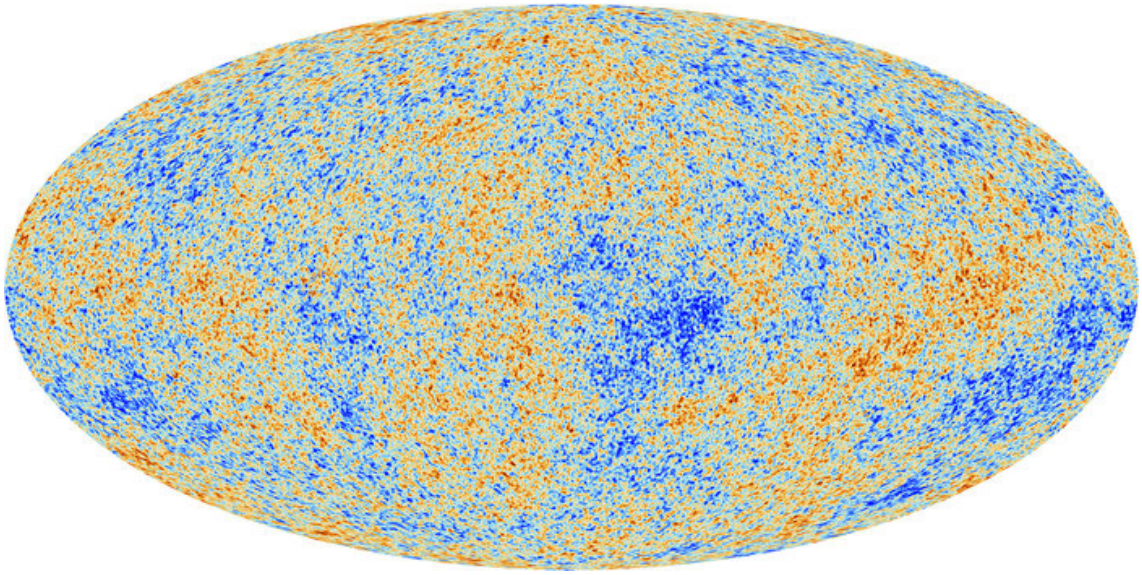

Figure 2.1.: *The Mollweide projection of the CMB anisotropies measured by the Planck telescope after foregrounds and the monopole have been removed. The red to blue colour scale correspond to a linear temperature variations from* $+200\mu K$ *to* $-200\mu K$ *about the average temperature of* $2.728K$ *[5].*

CMB, obtained after subtracting away the motion of the Earth, Sun and Galaxy, illustrates a high degree of isotropy with $|\Delta T(\theta)/T| \lesssim 10^{-5}$. Fig. (2.1) shows the CMB temperature anisotropy map with a temperature of $2.728 \pm 0.004K$. Isotropy is also seen at closer distances via galaxy surveys like the Two-degree-Field Galaxy Redshift Survey [6, 7] and the Sloan Digital Sky Survey [8]. Fig. (2.2) shows a 2-dimensional slice through the local universe illustrating the filaments of galaxies on small scales. However, on scales larger than 100 Mpc[2] no structures are seen, this is sometimes referred to as the homogeneity scale.

Temperature inhomogeneities at the time of recombination (the period during which the CMB forms) would result in significant temperature anisotropies. The high level of observed temperature isotropy in the CMB and isotropy observed in galaxy distributions on LSS surveys supports our belief in homogeneity of the universe on the largest scales [4]. Direct evidence of homogeneity is more difficult to obtain as measures of large spatial scales probe different time scales and a complete understanding of the evolution of the universe is needed. The validity of homogeneity is still debated [9].

Secondly, we assume there exists a geometric theory of gravitation that describes our universe. Although there are other alternatives (see [10]), the ΛCDM model takes Einstein's theory of general relativity to be the correct description of gravity. General Relativity has been tested extensively and remains the leading theory of gravity [11]

The last assumption is that the matter content of the universe is composed of the standard model particles, a form of Cold Dark Matter (CDM) and a cosmological

[2]The standard astronomical unit of length is Mpc$= 3.09 \times 10^{22}m$.

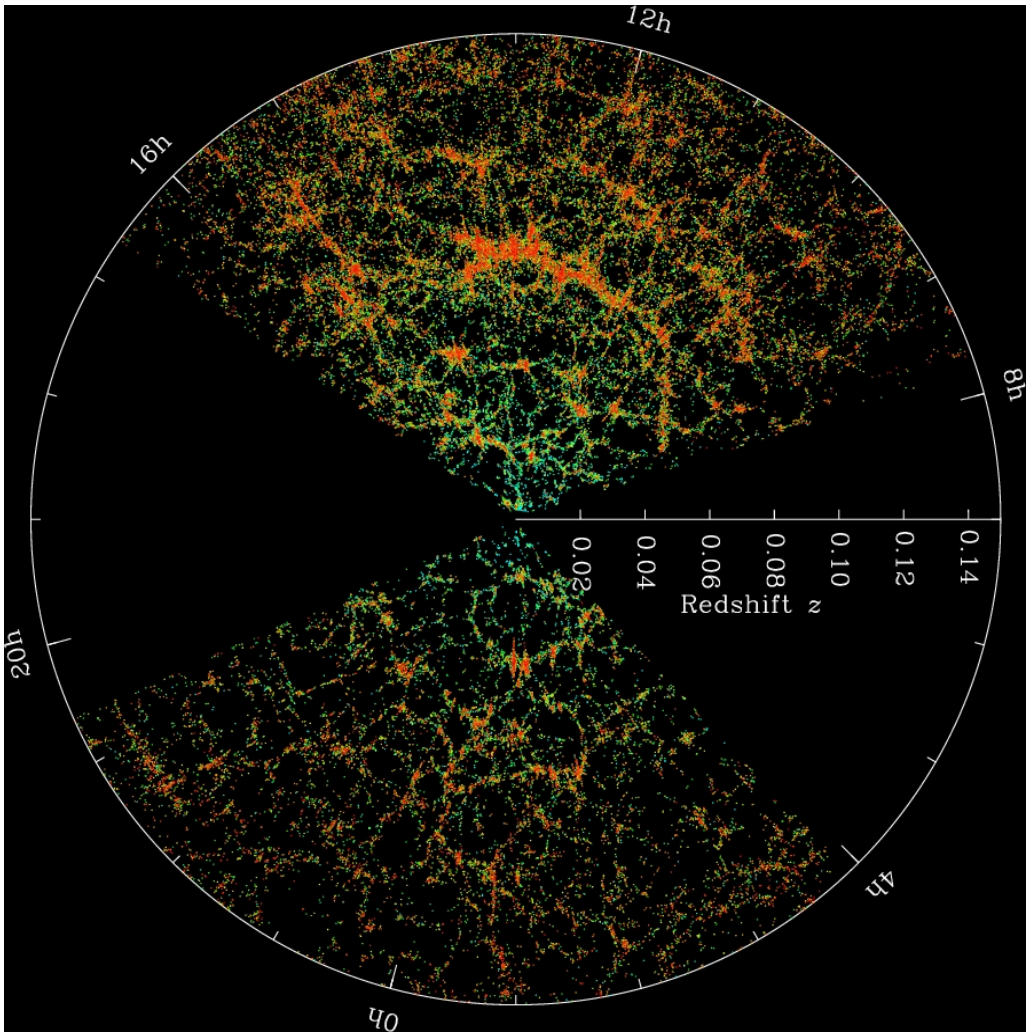

Figure 2.2.: *The SDSS's 2-dimensional map of the universe. At the center is Earth and each dot represents a galaxy. The colouring represents the green-red colouring of the galaxy (an indicator for the age of the galaxy as red stars are older). Image courtesy of the SDSS collaboration and M. Blanton*

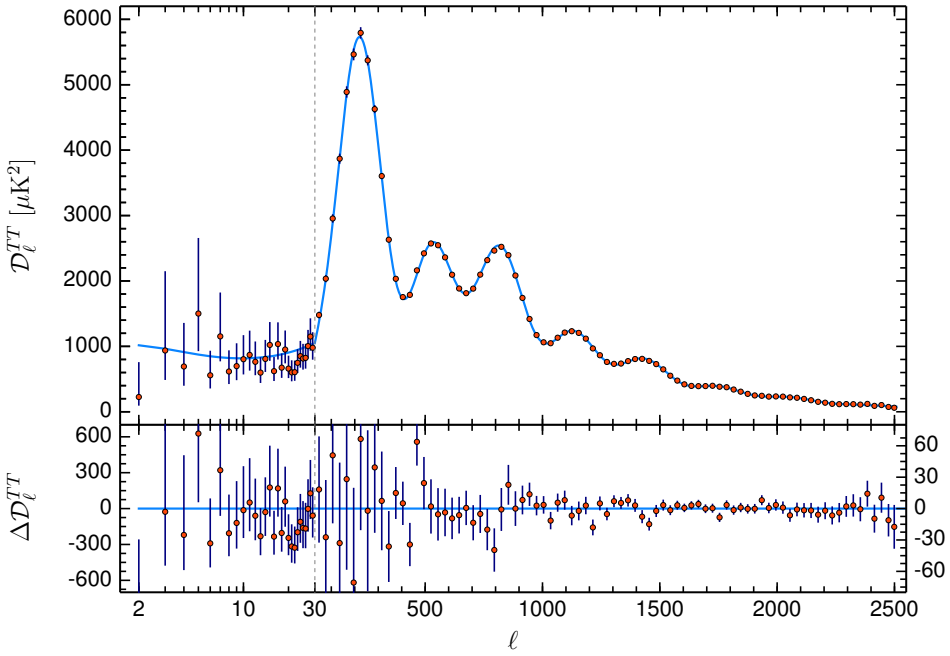

Figure 2.3.: *Planck 2018 CMB angular power spectra of temperature-temperature (TT) correlations [3], compared with the base-ΛCDM best fit to the Planck TT,TE,EE+lowE+lensing data (blue curves). Beneath are the residuals of this fit.*

constant Λ. Standard model particles includes; baryonic matter which is a form of matter directly observable from the emission lines of luminous objects (stars) and non-directly by the absorption lines of non-luminous objects (gas) and relativistic particles such as photons and neutrinos.

From observations of galaxy rotation curves, galaxy cluster dynamics and gravitational lensing combined with our assumption of general relativity we require there to be much more non-luminous 'dark' matter than is visible. The nature of this matter is uncertain and the hunt for understanding its composition is a large topic in particle and astroparticle physics today. Cosmological effects of this dark matter require it to be pressureless and non-relativistic, hence the dark matter is referred to as 'cold'.

The cosmological constant, Λ, is the value of the vacuum energy density of space that accounts for the accelerated expansion of the late universe. Observations of type Ia supernova (SNIa) have shown that the universe is not just expanding but that the rate of this expansion is increasing [12, 13]. These assumptions here have also been used to correctly predict the peaks in the angular power spectrum of the CMB anisotropies [3] (with the TT-correlation spectrum seen in Fig. (2.3)). This also illustrates the need for Λ without the need for supernova data.

2.2. Cosmic Dynamics

In this section, we will discuss the mathematical framework for ΛCDM and its matter content. After we have formulated this convariantly, we will obtain the evolution equations of the background cosmology.

2.2.1. The FLRW Model

As we have discussed, it is usual to assume ΛCDM describes the universe, at least from the time of nucleosynthesis to today. If general relativity works well for ΛCDM it is reasonable to assume it works well for earlier phases. The field equations of Einstein's general relativity can be obtained from variation of the Einstein-Hilbert action,

$$S_{EH} = \frac{1}{2} M_{\rm pl}^2 \int d^4x \sqrt{-g}\,(R - 2\Lambda)\ , \tag{2.1}$$

where $M_{\rm pl}$ is the reduced planck mass defined in Sec. (1.2). The space-time metric is denoted as $g_{\mu\nu}$ where the determinant is labeled g. The Ricci scalar, R, is the scalar curvature of the space-time metric, $g_{\mu\nu}$. Varying the above action, Eqn. (2.1), with respect to the metric gives

$$R^{\mu\nu} - \frac{1}{2} g^{\mu\nu} R - g^{\mu\nu}\Lambda = 0\,, \tag{2.2}$$

which is the gravitational field equation in the absence of matter and where $R^{\mu\nu}$ is the Ricci tensor of the metric $g_{\mu\nu}$. The Einstein tensor is defined as Eqn. (2.2) in the absence of Λ,

$$G_{\mu\nu} = R^{\mu\nu} - \frac{1}{2} g^{\mu\nu} R\,. \tag{2.3}$$

This is a conserved tensor under a covariant derivative,

$$G^{\mu\nu}_{;\nu} = 0\,, \tag{2.4}$$

as can be shown by use of the Bianchi identities,

$$3R_{\alpha\mu(\nu\sigma;\beta)} = 0\,. \tag{2.5}$$

Using the symmetries of the ΛCDM model we can prescribe the space-time metric $g_{\mu\nu}$ that describes the geometry of the universe at large scales to be the Friedmann-Lemaître-Robertson-Walker (FLRW) metric [14] with line element,

$$ds^2 = -dt^2 + a^2(t)\left[\frac{dr^2}{1-\kappa r^2} + r^2 d\theta^2 + r^2 \sin^2\theta d\phi^2\right] = -dt^2 + a^2(t)\gamma_{ij} dx^i dx^j\ , \tag{2.6}$$

in spherical comoving coordinates (r, θ, ϕ) where $a(t)$ is the scale factor (a dimensionless parameter of the relative expansion of the universe at a coordinate time t) and

κ is a parameter that represents the global geometry of space. For positive spatial curvature $\kappa > 0$, for negative spatial curvature $\kappa < 0$ and for flat spatial curvature $\kappa = 0$. Here we have also introduced the time-independent three dimensional spatial metric γ_{ij} for convenience later on. By virtue of a growing scale factor the FLRW models are very effective at explaining cosmological features of expansion and evolution of the universe. Now that we have our space-time metric corresponding to Eqn. (2.6), let us now take a look at the stress-energy tensor $T^{\mu\nu}$.

2.2.2. Matter Content

The matter content in ΛCDM can be simply described by many perfect fluids which are characterised by only their energy density ρ and pressure p. In a similar fashion to Eqn. (2.1) we can write the action for the matter sector,

$$S_M = \frac{1}{2}\int d^4x\sqrt{-g}\mathcal{L}\,, \tag{2.7}$$

where $\mathcal{L}$ is the matter Lagrangian. The energy-momentum tensor can be obtained from varying the action with respect to the metric,

$$T_{\mu\nu} = g_{\mu\nu}\mathcal{L} - 2\frac{\delta\mathcal{L}}{\delta g^{\mu\nu}}\,. \tag{2.8}$$

Using this result and Eqn. (2.2) we can write the general form of the gravitational field equations for a universe containing matter,

$$R^{\mu\nu} - \frac{1}{2}g^{\mu\nu}R - g^{\mu\nu}\Lambda = M_{\rm pl}^{-2}T^{\mu\nu}\,. \tag{2.9}$$

The most general form of the energy-momentum tensor for a fluid is given as,

$$\bar{T}_{\mu\nu} = (\rho + p)u_\mu u_\nu + pg_{\mu\nu} + 2q_{(\mu}u_{\nu)} + \pi_{\mu\nu}, \tag{2.10}$$

where u_μ is the relative 4-velocity between the fluid and the observer which satisfies $u^\mu u_\mu = -1$[3]. The energy density measured by an observer at rest is $\rho = T_{\mu\nu}u^\mu u^\nu$, the pressure is $p = T_{\mu\nu}(g^{\mu\nu}+u^\mu u^\nu)/3$, the energy flux relative to u^μ is $q^\mu = -T_{\lambda\kappa}u^\lambda(g^{\kappa\mu}+u^\kappa u^\mu)$ and the anisotropic pressure tensor is defined as $\pi_{\mu\nu}$ and satisfies $\pi_{\mu\nu}u^\mu = \pi^\mu_\mu = 0$.

In cosmology it is common to model the background matter content as a perfect fluid (one characterized only by its energy density and pressure). For perfect fluids we may set $q^\mu = 0$ and $\pi_{\mu\nu} = 0$, such that Eqn. (2.10) becomes

$$\bar{T}_{\mu\nu} = (\rho + P)u_\mu u_\nu + Pg_{\mu\nu} \tag{2.11}$$

[3]We have set $c = 1$ and will continue to work in these units.

The different components of the stress-energy tensor may be broken up into the energy density T^{00}, the momentum density T^{0i} and the stress T^{ij}. For a perfect isotropic fluid the energy density is equivalent to $T^{00} = \rho$ and pressure $T^{ij} = p\delta^{ij}$. The momentum density is defined as $T^{0i} = (\rho + p)u^i$.

The properties of our matter can be defined by the equation of state,

$$\omega = \frac{p}{\rho}\,. \tag{2.12}$$

In the ΛCDM model the fluids we are interested in have different equations of state. Non-relativistic matter (such as baryons and CDM) will have $\omega = 0$, relativistic matter (such as photons and neutrinos) will have $\omega = 1/3$ and dark energy will have an equation of state of $\omega = -1$.

2.2.3. The Evolution and Expansion Equations

During the evolution of the energy density and pressure we require that the total energy and momentum be conserved. The covariant conservation equation (or continuity equation) is found from imposing the covariant derivative on Eqn. (2.9) where Eqn. (2.4) and $g_{\mu\nu;\alpha} = 0$ implies,

$$T^{\mu\nu}_{\ ;\nu} = 0\,. \tag{2.13}$$

Solving this conservation equation we write the evolution of the energy density (the continuity equation of the fluid with energy density ρ and pressure p),

$$\dot{\rho} = -3H(\rho + p)\,, \tag{2.14}$$

where we have defined the Hubble parameter as $H = \dot{a}/a$. By integrating the above equation we can derive how the energy density changes with respect to time in an expanding universe. For fluids with an equation of state ω, defined in Eqn. (2.12), the energy density is approximately,

$$\rho \sim a^{-3(1+\omega)}\,. \tag{2.15}$$

For CDM and baryonic matter $\rho_m \sim a^{-3}$ and for radiation $\rho_r \sim a^{-4}$ meaning that the energy of these particles will redshift as the universe expands. However, for dark energy the energy density remains a constant.

From the metric of Eqn. (2.6) we can calculate the components of the Ricci tensor as,

$$\begin{aligned} R_{00} &= -3\frac{\ddot{a}}{a}\,, \\ R_{ij} &= \gamma_{ij}\left(2\dot{a}^2 + a\ddot{a} + 2\kappa\right)\,. \end{aligned} \tag{2.16}$$

This in combination with the gravitational field equation in Eqn. (2.9) gives us a set of two evolution equations for the expansion of the universe. For the 00-components we have the Friedmann equation,

$$H^2 = \frac{\rho}{3M_{\rm pl}^2} + \frac{\Lambda}{3} - \frac{\kappa}{a^2}\,. \tag{2.17}$$

The second is the Raychaudhuri equation, derived from the trace components,

$$\frac{\ddot{a}}{a} = -\frac{1}{6M_{\rm pl}^2}\left(\rho + 3p\right) + \frac{\Lambda}{3}\,. \tag{2.18}$$

The Friedmann equation governs the time evolution of the FLRW universe. It illustrates that a positive $\Lambda > (\rho+3p)/2M_{\rm pl}^2$ the expansion of the universe is accelerating.

From Eqn. (2.17) there is a critical energy density, necessary to balance out the left and right hand side of the equation in the absence of curvature, defined as $\rho_{crit} = 3M_{\rm pl}^2H^2$. It is often used to normalize the density parameter $\Omega_i = \rho_i/\rho_{crit}$ for the fluids. In the case of dark energy $\Omega_\Lambda = \Lambda/3H^2$ and the spatial curvature parameter $\Omega_\kappa = -\kappa/(H^2a^2)$. The total matter density parameter is then,

$$\Omega_m = \sum_i \Omega_i = 1 - \Omega_\kappa\,, \tag{2.19}$$

and can be used to rewrite the Freidmann equation, giving,

$$H^2 = H_0^2\left(\sum_i \Omega_i \left(\frac{a}{a_0}\right)^{-3(1+\omega_{i\,0})} + \Omega_{k\,0}\left(\frac{a}{a_0}\right)^{-2}\right)\,, \tag{2.20}$$

where all quantities with a subscript '0' are evaluated today. If the curvature of the universe is observationally small then $\Omega_m \approx 1$, this is a result that is backed up observationally [3].

2.2.4. Problems of the Big Bang Model

The hot big bang model is exceptionally good at explaining many aspects of our universe, however, there are certain aspects of the cosmos left unexplained. In particular, either the universe as we see it today requires finely-tuned initial conditions which is highly unlikely or there was an earlier phase that gives rise to the observed universe today. There are three main problems that exist in the Big Bang model which imply fine tuned initial conditions. Below we will discuss each of these.

The first is the flatness problem referring to the problem of why the parameter κ is observed to be so close to zero [3]. For the universe to be so flat today the early universe must have been significantly flatter. The definition of the density parameter Ω_κ in Eqn. (2.19), implies that when $\Omega_\kappa = 0$ is an unstable point in the parameter space, since aH decreases with time during matter or radiation dominance such that

Ω_m diverges away from 1. For example, this would require a density parameter of $\Omega_k \sim 10^{-16}$ at the time of nucleosynthesis. This would require fine tuning of the initial conditions.

The second is the Horizon problem. The comoving (or particle) horizon is the maximum distance between two points that have been in causal contact at some point in the past. At the time of last scattering the CMB consisted of roughly 10^6 causally disconnection regions [15]. The observed temperature of the CMB is highly uniform and exhibits high levels of isotropy and homogeneity. It is impossible then to reconcile the fact that with so many causally disconnected regions which did not have time to communicate with one another, we are still left with an extremely uniform CMB. This would require each patch to have the same fine-tuned initial conditions.

The third problem is the Monopole problem (or more generally, the relic density problem). This problem is related to the absence of hypothetical particles that formed in the very early universe when energies were of order of the GUTs scale. Such particles include cosmic strings [16], domain walls [17] and magnetic monopoles [18] and are often the result of some symmetery breaking of a field at high energies. The most notorious of these are the magnetic monopoles which are believed to be heavy and stable enough to still exist in the universe today. However, there are no observational evidence of such particles existing and the conventional hot big bang model provides no known mechanism to dilute the number density of these relics to below observational limits.

Lastly the hot big bang model does not provide us with an explanation for the initial conditions of the structure we observe in the universe. Today we live in a universe containing clusters of galaxies with large scale structure. The growth of this structure required initial fluctuations of just the right amplitude and scale dependence to explain observations.

2.3. Cosmic Inflation

Cosmic inflation is the acceleration of the scale factor in the early universe [19, 20]. Inflation is usually driven by a scalar field (or ensemble of fields). As we will see this rapid growth both solves the flatness and horizon problem, and the quantum fluctuations of this field, responsible for ripples in the energy density of the early universe, providing the initial conditions that seed the growth of structure in the universe.

In the standard big bang cosmology the comoving Hubble radius $\mathcal{H}^{-1} = (aH)^{-1}$ is strictly increasing, which then gives rise to the above mentioned problems. Under a period of exponential expansion, these problems can be made to go away because

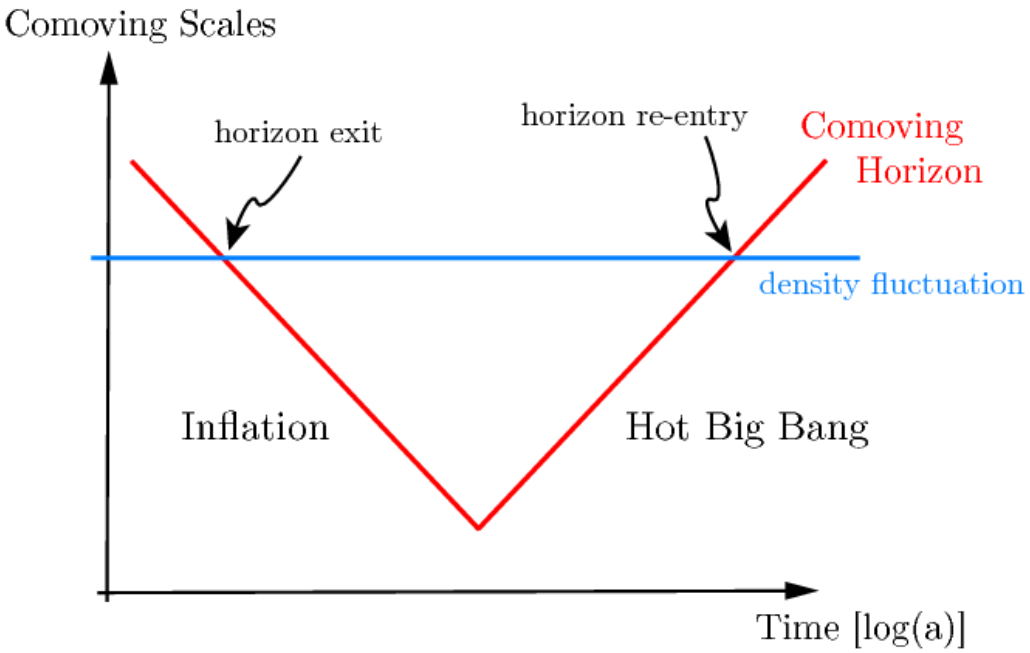

Figure 2.4.: *Evolution of the comoving Hubble radius* $(aH)^{-1}$ *in the early universe. During inflation the comoving Hubble radius is decreasing, after inflation ends it begins to grow. Quantum fluctuations that grow on sub-horizon scales become constant at horizon exit and remain constant until they re-enter the horizon at a later time [21]*

the Hubble radius is decreasing,

$$\frac{d}{dt}\left(aH\right)^{-1} < 0\,. \tag{2.21}$$

In Fig. (2.4) the evolution of the comoving Hubble radius is illustrated over a period from the beginning of inflation to today. In this period it is necessary for the scale factor $\ddot{a}(t) > 0$, and to quantify the length of inflation we define the number of e-folds as,

$$N = \ln\left(\frac{a_f}{a_i}\right)\,, \tag{2.22}$$

where a_i is the scale factor at the beginning of inflation and a_f is the scale factor at the end.

Inflation solves the problems of the hot big bang in the following ways: By examination of Eqn. (2.20) it is clear that for a non-flat universe undergoing accelerated expansion, the RHS will decrease and be attracted to a solution of $\Omega_m = 1$. To quantify the amount of observable inflation needed, consider,

$$\left|\frac{\Omega_\kappa(t_f)}{\Omega_\kappa(t_i)}\right| = \left(\frac{a_f}{a_i}\right)^{-2} = e^{-2N}\,, \tag{2.23}$$

where 'i' is the beginning of inflation and 'f' is the end of inflation. For example one would require more than 70 e-folds of inflation to have occurred to have $|\Omega_\kappa(t_f)| \lesssim 10^{-60}$ from an initial $\Omega_\kappa(t_i) \sim \mathcal{O}(1)$.

The horizon problem is also solved by the fact that the comoving Hubble radius is decreasing during inflation. A small causally connected patch can then be expanded to a size greater than the current observable universe, freezing in the physical properties of that patch. So the 10^6 seemingly disconnected regions were in fact not disconnected in the past [15]. To determine how much inflation is needed to solve the horizon problem we find the relation between the particle horizon now $d_H(t_0)$ and at the end of inflation $d_H(t_f)$,

$$e^N \sim \frac{T_0}{T_f}\frac{d_H(t_0)}{d_H(t_f)}\,, \tag{2.24}$$

where T_0 is the temperature today and T_f is the temperature at the end of inflation. Finally, as monopoles at the beginning of inflation are separated by a length scale defined by the speed of propagation ($\sim c$) times the scale over which the symmetry is broken we would expect one monopole per Hubble volume. They are therefore rapidly diluted away by the enormous expansion during inflation.

In order to solve these problems there must be approximately $N \geqslant 50-70$ e-folds of inflation depending on the energy scale of inflation and the reheating temperature. Scales of the size of the CMB today therefore represent modes produced by the fluctuations $50-70$ e-folds before the end of inflation. This is illustrated in Fig.(2.4) where the earliest scales to exit the horizon are the last to re-enter it. The amount of inflation observable to us corresponds to that which has already re-entered our horizon as everything outside of our horizon is unobservable. The CMB anisotropies, however, only probe over 4 e-folds of inflation. However, there are no upper limits on the total amount of inflation, this is referred to as Eternal Inflation [22, 23].

2.3.1. Single-Field Slow-Roll Inflation

To obtain accelerated expansion in General Relativity, one requires a source of negative pressure. Here we demonstrate how this can be achieved through scalar fields. For simplicity we start with the simplest inflationary model where one light scalar field drives inflation, is called the inflaton. As we have seen in the previous sections the evolution of the universe can be determined by its matter content. As in Eqn. (2.7) we construct the action for a single canonical scalar field ϕ evolving in a potential $V(\phi)$,

$$S = -\int d^4x\sqrt{-g}\left[\frac{1}{2}\partial_\mu\phi\partial^\mu\phi + V(\phi)\right]\,, \tag{2.25}$$

and its energy-momentum tensor takes the form,

$$T_{\mu\nu} = \partial_\mu\phi\partial_\nu\phi - \left(\frac{1}{2}\partial_\alpha\phi\partial^\alpha\phi + V(\phi)\right)g_{\mu\nu}\,. \tag{2.26}$$

This can then be compared directly with Eqn. (2.10), so that the scalar fields in

a homogeneous and isotropic space-time can be represented as fluids with energy density,

$$\rho = \frac{\dot{\phi}^2}{2} + V(\phi)\,, \tag{2.27}$$

and pressure,

$$p = \frac{\dot{\phi}^2}{2} - V(\phi)\,. \tag{2.28}$$

We can redefine the Raychaudhuri equation in terms of the scalar field,

$$\frac{\ddot{a}}{a} = -\frac{1}{3M_{\rm pl}}\left(\dot{\phi}^2 - V\right)\,, \tag{2.29}$$

where we have neglected Λ and assumed $\kappa = 0$. When the potential energy is greater than the kinetic (i.e. $\dot{\phi}^2 < V$) we enter a period of accelerated expansion and when it's much larger $\dot{\phi}^2 \ll V$ the expansion is close to exponential. This condition for exponential expansion is called the slow-roll assumption. In addition to the Raychaudhuri equation we also have the Friedmann equation,

$$H^2 = \frac{1}{3M_{\rm pl}^2}\left(\frac{1}{2}\dot{\phi}^2 + V\right)\,, \tag{2.30}$$

and using $\dot{H} = \ddot{a}/a - H^2$ and the above relation we can rewrite the Eqn. (2.29) as,

$$\dot{H} = -\frac{\dot{\phi}^2}{2M_{\rm pl}^2}\,. \tag{2.31}$$

The Klein-Gordon equation is also obtained by applying the continuity equation from Eqn. (2.13) to Eqn. (2.26),

$$\ddot{\phi} + 3H\dot{\phi} + V_{,\phi} = 0\,, \tag{2.32}$$

where $V_{,\phi}$ is the derivative of the potential with respect to the scalar field. Some predictions of inflation can be computed without specifying the exact form of the inflaton's potential, via the slow-roll parameters which we define below. The term 'slow-roll' comes from the fact that the potential energy is dominant and near constant for the majority of the inflationary epoch and in effect the field "slowly rolls" down the potential and speeds up as it reaches the minimum of the potential. As well as requiring that $\dot{\phi}^2 \ll V$ we also need inflation to last sufficiently long and that condition is met when $\ddot{\phi} \ll 3H\dot{\phi}^2$. Then, the evolution equations become,

$$\begin{aligned} H^2 &\simeq \frac{1}{3M_{\rm pl}^2}V\,, \\ 3H\dot{\phi} &\simeq -V_{,\phi}\,, \end{aligned} \tag{2.33}$$

so in the slow-roll regime the Hubble parameter is approximately constant corre-

sponding to the space-time being approximately de-Sitter, $a(t) \sim e^{Ht}$.

In order to quantify the flatness of the potential and the duration of inflation we now introduce the slow-roll parameters as follows:

$$\epsilon_H = -\frac{\dot{H}}{H^2}\,, \quad \epsilon_V = \frac{M_{\rm pl}^2}{2}\left(\frac{V_{,\phi}}{V}\right)^2\,, \tag{2.34}$$

where ϵ_H is the Hubble slow-roll parameter and ϵ_V is the potential slow-roll parameter and are related by $\epsilon_H \approx \epsilon_V$ when $\epsilon_H < 1$ which corresponds to slow-roll expansion. This condition comes from the requirement that $\dot{\phi}^2 \ll V$ and the second equation in Eqn. (2.33). For brevity we will define $\epsilon = \epsilon_V = \epsilon_H$.

The second slow-roll parameter, η comes from the condition that accelerated expansion will only be sustained for a sufficiently long period of time for a small enough second time derivative of ϕ,

$$\eta_H = \epsilon - \frac{\dot{\epsilon}}{2H\epsilon}\,, \quad \eta_V = M_{\rm pl}^2\left(\frac{V_{,\phi\phi}}{V}\right)\,, \tag{2.35}$$

where $|\eta_H| < 1$ corresponds to a small fractional change of ϵ per e-fold. In the slow-roll limit η_H and η_V may be related by $\eta_H \approx \eta_V - \epsilon_V$. To successfully inflate the universe (i.e. the slow-roll conditions) one needs $\epsilon_H, |\eta_H| < 1$ or $\epsilon_V, |\eta_V| \ll 1$. When the slow-roll conditions are violated, inflation ends, corresponding to $\epsilon_H = 1$ or $\epsilon_V \approx 1$.

The number of e-folds between two arbitrary points in time is calculated as,

$$N_H(t_i, t_f) = \int_{t_i}^{t_f} H dt\,, \tag{2.36}$$

and can be reformulated into the number of e-folds between two field values before inflation ends, given by,

$$N_H(\phi_i, \phi_f) = \int_{\phi_i}^{\phi_f} \frac{H}{\dot{\phi}} d\phi \approx \int_{\phi_i}^{\phi_f} \frac{1}{\sqrt{2\epsilon_H}} d\phi\,, \tag{2.37}$$

which is defined on the RHS in terms of the Hubble slow-roll parameter. We may also calculate this as a function of the potential,

$$N_V(\phi_i, \phi_f) = \int_{\phi_i}^{\phi_f} \frac{V}{V_{,\phi}} d\phi \approx \int_{\phi_i}^{\phi_f} \frac{1}{\sqrt{2\epsilon_V}} d\phi\,. \tag{2.38}$$

2.4. The Perturbed Cosmology

The universe today has a large scale structure comprising of clusters of galaxies. The evolution towards this structure may be understood through the cosmological perturbation theory. As our background cosmology forbids such structures we assume

the inhomogeneities are seeded from perturbations in the primordial density caused by fluctuations of the scalar field during a period of inflation. To illustrate such a perturbation we consider a scalar field[4] ϕ and split the field into its homogeneous background and inhomogeneous perturbation [24],

$$\phi(\tau, x^i) = \phi_0(\tau) + \delta\phi(\tau, x^i)\,, \tag{2.39}$$

where we have switched to conformal time $t \to \tau$.

Our universe's geometry can be approximately described by a flat FLRW background with a perturbed space-time. We then assume that more generally the metric in cosmology can be decomposed into background quantities with inhomogeneous perturbations on top. Using the background cosmology we decompose our 4–dimensional space-time into spatial hypersurfaces with 3 dimensions and one temporal dimension. However, let us first define the perturbations to a tensor more generally. A tensor can be split into the background and inhomogeneous perturbations,

$$T^{full}_{\mu\nu}(\tau, x^i) = T^{(0)}_{\mu\nu}(\tau) + \epsilon T^{(1)}_{\mu\nu}(\tau, x^i) + \frac{1}{2}\epsilon^2 T^{(2)}_{\mu\nu}(\tau, x^i) + \cdots\,, \tag{2.40}$$

where background quantities are dependent only on time. Here the expansion has been made to second order $T^{(2)}$ but these shall be omitted from henceforth and only first order $T^{(1)}$ (linear perturbation) will be discussed. Likewise vectors can be decomposed into spatial and temporal parts. If we consider a four vector $\mathcal{U}^\mu$ we may express it in the form,

$$\mathcal{U}^\mu = \begin{pmatrix} \mathcal{U}^0 \\ \\ \mathcal{U}^i \end{pmatrix}\,, \tag{2.41}$$

where $\mathcal{U}^0$ is the temporal part and $\mathcal{U}^i$ is the spatial part. If we were working in Minkowski space-time the space decomposes as $\mathbb{R}^{(4)} \to \mathbb{R}^{(3,1)}$. In this instance we may decompose the spatial components again using Helmholtz's theorem into its gradient and curl part,

$$\mathcal{U}^i = \delta^{ij}\mathcal{U}_{,j} + \mathcal{U}^i_{vec}, \tag{2.42}$$

where $\partial\mathcal{U}^i_{vec}/\partial x^i = 0$. For our FLRW cosmology we assume an isotropic background and this entails that all spatial vectors vanish. This however is not the case for perturbations on top of our background as we shall see.

We first consider the perturbations to the metric by separating out the scalar, vector and tensor part. The perturbations $\delta g_{\mu\nu}$ to the metric of the line element in

[4]Scalar fields are a common component of models of inflation. The classical example of inflation is driven by a single scalar field and motivated by the presumed existence of scalar fields in high energy physics. It is therefore important to examine the perturbations to the scalar field.

Eqn. (2.6) is defined as,

$$\delta g_{\mu\nu} = a^2 \begin{pmatrix} -2\phi_1 & B_i \\ B_i & 2C_{ij} \end{pmatrix}. \tag{2.43}$$

Clearly we have associated the perturbation to the temporal part of the metric to an arbitrary scalar ϕ_1 (referred to as the lapse function), the $0-i$ components to a vector B_i and the $i-j$ components to the tensor quantity C_{ij}. We can further decompose the vector and tensor components into scalar, vector and tensor parts (SVT decomposition [1]) so that,

$$B_i = B_{,i} - B_i^{vec}, \tag{2.44}$$

$$C_{ij} = -\psi_1\delta_{ij} + E_{,ij} + F_{(i,j)} + \tfrac{1}{2}h_{ij}\,, \tag{2.45}$$

where we have picked up three additional scalars B, ψ_1 and E (each exhibiting a single degree of freedom), two additional vectors B_i^{vec} and F_i (which are divergent free and each have two degrees of freedom) and one additional tensor h_{ij} (which is traceless and transverse and has two degrees of freedom), the metric perturbation. The metric perturbation, ψ_1, will later be identified directly with the intrinsic scalar curvature of spatial hypersurfaces [25]. In total there are 10 degrees of freedom [24, 25]. Under this decomposition of the metric the governing equations decouple for the inhomogeneous cosmology at linear order. The corresponding components of the metric are,

$$g_{00} = -a^2(1+2\phi_1)\,, \tag{2.46}$$

$$g_{0i} = a^2 B_i\,, \tag{2.47}$$

$$g_{ij} = a^2[\delta_{ij} + C_{ij}]. \tag{2.48}$$

2.4.1. Perturbing Matter

We consider a small perturbation away from the background energy–momentum tensor given in Eqn. (2.10) and setting $q_\mu = 0$ to define $\bar{T}_{\mu\nu}$ to form the perturbed stress–energy tensor $T_{\mu\nu}$,

$$T_{\mu\nu} = \bar{T}_{\mu\nu} + \delta T_{\mu\nu}. \tag{2.49}$$

Likewise we define the perturbed energy–density and the pressure to linear order as,

$$\rho = \rho_0 + \delta\rho, \quad P = P_0 + \delta P\,. \tag{2.50}$$

The perturbation of fluid energy–momentum tensor is $\delta T_{\mu\nu}$,

$$\delta T_{\mu\nu} = (\delta\rho + \delta P)\bar{u}_\mu\bar{u}_\nu + \delta P\bar{g}_{\mu\nu} + 2(\rho_0 + P_0)\bar{u}_{(\mu}\delta\bar{u}_{\nu)} + P_0\delta g_{\mu\nu} + a^2 P_0\pi_{\mu\nu}. \tag{2.51}$$

The fluid four velocity has been decomposed in the background quantities and inhomogeneous perturbations, $u^\mu = \bar{u}^\mu + \delta u^\mu$ which satisfies $u_\mu u^\mu = -1$. The solutions at background level are $\bar{u}^\mu = a^{-1}\delta^\mu_0$ and $\bar{u}_\mu = -a\delta^0_\mu$, where δ^0_μ is the Kronecker delta. Since the norm of $\bar{u}^\mu + \delta u^\mu$ should be equal to -1 we infer,

$$\bar{u}^\mu \delta u_\mu + \delta g_{\mu\nu}\bar{u}^\mu\bar{u}^\nu = 0. \tag{2.52}$$

Solving Eqn. (2.52) we extract the perturbations to the velocity as $\delta u_0 = -a\phi_1$ and $\delta u^i = v^i/a$. The temporal and spatial components of perturbations to the fluid velocity are,

$$\delta u^\mu = a^{-1}(-\phi_1, v^i), \quad \delta u_\mu = a(-\phi_1, v_i + B_i). \tag{2.53}$$

The fully perturbed fluid velocity at linear order is,

$$\begin{aligned} u_0 =& -a\left[1+\phi_1\right], \\ u_i =& a\left[v_i + B_i\right], \end{aligned} \tag{2.54}$$

$$\begin{aligned} u^0 =& a^{-1}\left[1-\phi_1\right], \\ u_i =& a\left[v^i\right]. \end{aligned} \tag{2.55}$$

and v is decomposed into a scalar and a vector part according to $v^i = \delta^{ij}v_{,j} + \bar{v}^i_{vec}$. The anisotropic stress tensor then only consists of a spatial part that decouples under decomposition to scalars $\bar{\pi}$, vectors $\bar{\pi}_i$ and tensors $\bar{\pi}_{ij}$. It is symmetric and orthogonal to u^μ so that $u^\mu\pi_{\mu\nu} = 0$. Implying that we can set $\pi_{00} = \pi_{i0} = 0$, the remaining component to the anisotropic stress is,

$$\pi_{ij} = a^2\left[\bar{\pi}_{,ij} - \frac{1}{3}\nabla^2\bar{\pi}\delta_{ij} + \bar{\pi}_{(j,i)} + \bar{\pi}_{ij}\right]. \tag{2.56}$$

Perturbations in the four velocity induce non-vanishing energy flux components T^0_j and momentum density T^i_0. The components of the perturbations to the energy–momentum tensor of rank $(1,1)$ (for rank $(0,2)$ see Appendix. (A.3)) are then,

$$\delta T^0_0 = -\delta\rho\,, \tag{2.57}$$

$$\delta T^0_i = (\rho_0 + P_0)(v_{,i} + \bar{v}^{vec}_i + B_{,i} + \bar{B}^{vec}_i)\,, \tag{2.58}$$

$$\delta T^i_j = \delta P\delta^i_j + P_0 a^{-2}\pi^i_j. \tag{2.59}$$

The mixed upper and lower indices form of the perturbed energy–momentum tensor is often more efficient for calculations during inflation, as we will see when calculating the energy-momentum tensor for a scalar field. We can then apply the conservation equation, Eqn. (2.13), and the following constraints are obtained,

$$\delta\rho' + 3\mathcal{H}(\delta\rho + \delta P) - 3(\rho_0 + P_0)\psi' + (\rho_0 + P_0)\nabla^2(\mathcal{V} + \sigma) = 0 \tag{2.60}$$

and

$$\mathcal{V}' + \left(1 - 3\frac{P_0'}{\rho_0'}\right)\mathcal{H}\mathcal{V} + \psi + \frac{1}{\rho_0 + P_0}\left(\delta P + \frac{2}{3}\nabla^2\pi\right) = 0, \tag{2.61}$$

where $\mathcal{V} = v + B$ is the total covariant velocity perturbation and $\sigma = E' - B$ is the shear scalar. The perturbation to the scalar energy–momentum tensor in Eqn. (2.26) is,

$$\begin{aligned}\delta T_{\mu\nu} =& 2\partial_{(\nu}\phi_0\partial_{\mu)}\delta\phi_0\,, - \left(\frac{1}{2}g^{\alpha\beta}\phi_{0,\alpha}\phi_{0,\beta} + V\right)\delta g_{\mu\nu}\,, \\ & - g_{\mu\nu}\left(\frac{1}{2}\delta g^{\alpha\beta}\phi_{0,\alpha}\phi_{0,\beta} + \frac{1}{2}g^{\alpha\beta}\delta\phi_{,\alpha}\phi_{0,\beta} + V'\delta\phi\right).\end{aligned} \tag{2.62}$$

Separating the components of the scalar energy–momentum tensor of rank $(1,1)$ (for rank $(0,2)$ see Appendix. (A.3)) [26] we get,

$$\delta T^0_0 = \; a^{-2}\phi_0'\left(\phi_1\phi_0' - \delta\phi'\right) - V_{,\phi}\delta\phi \tag{2.63}$$

$$\delta T^0_i = \; -a^{-2}\phi_0'\delta\phi_{,i} \tag{2.64}$$

$$\delta T^i_j = \; -\left[a^{-2}\phi_0'\left(\delta\phi' - \phi_0'\phi_1\right) - V_{,\phi}\delta\phi\right]. \tag{2.65}$$

We may then perform a covariant derivative, again by Eqn. (2.13), and we can obtain the perturbed Klein-Gordon equation,

$$\delta\phi'' + 2\mathcal{H}\delta\phi' + 2a^2V_{,\phi}\phi_1 - 3\phi_0'\psi' - \phi_0'\phi_1{}' + a^2V_{,\phi\phi}\delta\phi = 0. \tag{2.66}$$

Having constructed the components of the stress–energy tensor for both the perfect fluid and scalar field we can find the relations between the energy density, pressure and the scalar field for a linearly perturbed cosmology. The two quantities we obtain are,

$$\delta\rho = \frac{1}{a^2}\phi'(\delta\phi' - \phi'\phi_1) + V_{,\phi}\delta\phi \tag{2.67}$$

$$\delta P = \frac{1}{a^2}\phi'(\delta\phi' - \phi'\phi_1) - V_{,\phi}\delta\phi \tag{2.68}$$

The components of the energy momentum tensor for a scalar can be perturbed to second order in perturbation theory, see Refs. [27–29].

2.4.2. Perturbing the Einstein Equations

The perturbations to the Einstein equations are

$$\delta G_{\mu\nu} = 8\pi G\delta T_{\mu\nu}\,. \tag{2.69}$$

In Appendix (A.2) we derive the full set of pertrubations to the metric components of the Einstein equations. The perturbed curvature of the spatial sections is,

$$\delta^3 R = -\frac{4}{a^2}\nabla^2\psi\,, \tag{2.70}$$

where δ^3 refers to the three dimensional curvature scalar obtain from the trace of the Ricci tensor without including the temporal part. Considering only the scalar perturbations we write the perturbations to the Einstein equation using the equation $\delta G_{\mu\nu} = 8\pi G \delta T_{\mu\nu}$. The $0-0$ component is,

$$3\mathcal{H}(\mathcal{H}\phi_1 + \psi') - \nabla^2(\psi + \mathcal{H}\sigma) = -4\pi G a^2 \delta\rho. \tag{2.71}$$

The $0-i$ component of the Einstein equation is,

$$\mathcal{H}\phi_1 + \psi' = -4\pi G a^2(\rho_0 + P_0)(v + B). \tag{2.72}$$

The off-trace components of the Einstein equation $i-j$ for $i \neq j$ represents the evolution equation of the scalar shear,

$$\sigma' + 2\mathcal{H}\sigma + \psi - \phi_1 = 8\pi G a^2 \Pi, \tag{2.73}$$

while the trace $i-i$ of the Einstein equation is,

$$\psi'' + 2\mathcal{H}\psi' + \mathcal{H}\phi_1' + \left(2\frac{a''}{a} - \frac{a'^2}{a^2}\right)\phi_1 = 4\pi G a^2\left(\delta P + \frac{2}{3}\nabla^2\Pi\right)\,. \tag{2.74}$$

In essence these are the perturbed Friedmann equations.

2.5. The Gauge Invariant Cosmology

From the decomposition of the perturbed cosmology into a unique background and perturbed quantities about this background comes the issue of gauge dependence. General relativity is covariant, that under a change of coordinates $x^\mu \to \tilde{x}^\mu$, it remains unchanged. However, perturbations are coordinate dependent and change under coordinate transformations. Transformation laws can then be found by allowing the perturbations to change.

One way of seeing this is by embedding the four dimensional manifold $\mathcal{M}_\epsilon$ into a higher dimensional domain $\mathcal{N}$ that also allows for the perturbation parameters to vary, the 'ϵ' is there to represent the perturbed cosmology [30, 31]. This higher dimensional domain is foliated by an infinite number of manifolds $\mathcal{M}$ mapped to one another such that $\mathcal{N} = \mathcal{M} \times \mathcal{R}$. The perturbations and the background live on the manifold $\mathcal{M}_\epsilon$. We may define just the background quantities alone as the manifold in which $\epsilon = 0$ denoted $\mathcal{M}_0$ on which a coordinate system x^μ lives. We

map from the background where there is one coordinate system into the perturbed cosmology where there are many coordinate systems that are close together. This splitting between the manifolds on $\mathcal{N}$ is our cause for concern and the dependence on the gauge mapping is called the gauge problem.

The solution comes from knowing how these quantities transform, which gives us the gauge transformations. The gauge transformation moves from one coordinate system x^μ to another $\tilde{x}^\mu$ on $\mathcal{M}_\epsilon$ while preserving the coordinate system on $\mathcal{M}_0$. There are two approaches to gauge transformations: the active and passive approach [30, 31]. In the active approach, perturbed quantities change under a mapping which induces the transformation at the coordinate point. In the passive approach the relation between the choice of coordinates are specified at the same physical point.

The active approach [32] requires us to specify the gauge generator, ξ^μ, so that we may then define the transformation as an exponential mapping at the coordinate point for a tensor,

$$\tilde{T} = e^{\pounds_\xi} T, \tag{2.75}$$

where $\pounds_\xi$ is the Lie derivative with respect to ξ^λ. By expanding the exponential map to linear order, we may then define the transformation as,

$$\tilde{T} = \tilde{T}_0 + \epsilon\delta\tilde{T}_1 = T_0 + \epsilon\delta T_1 + \epsilon\pounds_\xi T_0. \tag{2.76}$$

The Lie derivatives of a scalar, vector and tensor are [30, 32],

$$\pounds_\xi\varphi = \xi^\lambda\varphi_{,\lambda}\,, \tag{2.77}$$

$$\pounds_\xi V_\mu = V_{\mu,\alpha}\xi^\alpha + V_\alpha\xi^\alpha_{,\mu}\,, \tag{2.78}$$

$$\pounds_\xi T_{\mu\nu} = T_{\mu\nu,\lambda}\xi^\lambda + T_{\mu\lambda}\xi^\lambda_{,\nu} + T_{\lambda\nu}\xi^\lambda_{,\mu}. \tag{2.79}$$

We can decompose the vector field ξ^μ in a temporal α and spatial β scalar part and a divergence-free spatial vector γ^i,

$$\xi^0 = \alpha, \quad \xi^i = \partial^i\beta + \gamma^i. \tag{2.80}$$

For the gauge transformation of a four-scalar such as the energy–density in Eqn. (2.50), ρ_0 remains unchanged under the change of coordinates $\tilde{x}^\mu$ to x^μ. Applying equation (2.77) we obtain,

$$\tilde{\rho}(\tilde{x}^\mu) = \rho_0(x^0) + \epsilon\left(-\rho_0'(x^0)\xi^0(x\mu) + \tilde{\delta\rho}(x^\mu)\right), \tag{2.81}$$

where we find the transformation law,

$$\tilde{\delta\rho} = \delta\rho + \rho_0'\xi^0 = \delta\rho + \rho_0'\alpha. \tag{2.82}$$

Now consider the gauge transformation of a vector. We will take the example of the four-vector u_μ as in Eqn. (2.42) and applying the Eqn. (2.78) the transformation law of the perturbation is,

$$\delta\tilde{U}_\mu = \delta U_\mu + U'_{(0)\mu}\alpha + u_{(0)\lambda}\xi^\lambda_{,\mu} \tag{2.83}$$

We now focus on the metric at first order and how it changes under a gauge transformation. To determine the transformation rules of each perturbation variable we look back at the metric components and find their Lie derivatives,

$$\begin{aligned}
\pounds_\xi g_{00} &= -2a^2(\tau)(\alpha' + \mathcal{H}\alpha), && (2.84)\\
\pounds_\xi g_{0i} &= a^2(\tau)(-\alpha_{,i} + (\beta_{,i} + \gamma_i)'), && (2.85)\\
\pounds_\xi g_{ij} &= a^2(\tau)((\beta_{,i} + \gamma_i)_{,j} + (\beta_{,i} + \gamma_i)_{,i} + \mathcal{H}\alpha\delta_{ij}). && (2.86)
\end{aligned}$$

We only need Eqn. (2.76) and (2.77) to determine the change of δg_{00}. The transformation of the metric components δg_{0i} contains both vector and scalar perturbations so we must also use Eqn. (2.78) here. We break up B_i into a vector and scalar component, the vector component is,

$$\tilde{B}_{(vec)i} = B_{(vec)i} + \xi'_i - \alpha_{,i}\,, \tag{2.87}$$

and the scalar part is found by taking the divergence and removing the Laplacian,

$$\tilde{B} = B + \beta' - \alpha\,. \tag{2.88}$$

Using Eqn. (2.79) we form the transformation law for the spatial part of the metric δg_{ij},

$$2\tilde{C}_{ij} = 2C_{ij} + 2\mathcal{H}\alpha\delta_{ij} + \xi_{(i,j)}, \tag{2.89}$$

and then apply the decomposition of the tensor C_{ij} as defined in Eqn. (2.44). In order to solve for the transformation of each variable we need to find three conservation equations using Eqn. (2.13). The first is the trace of Eqn. (2.89), and yields equations formed of the scalar perturbations,

$$-3\tilde{\psi} + \nabla^2\tilde{E} = -3\psi + \nabla^2 E + 3\mathcal{H}\alpha + \nabla^2\beta\,, \tag{2.90}$$

and by applying $\partial_i\partial_j$ to Eqn. (2.89) we get the second equation,

$$-\nabla^2\tilde{\psi} + \nabla^2\nabla^2\tilde{E} = -\nabla^2\psi + \nabla^2\nabla^2 E + \mathcal{H}\nabla^2\alpha + \nabla^2\nabla^2\beta\,. \tag{2.91}$$

These two equations allow us to find the transformation of the scalars $\tilde{\psi}$ and $\tilde{E}$. The

third is obtained by taking the divergence of Eqn. (2.89), yeilding,

$$2\partial^j \tilde{C}_{ij} = 2\partial^j C_{ij} + 2\mathcal{H}\alpha_{,i} + \nabla^2 \xi_{,i} + \nabla^2 \beta_{,i} \,. \tag{2.92}$$

By substitution of the scalars $\tilde{\psi}$ and $\tilde{E}$ into the above equation, we find,

$$\nabla^2 \tilde{F}_i = \nabla^2 F_i + \nabla^2 \gamma^i \tag{2.93}$$

In this manner we determine the transformation of all the metric perturbations at linear order. They are,

Scalar	Vector	Tensor
$\tilde{\phi_1} = \phi_1 + \alpha' + \mathcal{H}\alpha$	$\tilde{B}^i = B^i - \gamma^{i\prime}$	$\tilde{h}_{ij} = \bar{h}_{ij}$
$\tilde{B} = B - \alpha + \beta'$	$\tilde{F}^i = F^i + \gamma^i$	
$\tilde{\psi} = \psi - \mathcal{H}\alpha$		
$\tilde{E} = E + \beta$		

(2.94)

To first order the tensor h_{ij} is gauge–independent (not dependent on the quantities α, β or γ). We may now define the transformation of a fluid four velocity using Eqn. (2.83),

$$\tilde{v_i} + \tilde{B_I} = v_i + B_i - \alpha_{,i} \,. \tag{2.95}$$

Using the transformation of the metric perturbations B_i and decomposing the vector into a scalar and divergent free vector part we obtain,

$$\tilde{v} = v - \beta' \,, \tag{2.96}$$

for the scalar part and the vector part is,

$$\tilde{v}_{(vec)i} = v_{(vec)i} - \gamma_i \,. \tag{2.97}$$

Combinations of the metric perturbations may be made that are gauge-invariant so as to remain unchanged under a change of coordinates.

2.5.1. Different Gauges

We can make use of Eqns. (2.94) to remove the gauge dependencies α and β. By doing so create gauge-invariant quantities. One gauge–dependent quantity we wish

to fix to a gauge are the scalar curvature perturbations and we do this by a suitable choice of α, β and γ^i. We will briefly overview a few choices of gauges from the review Ref. [30]:

- Longitudinal Gauge. It was argued that only variables explicitly invariant under gauge transformations should be considered [33], in that work the gauge invariant variables were defined. These are the Bardeen variables in what is known as the longitudinal gauge (as we will see in the next section),

$$\Psi = \psi - \mathcal{H}(B - E'), \tag{2.98}$$
$$\Phi = \phi_1 + (B - E') + (B - E')', \tag{2.99}$$
$$\Phi^i = F'^i - B^i. \tag{2.100}$$

  Here we initially had 10 degrees of freedom (d.o.f.) $(\phi_1, B, \psi, E, B^i, F^i, h_{ij})$ and 4 gauge degrees of freedom $(\alpha, \beta, \gamma^i)$ that are absorbed now into the gauge invariant quantities $(\Phi, \Psi, \Phi^i, \tilde{h}_{ij})$ of $10 - 4 = 6$ degrees of freedom. It is a choice of gauge in which,

$$\tilde{E} = 0, \quad \tilde{B} = 0\,. \tag{2.101}$$

  this choice results in a vanishing of what is called the shear,

$$\sigma = B - E'\,. \tag{2.102}$$

  The shear transforms as,

$$\tilde{\sigma} = \sigma + \alpha = 0 \tag{2.103}$$

  as it is a scalar. The gauge generators are then,

$$\alpha = -\sigma \;\text{ and }\; \beta = -E\,. \tag{2.104}$$

  From this we obtain the first two equations in Eqns. (2.98). This is referred to as the Longitudinal gauge [25] and coincides with the orthogonal zero-shear gauge [33, 34] and the conformal Newton gauge [35, 36] as it resembles Newtonian equation on small scales.

  There is an extension to this gauge, called the Poisson gauge [35, 37]. In the Poisson gauge there is an addition condition that a vector perturbation should vanish. There are two choices, in addition to (2.101); one, by taking the divergence of the g_{0i} components of the metric such that $B^i_{(vec)} = 0$ or by taking the divergence of the spatial part of the metric g_{ij} such that $F_i = 0$.

- Flat Gauge. By choice of the gauge transformations the diagonal elements of the metric can be set to zero so that the scalar curvature perturbations are zero or rather that the curvature is uniform [24]. The requirement is that the

following metric scalar perturbation transformations are $\tilde{\psi} = \tilde{E} = 0$ as well as the vector perturbation $\tilde{F}_{vec} = 0$. This choice is referred to as the flat gauge and the gauge generators are

$$\alpha = \frac{\psi}{\mathcal{H}}, \quad \beta = -E, \quad \gamma^i = -F^i_{vec}. \tag{2.105}$$

Now that we have an expression for the temporal part of the gauge generator α, we can relate the lapse function to the curvature scalar,

$$\tilde{\phi}_{1f} = \phi_1 + \psi + \left(\frac{\psi}{\mathcal{H}}\right)'. \tag{2.106}$$

Furthermore, matter scalar quantities can be rewritten. The density perturbations transform as

$$\delta\tilde{\rho}_f = \delta\rho + \rho_0' \frac{\psi}{\mathcal{H}}, \tag{2.107}$$

and the scalar field perturbations transform as

$$\delta\tilde{\phi}_f = \delta\phi + \phi_0' \frac{\psi}{\mathcal{H}} \tag{2.108}$$

- Uniform Density Gauge. In this gauge the metric components are not restricted, instead the density perturbations are zero and space is foliated into hypersurfaces where the density is uniform [38]. In this form the gauge transformation of α is,

$$\alpha = -\frac{\delta\rho}{\rho_0'}. \tag{2.109}$$

To illustrate that the perturbations to the density are gauge-invariant we have,

$$\tilde{\rho_u} = \delta\rho + \rho_0' \left(-\frac{\delta\rho}{\rho_0'}\right) = 0. \tag{2.110}$$

The transformations of the scalar curvature [39] are,

$$\tilde{\phi}_{1u} = \phi_1 - \frac{\mathcal{H}\delta\rho}{\rho_0'} - \left(\frac{\delta\rho}{\rho_0'}\right)'. \tag{2.111}$$

and

$$\tilde{\psi_u} = \psi + \frac{\mathcal{H}\delta\rho}{\rho_0'} = -\zeta. \tag{2.112}$$

We relabel the curvature perturbation ψ as ζ in order to distinguish it from the other gauges. In the absence of gravitational waves the spatial metric may be written as $h_{ij} = a^2 e^{2\zeta}\delta_{ij}$. The perturbation to the scalar field in the uniform-density gauge is,

$$\delta\tilde{\phi} = \delta\phi - \phi_0' \frac{\delta\rho_1}{\rho_0'}. \tag{2.113}$$

- Comoving Gauge. The comoving gauge tracks the motion of matter and requires that both the fluid velocity and the momentum vanish such that there is no net flux of energy ($\delta T^0_i = 0$) at the hypersurface [24]. The vanishing of matter fluid 3-velocity $\tilde{v}_i = 0$ on constant time hypersurface also requires that $\tilde{v}_i + \tilde{B}_i = 0$, the vanishing of momentum. The gauge transforming quantity α is,

$$\alpha = v + B\,. \tag{2.114}$$

The transformation of the lapse function of the metric are,

$$\tilde{\phi}_{c1} = \phi_1 + \mathcal{H}(v + B) + (v' + B')\,, \tag{2.115}$$

$$\tilde{\psi}_c = \psi - \mathcal{H}(v + B). \tag{2.116}$$

The scalar quantity associated to the density perturbations transforms as,

$$\tilde{\delta\rho}_c = \delta\rho + \rho_0'(v + B). \tag{2.117}$$

In the case of single field inflation, by relating the perturbations to the stress energy tensor in Eqn. (2.58) and Eqn. (2.64),

$$(\rho_0 + P_0)(v + B) = -\frac{1}{a^2}\phi'\delta\phi_{,i}\,, \tag{2.118}$$

and then substituting in the expressions for the energy-density and pressure,

$$\rho_0 = \frac{1}{2a^2}\phi_0'^2 - V(0), \quad P_0 = \frac{1}{2a^2}\phi_0'^2 + V(0), \tag{2.119}$$

allows us to switch between the momentum of the fluid and the evolution of the scalar field

$$\phi'^2(v + B) = -\phi'\delta\phi, \tag{2.120}$$

$$(v + B) = -\frac{\delta\phi}{\phi_0'}. \tag{2.121}$$

The redefinition of the momentum provides us with a gauge invariant scalar field perturbation,

$$\tilde{\delta\phi}_{1c} = \delta\phi_1 + \phi_0'(v + B) \tag{2.122}$$

$$= \delta\phi_1 - \phi_0'\left(\frac{\delta\phi_1}{\phi_0'}\right) = 0. \tag{2.123}$$

Reformulating the transformation of the density perturbations gives us,

$$\tilde{\delta\rho} = \delta\rho - \frac{\rho_0'\delta\phi}{\phi'}. \tag{2.124}$$

The curvature perturbation in the comoving gauge is conventionally labeled $\mathcal{R}$ and is,

$$\tilde{\psi_c} = \mathcal{R} = \psi + \mathcal{H}\frac{\delta\phi}{\phi_0'}. \tag{2.125}$$

2.5.2. Relating the Gauges

The quantities in one guage can be related to the quantities in another gauge. As we simplified our expressions for the transformation of cosmological quantities such as the curvature perturbation by setting certain metric or matter perturbations to zero, the information of the dynamics within the system is not lost but instead is contained in the gauge invariant quantities themselves. Relating this information between the different gauges can be done by careful algebraic substitution. We can relate the gauge invariant density perturbations in the flat gauge, Eqn. (2.107), to the uniform density curvature perturbations, Eqn. (2.112), and obtain,

$$-\zeta = \frac{\mathcal{H}}{\rho_0'}\tilde{\delta\rho}_f\,. \tag{2.126}$$

The curvature perturbations in the comoving gauge and the uniform density gauge can be related. We first take the definition of the comoving curvature perturbations from Eqn. (2.116) and substitute $(v + B)$ for $(\tilde{\delta\rho_c} + \delta\rho)/\rho_0'$ from the density perturbation of Eqn. (2.117) to form,

$$\mathcal{R} = \psi - \frac{\mathcal{H}}{\rho'}(\delta\rho_c - \delta\rho)\,. \tag{2.127}$$

This may then be substituted for ψ in the equation for the curvature perturbation of the uniform density gauge in Eqn. (2.112) and only the gauge invariant density perturbation within the comoving gauge remains. The relation is

$$\zeta = -\mathcal{R} - \frac{\mathcal{H}}{\rho_0'}\delta\rho_c\,. \tag{2.128}$$

2.5.3. Adiabaticity of Fluctuations

As well as an overall density perturbation that contributes to the curvature perturbations of the universe there may be many components of the fluid that exchange relative density perturbations between themselves. The relative density perturbation will contribute to the isocurvature (entropy) perturbations. To identify this entropic contribution we define the pressure as a function of the energy density and entropy S as $P = p(\rho, S)$. The pressure perturbations can be then found by a linear expansion about these parameters of our system,

$$\delta P = \frac{\delta P}{\delta S}|_\rho \delta S + \frac{\delta P}{\delta \rho}|_S \delta\rho\,, \tag{2.129}$$

this is our equation of state where the adiabatic sound speed is identified as,

$$c_a^2 = \left.\frac{\delta P}{\delta \rho}\right|_S . \tag{2.130}$$

The first term on the right hand side of Eqn. (2.129) can be identified as the non-adiabatic pressure. The non-adiabatic pressure is defined as [40],

$$\delta P_{nad} = \delta P - \delta\rho \frac{P_0'}{\rho_0'} \neq 0 , \tag{2.131}$$

For an adiabatic system there is a single degree of freedom so this Eqn. (2.131) would be zero, additional degrees of freedom may result in non-adiabatic pressure perturbations. In this sense a multifluid system can split the non-adiabatic pressure perturbations into an intrinsic part that occurs within each fluid (as we outlined above) and the relative pressure perturbations that are due to the energy transfer between fluids. The gauge invariant form of the relative perturbations between fluids can be defined as

$$S_{IJ} = 3\mathcal{H}\left(\frac{\delta\rho_J}{\rho_J'} - \frac{\delta\rho_I}{\rho_I'}\right) = 3\mathcal{H}\left(\zeta_I - \zeta_J\right) . \tag{2.132}$$

The relative non-adiabatic pressure [41, 42] is then,

$$\delta P_{rel} = -\frac{1}{6\mathcal{H}\rho'} \sum_{I,J} \rho_I' \rho_J' \left(c_I^2 - c_J^2\right) S_{IJ} . \tag{2.133}$$

An adiabatic fluid defines the equation of state,

$$\delta P = c_s^2 \delta\rho , \tag{2.134}$$

where c_s is the adiabatic sound speed. This inherently means we have a single degree of freedom proportional to the energy density [43, 44]. The local variance of each density fluctuation follows a time translation to a surface of uniform energy density which corresponds to adiabatic curvature perturbations. For multiple fluids with no transfer of energy between them adiabatic fluctuations occur when there is a common time-shift in the background density or pressure. In general the matter content of the universe need not be so restricted to one degree of freedom.

2.5.4. Evolution of Gauge–Invariant Quantities

In order to see how the curvature perturbations evolve with time we take the conformal time derivative of the curvature perturbations. The evolution is important particularly during the epoch of cosmic inflation. The slow-roll regime has become the standard model of inflation where the curvature perturbations freeze out on the

super-horizon scales. There is also a coincidence of the curvature perturbations in the different gauges on these scales. On super-horizon scales the perturbation in density in the comoving gauge may be ignored. The justification for this is that on large scales the spatial gradient is negligible. If we examine Eqn. (2.128) and set $\delta\rho_c = 0$, the curvature perturbation in the comoving and uniform density gauges coincide. Thus their evolution should be the same. There are numerous cases in which this may not be true, for example in multifield inflation [38, 41, 45]. In general we should not limit ourselves to a specific super-horizon scale: we take the time derivative of Eqn. (2.112) and expand it so that we get,

$$\begin{aligned}\zeta' &= -\left(\psi + \mathcal{H}\frac{\delta\rho}{\rho_0'}\right)' \\ &= -\psi' - \mathcal{H}'\frac{\delta\rho}{\rho_0'} - \mathcal{H}\frac{\delta\rho'}{\rho_0'} + \mathcal{H}\frac{\delta\rho_1\rho_0''}{\rho_0'^2}.\end{aligned} \tag{2.135}$$

Substituting Eqn. (2.60), Eqn. (2.14) (in conformal time) and its second derivative,

$$\rho'' = -3\mathcal{H}'(\rho + P) - 3\mathcal{H}(\rho' + P'), \tag{2.136}$$

we get,

$$\zeta' = -\mathcal{H}\frac{\delta P}{\rho + P} + \mathcal{H}\frac{P'}{\rho'}\frac{\delta\rho}{(\rho + P)} - \frac{1}{3}\nabla^2(\mathcal{V} + \sigma), \tag{2.137}$$

where $\mathcal{V} = v + B$ is the total covariant velocity perturbation. From our definition of the non-adiabatic pressure in Eqn. (2.131) this reduces to the form,

$$\zeta' = -\mathcal{H}\frac{\delta P_{nad}}{\rho + P} - \Sigma_{\mathcal{V}}, \tag{2.138}$$

where we have abbreviated the spatial gradient to $\Sigma_{\mathcal{V}}$,

$$\Sigma_{\mathcal{V}} = \frac{1}{3}\nabla^2(\mathcal{V} + \sigma)\,. \tag{2.139}$$

The perturbation ζ is constant if there are no sources of non-adiabatic pressure and spatial gradients are neglected. This is true in single-field slow-roll inflation evaluated on large scales where gradients can be ignored. The evolution of the comoving curvature perturbation is constructed from the perturbed Einstein equations and energy momentum equations.

2.6. Statistics of Curvature Perturbations

Having defined ζ and studied its evolution, in this section we will illustrate how quantities such as the ζ, calculated from the theory, can be related to observables. Observations of the CMB are used to calculate the statistics of temperature fluctua-

tions that are related to the statistics of ζ, likewise for observations of LSS. Current observations have a good measure on the statistics of two- and three-point correlations for temperature anisotropies in the CMB and in this section we will show the equivalent constraints on the statistics of ζ.

2.6.1. Two-Point Statistics

In general, we are only interested in the statistics of the curvature perturbations once ζ becomes constant, which as we have shown in Eqn. (2.138) occurs when the entropy perturbation dies out. In single-field slow-roll models of inflation this will occur a few e-folds after the modes of interest have crossed the horizon, in multi-field models of inflation it may be necessary to track the statistics over a long period of time (and often until inflation has ended) as ζ may continue to evolve.

While the perturbations of ζ average to be zero, the variance is non-zero. In fourier space we can parameterise the variance of the perturbations of ζ for a wavenumber k using the power spectrum. This tells us the amplitude of the variance at a particular value of k. The variance of the curvature perturbation $\zeta(\mathbf{x}$ at some point $\mathbf{x}$ can be written as,

$$\langle[\zeta(\mathbf{x}]^2\rangle = \langle \int \frac{d^3\mathbf{k_1}}{(2\pi)^{3/2}} \frac{d^3\mathbf{k_2}}{(2\pi)^{3/2}} \zeta(\mathbf{k_1})\zeta(\mathbf{k_2}) e^{i(\mathbf{k_1}+\mathbf{k_2})\cdot\mathbf{x}} \rangle \,. \tag{2.140}$$

Assuming statistical homogeneity the variance should be independent of $\mathbf{x}$, therefore $\langle\zeta(\mathbf{k_1})\zeta(\mathbf{k_2})\rangle \propto \delta(\mathbf{k_1}+\mathbf{k_2})$. Assuming isotropy the proportionality constant can only be a function of $k = |\mathbf{k}|$. We may then define the power spectrum $P(k)$ as the Fourier equivalent of the two-point function of ζ,

$$\langle\zeta(\mathbf{k_1})\zeta(\mathbf{k_2})\rangle = (2\pi)^3\delta(\mathbf{k_1}+\mathbf{k_2})P(k) \,. \tag{2.141}$$

As implied by the delta function of wavevectors $\mathbf{k_1}$ and $\mathbf{k_2}$, the power spectrum has a single degree of freedom, namely the scale dependence. It is often useful to then define the dimensionless power spectrum,

$$\mathcal{P}(k) = \frac{k^3}{2\pi^2} P(k) \,, \tag{2.142}$$

which is nearly independent of k for inflationary perturbations on super-horizon scales [5] and as a result it is often customary to normalize models with a non-adiabatic evolution to this. Conventionally we choose a pivot scale $k_\star$ usually set by observational constraints, i.e. , for the Planck temperature mapping a pivot scale of 0.05Mpc^{-1} [5] and later 0.002Mpc^{-1} [46] as parameters decorrelate at these pivot

[5] We will discuss this later when considering just field-correlations in Eqn. (4.20): at horizon crossing for a canonical light field $G_{IJ} = \delta_{IJ}$, the dimension-full power spectrum is $P(k) = H^2/2k^3$.

scales. The measured amplitude at the pivot scale of $k_\star = 0.05\text{Mpc}^{-1}$ is,

$$\mathcal{P}(k_\star) = (2.196 \pm 0.060) \times 10^{-9} \,. \tag{2.143}$$

From the perspective of inflationary dynamics such modes exit the horizon between 50 and 60 e-folds before inflation ends. The amplitude of the power spectrum will have some scale-dependence which is measured by the parameter n_s, the spectral index,

$$n_s - 1 = \frac{d \ln \mathcal{P}(k)}{d \ln k} \,. \tag{2.144}$$

When there is more power on the small wavelengths (UV-spectrum with $n_s > 1$) we say the spectrum is blue-tilted. When there is more power on the long wavelengths (IR-spectrum with $n_s < 1$) we say the spectrum is red-tilted.

It is also possible that the spectral index will exhibit a running, such that it is wavelength dependent. We define this running as,

$$\alpha_s = \frac{d \ln n_s}{d \ln k} \,. \tag{2.145}$$

2.6.2. Three-Point Statistics

Similar to the construction of the power spectrum for the two-point function in Eqns. (2.140) and (2.141), we can construct the bispectrum $B(k_1, k_2, k_3)$ for the statistics of the three-point function as

$$\langle \zeta(\mathbf{k_1}) \zeta(\mathbf{k_2}) \zeta(\mathbf{k_3}) \rangle = (2\pi)^3 \delta(\mathbf{k_1} + \mathbf{k_2} + \mathbf{k_3}) B(k_1, k_2, k_3) \,, \tag{2.146}$$

where the delta function, coming from out assumption of statistical homogeneity, implies that the wavevectors form a triangle in Fourier space. Additionally, statistical isotropy entails that the orientation of this triangle is irrelevant, so that only its shape and overall scale matter, hence the dependence on the three wavenumbers $k_i = |\mathbf{k}_i|$. The bispectrum shape can be classified into three limiting sets of configurations, as seen in Fig. (2.5): the squeezed (local) limit ($k_1 \ll k_2 = k_3$) is the large scale limit, the equilateral limit ($k_1 = k_2 = k_3$) and the orthogonal (folded) limit. We will soon discuss the physical significance of each of these configurations.

A quantity for quantifying the amplitude of the bispectrum is by defining the reduced bispectrum as

$$f_{nl}(k_1, k_2, k_3) = \frac{5}{6} \frac{B(k_1, k_2, k_3)}{P(k_1)P(k_2) + P(k_1)P(k_3) + P(k_2)P(k_3)} \,, \tag{2.147}$$

where, by putting a constraint on the overall scale, $k_s = k_1 + k_2 + k_3$, we can parameterize any shape by the α and β quantities[6] such that,

[6] We note that α and β in this context is different from the gauge terms we used in Sec. (2.5).

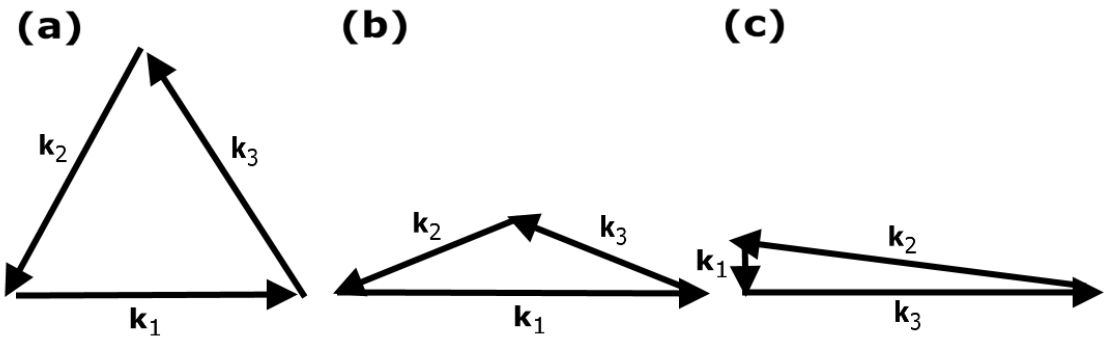

Figure 2.5.: *The bispectrum configurations are often classified in terms of three different limits: the equilateral limit (a), the orthogonal (folded) limit (b) and the squeezed (local) limit (c).*

$$\begin{aligned} k_1 &= \frac{k_s}{4}(1+\alpha+\beta)\,, \\ k_2 &= \frac{k_s}{4}(1-\alpha+\beta)\,, \\ k_3 &= \frac{k_s}{2}(1-\beta)\,, \end{aligned} \tag{2.148}$$

with the allowed values of (α, β) falling inside the triangle in the α, β plane with vertices $(-1, 0)$, $(1, 0)$ and $(0, 1)$. The reduced bispectrum measures the relative non-linearity between the two- and three-point functions. Equivalently to the power spectrum we form the dimensionless bispectrum,

$$\mathcal{B} = (k_1 k_2 k_3)^2 B(k_1, k_2, k_3)\,, \tag{2.149}$$

which is often related to the 'shape function' denoted $S(k_1, k_2, k_3)$ [47] by some normalisation,

$$\mathcal{B}(k_1, k_2, k_3) = (2\pi)^4 \mathcal{P}(k_\star)^2 S(k_1, k_2, k_3)\,, \tag{2.150}$$

where $\mathcal{P}(k_\star)$ comes from Eqn. (2.143).

Note that in the approximation of an exactly scale-invariant power spectrum, f_{nl} and S are related by

$$f_{nl}(k_1, k_2, k_3) = \frac{10}{3} \frac{S(k_1, k_2, k_3)}{k_1^2/(k_2 k_3) + 2\,perms.}\,, \tag{2.151}$$

where *perms* indicates permutations over the k's. A bispectrum that is equilateral-like in shape will peak in amplitude for equilateral configurations at about $(\alpha, \beta) = (0, 1/3)$ as seen in Fig. (2.6). These non-Gaussian shapes are generated by derivative interactions and are often a feature of inflationary models with non-canonical kinetic

terms [48]. We define the equilateral shape template [49] as

$$S^{eq} = \frac{9}{10} f_{nl}^{eq} \left[-\left(\frac{k_1^2}{k_2 k_3} + 2\,perms. \right) + \left(\frac{k_1}{k_2} + 5\,perms. \right) - 2 \right] , \tag{2.152}$$

where f_{nl}^{eq} is a constant representing the amplitude for this shape.

A bispectrum that is orthogonal-like in shape will peak in amplitude for folded configurations at about $(\alpha, \beta) = (0, 0), (-1/2, 1/2)$ and $(1/2, 1/2)$ in Fig. (2.6). Signatures in this configuration can be generated in models with non Bunch-Davies vacuum [50]. Large amplifications of these signatures have been generated in multi-field DBI Galileon inflation [47, 51] and, as we will examine in Ch. (8), models boasting large negative field-space curvature such as Sidetracked inflation [52]. The shape template for orthogonal non-Gaussianity [53] is

$$S^{orth} = \frac{27}{10} f_{nl}^{orth} \left[-\left(\frac{k_1^2}{k_2 k_3} + 2\,perms. \right) + \left(\frac{k_1}{k_2} + 5\,perms. \right) - \frac{8}{3} \right] , \tag{2.153}$$

where f_{nl}^{orth} is a constant representing the amplitude for this shape.

The super-horizon growth of perturbations in multi-field models of inflation amplify the local non-Gaussian shape. This arises from interactions between growing modes outside of the horizon, as opposed to the modes which quickly freeze out and become constant a few e-folds after horizon crossing. The interacting modes appear in local combinations of the terms $(k_1^3 k_2^3)^{-1}$. There are called 'local' as the evolution is local in space and quantities local in positional space translate to non-localities in momentum space. In the squeezed limit when $(k_1 \ll k_2 = k_3)$ the behaviour of the amplitude of f_{nl} is $(k_1/k_2)^{-1}$ [48]. The template for the local shape is

$$S^{local} = \frac{3}{10} f_{nl}^{local} \left(\frac{k_1^2}{k_2 k_3} + 2\,perms. \right) , \tag{2.154}$$

where f_{nl}^{local} is a constant representing the amplitude for this shape. In Fig. (2.6) the shape peaks in the squeezed configurations located in the corners of the triangles in Eqn. (2.148).

For multiple light fields with canonical kinetic terms in a potential where trajectories exhibit minimal bending it has been shown [54, 55] that the contributions to non-Gaussiansity are dominated by f_{nl}^{local}.

2.7. Quantization of the Fields

To begin our discussion of quantum fluctuations we must first describe the background geometry that they live on. Inflation as a theory of accelerated expansion describes our universe as a de Sitter like universe. During this phase of our uni-

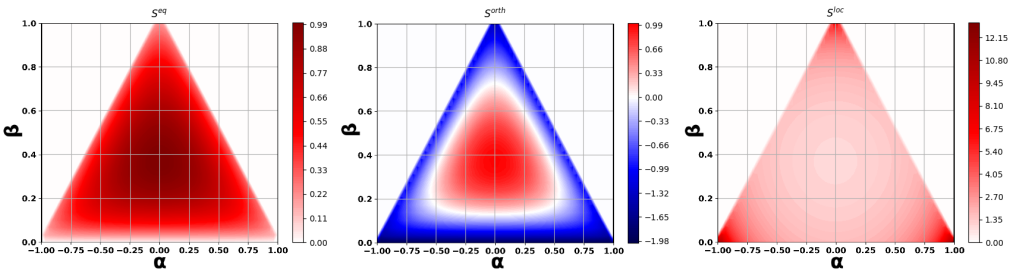

Figure 2.6.: *Using the coordinate system in Eqn. (2.148) we can visualize the shape templates: on the left is the equilateral template (Eqn. (2.152)), in the middle is the orthogonal template (Eqn. (2.153)) and on the right is the local template (Eqn. (2.154)).*

verse the space-time can be represented as a four-dimensional timelike hyperboloid embedded in a five-dimensional Minkowski space-time [56, 57]. Generally this is true for any D-dimensional timelike hyperboloid embedded in a $D+1$-dimensional Minkowski space-time. To illustrate we construct the line element where we have embedded the hyperboloid in the five-dimensional space. This metric is of the form

$$ds^2 = -dX_o^2 + dX_1^2 + dX_3^2 + dX_4^2\,, \tag{2.155}$$

where $\sqrt{X_\mu X^\mu} = H^{-2}$ is the de Sitter radius.

By choice of coordinates Eqn. (2.155) can take the form of an FLRW line element for an open, closed or flat universe. Various coordinate systems can be chosen for flat space. For example under a particular choice of coordinates we obtain the de Sitter induced line element for flat slicing,

$$dS^2_{flat} = -dt^2 + e^{2Ht}\delta_{ij}dx^i dx^j\,. \tag{2.156}$$

In conformal time this space-time takes the form,

$$dS^2_{flat} = \frac{1}{(H\tau)^2}\left(-d\tau^2 + \delta_{ij}dx^i dx^j\right)\,. \tag{2.157}$$

2.7.1. Quantizing Scalar Perturbations

We will now outline the quantization procedure for a single field; a more detailed description can be found in [21]. This calculation will be preformed in the flat gauge defined in Sec. (2.5.1). We first promote the scalar field to the status of a quantum operator $\hat{\delta\phi}(\mathbf{x}, t)$, defined as,

$$\hat{\delta\phi}(\mathbf{x}, t) = \int \frac{d^3\mathbf{k}}{(2\pi)^{3/2}}\left[\delta\phi_k(t)e^{i\mathbf{k}\cdot\mathbf{x}}\hat{a}_\mathbf{k} + \delta\phi_k^\star(t)e^{-i\mathbf{k}\cdot\mathbf{x}}\hat{a}^\dagger_\mathbf{k}\right]\,, \tag{2.158}$$

where $\delta\phi_k(t)$ is the mode function and the annihilation operator $\hat{a}_{\mathbf{k}}$ and creation operators $\hat{a}^\dagger_{\mathbf{k}'}$ satisfy the relation,

$$\left[\hat{a}_{\mathbf{k}}, \hat{a}^\dagger_{\mathbf{k}'}\right] = 2\pi\delta^3(\mathbf{k}-\mathbf{k}') \quad \text{and} \quad [\hat{a}_{\mathbf{k}}, \hat{a}_{\mathbf{k}'}] = \left[\hat{a}^\dagger_{\mathbf{k}}, \hat{a}^\dagger_{\mathbf{k}'}\right] = 0\,. \tag{2.159}$$

The mode function is a solution to the massless Klein-Gordon equation and satisfies,

$$\ddot{\delta\phi}_k + 3H\dot{\delta\phi}_k + \frac{k^2}{a^2}\delta\phi_k = 0\,, \tag{2.160}$$

where we make the assumption that they are free fields and are massless. This assumption holds for modes which are deep within the horizon. By converting to conformal time and rescaling our mode function as $\nu = a\delta\phi$ we find that the Klein-Gordon equation becomes,

$$\nu_k'' + \left(k^2 - \frac{a''}{a}\right)\nu_k = 0\,, \tag{2.161}$$

with an effective time-dependent mass term $m^2 = -a''/a$. In de Sitter space the scale factor can be read off from Eqn. (2.157), $a(\tau) = -1/H\tau$ and we get,

$$\nu_k'' + \left(k^2 - \frac{2}{\tau^2}\right)\nu_k = 0\,. \tag{2.162}$$

The general solution of this is

$$\nu_k(\tau) = \left[A(k)H^{(1)}_{3/2}(-k\tau) + B(k)H^{(2)}_{3/2}(-k\tau)\right]\,, \tag{2.163}$$

with $A(k)$ and $B(k)$ as arbitrary functions to be determined later after canonical quantization, $H^{(1,2)}_{3/2}$ are the Hankel functions of the first and second kind. The Hankel function is a linear combination of the Bessel functions of the first and second kind, expanding it out to linear order (for small arguments) and substituting it back in to Eqn. (2.163) we obtain the general form of the solution,

$$\nu_k(\tau) = A(k)e^{-ik\tau}\left(1 + \frac{1}{ik\tau}\right) + B(k)e^{ik\tau}\left(1 - \frac{1}{ik\tau}\right)\,. \tag{2.164}$$

Now we may impose the canonical quantization rules on the operators $\hat{\nu}$ and its conjugate momentum $\hat{\pi}(x)$,

$$[\hat{\nu}_{\mathbf{k},\tau}, \hat{\pi}_{\mathbf{k}',\tau}] = 2\pi\delta^3(\mathbf{k}-\mathbf{k}') \quad \text{and} \quad [\hat{\nu}_{\mathbf{k},\tau}, \hat{\nu}_{\mathbf{k},\tau}] = [\hat{\pi}_{\mathbf{k},\tau}, \hat{\pi}_{\mathbf{k},\tau}] = 0\,. \tag{2.165}$$

From the commutation rules of the annihilation and creation operators, this implies that

$$\nu_k\nu_k^{\star\prime} - \nu_k^\star\nu_k' = i\,, \tag{2.166}$$

which upon solving we find a solution to the functions $A(k)$ and $B(k)$,

$$A(k)^2 - B(k)^2 = \frac{1}{2k}\,. \tag{2.167}$$

Here we can make a choice of only the positive frequency modes. With this choice, as $k\tau \to -\infty$, $\nu_k \to e^{-ik\tau}/\sqrt{2k}$, we can set $B(k) = 0$. This is referred to as the Bunch-Davies vacuum [58]. We may now define the correlation function of ν as,

$$\langle 0\,|\hat{\nu}(\mathbf{x},\tau)\hat{\nu}(\mathbf{x}',\tau)|\,0\rangle = \int \frac{d^3\mathbf{k}}{(2\pi)^3}\,|\nu_k|^2\,e^{i\mathbf{k}\cdot(\underline{\mathrm{X}}-\mathbf{x}')}\,, \tag{2.168}$$

which corresponds to the dimension full power spectra,

$$P_\nu(k) = |\nu_k|^2\,. \tag{2.169}$$

We now have our solution satisfying this initial condition,

$$\delta\phi_k = \frac{H\tau}{\sqrt{2k}}\left(1 + \frac{1}{ik\tau}\right)e^{-ik\tau} \tag{2.170}$$

where we have converted back to our mode function $\delta\phi_k$. We may now deduce the power spectra by determining the variance of the field fluctuations,

$$P_{\delta\phi}(k) = |\delta\phi_k|^2 = \frac{|\nu_k|^2}{a^2}\,. \tag{2.171}$$

Taking the limit of Eqn. (2.168) on super-horizon scales, where $k\tau \ll 1$, the scale invariant dimensionless power spectrum is,

$$\mathcal{P}_{\delta\phi}(k) = \left(\frac{H_\star}{2\pi}\right)^2\,, \tag{2.172}$$

where $H_\star$ is evaluated at horizon crossing.

We can relate $\delta\phi$ to the curvature perturbation in the comoving gauge $\mathcal{R}$ and repeat this procedure. Using the curvature perturbation from Eqn. (2.125) and substituting $|\mathcal{R}| = |\nu_k/z|$ where,

$$z = \frac{a\phi'}{\mathcal{H}}\,, \tag{2.173}$$

we get the governing equation in the comoving gauge,

$$\mathcal{R}'' - \frac{z'^2}{z}\mathcal{R}' + k^2\mathcal{R} = 0\,, \tag{2.174}$$

where an effective mass can be defined as $m_{eff}^2 = -z'/z$. In the limit outside the horizon where $\dot{a} = a$ and $H = const.$, the solution grows like,

$$\nu_k \propto z; \quad k^2 \ll z''/z\,, \tag{2.175}$$

and the comoving curvature perturbation on super-horizon scales no longer evolves and $\mathcal{R}' \propto 0$. From Eqn .(2.128) we know that the comoving curvature perturbations can be related to the uniform density perturbations meaning $|\zeta| = |\nu_k/z|$. This implies that the power spectrum is given by,

$$\mathcal{P}_\mathcal{R} = \mathcal{P}_\zeta = \frac{k^3}{2\pi^2}\left|\frac{\nu_k}{z}\right|^2 . \tag{2.176}$$

These calculations can be extended to the three-point function. We defer this discussion until Ch. (4) where the in–in formalism is used.

2.7.2. Quantizing Tensor Perturbations

Tensor modes during inflation are easier to compute in comparison. Tensor modes are responsible for the initial amplitude of gravitational waves, whose oscillations begin at horizon entry [4]. The amplitude of these gravitational waves, if large enough, are detectable. Here we will only consider the tensor perturbation h_{ij} in Eqn. (2.43) such that the form our line element is,

$$ds^2 = a^2(\tau)\left[-d\tau^2 + (\delta_{ij} + h_{ij})\, dx^i dx^j\right] . \tag{2.177}$$

Expanding the Einstein-Hilbert action (2.1) to second order with the line element above [21] we get,

$$S_{(2)} = -\frac{M_{\rm pl}^2}{8}\int d^3x d\tau a^2 h^{ij}\left[h''_{ij} + 2\frac{a'}{a}h'_{ij} - \partial^2 h_{ij}\right] . \tag{2.178}$$

We can decompose the tensor perturbations into an orthogonal basis of polarizations $s \in (+, \times)$. The Fourier expansion of the perturbation mode is,

$$h_{ij} = \int \frac{d^3k}{(2\pi)^3}\sum_s e^s_{ij}(k) h^s_{\mathbf{k}}(\tau) e^{i\mathbf{k}\cdot\mathbf{x}} + c.c. , \tag{2.179}$$

where $\mathbf{k}$ is the comoving wavenumber and '$+c.c.$' denotes the addition of the complex conjugate. The tensors e_{ij} obey the relations $e_{ii} = k^j e_{ij=0}$ and $e^s_{ij}(k)e^{s'}_{ij}(k) = 2\delta_{ss'}$. The action in Fourier space is then,

$$S_{(2)} = M_{\rm pl}^2 \sum_s \int d\tau dk \frac{a^4}{4}\left[h^{s'}_{\mathbf{k}} h^{s'}_{\mathbf{k}} - k^2 h^s_{\mathbf{k}} h^s_{\mathbf{k}}\right] \tag{2.180}$$

Each polarization of the tensor modes behaves like a canonically-normalized free scalar field. Due to the stochastic nature of the tensor perturbations they are generally considered to be invariant under parity transformations. This means that cross

correlations between polarizations vanish and we have,

$$4\langle h_s(\mathbf{k_1})h_s(\mathbf{k_2})\rangle = (2\pi)^3\frac{2\pi^2}{k^3}\mathcal{P}_h(k)\delta^3(\mathbf{k}-\mathbf{k}')\,, \tag{2.181}$$

where $\mathcal{P}_h$ is the dimensionless power spectrum of tensor perturbations. We can write the Sasaki-Mukhanov equation[7],

$$v_k^{s\prime\prime} + w_k(\tau)^2 v_k^s = 0\,, \tag{2.182}$$

where $v_k^s = aM_{\rm pl}h_{\mathbf{k}}^s/2$ is a redefinition of the tensor mode to a canonically normalized field. The frequency component $w_k(\tau)$ takes the form of [59]

$$w_k^2(\tau) \approx k^2 - \frac{2}{\tau^2} \quad \text{de Sitter}\,. \tag{2.183}$$

The calculation for the power spectrum follows from that given in Sec. (2.7.1). We can then define the dimensionaless power spectrum for each polarization evaluated at horizon crossing when $k \approx aH$ is,

$$\mathcal{P}_h(k) = \frac{4}{M_{\rm pl}^2}\left(\frac{H_\star}{2\pi}\right)^2\,, \tag{2.184}$$

where $H_\star$ is evaluated at horizon crossing. The total tensor power spectrum is then obtained by summing over all polarizations,

$$\mathcal{P}_T(k) = \frac{8}{M_{\rm pl}^2}\left(\frac{H_\star}{2\pi}\right)^2\,. \tag{2.185}$$

In slow-roll models of inflation the amplitude of tensor perturbations will be much smaller than the amplitude of curvature perturbations and it is standard to define the ratio of tensor to scalar perturbations as,

$$r = \frac{\mathcal{P}_T^2}{\mathcal{P}_\zeta^2}\,. \tag{2.186}$$

This is one of the key observables that is used to test our models of inflation.

2.8. Models of Inflation

Single-field models

In single-field inflation, models are generally classified into two categories, small-field and large-field inflation. In large-field inflation the field evolution spans super-Planckian values $\Delta\phi > M_{\rm pl}$ and the inflaton field starts at large field values and then rolls down to the minimum $V(\phi = 0) = 0$. The archetypal large-field model is

[7] We will see that this comes from the action in Eqn. (2.177).

chaotic inflation [60], which has a potential of the form,

$$V(\phi) = \lambda_n \phi^n \,, \tag{2.187}$$

where λ_n is a coupling constant. Examples of other large-field inflation models include models with exponential potentials [61] and natural inflation [62] where the potential is sinusoidal (often justified in models containing axionic particles predicted from string theory [63]). In terms of the slow-roll parameters these models obey $-\epsilon < \eta \leqslant \epsilon$ (from Eqns. (2.34) and (2.35)). The second derivative of the potential also satisfies $V_{,\phi\phi} > 0$ meaning that the slow-roll parameter is $\eta_V > 0$. An interesting feature of large-field inflation is that they can produce a large tensor to scalar ratio r that may be possible to detect [64]. This can be seen using the approximate relation, the Lyth bound

$$\frac{\Delta\phi}{M_{\rm pl}} = \mathcal{O}(1) \times \left(\frac{r}{0.01}\right)^{1/2} \,. \tag{2.188}$$

For approximately Planckian values of the field variations $\Delta\phi$ (over a number of e-folds observable in the CMB) one could expect a value of $r \sim 0.01$.

In contrast, in small-field inflation the field spans a small (sub-Planckian) distance, $\Delta\phi < M_{\rm pl}$. These models invoke very flat potentials when the field is far from the minimum. Here the first slow-roll parameter satisfies $\eta < -\epsilon$. Likewise, the second derivative of the potential is negative $V_{,\phi\phi} < 0$ in the region of the potential where inflation occurs meaning the second slow-roll parameter is negative $\eta_V < 0$ (hence $\epsilon > 0$). Since the energy scales are smaller, the amplitude of gravitational waves produced will be too small to be detected. The type of potentials in this class have minimums displaced from $\phi = 0$, an example of such a potential is,

$$V(\phi) = \Lambda^4 \left[1 - \left(\frac{\phi}{\mu}\right)^n\right] \,, \tag{2.189}$$

where Λ sets the overall scale of the potential and μ is a dimensionless coupling constant. This model belongs to a category of hilltop inflation models [65].

In the above examples we have limited ourselves to a classification of models that admit slow-roll behavior, but this need not be the case. It can also be interesting to consider models with features in the potential that temporarily violate the slow-roll conditions as they often produce large observable signatures. An example of such a feature is a step in the potential [66, 67],

$$V(\phi) = V_0 \left[1 + cF\left(\frac{\phi_f - \phi}{d}\right)\right] \,, \tag{2.190}$$

where V_0 is a potential that supports slow-roll inflation in the limit where $c \to 0$, ϕ_f is the field value about where the step occurs, d is the width of the step and F

is a function that transition between $+1$ and -1 often defined as $-\tanh(x)$. Such features can produce highly scale dependent power-spectra and observable bispectra.

Departing from the single-field slow-roll inflation paradigm, we have a plethora of inflationary models with different theoretical motivations and different observational predictions. Below we outline a few of these categories.

Canonical multi-field inflation

In general, from the perspective of high-energy physics it is more realistic to have more than one dynamically relevant scalar field during inflation [68, 69]. The addition of more fields expands the possibilities for the inflationary dynamics leading to a loss in the predictive power of the theory. In assisted inflation [70, 71] a collection of fields each with a value of $\phi_i \ll M_{\rm pl}$ can approximate the single large field models by a rotation of the field basis into one direction with $\phi \gg M_{\rm pl}$ with predictions that converge in the large number $N > 100$ of field limit [72]. However in the case of N sinusoidal fields the individual expansion of each ϕ_i can remain relevant as in the case of N-flation [73]. With an increase in the number of fields comes a larger parameter space and a hierarchy of masses giving rise to different inflationary dynamics. A generic action for such a model is given as,

$$S = \frac{1}{2}\int d^4x\sqrt{-g}\left[M_{\rm pl}^2 R - \delta_{IJ}g^{\mu\nu}\partial_\mu\phi^I\partial_\nu\phi^J - 2V(\phi^I,\phi^J)\right] . \tag{2.191}$$

As an example of an anayltically tractable proxy for N-flation [74] we can can consider the potential for two fields ϕ and χ,

$$V(\phi,\chi) = \frac{1}{4}g\phi^4 + \Lambda^2\left(1-\cos\frac{2\pi\chi}{f}\right) . \tag{2.192}$$

This is refered to as the Axion-Quartic model and aims to encapsulate the physics of N-flation where one of the fields initially lies near a hilltop of the axionic potential [75, 76]. This region has a large and negative slow-roll parameter η, while ϵ remains small. This then generates large local non-gaussianity, $f_{nl}^{local} = \mathcal{O}(10)$.

Another popular example is the curvaton scenario [77] where we have an inflationary field ϕ and a light spectator field χ. Here the field ϕ drives inflation while the primordial density pertrubations are generated by the curvaton field χ. In this scenario $V(\chi)$ is almost flat and its mass is much less than the Hubble parameter. During inflation the curvatons conribution to the density is negligible and is essential frozen. After inflation the Hubble parameter decreases and when $H \sim m(\chi)$ the curvaton unfreezes and oscillates about its minimum. The coherent curvaton oscillations correspond to pressureless matter which dominates the energy density of the Universe imposing its own curvature perturbation. A more detailed review of multifield inflation with the kind of action in Eqn. (2.191) can be found in Ref. [78].

Non-canonical multi-field inflation

In non-canonical models of inflation the action contains a modified kinetic term [79]. Compared to Eqn. (2.191), the action is of a modified form,

$$S = \frac{1}{2}\int d^4x\sqrt{-g}\left[M_{\rm pl}^2 R - P(\phi^I, X) - 2V(\phi^I, \phi^J)\right] . \tag{2.193}$$

where $P(\phi^I, X)$ is some function of the kinetic term $X = G_{IJ}g^{\mu\nu}\partial_\mu\phi^I\partial_\nu\phi^J$ and some fields ϕ^I. $P(\phi^I, X)$ is the most general form and can contain couplings between derivatives of the fields $P(\phi^I, X)$ [80]. The simplest form of this action contains just $P(\phi^I, X) = X$. In this case, it corresponds having a field-space metric G_{IJ} instead of the delta function in Eqn. (2.191) which may be Euclidean and hence have flat scalar curvature in field-space or be non-Euclidean and have some curvature in field-space. A non-trivial field-space metric can be just as important as the fields' potential energy in determining the fields' dynamics, and hence the observational predictions of inflationary models. While this is not exclusively limited to multi-field scenarios (i.e. DBI inflation [81, 82]) it can be motivated by Supersymmetry models of inflation with Kahlër manifolds, D-brane inflation [83], etc. It is one of the main objectives of this thesis to explore these models in more detail, which we will do in later chapters.

Non-minimal coupling to gravity and modified gravity

In these models one or many fields, such as the inflaton, may be coupled to the Ricci Scalar [59]. One such coupling may appear as $f(\phi^I)g^{\mu\nu}R_{\mu\nu}(\Gamma)$ where Γ is the connection. We need not specify whether the connection is of the Levi-Civita form, $\Gamma = \Gamma(g_{\mu\nu})$, as it may be determined independently (i.e. in the Palatini theory of gravity [84, 85]). In general, any departure away from the Einstein-Hilbert theory of gravity, due to perhaps some high-energy modifications to gravity, can be reformalized as a non-minimally coupled system of scalar fields and potential [86]. The action is of the form,

$$S = \frac{1}{2}\int d^4x\sqrt{-g}\left[M_{\rm pl}^2 F(R, \phi^I) - \delta_{IJ}g^{\mu\nu}\partial_\mu\phi^I\partial_\nu\phi^J - 2V(\phi^I, \phi^J)\right] . \tag{2.194}$$

In this form we would need to rederive the Friedmann equation for this model, however as gravity is invariant under conformal transformation it can be turned into something of the form of Eqn. (2.193) making it possible to calculate the observables from inflation in a simpler way. We will discuss this class of model in Ch. (7).

For both Non-canonical and Non-minimal coupling models of inflation calculation of the observables can not be done analytically. This is also the case for certain canonical models of inflation and non-slow-roll models. In these instances numerical methods are often the only way to acquire results.

2.9. End of Inflation

At the end of inflation, when $\epsilon = 1$, the field oscillates around the minimum of the potential and the energy density of the universe is locked up in the homogeneous scalar fields. In order for the universe to transition from this 'cold' state to a 'hot' one, as in the hot big bang model, we require that the universe establishes equilibrium through the reheating process [87]. The process of the inflaton decaying into a collection of matter and radiation particles can be complex as we have additional decay parameters. These effects may be possible to calculated perturbatively, or, non-perturbative effects such as parametric resonances and tachyonic instabilities can be as significant. The latter leads to a exponential growth in the number density of the decay particles and this process is called preheating. In this section we will give an brief overview of these processes that occur after inflation has ended.

2.9.1. Reheating

During inflation the fields are slowly rolling and the potential energy of the fields dominates. When inflation ends the fields begin to oscillate about the minimum of the potential and the energy can be released into other forms of matter and radiation [88]. Initially the coherent oscillations may be considered as isolated scalar particles coupled to lighter fields. This interaction means that the field ϕ decays perturbatively into species A and at a decay rate Γ_A^I. This additional term appears in the Klein-Gordon equation (from Eqn. (2.195)),

$$\ddot{\phi}_I + \left(3H + \frac{1}{2}\Gamma_A^I\right)\dot{\phi}_I + V_{,I} = 0\,, \tag{2.195}$$

equivalent to the $3H\dot{\phi}$ term the decay term acts as an additional dampening to the harmonic oscillator evolution of ϕ [89]. The interactions in the above equation only become relevant when the Hubble parameter decreases to the point where $H \sim \Gamma_{Tot}$, where Γ_{Tot} is the sum of the decay rates. So this equation is only valid at the end of inflation when the fields are oscillating rapidly about their minimum. In addition to this the continuity equation for the decay products can be formed,

$$\dot{\rho}_A + 3H(\rho_A + p_A) = \frac{1}{2}\sum_I^N \Gamma_A^I \dot{\phi}_I^2\,, \tag{2.196}$$

where the decay fluids will have an equation of state of $p_\gamma = \rho_\gamma/3$ for radiation and $p_m = 0$ for matter [90]. For perturbative reheating to work we require that the couplings are small. In addition this method cannot take into account the Bose condensation effects [88]. This occurs if the phase space of decay products is densely populated and leads to an exponential increase in the decay efficiency.

2.9.2. Preheating

The above perturbative analysis may only be valid at the late stages of reheating when most of the energy density of the inflationary fields have decayed to relativistic species. In the early period of oscillations another effect may be dominant, preheating. During the preheating stage particles are produced by a mechanism of parametric resonance. By this we mean the resonance effect exhibited by an oscillator with a time-dependent frequency. Preheating can also occur even when there are no oscillations, such as in situations like kination [91]. As well as the standard form of reheating, which is model dependent and converts initially homogeneous oscillating fields into particles of different species there can be tachyonic preheating which converts particles into the same species [92]. Another variation of preheating is known as instant preheating. This mechanism ends after the first passage of the field through $\phi = 0$, hence the name 'instant'.

2.10. Observational Constraints on Inflation

In recent years the quantity and quality of observational data has increased vastly. The mapping of the CMB has been the most important source of evidence for inflation. Much of this advancement has been made through satellite missions and ground based telescopes. Balloon based telescopes have also been used such as CBI[93], VSA [94], ACBAR [95], BOOMERANG [96] and Spider [97]. From 1989 to 1993 the COBE satellite [98] collected evidence in support of the hot big bang model by observing the near perfect black-body spectrum of the CMB and some faint clues of anisotropies in the temperature power spectrum. This spacecraft was then succeeded by WMAP [99] which operated from 2001 to 2010. Thanks to its vastly improved resolution the first detailed map of the anisotropies could be obtained. WMAP collected cosmological data for a wide range of parameters, from the age of the universe to the precise fraction of dark matter, baryonic matter and dark energy. From this data the strong evidence for inflation was found, such as the flatness of the early universe and the tilt of the spectrum. In 2009 the Planck telescope was launched [100–102] with improved equipment for measuring the temperature anisotropies. While the Planck mission was completed in 2013, the data from that mission is still being analysed to this day. Three sets of result releases have been made since the mission has ended [5, 46, 103] with the latest giving the most refined constraints on inflation to date. These results in combination with results from ground based experiments BICEP1, BICEP2, Keck Array, and BICEP3 have lead not only to the validation of slow-roll inflationary predictions but also to the exclusion of many of the simplest models of inflation. The results of the combination of these surveys are as follows: The spectral index has been

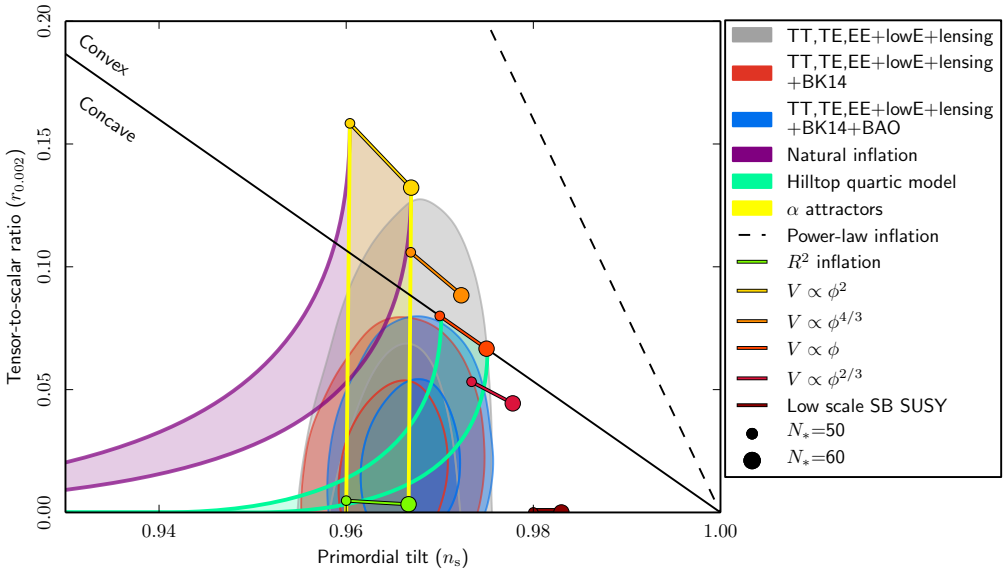

Figure 2.7.: *Constraints on the observed spectral index n_s and the tensor to scalar ratio r by Planck alone and in combination with BK14 or BK14 plus BAO (Baryonic acoustic oscillations) data, compared to the theoretical predictions of selected inflationary models [103]*

measured [103] to be,

$$n_s = 0.9649 \pm 0.0042\,. \tag{2.197}$$

The limits on the tensor to scalar ratio [103] is,

$$r < 0.1\,. \tag{2.198}$$

In Fig. (2.7) we see how these constraints have restricted the parameter space of models. In addition to these results we also have constraints on non-Gaussianities produced during inflation [46],

$$\begin{aligned} f_{nl}^{eq} &= -4 \pm 43\,, \\ f_{nl}^{ort} &= -26 \pm -21\,, \\ f_{nl}^{local} &= 0.5 \pm 5.0\,. \end{aligned} \tag{2.199}$$

3. Cosmological Perturbation Theory in Curved Field-Space

In this chapter, using the tools of cosmological perturbation theory, we derive the perturbed action and density perturbations at second order for models of inflation with a curved field-space metric. In Sec. (3.1) we present the ADM approach to cosmological perturbations. We then calculate the perturbed equations of motion for a generic non-canonical multifield model of inflation using a covaraint setup over the field-space indices in Sec. (3.2). Finally, in Sec. (3.3) we introduce the novel calculation of the curvature pertrubations for this model in the unifrom density gauge.

We begin by deriving the action to cubic order, and the Hamiltonian equations of motion, for covariant field-space perturbations defined on flat hypersurfaces. As we will now discuss, the calculations mirror those presented in Ref. [78, 104] but generalized to the case of a non-trivial field-space metric.

We begin with the action for $\mathcal{N}$ scalar fields minimally coupled to gravity,

$$S = \frac{1}{2}\int d^4x\sqrt{-g}\left[M_{\rm p}^2 R - G_{IJ}g^{\mu\nu}\partial_\mu\phi^I\partial_\nu\phi^J - 2V\right] , \tag{3.1}$$

where R is the Ricci scalar associated with the space-time metric $g_{\mu\nu}$, G_{IJ} is the $\mathcal{N}$ dimensional field-space metric, and where upper case Roman indices run from 1 to $\mathcal{N}$, which are raised and lowered by G_{IJ}. This is a subset of models described by the action in Eqn. (2.193) where $P(\phi^I, \phi^J) = G_{IJ}$ is a function of the fields $G_{IJ}(\phi^I, \phi^J)$.

For a flat Friedmann-Robertson-Walker (FRW) cosmology in Eqn. (2.6) with $\kappa = 0$ this action leads to the background equations of motion,

$$\begin{aligned} 3M_{\rm p}^2H^2 =& \frac{1}{2}G_{IJ}\dot\phi^I\dot\phi^J + V \,, \\ D_t\dot\phi_I + 3H\dot\phi_I =& -V_I \,, \end{aligned} \tag{3.2}$$

where the covariant time derivative of a field-space vector, U^I, is defined as

$$D_tU^I = \dot U^I + \dot\phi^M\Gamma^I_{MN}U^N \,, \tag{3.3}$$

and t indicates cosmic time, with a over-dot indicating differentiation with respect

to cosmic time. This is the multifield covariant form of Eqns. (2.29) and (2.30). The connection Γ^I_{MN} is the Levi-Civita connection compatible with the field-space metric G_{IJ}.

3.1. Metric Perturbations of the ADM Metric

As we have discussed in the Sec. (2.5) 4D space-time can be foliated into spatial hypersurfaces. Each hypersurface (which we will call Σ_t) is a 3D Riemannian surface of constant time t. This space is globally hyperbolic and the foliation can be performed in various ways. This slicing (or threading) is a guage choice and the gauge dependencies can be addressed by fixing the gauge. An approach to looking at metric perturbations is to begin with the Arnowitt-Deser-Misner (ADM) metric [105]. It proves convenient to follow Refs. [54, 104, 106, 107], employing the (3+1) ADM decomposition of space-time, such that

$$g_{00} = -(N^2 - N_i N^i), \quad g_{0i} = N_i, \quad g_{ij} = \gamma_{ij}\,, \tag{3.4}$$

where γ_{ij} is the metric of 3-dimenstional spatial hypersurface, N is the lapse function and N^i is the shift vector. The projection normal to Σ_t has components $n^\alpha = (1, -N^i)/N$ and contracted with the metric $g_{\alpha\beta}$ is $n_\alpha = N(-1, 0, 0, 0)$; a unit normal timelike vector satisfying the condition $n_\alpha n^\alpha = -1$. Likewise we define a vector t^α which satisfies $t^\alpha \nabla_\alpha t = 1$ such that $t^\alpha = N n^\alpha + N^\alpha$ where we can construct the lapse function and shift vector as,

$$N = -t^\alpha n_\alpha\,, \quad N_\alpha = (g_{\alpha\beta} + n_\alpha n_\beta) t^\beta. \tag{3.5}$$

A geometrical interpretation of N is the lapse of proper time along the normal vector and N_α as being the shift of spatial coordinates with respect to the normal vector. As time increases, we iterate from one hypersurface to the next whereby 4D space-time is seen as the time evolution of the 3D Riemannian space [108].

In order to obtain Einstein's field equations it is necessary to use the variational principle with the Einstein-Hilbert action in Eqn. (2.1) (setting $\Lambda = 0$) where R, the scalar space-time curvature, may be split into intrinsic and extrinsic components. This result combined with the action in Eqn. (3.1) is written as

$$S = \frac{1}{2}\int d^4x\sqrt{h}\left(M_{\rm p}^2\left[N R^{(3)} + \frac{1}{N}(E_{ij}E^{ij} - E^2)\right] + \frac{1}{N}\pi^I\pi_I - N G_{IJ}\partial_i\phi^I\partial^i\phi^J - 2NV\right), \tag{3.6}$$

where $R^{(3)}$ is the Ricci scalar of the 3-metric h_{ij}. The quantity E_{ij} is proportional to the extrinsic curvature on slices of constant t, with

$$E_{ij} = \frac{1}{2}(\dot{\gamma}_{ij} - N_{i;j} - N_{j;i}), \tag{3.7}$$

where a bar denotes covariant derivatives with respect to the three metric. The quantity π^I is defined as

$$\pi^I = \dot{\phi}^I - N^j \phi^I_{;j}. \tag{3.8}$$

3.1.1. Metric Perturbations

Working in the spatially flat gauge, and considering only scalar perturbations[1], one has $R^{(3)} = 0$ and $h_{ij} = a^2\delta_{ij}$, and the only perturbations to the space-time metric are given by

$$\begin{aligned} N &= 1 + \Phi_1 + \Phi_2 + \cdots \\ N_i &= \theta_{1\,,i} + \theta_{2\,,i} + \cdots , \end{aligned} \tag{3.9}$$

where Φ_1 and Φ_2 are the first and second order perturbations in the lapse, and θ_1 and θ_2 are the first and second order perturbations in the shift. This involves similar techniques to those reviewed in Sec. (2.5) but now up to second order.

3.1.2. Field Perturbations

Next, we consider the perturbations to the matter sector and hence to the scalar fields present. In the previous chapter we had fluid or radiation perturbations, where now we only scalar fields. The field perturbations, $\delta\phi^I(x,t)$, are defined by the expression $\phi^I = \phi^I_0(t) + \delta\phi^I(x,t)$. These field perturbations are not, however, covariant under relabeling of field-space, and it proves convenient to work with a different set of perturbations that are covariant, which we label Q^I. These were first introduced by Gong & Tanaka [109]. The idea is to consider the geodesic that links together the position in field-space labeled by ϕ^I_0 and that labelled by ϕ^I, and an affine parameter parameterizing this trajectory denoted λ. The coordinate displacement $\delta\phi^I$ can then be expressed by the series expansion about the point $\lambda = 0$ as

$$\delta\phi^I = \left.\frac{d\phi^I}{d\lambda}\right|_{\lambda=0} + \left.\frac{1}{2!}\frac{d^2\phi^I}{d\lambda^2}\right|_{\lambda=0} + \cdots . \tag{3.10}$$

We can then form the geodesic equation

$$D^2_\lambda \phi^I = \frac{d^2\phi^I}{d\lambda^2} + \Gamma^I_{JK}\frac{d\phi^J}{d\lambda}\frac{d\phi^K}{d\lambda} = 0\,, \tag{3.11}$$

and define $Q^I = \mathrm{d}\phi^I/\mathrm{d}\lambda|_{\lambda=0}$ and $D_\lambda = Q^I\nabla_I$ (where ∇_I is the covariant derivative defined in Eqn. (1.12)). Using this geodesic equation, the expansion (3.10) can be rewritten as

$$\delta\phi^I = Q^I - \frac{1}{2!}\Gamma^I_{JK}Q^JQ^K\,, \tag{3.12}$$

[1] Although beyond linear order vector and tensor perturbations do couple to the scalar perturbations, they do not affect the calculation of the scalar three point function which follows from the third-order action involving only scalar perturbations.

which relates field perturbations to the covariant perturbations. The time derivative of field fluctuations, $\delta\dot{\phi}^I$, can also be written in terms of covariant quantities as

$$\delta\dot{\phi}^I = D_t Q^I - \dot{\phi}^M \Gamma^I_{MN} Q^N - \frac{1}{2}\Gamma^I_{JK,M}\dot{\phi}^M Q^J Q^K - \Gamma^I_{(JK)} D_t Q^J Q^K + \Gamma^I_{(JK)}\Gamma^J_{MN} Q^K \dot{\phi}^M Q^N \,, \tag{3.13}$$

as can a perturbation to the field-space metric, and using (3.12) and (1.13) we find

$$\begin{aligned}\delta G_{IJ} \;=\; & 2\Gamma_{(IJ)K}Q^K - \Gamma_{(IJ)K}\Gamma^K_{MN}Q^M Q^N + \Gamma_{(IM)L}\Gamma^M_{JK}Q^K Q^L + \Gamma_{(JM)L}\Gamma^M_{IK}Q^K Q^L \\ & + \frac{1}{2}(G_{IM}\Gamma^M_{JK,L} + G_{JM}\Gamma^M_{IK,L})Q^K Q^L \,. \end{aligned} \tag{3.14}$$

Here we have adopted the notation of using (IJ) parenthesis to illustrate symmetrization over the indices I and J. A bar $|$ is used to exclude certain indices from the symmetrization procedure, for example, $(I|J|K)$ symmetrizes I and K but not J.

3.2. The Perturbed Action

The next step is to insert our perturbed expressions for N, N_i and ϕ^I into (3.6) to calculate the perturbed action. Expanding order by order, the first order action simply leads back to the background equations, while the action at second and higher order lead to the dynamics of the perturbations. After some integration by parts and discarding total derivatives, one finds the action at second and third order can be written in the form given by Elliston *et al.* [104]

$$\begin{aligned} S_{(2)} = \frac{1}{2}\int d^4x a^3 \Big(& \Phi_1 \Big[-6M_{\rm p}^2 H^2 \Phi_1 + G_{IJ}\dot{\phi}^I\dot{\phi}^J\Phi_1 \\ & -2G_{IJ}\dot{\phi}^I D_t Q^J - 2V_{;I}Q^I \Big] - \frac{2}{a^2}\partial^2\theta_1 \Big[2M_{\rm p}^2 H\Phi_1 - G_{IJ}\dot{\phi}^I Q^J \Big] \\ & + R_{KIJL}\dot{\phi}^K\dot{\phi}^L Q^I Q^J + G_{IJ}D_t Q^I D_t Q^J - G_{IJ}\partial^i Q^I \partial_j Q^J - V_{;IJ}Q^I Q^J \Big) \,, \end{aligned} \tag{3.15}$$

and

$$\begin{aligned} S_{(3)} = \frac{1}{2}\int d^4x a^3 \Big(& 6M_{\rm p}^2 H^2 \Phi_1^3 + 4M_{\rm p}^2 \frac{H}{a^2}\Phi_1^2 \partial^2\theta_1 - \frac{M_{\rm p}^2\Phi_1}{a^4}(\partial_i\partial_j\theta_1\partial_i\partial_j\theta_1 - \partial^2\theta_1\partial^2\theta_1) \\ & - G_{IJ}\dot{\phi}^I\dot{\phi}^J\Phi_1^3 + 2\Phi_1^2\dot{\phi}^I D_t Q^J + \frac{2}{a^2}\Phi_1 G_{IJ}\dot{\phi}^I\partial_i\theta_1\partial_i Q^J - \Phi_1 R_{L(IJ)M}\dot{\phi}^L\dot{\phi}^M Q^I Q^J \\ & - \Phi_1\Big(G_{IJ}Q^I Q^J + \frac{1}{a^2}G_{IJ}\partial^i Q^I\partial_j Q^J \Big) - \frac{2}{a^2}\partial_i\theta_1 G_{IJ}D_t Q^I\partial_i Q^J + \frac{4}{3}R_{I(JK)L}\dot{\phi}^L D_t Q^I Q^J Q^K \\ & + \frac{1}{3}R_{(I|LM|J;K)}\dot{\phi}^L\dot{\phi}^M Q^I Q^J Q^K - \frac{1}{3}V_{;(IJK)}Q^I Q^J Q^K - V_{;(IJ)}\Phi_1 Q^I Q^J \Big) \,, \end{aligned} \tag{3.16}$$

where R_{IJKL} is the Riemann tensor compatible with the field-space metric G_{IJ}, and $R_{IJKL;M}$ its covariant derivative.

Constraint equations

Varying the action with respect to the lapse and shift leads to two constraint equations that can be used to get expressions for the perturbations in the lapse and shift in terms of the covariant Q^I perturbations[110]. These can be substituted back into the action to express the perturbed action only in terms of Q^I. To do so we only need the constraint equations at linear order (as explained in [106]), but later we will also need them at second order too, so we provide the full expressions here.

Considering first, the variation with respect to the shift, at linear order one finds

$$\Phi_1 = \frac{1}{2M_{\rm p}^2 H} G_{IJ}\dot{\phi}^I Q^J, \tag{3.17}$$

while at second order

$$\begin{aligned}\Phi_2 = \frac{\Phi_1^2}{2} + \frac{\partial^{-2}}{2M_{\rm p}^2 H}\Big[&-\frac{M_{\rm p}^2}{a^2}\partial_i\partial_j\Phi_1\partial_i\partial_j\theta_1 + \frac{M_{\rm p}^2}{a^2}\partial^2\Phi_1\partial^2\theta_1 \\ &+G_{IJ}(\partial_i D_t Q^I)\partial_i Q^J + G_{IJ}D_t Q^I\partial^2 Q^J\Big]\,.\end{aligned} \tag{3.18}$$

On large scales where spatial gradients decay, one then finds that

$$\Phi_2 = \frac{\Phi_1^2}{2} + \frac{\partial^{-2}}{2M_{\rm p}^2 H}\left[G_{IJ}(\partial_i D_t Q^I)\partial_i Q^J + G_{IJ}D_t Q^I\partial^2 Q^J\right]\,. \tag{3.19}$$

Next, varying the action with respect to the lapse, at linear order we have

$$\partial^2\theta_1 = -3a^2 H\Phi_1 + \frac{a^2}{2M_{\rm p}^2 H}G_{IJ}\Phi_1\dot{\phi}^I\dot{\phi}^J - \frac{a^2}{2M_{\rm p}^2 H}G_{IJ}\dot{\phi}^I D_t Q^J - \frac{a^2}{2M_{\rm p}^2 H}V_{;I}Q^I\,, \tag{3.20}$$

and at second order

$$\begin{aligned}\partial^2\theta_2 =&2\Phi_1\partial^2\theta_1 - \frac{1}{4a^2 H}\left(\partial_i\partial_j\theta_1\partial_i\partial_j\theta_1 - \partial^2\theta_1\partial^2\theta_1\right) + \frac{a^2}{2M_{\rm p}^2 H}G_{IJ}\Phi_1\dot{\phi}^I D_t Q^J \\ &+\frac{1}{2M_{\rm p}^2 H}G_{IJ}\dot{\phi}^I\partial_i\theta_1\partial_i Q^J - \frac{a^2}{4M_{\rm p}^2}G_{IJ}D_t Q^I D_t Q^J - \frac{1}{4M_{\rm p}^2 H}G_{IJ}\partial_i Q^I\partial_i Q^J \\ &-\frac{a^2}{4M_{\rm p}^2}V_{;(IJ)}Q^I Q^J + \frac{a^2 H}{2}(2\Phi_2 - 3\Phi_1^2)(\epsilon - 3) - \frac{a^2}{4M_{\rm p}^2}R_{L(IJ)M}\dot{\phi}^L\dot{\phi}^M Q^I Q^J\,,\end{aligned} \tag{3.21}$$

where $\epsilon = -\dot{H}/H^2$ is the slow-roll parameter from Eqn. (2.34). Using these latter expressions and again taking the large scale super-horizon limit one finds the additional relation

$$6H\Phi_1 = \frac{1}{M_{\rm p}^2 H}G_{IJ}\Phi_1\dot{\phi}^I\dot{\phi}^J - \frac{1}{M_{\rm p}^2 H}G_{IJ}\dot{\phi}^I D_t Q^J - \frac{1}{M_{\rm p}^2 H}V_{;I}Q^I\,, \tag{3.22}$$

at first order, and

$$\frac{1}{2}G_{MN}D_tQ^MD_tQ^N = 2\Phi_1 G_{IN}\dot{\phi}^I D_tQ^N - \frac{1}{2}V_{;(MN)}Q^MQ^N - M_{\rm p}^2H^2(3\Phi_1^2 - 2\Phi_2)(\epsilon - 3) - \frac{1}{2}R_{I(MN)J}\dot{\phi}^I\dot{\phi}^JQ^MQ^N\,, \tag{3.23}$$

at second order.

The Fourier space action

Finally, using the equations for Φ (3.17) and θ (3.20) in terms of Q^I one can write the quadratic and cubic parts of the action (3.15) and (3.16) solely in terms of Q^I. It is convenient at this stage to move from real space to Fourier space. After doing so, to keep our expressions to a manageable size, we follow the extended summation convention introduced in Ref. [78] and in the notation section, Sec. (1.2), in Eqn. (1.1). When considering Fourier space quantities we use bold font indices, $\mathbf{I}, \mathbf{J}, \ldots$ to indicate that the usual summation over fields is accompanied by an integration over Fourier space as defined in Eqn. (1.1). Using this notation the action reads

$$S_{(2)} = \frac{1}{2}\int dta^3\left(G_{\mathbf{IJ}}(\mathbf{k}_I,\mathbf{k}_J)(D_tQ^{\mathbf{I}}(\mathbf{k}_I)D_tQ^{\mathbf{J}}(\mathbf{k}_J) + M_{\mathbf{IJ}}(\mathbf{k}_I,\mathbf{k}_J)Q^{\mathbf{I}}(\mathbf{k}_I)Q^{\mathbf{J}}(\mathbf{k}_J)\right)\,, \tag{3.24}$$

at second order and

$$\begin{aligned} S_{(3)} = \frac{1}{2}\int dta^3\,\big(&A_{\mathbf{IJK}}(\mathbf{k}_I,\mathbf{k}_J,\mathbf{k}_K)Q^{\mathbf{I}}(\mathbf{k}_I)Q^{\mathbf{J}}(\mathbf{k}_J)Q^{\mathbf{K}}(\mathbf{k}_K) \\ &+B_{\mathbf{IJK}}(\mathbf{k}_I,\mathbf{k}_J,\mathbf{k}_K)D_tQ^{\mathbf{I}}(\mathbf{k}_I)Q^{\mathbf{J}}(\mathbf{k}_J)Q^{\mathbf{K}}(\mathbf{k}_K) \\ &+C_{\mathbf{IJK}}(\mathbf{k}_I,\mathbf{k}_J,\mathbf{k}_K)D_tQ^{\mathbf{I}}(\mathbf{k}_I)D_tQ^{\mathbf{J}}(\mathbf{k}_J)Q^{\mathbf{K}}(\mathbf{k}_K)\big)\,, \end{aligned} \tag{3.25}$$

at third order, where we have defined

$$G_{\mathbf{IJ}}(\mathbf{k}_I,\mathbf{k}_J) = (2\pi)^3\delta(\mathbf{k}_I+\mathbf{k}_J)G_{IJ} \tag{3.26}$$

$$M_{\mathbf{IJ}}(\mathbf{k}_I,\mathbf{k}_J) = (2\pi)^3\delta(\mathbf{k}_I+\mathbf{k}_J)\left(\frac{k_I^2}{a^2}G_{IJ} - m_{IJ}\right) \tag{3.27}$$

$$A_{\mathbf{IJK}}(\mathbf{k}_I,\mathbf{k}_J,\mathbf{k}_K) = (2\pi)^3\delta(\mathbf{k}_I+\mathbf{k}_J+\mathbf{k}_K)a_{IJK} \tag{3.28}$$

$$B_{\mathbf{IJK}}(\mathbf{k}_I,\mathbf{k}_J,\mathbf{k}_K) = (2\pi)^3\delta(\mathbf{k}_I+\mathbf{k}_J+\mathbf{k}_K)b_{IJK} \tag{3.29}$$

$$C_{\mathbf{IJK}}(\mathbf{k}_I,\mathbf{k}_J,\mathbf{k}_K) = (2\pi)^3\delta(\mathbf{k}_I+\mathbf{k}_J+\mathbf{k}_K)c_{IJK}\,. \tag{3.30}$$

with

$$m_{IJ} = V_{;IJ} - R_{IKLJ}\dot{\phi}^K\dot{\phi}^L - \frac{3+\epsilon}{M_{\rm p}^2}\dot{\phi}_i\dot{\phi}_J - \frac{(\dot{\phi}_I D_t\dot{\phi}_J + \dot{\phi}_J D_t\dot{\phi}_I)}{HM_{\rm p}^2}\,, \tag{3.31}$$

and

$$\begin{aligned} a_{IJK} =& -\frac{1}{3}V_{;IJK} - \frac{\dot\phi_I V_{;JK}}{2HM_{\rm p}^2} + \frac{\dot\phi_I\dot\phi_J\xi_K}{8H^2M_{\rm p}^4} + \frac{\dot\phi_I\xi_J\xi_K}{32H^3M_{\rm p}^4}\left(1-\frac{(\mathbf{k}_J\cdot\mathbf{k}_K)^2}{k_J^2k_K^2}\right) \\ &+ \frac{\dot\phi_I\dot\phi_J\dot\phi_K}{8HM_{\rm p}^4}\left(6\frac{G_{MN}\dot\phi^M\dot\phi^N}{H^2M_{\rm p}^2}\right) + \frac{\dot\phi_I G_{JK}}{2HM_{\rm p}^2}\frac{\mathbf{k}_J\cdot\mathbf{k}_K}{a^2} \\ &- \frac{1}{2}\frac{G_{NK}\dot\phi^L\dot\phi^M\dot\phi^N K R_{L(IJ)M}}{M_{\rm p}^2H} + \frac{1}{3}\dot\phi^L\dot\phi^M R_{(I|LM|J;K)}\,, \end{aligned} \tag{3.32}$$

$$b_{IJK} = \frac{\dot\phi_I\dot\phi_J\dot\phi_K}{4H^2M_{\rm p}^4} - \frac{\dot\phi_I\xi_J\dot\phi_K}{8H^3M_{\rm p}^4}\left(1-\frac{(\mathbf{k}_J\cdot\mathbf{k}_K)^2}{k_J^2k_K^2}\right) - \frac{\xi_I G_{JK}}{2HM_{\rm p}^2}\frac{\mathbf{k}_I\cdot\mathbf{k}_J}{k_I^2} + \frac{4}{3}\dot\phi^L R_{I(JK)L}\,, \tag{3.33}$$

$$c_{IJK} = -\frac{G_{IJ}\dot\phi_K}{2HM_{\rm p}^2} + \frac{\dot\phi_I\dot\phi_J\dot\phi_K}{8H^3M_{\rm p}^4}\left(1-\frac{(\mathbf{k}_I\cdot\mathbf{k}_J)^2}{k_I^2k_J^2}\right) + \frac{G_{IJ}\dot\phi_K}{HM_{\rm p}^2}\frac{\mathbf{k}_I\cdot\mathbf{k}_K}{k_I^2}\,, \tag{3.34}$$

where

$$\xi_I = 2D_t\dot\phi_I + \frac{\dot\phi_I}{H}\frac{G_{NM}\dot\phi^N\dot\phi^M}{M_{\rm p}^2}\,. \tag{3.35}$$

Here a_{IJK} is to be symmetrised over all three indices, b_{IJK} over J & K and c_{IJK} over I & J. Each index permutation will have a corresponding exchange of wavenumber associated with the indices.

3.3. The Curvature Perturbation

As we have seen quantities in one gauge can be related to quantities in another guage. Here we have worked with the quantities Q^I defined on flat hypersurfaces but need to relate it the to ζ to make consistent with observational constraints. This is what we proceed to do now. Here we extend the calculation to the case of a non-trivial field-space metric.

A first step in the calculation of ζ in terms of field-space fluctuations on a flat hypersurface is to relate ζ to the total density perturbation on the flat hypersurface $\psi = 0$. This calculation was performed in Ref. [111], and is unchanged in our new setting. Utilizing the perturbation theory framework in Sec. (2.5.1) but including terms up to second order we can find an equation like Eqn. (2.112) but to second order we obtain,

$$\zeta = -H\frac{\delta\rho}{\dot\rho} + H\frac{\dot\delta\rho\delta\rho}{\dot\rho^2} - \frac{H}{2}\frac{\ddot\rho\delta\rho^2}{\dot\rho^3} + \frac{\dot H}{2}\frac{\delta\rho^2}{\dot\rho^2}\,. \tag{3.36}$$

3.3.1. The Density Perturbation

The new element for the non-trivial field-space case is therefore to calculate $\delta\rho$ in this setting. In general, one finds that $\rho = -T^{00}/g^{00}$ [24], where $T_{\mu\nu}$ is the energy momentum tensor. The perturbation in the density up to second order is therefore

$$\delta\rho = \delta T^{00} + \rho\delta g^{00} + \left(\delta T^{00} + \rho\delta g^{00}\right)\delta g^{00}\,. \tag{3.37}$$

The energy–momentum tensor Eqn. (2.26) can be rewritten for an arbitrary number of scalar fields with non-trivial field-space metric given by,

$$T_{\mu\nu} = G_{IJ}\partial_\mu\phi^I\partial_\nu\phi^J - \frac{1}{2}G_{IJ}g_{\mu\nu}\partial^\lambda\phi^I\partial_\lambda\phi^J - g_{\mu\nu}V. \tag{3.38}$$

This leads to the background energy density $\rho = \frac{1}{2}G_{IJ}\dot\phi^I\dot\phi^J + V$ as expected. Perturbing Eqn. (3.38) and using Eqn. (3.37) and recalling that

$$\begin{aligned} g^{00} + \delta g^{00} &= -1 + 2\Phi_1 + 2\Phi_2 - 3\Phi_1^2 \\ g^{0i} + \delta g^{0i} &= \partial^i\theta_1 + \partial^i\theta_2 - 2\Phi_1\partial^i\theta_1 \\ g^{ij} + \delta g^{ij} &= h^{ij} - \partial^i\theta_1\partial^j\theta_1\,, \end{aligned} \tag{3.39}$$

one finds that

$$\begin{aligned} \delta\rho =& \frac{1}{2}G_{IJ}(\dot\phi^I\dot{\delta\phi}^J + \dot\phi^J\dot{\delta\phi}^I) - \Phi_1 G_{IJ}(\dot\phi^I\dot{\delta\phi}^J + \dot\phi^J\dot{\delta\phi}^I) + \frac{1}{2}\delta G_{IJ}(\dot\phi^I\dot{\delta\phi}^J + \dot\phi^J\dot{\delta\phi}^I) \\ &+ \frac{1}{2}G_{IJ}\dot{\delta\phi}^I\dot{\delta\phi}^J - \Phi_1 G_{IJ}\dot\phi^I\dot\phi^J + \frac{1}{2}(3\Phi_1 - 2\Phi_2)G_{IJ}\dot\phi^I\dot\phi^J + \frac{1}{2}\delta G_{IJ}\dot\phi^I\dot\phi^J \\ &- \Phi_1\delta G_{IJ}\dot\phi^I\dot\phi^J + V_{;I}\delta\phi^I + \frac{1}{2}V_{;(IJ)}\delta\phi^I\delta\phi^J\,. \end{aligned} \tag{3.40}$$

Finally, we need to rewrite this expression in terms of the covariant perturbations, Q^I instead of the raw field perturbations $\delta\phi^I$. Collecting some terms together and applying the relations (3.12), (3.13) and (3.14) we obtain a neat expression which at linear order gives

$$\delta\rho_1 = -\Phi_1 G_{IJ}\dot\phi^I\dot\phi^J + G_{(IJ)}\dot\phi^I D_t Q^J + V_{;I}Q^I\,, \tag{3.41}$$

which is a covariant form of Eqn. (2.67) and at second order

$$\begin{aligned} \delta\rho_2 =& \frac{1}{2}R_{L(IJ)M}\dot\phi^L\dot\phi^M Q^I Q^J + \frac{1}{2}V_{;(IJ)}Q^I Q^J - 2\Phi_1 G_{(IJ)}\dot\phi^I D_t Q^J \\ &+ \frac{1}{2}G_{IJ}\dot\phi^I\dot\phi^J(3\Phi_1^2 - 2\Phi_2) + \frac{1}{2}G_{IJ}D_tQ^I D_tQ^J. \end{aligned} \tag{3.42}$$

Moreover, one can use Eqs. (3.17) and (3.18) to substitute for Φ_1 and Φ_2 and write $\delta\rho$ entirely in terms of the covariant perturbations Q^I. There are in fact a number

of equivalent ways to write $\delta\rho$ as a function of the field-space perturbations using Eqn. (3.22) and (3.23), which on substitution into Eqn. (3.36) lead to equivalent ways to write ζ in terms of Q^I. Different possibilities were discussed at length in Ref. [111] for the canonical case. For the numerical implementations of Ref. [78] the simplest of these was used, which follows from the use of Eqn. (3.17) and (3.18), and in the non-trivial field-space case leads to

$$\delta\rho_1 = -3HG_{IJ}\dot{\phi}^I Q^J \,, \tag{3.43}$$

and

$$\begin{aligned}\delta\rho_2 &= 3M_{\rm p}^2H^2(3\Phi_1^2 - 2\Phi_2) \\ &= \frac{3}{2M_{\rm p}^2}\dot{\phi}_I\dot{\phi}_J Q^I Q^J - 3H\partial^{-2}\left(G_{IJ}(\partial_i D_t Q^I)\partial^i Q^J + G_{IJ}D_tQ^I\partial^2 Q^J\right).\end{aligned} \tag{3.44}$$

Substituting Eqns. (3.43) and (3.44) into Eqn. (3.36) one finds

$$\zeta_{(1)} = -\frac{1}{2M_{\rm p}^2H\epsilon}G_{IJ}\dot{\phi}^I Q^J \,, \tag{3.45}$$

and

$$\begin{aligned}\zeta_{(2)} =& \frac{1}{6M_{\rm p}^2H^2\epsilon}\left[\left(\frac{1}{M_{\rm p}^2}\dot{\phi}_I\dot{\phi}_J\left[-\frac{3}{2}+\frac{9}{2\epsilon}+\frac{3}{4\epsilon^2M_{\rm p}^2H^3}V_{;K}\dot{\phi}^K\right]\right)Q^IQ^J\right. \\ &\left.+\left(\frac{3}{M_{\rm p}^2H\epsilon}\dot{\phi}_I\dot{\phi}_J\right)Q^ID_tQ^J - 3H\partial^{-2}\left(G_{IJ}(\partial_iD_tQ^I)\partial^iQ^J + G_{IJ}(D_tQ^I)\partial^2Q^J\right)\right].\end{aligned} \tag{3.46}$$

To calculate the statistics of ζ we introduce new notation to know how it is related to the set of perturbations $\delta X^a = \{Q^I, P_J\}$. Where the canonical momentum P^I is defined as,

$$P_I = \frac{\delta S}{\delta(D_tQ^I)} \,, \tag{3.47}$$

and by utilizing Eqns. (3.24) and (3.25) we obtain,

$$P_I = a^3\left(D_tQ_I + \frac{1}{2}B_{\mathbf{JK}I}Q^{\mathbf{J}}Q^{\mathbf{K}} + C_{I\mathbf{JK}}P^{\mathbf{J}}Q^{\mathbf{K}}\right) \,, \tag{3.48}$$

where bold indices are defined using Eqn. (1.1). We require only the form of this relation on super-horizon scales, and we write it in the form

$$\zeta(\mathbf{k}) = N_{\mathbf{a}}\delta X^{\mathbf{a}} + \frac{1}{2}N_{\mathbf{ab}}\delta X^{\mathbf{a}}\delta X^{\mathbf{b}} \,, \tag{3.49}$$

where

$$\begin{aligned} N_{\mathbf{a}}(\mathbf{k}) =& (2\pi)^3\delta(\mathbf{k}-\mathbf{k_a})N_a \\ N_{\mathbf{ab}}(\mathbf{k},\mathbf{k_a},\mathbf{k_b}) =& (2\pi)^3\delta(\mathbf{k}-\mathbf{k_a}-\mathbf{k_b})N_{ab}(\mathbf{k_a},\mathbf{k_b})\,. \end{aligned} \tag{3.50}$$

For the case of multifield inflation with canonical kinetic terms, N_a and N_{ab} were calculated in Ref. [111] (also see Refs. [112, 113]). On moving to Fourier space we can identify expressions for the N tensors defined above, and we find that

$$N_a = -\frac{1}{2M_{\rm p}^2 H\epsilon}\dot{\phi}_I \begin{pmatrix} 1 \\ \\ 0 \end{pmatrix} \tag{3.51}$$

$$N_{ab} = -\frac{1}{3M_{\rm p}^2H^2\epsilon}\begin{pmatrix} \frac{1}{M_{\rm p}^2}\dot{\phi}_I\dot{\phi}_J\left[-\frac{3}{2}+\frac{9}{2\epsilon}+\frac{3}{4\epsilon^2M_{\rm p}^2H^3}V_{;K}\dot{\phi}^K\right] & \frac{3}{H\epsilon}\frac{\dot{\phi}_I\dot{\phi}_J}{M_{\rm p}^2}-G_{IJ}\frac{3H}{k^2}\left(\mathbf{k_a}\cdot\mathbf{k_b}+k_a^2\right) \\ \\ \frac{3}{H\epsilon}\frac{\dot{\phi}_I\dot{\phi}_J}{M_{\rm p}^2}-G_{IJ}\frac{3H}{k^2}\left(\mathbf{k_a}\cdot\mathbf{k_b}+k_b^2\right) & 0 \end{pmatrix}. \tag{3.52}$$

These equations will be used in Ch. (5) in our implementation of the transport method to calculate the power spectrum and bispectrum for inflationary perturbations. We emphasize that we do not assume slow-roll, thus our implementation covers the full basis of perturbations (Q, P), unlike other methods as discussed in Sec. (5.1).

4. Quantization and the Quantum Sub-Horizon in Curved Field-Space

One of the sucesses of inflation is the captivating realization that quantum fluctuations of light ($m < H$) scalar field(s) can be related to the large scale structure of the universe. In Sec. (4.1) we introduce the framework for describing quantum fields in cosmology in the interaction picture. Using this formalism we go on to calculate the two-point statistic in Sec. (4.2) and the three-point statistics in Sec. (4.3). Finally we calculate the two-point statistics for the tensor modes in Sec. (2.7.2).

In this chapter we will review the in–in formalism and calculate the correlation functions deep inside the horizon for models of inflation with a curved field-space metric. The in–in formalism can be used to calculate the correlation function at horizon crossing or as initial conditions for super-horizon techniques. However, as we will discuss in Sec. (5.1) there are disadvantages to this for certain models. Instead, our approach is to utilize the in–in formalism deep inside the horizon, and evolve outwards using the transport method, as we will see in Ch. (5).

4.1. The Interaction Picture

We begin to construct our formalism of evaluating correlation functions using the Heisenberg picture of quantum mechanics in which operators $\mathcal{O}$ incorporate time dependence and states are time independent. The Hamiltonian is constructed from Eqns. (3.24) and (3.25) such that $H_{int} = -\int \mathcal{L}_{(3)} d^3x$ and is a function of the field perturbation Q_I and canonical momenta P_J, which are covariant under transformations in field-space. It can then be shown that P_I along with Q_I satisfy the canonical commutation algebra,

$$\left[Q^I(\mathbf{k}_I, t), P_J(\mathbf{k}_J, t')\right] = i(2\pi)^3 \delta^I_J(\mathbf{k}_I + \mathbf{k}_J)\delta(t - t')\,. \tag{4.1}$$

At this stage it is helpful to rescale P_I such that $P_I \to a^3 P_I$, where for convenience we employ the same symbol for the rescaled momentum, and use it solely from here

on. In terms of the rescaled momentum,

$$D_t Q_I = P_I - \frac{1}{2} B_{\mathbf{JK}I} Q^{\mathbf{J}} Q^{\mathbf{K}} - C_{I\mathbf{JK}} P^{\mathbf{J}} Q^{\mathbf{K}} + \cdots . \tag{4.2}$$

The Hamiltonian is then given by,

$$\begin{aligned} H_t = \int dt \frac{a^3}{2} \Bigg(& \underbrace{G_{\mathbf{IJ}} P^{\mathbf{I}} P^{\mathbf{J}} - M_{\mathbf{IJ}} Q^{\mathbf{I}} Q^{\mathbf{J}}}_{H_0} \\ & \underbrace{- A_{\mathbf{IJK}} Q^{\mathbf{I}} Q^{\mathbf{J}} Q^{\mathbf{K}} - B_{\mathbf{IJK}} Q^{\mathbf{I}} Q^{\mathbf{J}} P^{\mathbf{K}} - C_{\mathbf{IJK}} P^{\mathbf{I}} P^{\mathbf{J}} Q^{\mathbf{K}}}_{H_{int}} \Bigg) , \end{aligned} \tag{4.3}$$

where we have labelled the 'free' part of the Hamiltonian as $H_0(Q^I(t), P_J(t); t)$, and the 'interaction' part as $H_{int}(Q^I(t), P_J(t); t)$. In terms of the perturbation theory outlined in Ch. (3) the 'free' part will describe the evolution of two-point correlation function at leading order. Components of the 'interaction' part will contribute to the evolution of the three-point correlation functions at leading order.

Finally Hamilton's equations provide us with the evolution equations for Q^I and P^I, which are,

$$D_t Q^I = -i[Q^I, H_t] \tag{4.4}$$

$$D_t P^I = -i[P^I, H_t] - 3H P^I , \tag{4.5}$$

where the evolution of P^I takes a slightly non-canonical form due to the rescaling of the canonical momenta. The solution to these evolution equations then follow,

$$\begin{aligned} Q^I(t) &= U^{-1}(t, t_0) Q^I(t_0) U(t, t_0) , \\ P_J(t) &= U^{-1}(t, t_0) Q_J(t_0) U(t, t_0) , \end{aligned} \tag{4.6}$$

where U is a unitary transformation satisfying,

$$\frac{d}{dt} U(t, t_0) = -i H_t(Q^I(t_0), P^J(t_0); t) U(t, t_0) , \tag{4.7}$$

and the initial condition $U(t_0, t_0) = 1$, where $t_0 \approx -\infty$ is an early enough time where modes are deep within the horizon.

The interaction picture is an intermediate representation between the Schrödinger picture (where the states are time dependent and operators are time independent) and the Heisenberg picture. The operators follow the evolution of the free Hamiltonian and the states evolve according to the interaction Hamiltonian. As the name suggests this picture is advantageous in many-body systems of interacting quantum particles [48]. We review the calculation for the expectation value $\langle \mathcal{O}(Q^I, P_J; t) \rangle$, where $\mathcal{O}$ is our operator evaluated in the ground state, following Refs. [114, 115]. Here we define new operators q^I and p^J, that are called the *interaction picture fields*,

that satisfy Eqns. (4.4) and (4.5) for the free part of the Hamiltonian. The solutions are defined as,

$$\begin{aligned} q^I(t) &= U_0(t,t_0)^{-1} Q^I(t_0) U_0(t,t_0) \\ p_J(t) &= U_0(t,t_0)^{-1} P_J(t_0) U_0(t,t_0)\,, \end{aligned} \tag{4.8}$$

where U_0 satisfies,

$$\frac{d}{dt} U_0(t,t_0) = -iH_0(Q^I(t_0), P^J(t_0); t) U_0(t,t_0)\,, \tag{4.9}$$

with $U_0(t_0,t_0) = 1$. If the operator is polynomial in Q^I and P_J the correlation function $\langle \mathcal{O} \rangle$ can be written as,

$$\langle \mathcal{O}(Q^I, P^J; t) \rangle = \langle F(t,t_0)^{-1} \mathcal{O}(q^I, p^J; t) F(t,t_0) \rangle\,, \tag{4.10}$$

where F is given as,

$$F(t,t_0) = U_0^{-1}(t,t_0) U(t,t_0)\,, \tag{4.11}$$

and satisfy,

$$\begin{aligned} \frac{dF(t,t_0)}{dt} &= -iU_0^{-1}(t,t_0) H_{int}(Q^I(t_0), P^J(t_0); t) U_0(t,t_0) F(t,t_0) \\ &= -iH_{int}(Q^I(t), P^J(t); t) F(t,t_0)\,, \end{aligned} \tag{4.12}$$

with $F(t_0,t_0) = 1$. This has the solution,

$$F(t,t_0) = \mathcal{T} exp\left(-i \int_{-\infty^+}^{t} H_I(q^I, p^J; t) dt \right)\,, \tag{4.13}$$

where $\mathcal{T}$ is the time-ordering operator such that products in the expansion of the exponential are written from left to right in decreasing order of time arguments. We can also define the anti-time-ordering operator, $\bar{\mathcal{T}}$, which writes products in the expansion of the exponential from left to right in increasing order of time arguments. The lower limit $-\infty^+$ denotes that the contour of integration should be deformed above the real axis into the positive imaginary half-plane at early times, with the fields appearing in the integrand defined by analytic continuation. The expectation value is then,

$$\begin{aligned} &\langle \mathcal{O}(P^I, Q^J; t) \rangle = \\ &\langle \bar{\mathcal{T}} exp\left(i \int_{-\infty^+}^{t} H_I(q^I, p^J; t) dt \right) \mathcal{O}(q^I, p^J; t) \mathcal{T} exp\left(-i \int_{-\infty^+}^{t} H_I(q^I, p^J; t) dt \right) \rangle\,. \end{aligned} \tag{4.14}$$

where all the field perturbations are now in the interaction picture. We integrate form $-\infty$ to some arbitrary point t. This is the in–in formalism. In the standard

calculations this is the time of horizon crossing, in our formalism it will be at a time within the horizon.

4.2. Two-Point Correlation Function

Following the approach of Ref. [78] (which is closely related to that of Ref. [116]), these are fixed at some early time at which all the wavenumbers of a given correlation are far inside the horizon during inflation, and where m_{IJ} is subdominant to $(k/a)^2 G_{IJ}$ in Eq. (3.27). In this limit it is reasonable to assume that the solution for the two-point correlation function of Q^I is well approximated by the de-Sitter space solution and we can use this solution to provide initial conditions for our numerical evolution. We note that it is only required that this solution be valid at some point long before all scales of interest cross the horizon, and moreover, that the numerical evolution is then free to evolve away from this solution, accounting for the complex dynamics that can subsequently occur in general inflationary models.

As introduced in Sec. (2.7.1), we can quantize our scalar pertrubations. By rescaling our mode function as $\nu^I(\tau, k) = aQ^I(\tau, k)$ it may by quantized by writing it in terms of the creation and annihilation,

$$\nu^I_{\mathbf{k}}(\tau) \to \nu(\tau)\hat{a}^I_{\mathbf{k}} + \nu^\star \hat{a}^{\dagger J}_{-\mathbf{k}}, \tag{4.15}$$

and satisfies Eqn. (2.166). Unlike Eqn. (2.159), the creation and annihilation satisfy

$$\left[\hat{a}^I_{\mathbf{k}}, \hat{a}^{\dagger J}_{\mathbf{k}'}\right] = 2\pi\delta(\mathbf{k} - \mathbf{k}')\Pi^{IJ}, \tag{4.16}$$

where Π^{IJ} solves the equation $D_\tau \Pi^{IJ} = 0$ [104] with a solution

$$\Pi^{IJ}(\tau_1, \tau_2) = \mathcal{P} \exp\left(-\int_{\tau_1}^{\tau_2} d\tau \Gamma^I_{KL}\left[\phi^M(\tau)\right] \frac{d\phi^K}{d\tau}\right) G^{LJ}(\tau_1)\,, \tag{4.17}$$

which transforms as a bitensor with the first index I transforming in the tangent space at point $\phi^M(\tau_2)$ and the second index J in the tangent space at point $\phi^M(\tau_1)$ and the exponential is path ordered which is indicated by $\mathcal{P}$. It defines a parallel transport along the direction of the phase space flow instead of the geodesic G_{IJ}.

The two-point function in de Sitter space is typically written in conformal time τ and takes the form [117, 118],

$$\langle Q^I(k_1, \tau_1) Q^J(k_2, \tau_2)\rangle = (2\pi)^3 \delta(k_1 + k_2)\Pi^{IJ} \frac{H^2}{2k^3}(1 + ik\tau_1)(1 - ik\tau_2)e^{ik(\tau_2 - \tau_1)}\,. \tag{4.18}$$

The two-point functions $\langle Q^I(\tau_1) P^J(\tau_2)\rangle$, and $\langle P^I(\tau_1) P^J(\tau_2)\rangle$ can then be calculated by differentiating Eq. (4.18), using the definition of P^I and accounting for the use of conformal time. For our purposes we only need to consider the limit $\tau_2 \to \tau_1$ with

$-\tau \gg 1$, which corresponds to equal time correlations on sub-horizon scales. In this limit $\Pi^{IJ} \to G^{IJ}$, and one finds initial conditions for the two point function for the various combinations of covariant field perturbation and momenta correlations. The calculation is similar to that presented in Ref. [118], though in that work the time variable used for the transport system was e-folds N, while in this paper we use cosmic time, t. For convenience we can write the two-point function as the tensor Σ^{ab},

$$\langle \delta X^a(\mathbf{k}_a)\delta X^b(\mathbf{k}_b)\rangle = (2\pi)^3\delta(\mathbf{k}_a+\mathbf{k}_b)\Sigma^{ab}(k_a)\,. \tag{4.19}$$

We now list the two-point correlation function that are valid deep in the horizon and may also be evaluated at horizon crossing.

- Field-Field correlation

Beginning with the expression for the two point function of Q^I (4.18) we consider the $-\tau \gg 1$ limit for the field-field correlations. We find

$$\begin{aligned}\langle Q^I(k_1,\tau)Q^J(k_2,\tau)\rangle &= (2\pi)^3\delta(k_1+k_2)\frac{G^{IJ}}{2k^3}H^2(\tau)(1-ik\tau)(1+ik\tau)\\ &\approx (2\pi)^3\delta(k_1+k_2)\frac{G^{IJ}}{2k^3}H^2(\tau)|k\tau|^2\\ &\approx (2\pi)^3\delta(k_1+k_2)\frac{G^{IJ}}{2a^2k}\,.\end{aligned} \tag{4.20}$$

The initial condition for Σ^{IJ}_* is then

$$\Sigma^{IJ}_{*Re} = \left.\frac{G^{IJ}}{2a^2k}\right|_*\,, \quad \Sigma^{IJ}_{*Im} = 0\,, \tag{4.21}$$

where a subscript '$\star$' denotes evaluation at the initial time.

- Field-Momentum correlation

Next recalling that at linear order $P^I = D_tQ^I$ and that the covariant derivative of the parallel propagator is zero, we consider the leading term in the expression for the field-momentum correlation of unequal time correlations, and subsequently take equal time limit for the case $-\tau \gg 1$. Recalling that $d\tau = dt/a(t)$ we find

$$\begin{aligned}\langle Q^I(k_1,\tau_1)P^J(k_2,\tau_2)\rangle &= (2\pi)^3\delta(k_1+k_2)\frac{\Pi^{IJ}}{2k^3}H(\tau_1)H(\tau_2)(1+ik\tau_1)\left(\frac{k^2\tau_2}{a}\right)e^{ik(\tau_2-\tau_1)}\\ &= (2\pi)^3\delta(k_1+k_2)\frac{G^{IJ}}{2k^3}H^2(\tau)\left(\frac{k^2\tau}{a}\right)(1-ik\tau)\\ &= (2\pi)^3\delta(k_1+k_2)\left(-\frac{G^{IJ}H}{2ka^2}+i\frac{G^{IJ}}{2a^3}\right).\end{aligned} \tag{4.22}$$

The real and imaginary parts of the initial conditions for this case are then

$$\Sigma^{IJ}_{*Re} = -\frac{G^{IJ}H}{2ka^2}\bigg|_*\,, \quad \Sigma^{IJ}_{*Im} = \frac{G^{IJ}}{2a^3}\bigg|_*\,. \tag{4.23}$$

- Momentum-Momentum correlation

We follow a similar procedure to consider the momentum-momentum correlation

$$\begin{aligned}\langle P^I(k_1,\tau_1)P^J(k_2,\tau_2)\rangle &= (2\pi)^3\delta(k_1+k_2)\frac{\Pi^{IJ}}{2k^3}H(\tau_1)H(\tau_2)\left(\frac{k^2\tau_1}{a}\right)\left(\frac{k^2\tau_2}{a}\right)e^{ik(\tau_2-\tau_1)}\\ &= (2\pi)^3\delta(k_1+k_2)\frac{G^{IJ}}{2k^3}H^2(\tau)\left(\frac{k^4\tau^2}{a^2}\right)\\ &= (2\pi)^3\delta(k_1+k_2)\frac{G^{IJ}k}{2a^4}.\end{aligned} \tag{4.24}$$

The initial conditions for $\Sigma^{ab}_{\rm Re}$ where also given by Dias, Frazer and Seery [118].

4.3. Three-Point Correlation Function

We now move on to calculating the three-point function using the in-in formalism we outlined in Eqn. (4.14). After expanding the exponents to first order we find that the non-vanishing terms that remain are given by,

$$\langle \delta X^a \delta X^b \delta X^c\rangle_\star = -i\int_{-\infty}^{\tau_{init}} d\tau \big\langle \big[\delta X^a_\star \delta X^b_\star \delta X^c_\star, \mathcal{H}_{\mathbf{efg}}\delta X^{\mathbf{e}}\delta X^{\mathbf{f}}\delta X^{\mathbf{g}}\big]\big\rangle_\star\,, \tag{4.25}$$

where $\mathcal{H}_{\mathbf{efg}}$ is the interaction part of the Hamiltonian extracted from the cubic part of the action in Eqn. (3.25).

The Hamiltonian contains the kernel tensors a_{IJK}, b_{IJK} and c_{IJK} and is defined as,

$$\mathcal{H}_{\mathbf{abc}} = \frac{1}{3}\left\{\begin{pmatrix} -3a_{\mathbf{IJK}} & -b_{\mathbf{IKJ}} \\ -b_{\mathbf{KJI}} & -c_{\mathbf{IJK}}\end{pmatrix}, \begin{pmatrix} -b_{\mathbf{IJK}} & -c_{\mathbf{KJI}} \\ -c_{\mathbf{IKJ}} & 0\end{pmatrix}\right\}, \tag{4.26}$$

where the indices are organized so that a block of field labels are followed by a block of momentum labels and are contracted over the internal legs only. The bold font

on the indices indicates that the usual summation over phase space indices is accompanied by an integration over Fourier space. This order is sufficient as all higher order terms are suppressed by factors of $Q \approx H/M_{\rm pl}$. We can rewrite Eqn. (4.25) by including the integration over Fourier space and removing bold indices,

$$\langle \delta X^a \delta X^b \delta X^c \rangle_\star = -i \int_{-\infty}^{\tau_{init}} d\tau \mathcal{H}_{efg} \int \frac{\Pi_i d^3 k_i}{(2\pi)^9} (2\pi)^3 \delta(\Sigma_i \mathbf{k}_i) \langle \delta X^a_\star \delta X^b_\star \delta X^c_\star \delta X^e \delta X^f \delta X^g \rangle \,. \tag{4.27}$$

By using Wick's theorem the 6-point correlation function above can be broken into six permutations of two-point correlation functions,

$$\begin{aligned} \langle \delta X^a \delta X^b \delta X^c \rangle_\star = & -i \int_{-\infty}^{\tau_{init}} d\tau \mathcal{H}_{efg} \int \frac{\Pi_i d^3 k_i}{(2\pi)^9} (2\pi)^3 \delta(\Sigma_i \mathbf{k}_i) \langle \delta X^a_\star \delta X^e \rangle \langle \delta X^b_\star \delta X^f \rangle \langle \delta X^c_\star \delta X^g \rangle \\ & + cyclic. \end{aligned} \tag{4.28}$$

Each permutation represents a different way of contracting a pair of internal and external legs of the Feynman diagram. For convenience we can write the three-point function as the tensor

$$\langle \delta X^a \delta X^b \delta X^c \rangle_\star = (2\pi)^3 \delta(\Sigma_i \mathbf{k_i}) B^{abc}_\star(k_1, k_2, k_3) \,. \tag{4.29}$$

We can rewrite the three-point function B_{abc} in terms of permutations of the two-point function Σ_{ab},

$$B^{abc}_\star = -6i \int_{-\infty}^{\tau_{init}} d\tau \mathcal{H}_{\mathbf{efg}} \Sigma^{a\mathbf{e}}(\tau_\star, \tau) \Sigma^{b\mathbf{f}}(\tau_\star, \tau) \Sigma^{c\mathbf{g}}(\tau_\star, \tau) + c.c. \tag{4.30}$$

If we then substitute Eqn. (4.26) into Eqn. (4.30) we get,

$$\begin{aligned} B^{abc}_\star = & -6i \int_{-\infty}^{\tau_\star} d\tau \frac{a^4}{2} \Big[A_{\mathbf{efg}} \Sigma^{a\mathbf{e}} \Sigma^{b\mathbf{f}} \Sigma^{c\mathbf{g}} \\ & - \frac{1}{3a} \left(B_{\bar{\mathbf{e}}(\mathbf{fg})} \Sigma^{a\bar{\mathbf{e}}} \Sigma^{b\mathbf{f}} \Sigma^{c\mathbf{g}} + B_{(\mathbf{e}|\bar{\mathbf{f}}|\mathbf{g})} \Sigma^{a\mathbf{e}} \Sigma^{b\bar{\mathbf{f}}} \Sigma^{c\mathbf{g}} + B_{(\mathbf{ef})\bar{\mathbf{g}}} \Sigma^{a\mathbf{e}} \Sigma^{b\mathbf{f}} \Sigma^{c\bar{\mathbf{g}}} \right) \\ & - \frac{1}{3a^2} \left(C_{(\bar{\mathbf{ef}})\mathbf{g}} \Sigma^{a\bar{\mathbf{e}}} \Sigma^{b\bar{\mathbf{f}}} \Sigma^{c\mathbf{g}} + C_{(\bar{\mathbf{e}}|\mathbf{f}|\bar{\mathbf{g}})} \Sigma^{a\bar{\mathbf{e}}} \Sigma^{b\mathbf{f}} \Sigma^{c\bar{\mathbf{g}}} + C_{\mathbf{e}(\bar{\mathbf{fg}})} \Sigma^{a\mathbf{e}} \Sigma^{b\mathbf{f}} \Sigma^{c\bar{\mathbf{g}}} \right) \Big] \,, \end{aligned} \tag{4.31}$$

where the tensors Σ^{ab} have a dependence on two times (i.e. $\Sigma^{ab}(\tau_\star, \tau)$), τ representing the internal legs and $\tau_\star$ representing the external legs and the bars over the indices label P^I components. From our calculations of the two-point functions in Sec. (4.2)

we have,

$$\begin{aligned}\Sigma^{ab}(k) =& \frac{H^2}{2k^3}(1-ik\tau_\star)(1+ik\tau)\Pi^{ab}e^{ik(\tau-\tau_\star)}\\ \Sigma^{a\bar{b}}(k) =& \frac{H^2}{2k^3}(1+ik\tau_\star)(k^2\tau a^{-1})\Pi^{a\bar{b}}e^{ik(\tau-\tau_\star)}\\ \Sigma^{\bar{a}\bar{b}}(k) =& \frac{H^2}{2k^3}(k^2\tau_\star a^{-1})(k^2\tau a^{-1})\Pi^{\bar{a}\bar{b}}e^{ik(\tau-\tau_\star)}\,.\end{aligned} \tag{4.32}$$

We can now begin to explicitly calculate the three-point function by substituting Eqns. (4.32) into Eqn. (4.31). As we only need to integrate over the internal legs, the external components of Eqn. (4.32) can be brought outside. The time dependence of the b_{IJK} and c_{IJK} tensors which appear in the interaction Hamiltonian is slow-roll suppressed and their time dependence can be neglected. On the other hand, the a_{IJK} tensor contains fast changing terms proportional to $(k/a)^2 \approx (k\tau)^2$ which grow exponentially into the past and whose time dependence must be included. This splitting of the a_{IJK} into the fast and slow parts is best illustrated when we convert Eqn. (3.32) to conformal time $\tau = -1/aH$

$$a_{IJK} = \frac{\dot{\phi}_I G_{JK}}{2H^3 M_{\rm pl}^2}\frac{(\mathbf{k_J}\cdot\mathbf{k_K})}{\tau^2} + a_{IJK(slow)}. \tag{4.33}$$

It is also assumed that H and Γ^{ab} which appear in the expression for $\Sigma(\tau_1,\tau_2)$ are also sufficiently slowly varying that their time dependence can be neglected. The integral is dominated by its upper limit, and these assumptions mean that when evaluating it one takes $\Gamma^{IJ} \to G^{IJ}(\tau_\star)$ and $H \to H(\tau_\star)$. The assumptions need only be true for a short period around the time the initial conditions are fixed. In the resulting expressions for the initial conditions for B_{abc}, we keep both the terms which grow fastest as $\tau \to -\infty$ as well as the sub-leading terms.

To illustrate how this is evaluated in practice, let us consider this explicitly for the case of a field-field-field correlation.

- a,b,c $\to$ Field-Field-Field

Substituting in the expression for the two-point function we obtain

$$\begin{aligned}B_*^{abc} =& -\frac{iH^6}{8\Pi_i k_i^3}(1+ik_1\tau_\star)(1+ik_2\tau_\star)(1+ik_3\tau_\star)e^{-ik_s\tau_\star}\times\\ &\int_{-\infty}^{\tau_\star}\frac{d\tau}{H^2\tau^2}\left[\frac{\dot{\phi}^I G^{JK}}{4H}(\mathbf{k_2}\cdot\mathbf{k_3})(1-ik_1\tau)(1-ik_2\tau)(1-ik_3\tau)e^{ik_s\tau}\right.\\ &+\frac{a_s^{IJK}}{2H^2\tau^2}(1-ik_1\tau)(1-ik_2\tau)(1-ik_3\tau)e^{ik_s\tau}\\ &+\frac{b^{IJK}}{2H^2\tau^2}(1-ik_1\tau)(1-ik_2\tau)k_3^2\tau e^{ik_s\tau}\\ &\left.+\frac{c^{IJK}}{2}k_1^2k_2^2\tau^2(1-ik_3\tau)e^{ik_s\tau}+perms\right]+c.c.\,,\end{aligned} \tag{4.34}$$

where we assume that H and Π^{IJ} are sufficiently slowly varying to be taken as constants and that we can take $\Pi^{IJ} \to G^{IJ}$.

In order to perform the integration we need to know the time dependence of the tensors. As discussed earlier the a_{IJK} tensor contains fast and slow varying parts. The part containing terms quadratic in τ vary quickly and so are included in the integral separately (the first term in Eq. (4.34)), the remaining parts we label a_s^{IJK} and we assume can be considered constant in time. The next step is to perform the integration, recalling that the result is dominated by the upper limit (because the integral is highly oscillatory into the past). Keeping the leading and sub-leading terms in τ, and writing in terms of a and H, the final result is

$$\begin{aligned} B_*^{abc} =& \frac{1}{4a^4}\frac{1}{k_1\cdot k_2\cdot k_3\cdot k_s}\Big(-\left(c^{IJK}(k_1,k_2,k_3)\cdot(k_1\cdot k_2)+cyc.\right) \\ &+\left(a^2a_s^{IJK}(k_1,k_2,k_3)+cyc.\right)+\left(a^2Hb^{IJK}(k_1,k_2,k_3)\left(\frac{(k_1+k_2)\cdot k_3}{k_1\cdot k_2}-\frac{K2}{k_1\cdot k_2}\right)+cyc.\right) \\ &+\left(\frac{\dot\phi^I}{4H}G^{JK}(-{k_2}^2-{k_3}^2+{k_1}^2)+cyc.\right)\Big)\Big|_*\,, \end{aligned} \tag{4.35}$$

where $K2 \equiv k_1k_2 + k_1k_3 + k_2k_3$ and $k_s = k_1 + k_2 + k_3$. Repeating for the other correlations we find

- a,b,c $\to$ Momentum-Field-Field

$$\begin{aligned} B_*^{abc} =& -\frac{H}{4a^3K3}\left(-\frac{k_1^2(k_2+k_3)}{k_s}\cdot k_1\cdot k_2\cdot k_3\right)\Big(-\left(c^{IJK}(k_1,k_2,k_3)\cdot(k_1\cdot k_2)+cyc.\right) \\ &+\left(a^2a_s^{IJK}(k_1,k_2,k_3)+cyc.\right)+\left(\frac{G^{JK}\dot\phi^I}{4H}(-{k_2}^2-{k_3}^2+{k_1}^2)+cyc.\right)\Big) \\ &-\frac{H}{4a^3K3}\left(-\frac{k_1^2\cdot(k_2\cdot k_3)}{k_s}\right)\Big(\Big(c^{IJK}(k_1,k_2,k_3){k_1}^2{k_2}^2\left(1+\frac{k_3}{k_s}\right)+cyc.\Big) \\ &-\left(a^2a_s^{IJK}(k_1,k_2,k_3)\left(K2-\frac{k_1\cdot k_2\cdot k_3}{k_s}\right)+cyc.\right) \\ &+\left(b^{IJK}(k_1,k_2,k_3)\frac{k_1\cdot k_2\cdot {k_3}^2}{H}+cyc.\right) \\ &-\left(\frac{G^{IJ}\dot\phi^K}{4H}(-{k_1}^2-{k_2}^2+{k_3}^2)\left(K2+\frac{k_1\cdot k_2\cdot k_3}{k_s}\right)+cyc.\right)\Big)\Big|_*\,, \end{aligned} \tag{4.36}$$

where $K3 = k_1^3 + k_2^3 + k_3^3$.

- a,b,c $\to$ Momentum-Momentum-Field

$$
\begin{aligned}
B_*^{abc} = &- \frac{1}{4a^4K3}\frac{(k_1\cdot k_2\cdot k_3)^2\cdot k_1\cdot k_2}{k_s}\Big(-\left(c^{IJK}(k_1,k_2,k_3)\cdot(k_1\cdot k_2)+cyc.\right)\\
&+\left(a^2a_s^{IJK}(k_1,k_2,k_3)+cyc.\right)\\
&+\left(a^2Hb^{IJK}(k_1,k_2,k_3)\left(\frac{(k_1+k_2)\cdot k_3}{k_1\cdot k_2}+({k_1}^2\cdot {k_2}^2)\cdot k_1\cdot k_2\cdot {k_3}^2\right)+cyc.\right)\\
&-\left(\frac{G^{JK}\dot\phi^I}{4H}(-{k_2}^2-{k_3}^2+{k_1}^2)+cyc.\right)\Big)\Big|_*\,.
\end{aligned}
\tag{4.37}
$$

- a,b,c $\rightarrow$ Momentum-Momentum-Momentum

$$
\begin{aligned}
B_*^{abc} = &- \frac{H}{4a^3K3}\frac{{k_1}^2{k_2}^2{k_3}^2}{k_s}\Bigg(\left(c^{IJK}(k_1,k_2,k_3)\cdot(k_1\cdot k_2)^2\left(1+\frac{k_3}{k_s}\right)+cyc.\right)\\
&-\left(a^2a_s^{IJK}(k_1,k_2,k_3)\left(K2-\frac{k_1\cdot k_2\cdot k_3}{k_s}\right)+cyc.\right)+\left(\frac{b^{IJK}(k_1,k_2,k_3)}{H}k_1k_2\cdot {k_3}^2+cyc.\right)\\
&-\left(\frac{G^{JK}\dot\phi^I}{4H}(-{k_2}^2-{k_3}^2+{k_1}^2)\left(K2+\frac{k_1\cdot k_2\cdot k_3}{k_s}\right)+cyc\right)\Bigg)\Bigg|_*\,.
\end{aligned}
\tag{4.38}
$$

We reiterate that the calculation for the three-point function in our set up may be perform very early when the modes of interest are deep within the horizon. Using the in–in formalism we have reviewed in this chapter we can calculate the result in single-field inflation. We quote the result from Maldacena [106, 119] for the three-point function of ζ (which similarly obtained by the gauge relations in Sec. (2.5)),

$$
\langle\zeta(k_1)\zeta(k_2)\zeta(k_3)\rangle\sim(2\pi)^3\delta(\Sigma_i\mathbf{k_i})\frac{1}{M_{\rm pl}^4k_1^3k_3^3}\frac{\dot\rho_{t2}^4}{\dot\phi_{t2}^2}\frac{\dot\rho_{t3}^4}{\dot\phi_{t3}^2}\left(\frac{\ddot\phi_{t2}}{\dot\rho_{t2}\dot\phi_{t2}}+\frac{\dot\phi_{t2}^2}{\dot\rho_{t2}^2}\right)\,,
\tag{4.39}
$$

in the squeezed limit ($k_1=k_2\gg k_3$) which we defined in Sec. (2.6.2) where $t2$ is the time when modes k_1 and k_2 cross the horizons and $t3$ is the time when the mode k_3. Using the definition of the reduced bispectrum in Eqn. (2.147) we arrive at the famed consistency relation,

$$
f_{\rm NL}=\frac{5}{12}(1-n_s)\,,
\tag{4.40}
$$

in the squeezed limit. This result is calculated when the mode of interest is integrated over from deep inside the sub-horizon to the end of inflation, incorporating the sub- and super-horizon evolution of the mode. In contray to this, the transport method uses the in–in formalism only for its initial condition and incorporates the sub- and super horizon evolution in the transport equations. With these sets of equations as our initial conditions and the equation from Ch. (3) we have all the ingredients necessary our transport approach in the next chapter.

5. Evaluating Statistics from Inflation

In this chapter we examine the methods for calculating the statistics of curvature perturbations and tensor perturbations. Approximations can be made on super-horizon scales using methods such as δN [120]. We review this method in the context of the separate universe approach in Sec. (5.1). However, such methods are not accurate as they do not take into account the evolution of perturbations on sub-horizon scales nor do they easily allow for explicit scale dependence. We will then outline numerical methods, namely the Transport approach [121–123] in Sec. (5.2), which tracks the evolution of scale-dependent statistics from sub- to super-horizon scales. From this we extract relevant quantities that are used to examine inflationary predictions against our observations of the universe. Finally in Sec. (5.3) we calculate the statistics of tensor perturbations generated during inflation in both analytical and numerical formalisms.

5.1. Methods for Calculating the Statistics of Curvature Perturbations

The most commonly used method to study multiple fields in inflation is the δN formalism, which we review below. Statistics are calculated at horizon crossing using the in–in formalism from Sec. (4.1). They are evolved to the end of inflation using the separate universe approach and are analytically tractable in some circumstance. These methods are often convenient as they can be simple to compute and give us a precise understanding of mechanisms generating two- and three- point function growth. Analytically they are only applicable however when the models we are interested evolve according to the slow-roll assumptions, are not sensitive to sub-horizon effects, the fields are light and the potential is sum-seperable [124]. If the potential is feature-full and we have rapidly oscillating integrals (4.14) then it becomes difficult to solve and the solutions are not sufficiently accurate [78]. These are the motivations for the transport approach.

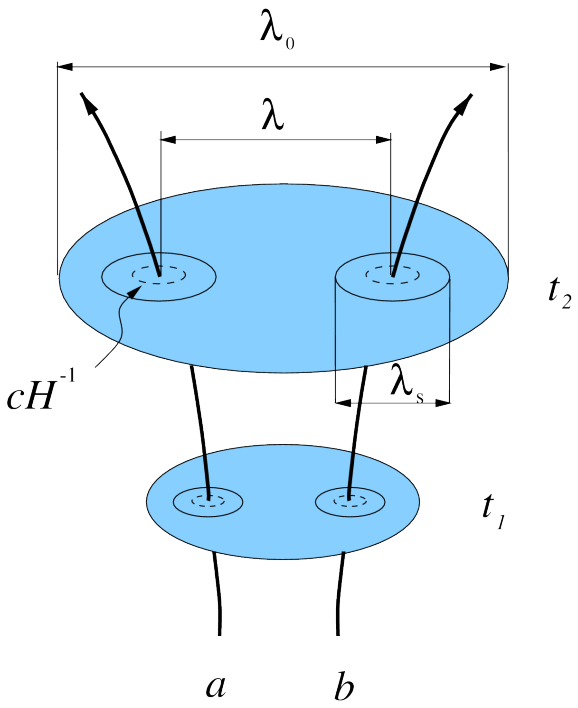

Figure 5.1.: *A diagram illustrating the seperate universe approach [38]. Each patch is on a different hypersurface foliated in 3-spatial dimensions and evolves intime. We work in natural units* $c = 1$.

5.1.1. The Separate Universe Picture

In Sec. (2.5.4) we assumed that the gradients on large scales can be ignored and illustrated the general conservation of curvature perturbations on scales larger than the comoving horizon size. In Eqn. (3.27) the perturbed equations of motion have terms that contain k/aH, which arises from the gradient of the curvature perturbations. These scale-dependent terms vanish on super-horizon scales as $k \to 0$. Thus, on super-horizon scales these terms may be ignored and one can employ the separate universe approach where each super-horizon patch of the universe evolves independently of one another. In practice we choose patches on scales larger than the horizon where the gradient terms are truly subdominant. Each patch of size $\lambda_s > H^{-1}$ acts as its own FLRW universe with homogeneous energy density and pressure, and we only need the initial conditions taken locally in each patch and evolve it using only the background equations. After each patch is evolved from a time t_1 to t_2 the curvature perturbations can then be calculated.

In Fig. (5.1) the evolution of two separate patches with the following hierarchy of scales $\lambda_0 \gg \lambda \gg \lambda_s > H^{-1}$ is illustrated. The integrated expansion between the two hypersurfaces along the world line of each patch is $N_i = N + \delta N_i$ where 'i' labels the patch and N is the background e-fold N. On scales greater than λ_s the homogeneous evolution equations are independent of the shorter wavelength perturbations. Each patch follows a trajectory along its worldline displaced from one another in the phase space of $(\phi^I, \dot{\phi}^I)$ with a distribution of initial conditions obtained using the

in–in formalism integrated from a time inside the horizon to horizon crossing (as in Ch. (4)). The trajectories along the world-lines can then be thought of as trajectories in field-space. Adiabatic perturbations are then defined as a translation in time along the background solutions. Isocurvature perturbations are normal to the time translations and distinguish between the different trajectories in phase-space. In this definition, the uniform density perturbations ζ, are perturbations in the locally-defined e-fold time (i.e. the time along each worldline) N [120]. The amount of expansion of one patch from some initial hypersurface (at time t_i) to the final slice of uniform energy density (at time t) is defined as $N(t,x) = \ln[\bar{a}(t,x)/a(t_i)]$ whereas the unperturbed amount of expansion is defined as $N_0(t) = \ln[a(t)/a(t_i)]$. We may then define ζ as,

$$\zeta(t,x) = \delta N = N(t,x) - N_0\,. \tag{5.1}$$

N is a function of the fields initial values, and so δN can be expressed as a Taylor expansion. Employing such an expansion we find an expression for ζ,

$$\zeta(t,x) = \delta N = \sum_I N_I \delta X_I + \frac{1}{2}\sum_{IJ} N_{IJ}\delta X_I \delta X_J + \cdots\,, \tag{5.2}$$

where the functions $N_I = \partial N/\partial X_I$ and $N_{IJ} = \partial^2 N/\partial X_I \partial X_J$ are functions of the background quantities evaluated at horizon crossing and δX^I are the field perturbations[1]. Then, we can calculate the two-point function,

$$\langle\zeta\zeta\rangle = N_I N_J \langle \delta X_I(\mathbf{k_1})\delta X_J(\mathbf{k_2})\rangle\,, \tag{5.3}$$

where we note that slow-roll is a required assumption for a few e-folds after horizon exit; this is also the requirement for calculating the quantum field correlator at horizon crossing. Similarly, we can calculate the three-point function,

$$\begin{aligned}\langle\zeta\zeta\zeta\rangle =& N_I N_J N_K \langle \delta X^I(\mathbf{k_1})\delta X^J(\mathbf{k_2})\delta X^k(\mathbf{k_3})\rangle \\ &+ N_{IJ}N_K N_L \int \frac{d^3q}{(2\pi)^3}\langle\delta X^I(\mathbf{k_1}-\mathbf{q})\delta X^K(\mathbf{k_2})\rangle\langle\delta X^J(\mathbf{q})\delta X^L(\mathbf{k_3})\rangle + cyclic\,,\end{aligned} \tag{5.4}$$

where the first term on the right hand side contains the non-linear interactions and the second term gives rise to the local non-gaussianity (as defined in Eqn. (2.154) in Sec. (2.6.2)). Considering solely the field-field correlations from Eqn. (4.20) the result for the power spectrum using Eqn. (2.142) and Eqn. (5.3) is,

$$\mathcal{P}(k) = N_I N_J G^{IJ}\left(\frac{H_\star}{2\pi}\right)^2\,, \tag{5.5}$$

[1] In the slow-roll regime these are $\delta X^I = Q^I$.

where $\star$ implies that we evaluate at horizon crossing which is where the k-dependence of the power spectrum arises from. By ignoring the non-Gaussian contributions to the bispectrum we can arrive at a k-independent expression for the local f_{nl} [120] (as defined in Sec (2.6.2)),

$$f_{nl} = \frac{5}{6}\frac{N_I N_J N^{IJ}}{\left[N_K N^K\right]^2} \,. \tag{5.6}$$

Note this result is analytical if one can calculate analytically N_I and N_{IJ}.

5.2. Numerical Methods for Calculating the Statistics of Curvature Perturbations

We could employ the δN, in–in or analytical methods for calculating statistics of inflation but as we will now discuss this is hard. Separate universe methods are successful at estimating statistics for simple models and a main motivation for using them is to make progress in obtaining analytical results.

δN provides one approach where analytics may be possible but for more complex models (models with large numbers of field) it's no longer straightforward to implement and possibly more cumbersome than if numerics were implemented. In order to calculate the two- and three- point statistics of ζ a model containing N-fields one will need to computed $2N$ coefficients of the N_I tensors, $2N(N+1/2)$ coefficients of the N_{IJ} tensor from Eqn. (5.3). In addition this method is only valid for light fields (less massive than the Hubble scale). These is a limiting factor in analytical approaches of δN.

In the in–in formalism calculating the correlation function may be hard as they may contain rapidly oscillating components [106, 116, 125] in the integrand of Eqn. (4.14). If this is the harmonic oscillator in Eqn. (4.14) we may ignore it up to horizon crossing but if there are oscillations in the potential then we cannot. In an adiabatic evolution under certain analytical prescriptions this will decay and leave insignificant contributions to the two- and three- point functions a few e-folds after horizon crossing. If the super-horizon evolution is characterized by non-adiabatic perturbations then components of the integrand will no longer be insignificant on super-horizon scales. If this is the case the integrals will no longer be rapidly oscillating but as long wavelength modes are large compared to the Hubble scale there may be a sensitivity to the mass spectrum and decay channel of the model [78]. However, it has been shown that numerical methods [116] are often the only way to calculate the correlation functions when these oscillations are significant; one such situation is when non-Gaussiantity is generated well before horizon crossing due to a rapid oscillation of the slow-roll parameters [126]. In addition analytical calculations in the in–in formalism become even more complex when we allow for a hierarchy of the external wavenumbers $\mathbf{k_i}$ in the three point functions $\langle \delta X_a \delta X_b \delta X_c \rangle$ (i.e. if we

wish to examine configurations other than equilateral) and the methods which do accommodate this involve lengthy factorizations which further increase the number of terms in our calculation

In addition this problem, the in–in formalism calculation of the correlation functions relies on the massless approximation whereby all fields are less massive than the Hubble scale. When fields are light in comparison to the Hubble scale the estimates of the correlation functions we obtain are universally applicable to any model of inflation. If the mass spectrum extends above the Hubble scale then this approximation breaks down and more specialized approaches must be made by keeping a subset of terms that capture the possible effects. However, it can be difficult to identify which terms are important as it is analytical not tractable. In both δN and the in–in formalism it is difficult to incorporate heavy fields.

5.2.1. Calculating Statistic for Models with Heavy Fields

While inflation is driven by light scalar fields the effects of additional heavy fields on the dynamics of inflation has recently been of interest [127]. There is a strong case for considering such fields if models have a UV completion in fundamental particle physics, such as Supergravity and String theory [83]. In Ch. (8) we examine a new class of model which features the non-trivial effects of heavy scalar fields. We can classify these models into three categories depending on both the influence of the heavy and light modes as well as how these modes affect one another.

In a Minkowski background, massive fields with $m_i \gg H$ are suppressed by the inverse of the mass [59, 128]. By virtue of the decoupling theorem, for scales below the mass of the heavy particle the full theory may be approximated arbitrarily closely by an effective theory of the light fields alone [129]. The heavy physics becomes negligible and one can integrate out the massive field leaving an effective single-field model whereby the light field tracks the minimum of the heavy field's potential. In a time dependent background, however more care needs to be taken, as dynamical effects arising from choices of initial conditions in the parameter space may compensate for how small $1/m_i$ is. If there is a bending in the field-space, as in Fig. (5.2), then there is an associated angular velocity $\dot{\theta}$ [131]. Bending terms like the angular velocity appear as couplings between adiabatic and isocurvature modes in the system, meaning care is required when integrating out the heavy mode as $\mathcal{O}(\dot{\theta}/m_i)$ could be unity or larger in the case where turning is rapid. In the case where the turning effects are small enough that the heavy modes track the minimum of the potential then only adiabatic excitations are relevant but due to the kinetic mixing of the fields the potential will be modified. The 'Gelaton' models [132] features a heavy field and non-canonical kinetic coupling, "the heavy field 'gels' to the light one", effectively getting dragged along by it and altering the light field dynamics. This results in a sound speed of less than 1 in the effective single-field description,

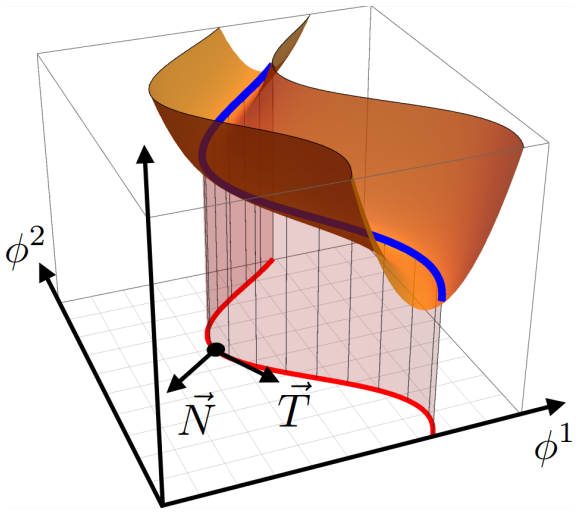

Figure 5.2.: *A diagram of a bending of the trajectory in field space [130]. Highlighted is the adiabatic projection $\vec{T}$ and the non-adiabatic (isocurvature) projection $\vec{N}$ along the evolution of the fields.*

resulting in large equilateral non-Gaussianity. There is a range of validity for this effective description to work, however, and in the simplest of scenarios predictions can be calculated analytically. In general however it is necessary to track the full evolution of both the heavy and light modes to account for not just the adiabatic fluctuations.

In the second case where the time dependent background effects are varying rapidly, such as a sharp turn where $\dot{\theta}/m_i \gg 1$, the heavy field can undergo a non-adiabatic evolution. With non-adiabatic evolution comes particle production and the excitation of both the heavy and light modes. The effects of particle production during inflation can largely impact the homogeneous background as well as the inflationary trajectory and the Hubble parameter, thus significantly altering the statistics of inflation. Such scenarios have been examined under special circumstances in the past [133, 134]. Three main contributions to the correlations of ζ are the particle production in the light modes (examined in Ref. [133] as the dominant contribution), the conversion of heavy modes into light modes (examined in Refs. [133, 134] but by neglecting particle production) and the response of heavy modes to light mode fluctuations. At the level of two-point statistics [127] it was found that features of heavy physics results in dampened superimposed oscillations onto the power spectrum. At the level of three-point statistics [135] the bispectrum was calculated under the effect of the periodic production of heavy degrees of freedom. Only in cases which limit to 'Gelaton' like behaviour can be studied analytically by use of effective field theories. In all non-adiabatic cases numerical methods are required when any of these effects are important, with effects like particle production making any analytical progress hard.

The third and final situation, the 'Quasi-single field inflation' model [136, 137], represents a mixture of the previous two. The heavy field has a mass of roughly

the same size as H and the trajectory turning rate is small enough that the heavy modes do not displace away from the minimum meaning there is negligible particle production from coupling to the background field configuration. However as the mass is small enough, particle production may still occur due to the metric couplings. The massive field will also have a cubic self-coupling which will parameterize the angular velocity $\dot{\theta}$ and the bispectrum can be generated through the conversion from the isocurvature modes to the curvature mode, once the inflaton trajectory turns. If $V''' > H$ then non-Gaussanities can be sizable [136]. We therefore wish to use an approach to calculating the effects of heavy fields during inflation, such an approach is the transport method.

5.2.2. The Transport Method

In this section we will review the framework for a method to numerically evolve the inflationary statistics. The method, developed by D. J. Mulryne et. al. [78, 121–123, 138], is called the Moment Transport method for inflationary statistics. This method evolves the statistical quantities (the moments or correlation functions) themselves rather than evolving a perturbed quantity ζ. The moments are evolved through a system of coupled ordinary differential equations called the transport equations. These equations were originally constructed for purely super-horizon evolutions for N-canonical fields [121, 123, 139] (and for non-canonical fields [104]) and then were later adapted for sub-horizon evolution [78, 122].

There are some strong advantages to this numerical approach. The first is that the treatment of Feynman integrals that rapidly oscillate one avoids in many other setups [140] as we evolve the statistics rather than evaluate the integrals (in Eqn. (4.14)) themselves. When compared with analytical or approximate methods a second advantage is that all effects up to tree-level are included so there is no need to make assumptions by discarding terms that may be relevant. By tracking each correlation function directly it is easier to pinpoint what are the terms that contribute any non-Gaussianity. A third advantage, and perhaps the strongest selling point of this method, is that we can track the evolution of these statistics from deep within the horizon in the quantum regime through horizon crossing to super-horizon scales where the correlation functions are classical statistical quantities and where we can evaluate observable quantities of the gauge invariant curvature perturbations. This makes the transport method a useful tool when calculating observables for different inflationary models.

In addition to this, in our implementation of the transport method we have excellent control of the accuracy, even for a large numbers of fields. The Transport method has been utilized in publicly available codes, for the non-canonical two-point correlators in `mTransport` [118], for the canonical three-point correlators [78] in `PyTransport` [141] and `CppTransport` [142], for non-canonical three-point cor-

relators in `PyTransport 2.0` [143] (as we will review in Ch. (6)) and more recently `CppTransport` [144].

Here, an important result of in this thesis is to derive the full transport equations that are valid during the quantum phase [122] and adapt them to the covariant field perturbations. Here we write the evolution equation of the Fourier modes of the covariant field and momentum fluctuations and for convenience we first label the full phase space of Heisenberg operations with the symbol $\delta X_a(k_a) = (Q^I(k_I), P^I(k_I)$ where a runs from 1 to $2N$ for N fields.

The expectation values we are interested in are then the two- and three-point functions of δX^a defined in Eqns. (4.19) and (4.29). As described, the equations of motion for these correlation functions follow directly from Eqns. (3.24) and (3.25) together with Ehrenfest's theorem, and can be presented in terms of equations of motion for Σ^{ab} and B^{abc}. By using Ehrenfest's theorem and from Eqn. (4.3) we may define the evolution of the expectation value of quantum operators as,

$$\begin{aligned} D_t\langle \delta Q^I\rangle &= \langle -i\left[\delta Q^I, \mathcal{H}\right]\rangle\,, \\ D_t\langle \delta P^I\rangle &= \langle -i\left[\delta P^I, \mathcal{H}\right]\rangle - 3H\langle P^I\rangle\,. \end{aligned} \tag{5.7}$$

Equivalently these two expressions are valid without the expectation brackets. In general, we can reformulate the above equation into a product of a matrix and the expectation value,

$$D_t\langle \delta X^{\rm a}\rangle = u^{\rm a}_{\rm b}\langle \delta X^{\rm b}\rangle + u^a_{bc}\langle \delta X^b \delta X^c\rangle \cdots\,, \tag{5.8}$$

where $u^{\rm a}_{\rm b}$ is a matrix to be computed from background quantities and the dots indicate higher order terms. The $u^{\rm a}_{\rm b}$ and higher order $u^{\rm a}_{\rm bc}$ tensors satisfy the relations,

$$\begin{aligned} u^{\rm a}_{\rm b} &= (2\pi)^3\delta(\mathbf{k}_a - \mathbf{k}_b)u^a_b(\mathbf{k}_a, \mathbf{k}_b)\,, \\ u^{\rm a}_{\rm bc} &= (2\pi)^3\delta(\mathbf{k}_a - \mathbf{k}_b - \mathbf{k}_c)u^a_{bc}(\mathbf{k}_a, \mathbf{k}_b, \mathbf{k}_c)\,. \end{aligned} \tag{5.9}$$

The evolution equation of the two-point function is also derived by the same theorem except now we apply the chain rule which takes the form,

$$D_t\langle \delta X^a \delta X^b\rangle = \langle (D_t\delta X^a)\delta X^b\rangle + \langle \delta X^a (D_t\delta X^b)\rangle\,. \tag{5.10}$$

In our covariant setting these take the form

$$D_t\Sigma^{ab}(k) = u^a{}_c(k)\Sigma^{cb}(k) + u^b{}_c(k)\Sigma^{ac}(k), \tag{5.11}$$

and

$$\begin{aligned} D_t B^{abc}(k_a,k_b,k_c) = {} & u^a{}_d(k_a)B^{dbc}(k_a,k_b,k_c) + u^b{}_d(k_b)B^{adc}(k_a,k_b,k_c) + u^c{}_d(k_c)B^{abd}(k_a,k_b,k_c) \\ & + u^a{}_{de}(\mathbf{k}_a,-\mathbf{k}_b,-\mathbf{k}_c)\Sigma^{db}(k_b)\Sigma^{ec}(k_c) \\ & + u^b{}_{de}(\mathbf{k}_b,-\mathbf{k}_a,-\mathbf{k}_c)\Sigma^{ad}(k_a)\Sigma^{ec}(k_c) \\ & + u^c{}_{de}(\mathbf{k}_c,-\mathbf{k}_a,-\mathbf{k}_b)\Sigma^{ad}(k_a)\Sigma^{be}(k_c)\,, \end{aligned} \tag{5.12}$$

where the covariant time derivative acts on Σ^{ab} in the following way

$$D_t\Sigma^{ab}(k) = \partial_t\Sigma^{ab}(k) + \mathbf{\Gamma}^a_c(k)\Sigma^{cb}(k) + \mathbf{\Gamma}^b_c(k)\Sigma^{ac}(k)\,, \tag{5.13}$$

and on B^{abc} as

$$\begin{aligned} D_t B^{abc}(k_a,k_b,k_c) = {} & \partial_t B^{abc}(k_a,k_b,k_c) + \mathbf{\Gamma}^a_d(k)B^{dbc}(k_a,k_b,k_c) \\ & + \mathbf{\Gamma}^b_d(k)B^{adc}(k_a,k_b,k_c) + \mathbf{\Gamma}^c_d(k)B^{abd}(k_a,k_b,k_c)\,, \end{aligned} \tag{5.14}$$

with $\mathbf{\Gamma}^a_b$ is defined as

$$\mathbf{\Gamma}^a_b = \begin{pmatrix} \Gamma^I_{JK}\dot{\phi}^K & 0 \\ 0 & \Gamma^I_{JK}\dot{\phi}^K \end{pmatrix}, \tag{5.15}$$

The u-tensors take the form

$$u^a{}_b = \begin{pmatrix} 0 & \delta^I_J \\ \tilde{m}^I_J & -3H\delta^I_J \end{pmatrix}, \tag{5.16}$$

where

$$\tilde{m}_{IJ} = -\frac{k^2}{a^2}G_{IJ} - m_{IJ}\,, \tag{5.17}$$

and

$$u^a{}_{bc} = \left\{ \begin{pmatrix} -b_{JK}{}^I & -c^I{}_{JK} \\ 3a^I{}_{JK} & b^I{}_{KJ} \end{pmatrix}, \begin{pmatrix} -c^I{}_{KJ} & 0 \\ b^I{}_{JK} & c_{KJ}{}^I \end{pmatrix} \right\}. \tag{5.18}$$

The two-point function will in general be complex, and can be divided into its real and imaginary parts

$$\Sigma^{ad} = \Sigma^{ad}_{\rm Re} + i\Sigma^{ad}_{\rm Im}\,, \tag{5.19}$$

with the real part symmetric under interchange of its indices, and the imaginary part anti-symmetric. Both parts independently satisfy Eqn. (5.11). On super-horizon scales the imaginary part decays to zero, indicating that on large scales the statistics of inflationary perturbations follow classical equations of motion.

B^{abc}, is in general also complex, but is real when only tree-level effects are included. In our numerical implementation of the transport system we evolve the real and imaginary parts of Σ^{ab} separately using Eqn. (5.11), and evolve B^{abc} according to the equation

$$\begin{aligned} D_t B^{abc}(k_a,k_b,k_c) =& u^a{}_d(k_a)B^{dbc}(k_a,k_b,k_c) + u^b{}_d(k_b)B^{adc}(k_a,k_b,k_c) + u^c{}_d(k_c)B^{abd}(k_a,k_b,k_c) \\ &+ u^a{}_{de}(\mathbf{k}_a,\mathbf{k}_b,\mathbf{k}_c)\Sigma^{db}_{\rm Re}(k_b)\Sigma^{ec}_{\rm Re}(k_c) - u^a{}_{de}(\mathbf{k}_a,\mathbf{k}_b,\mathbf{k}_c)\Sigma^{db}_{\rm Im}(k_b)\Sigma^{ec}_{\rm Im}(k_c) \\ &+ u^b{}_{de}(\mathbf{k}_b,\mathbf{k}_a,\mathbf{k}_c)\Sigma^{ad}_{\rm Re}(k_a)\Sigma^{ec}_{\rm Re}(k_c) - u^b{}_{de}(\mathbf{k}_b,\mathbf{k}_a,\mathbf{k}_c)\Sigma^{ad}_{\rm Im}(k_a)\Sigma^{ec}_{\rm Im}(k_c) \\ &+ u^c{}_{de}(\mathbf{k}_c,\mathbf{k}_a,\mathbf{k}_b)\Sigma^{ad}_{\rm Re}(k_a)\Sigma^{be}_{\rm Re}(k_b) - u^c{}_{de}(\mathbf{k}_c,\mathbf{k}_a,\mathbf{k}_b)\Sigma^{ad}_{\rm Im}(k_a)\Sigma^{be}_{\rm Im}(k_b), \end{aligned} \tag{5.20}$$

which follows from Eqn. (5.12) once Σ^{ab} is broken into real and imaginary parts, and which makes it clear that B^{abc} remains real if its initial conditions are real. In Sec. (4.2) we calculated the initial conditions for the two-point correlation function deep within the horizon. It is now possible to restructure these in tensorial form Σ^{ab},

$$\Sigma^{ab}_{*Re} = \frac{1}{2a^3k}\begin{pmatrix} aG^{IJ} & -aHG^{IJ} \\ -aHG^{IJ} & (k^2/a)G^{IJ} \end{pmatrix} \tag{5.21}$$

$$\Sigma^{ab}_{*Im} = \frac{1}{2a^3k}\begin{pmatrix} 0 & kG^{IJ} \\ -kG^{IJ} & 0 \end{pmatrix}. \tag{5.22}$$

Likewise the initial conditions for B^{abc} can be obtained from Sec. (4.3).

We now calculate the statistics of ζ (as we defined in Eqn. (3.49)) in the notation of Eqn. (3.50). In this notation the two and the three-point function of ζ are given

by

$$\begin{aligned}\langle\zeta(\mathbf{k_1})\zeta(\mathbf{k_2})\rangle =&(2\pi)^3\delta(\mathbf{k_1}+\mathbf{k_2})P(k)\\ \langle\zeta(\mathbf{k_1})\zeta(\mathbf{k_2})\zeta(\mathbf{k_3})\rangle =&(2\pi)^3\delta(\mathbf{k_1}+\mathbf{k_2}+\mathbf{k_3})B(k_1,k_2,k_3)\,,\end{aligned} \tag{5.23}$$

with the power spectrum and bispectrum from Eqns. (5.3) and (5.4) defined as,

$$\begin{aligned}P(k) =&N_aN_b\Sigma^{ab}_{\rm Re}(k)\\ B(k_1,k_2,k_3) =&N_aN_bN_cB^{abc}(k_1,k_2,k_3)+(N_aN_bN_{cb}(\mathbf{k_1},\mathbf{k_2})\Sigma^{ac}_{\rm Re}(k_1)\Sigma^{bd}_{\rm Re}(k_2)+2\,cyc.).\end{aligned} \tag{5.24}$$

5.3. Statistics of Tensor Perturbations

In Sec. (2.7.2) we detailed the calculation for two-point statistics of the tensor modes. We may also calculate the tensor power spectrum using the transport method. Similarly to the treatment of the field and field momentum fluctuations, we define a tensor momentum as $p_s = dh_s/dt$ and form the vector $Y^a_s = (h_s, p_s)$. We may then write the two-point function as,

$$\langle Y^a_s(\mathbf{k_1})Y^b_{s'}(\mathbf{k_2})\rangle = (2\pi)^3\delta_{ss'}\delta(\mathbf{k}+\mathbf{k}')\Upsilon^{ab}\,. \tag{5.25}$$

Following from Eqn. (5.11) the transport equations for Υ^{ab} can be written as,

$$\frac{d\Upsilon^{ab}}{dt} = \omega^a_c(k)\Upsilon^{cb}(k)+\omega^b_c(k)\Upsilon^{ac}(k)\,. \tag{5.26}$$

The matrices ω^a_b are computed as the massless limit of Eqn. (5.16) and are defined as ,

$$\omega^a_b(k) = \begin{pmatrix} 0 & 1 \\ -k^2/a^2 & -3H \end{pmatrix}, \tag{5.27}$$

and the initial conditions of the matrix of coefficients Υ^{ab} can also be computed, as in Sec. (2.7.2). They are equivalent to the massless limit of Eqn. (5.21) with some differences in normalization,

$$\Upsilon^{ab}(t_{init}) = \frac{1}{a^3kM^2_{\rm pl}}\begin{pmatrix} a & -aH \\ -aH & k^2/a \end{pmatrix}, \tag{5.28}$$

with all quantities on the RHS evaluated at t_{init}.

Having developed this covariant form of the transport equation. We are now in a position to employ these equation, together with the initial condition we have outlined in Ch. (4), in a numerical code.

6. Computing Statistics with PyTransport

In this chapter the transport method we have outlined in the previous chapter is put to use. We review the software available for computing the observables from inflation in Sec. (6.1), and outline where our code, `PyTransport 2.0`, fits and what advantages it has over the rest in Sec. (6.2). We then showcase its utility with a number of examples in Sec. (6.3) and then benchmark the codes performance in Sec. (6.4).

6.1. Software for Inflation

Computational simulations play a integral role in modern physics. Significant advancements in our understanding of the universe have been made thanks to the likes of Monte Carlo simulations of high energy particles colliding at the LHC and large N-body simulations of cosmic evolution in the Millennium simulation. Huge developments have been made in Monte Carlo techniques to calculate the tree-level matrix elements for a large class of Lagrangian-based models for particle phenomenology in the last 25 years. Codes like `Hegwig` [145], `CompHEP/CalcHEP` [146–148], `MadGraph/MadEvent` [149–152], `Sherpa` [153, 154], `Whizard` [155] and `FormCalc` [156, 157] generate the tree-level matrix elements that describe the hard scattering processes. These numerical tools have been used in combination with packages designed to generate the Feynman diagrams like `FeynRules` [158, 159] and `LanHEP` [160, 161]. Architecturally they are not too dissimilar from open-source code used to calculate the statistics from inflation but are, on a whole, far more developed. For two-point statistics of canonical inflation there exists open-source codes like `FieldInf` [162–164], `ModeCode/MultiModeCode` [72, 165–169] written in Fortran and `PyFlation` [170–172] written in Python. For three-point statistics of single-field canonical inflation there is `Bingo` [140, 173]. These implementations work on a case-by-case basis often requiring that derivatives of the potential and other model dependent terms be calculated separately and inputed manually. This is a major limitation as terms can be cumbersome in more complex (and interesting) models. For non-canonical models, terms like the Riemann tensor and its covariant derivative

(seen in (3.32) (3.33) (3.34)) which are of rank 4 and 5 respectively can grow in size dramatically with large numbers of fields making it impractical for manual entry of these terms. In reality users often resort to make assumptions about which terms are relevant and drop those that are not. It is therefore far better to automate this process, in a similar fashion to code used for particle physics phenomenology. This also means we can make fair comparisons between models without inconsistencies by making assumptions.

As outlined in Sec. (5.2.2) the Transport method is a numerical method that has a number of advantages over the alternatives which are used in the above implementations. Our implement of this method reduces the complexities of calculating the statistics, along with an automated method for deriving the derivatives of the potential the only complexities that arise are left to the initial conditions. This problem can be trivial as far enough back in time (deep in the horizon) the initial conditions of the two- and three- point functions are approximated by massless scalar fields. This leaves us with only the initial choice of field values and a choice of models parameters.

The first implementation of the transport approach to automatically calculate inflationary statistics was written in Mathematica in the code `mTransport` [118]. It computes the two-point correlation function of the curvature and tensor perturbations with an arbitrary field-space metric and scalar potential. It retains all the other benefits of the transport framework including accommodation of arbitrary mass hierarchies. While the code is sufficient for simple models with a small number of fields, it is too slow for complex models with large numbers of fields and can be inconvenient in some cases, such as Monte Carlo sampling. More recently the Transport method was implemented into code for canonical three-point statistics [78] in`CppTransport` [142] (written in C++) and in `PyTransport` [141] (written in Python and C++). Another major advantage is the choice of language, compared to mTransport (which is proprietary), both C++ and python are open-source and freely available, moreover, they are far quicker at evaluating the statistics and scale with the number of cores working on everything from a laptop to a parallelized cluster with thousands of cores.

For symbolic programming the CppTransport package utilizes the GiNaC computing algebra library. The translator component of the code converts the 'model description file' to customized C++ output necessary to evolve the dynamics and statistics. The model is then compiled. By utilizing the multi-process communication library MPI the calculations can be parallelized across multiple cores and multiple nodes in clusters. This task along with the integration is handled by the management system and then output data is saved into an SQLite database. Finally there is a visualization and reporting suite which enables post-processing analysis of the data easily read through an HTML interface. CppTransport was originally

designed to calculate statistics for canonical multifield models of inflation, recently it was updated to include more generic models, such a non-standard kinetic terms [144].

The package that we develop is `PyTransport`, which not only provides an independent verification of the transport other Transport implementations but has some advantages over the above packages that we will also outline in the next section.

6.2. PyTransport

`PyTransport` is a hybrid package of core C++ and Python interface. The symbolic programing is handled by sympy and gravipy. By utilizing Python's vast repositories of packages, high level analysis is straight forward to implement. It has minimal requirements, rapid deployment and with its Python interface means it is easily scriptable. For visualization libraries like mathplotlib and mayavi are available and jobs can be parallelized using Mpi4Py or similar packages. In this thesis we present a new version of the `PyTransport` package `PyTransport 2.0`, which extends the code to the case of a non-trivial field-space metric. Our new package allows users to specify both the potential and the field-space metric for a given model in a Python script. It automatically takes both these functions and generates a bespoke Python module. This module contains a number of useful functions including those needed to calculate the power spectrum and bispectrum of ζ. The package is available at github.com/jronayne/PyTransport.

6.2.1. Code Overview

As an interpreted language, Python can be slow for some tasks. This is circumvented in `PyTransport` by using C++ code, which is compiled into a Python module, to perform numerically intensive tasks with the result that the speed of the package is nearly indistinguishable from pure C++. The C++ code itself is kept as simple and clean as possible and can therefore easily be edited if required. `PyTransport` has been developed on OS X and Linux and is compatiable with Python 2.7 and 3. It can also be adapted to Windows systems, but this functionality has not yet been incorporated into the released package.[1]

The code is intended to be a reusable resource for inflationary cosmology. It enables users to quickly create a complied Python module(s) for any given model(s) of multifield inflation. The primary function of the complied module is to calculate the power-spectrum and bispectrum of inflationary perturbations produced by multifield inflation. To this end, the module contains a number functions that can be called from Python and that perform tasks such as calculating the background evolution of the cosmology, as well as the evolution of the two and three point functions. We also provide a number of further functions written in Python that perform common

[1] We thank Sean Butchers for work related to installing `PyTransport` on a Windows machine.

tasks such as calculating the power spectrum or bispectrum over a range of scales by utilizing the compiled module. The true power of the approach, however, is that users can rapidly write their own scripts, or adapt ours, to suit their own needs.

The transport approach to inflationary perturbation theory that the code employs can be seen as the differential version of the integral expressions of the In-In formalism. It is helpful numerically because it provides a set of ordinary differential equations for the correlation functions of inflationary perturbations. The code solves these equations from deep inside the horizon until some desired time after horizon crossing using a standard variable step size ordinary differential equation (ODE) routine with error control. Such off the shelf routines are extremely well tested, and provide an easy way to change the required accuracy. This is helpful in order to check convergence of the numerical solutions, or to respond to needs of models with very fine features.

The code is distributed in a folder called *PyTransportDist/*[2], which also contains a copy of the documentation in the *PyTransportDist/docs/* folder. The base code for `PyTransport` is written in C++ and has a simple object orientated structure. This code can be found in the *PyTransportDist/PyTransport/CppTrans* folder and we provide a few more details about its structure and functionality in appendix 1. The C++ code is deliberately as simple as possible to ensure transparency and adaptability. The idea of the `PyTransport` package as a whole is that after a potential and a field space metric (if the metric is non-Euclidean) are provided by the user the C++ code is automatically edited and complied into a Python module by supporting Python functions (called from the *PyTransportDist/PyTransport/PyTransSetup.py* file), meaning a lot of work is done for the user. The end result is a Python module consisting of a set of Python functions for a specific inflationary model, called the PyTrans*** module. The functions of this module provide key routines for inflationary cosmology (including calculating the evolution of the two and three point correlations). The asterisks, ***, indicate we can label the module with a tag telling us what model it corresponds to, and we can therefore install multiple modules if we want to work with many models simultaneously. The key functions available to these modules are defined in the file *PyTransportDist/PyTransport/PyTrans/PyTrans.cpp* (which is a C++ file defining the Python module). The scripts that edit the C++ code and compile the module are discussed further below in the setup section, and by default they place the compiled module in the local folder *PyTransportDist/PyTransport/PyTrans/lib/python/* to avoid access issues if, for example, you do not have root privileges. Other useful Python functions that perform common tasks, such as producing a power spectrum by looping over calls to the compiled module, can be found in *PyTransportDist/PyTransport/PyTransScripts.py*. Python treats functions written in Python inside a file, such as *PyTransScripts.py* and *Py-*

[2]If downloaded from GitHub, it will instead come in folder named PyTransport and labeled with the branch of the code.

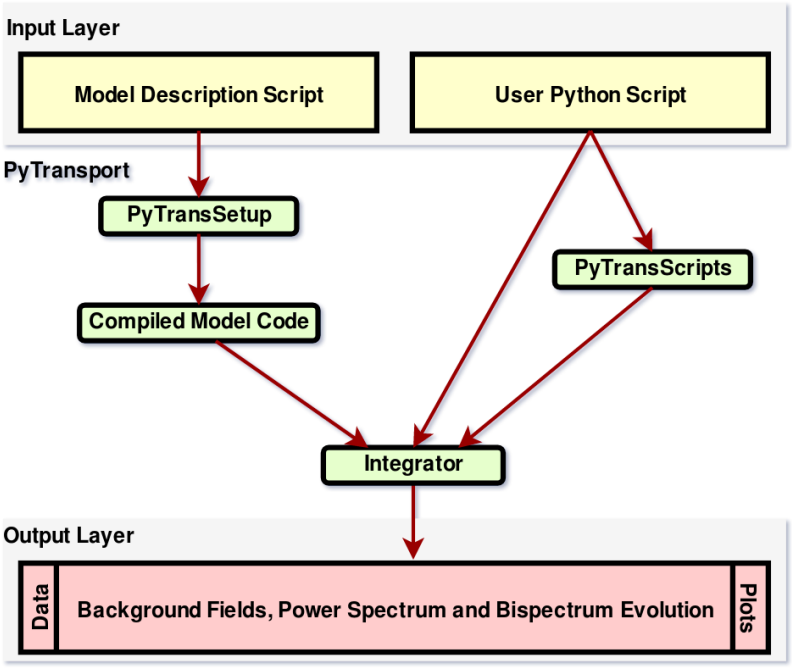

Figure 6.1.: *A block diagram showing the relation between the different components of* `PyTransport 2.0`.

TransSetup.py, in the same way as a compiled module. So there are effectively **three modules within PyTransport**, one to setup a compiled module for the potential we want to study (**PyTransSetup**), the compiled module itself (**PyTrans*****) (or multiple compiled modules labeled with different tags) and a module with various functions automating common tasks that use the functions of the compiled module (**PyTransScripts**). Also in the *PyTransportDist/* folder is an example folder *PyTransportDist/Examples* containing several example scripts for different models. The structure of the code is illustrated in Fig. (6.1). There are no dependencies external to the folders provided except for a working Python installation (with appropriate packages downloaded), and a C++ compiler – this is deliberate to make the code as easy as possible to use. An MPI installation such as openMPI is also needed if the module is required to be used across multiple cores.

We note that all the C++ code is written by the transport team except for an included Runge-Kutta-Fehlberg (rkf45) integrator routine written by John Burkardt and distributed under a GNU LGPL license detailed here[3]. We choose this lightweight integrator over other options, such as using integrators included with the BOOST library, so that it could easily be included with the distribution with no external dependencies being introduced.

[3]https://people.sc.fsu.edu/~jburkardt/f_src/rkf45/rkf45.html

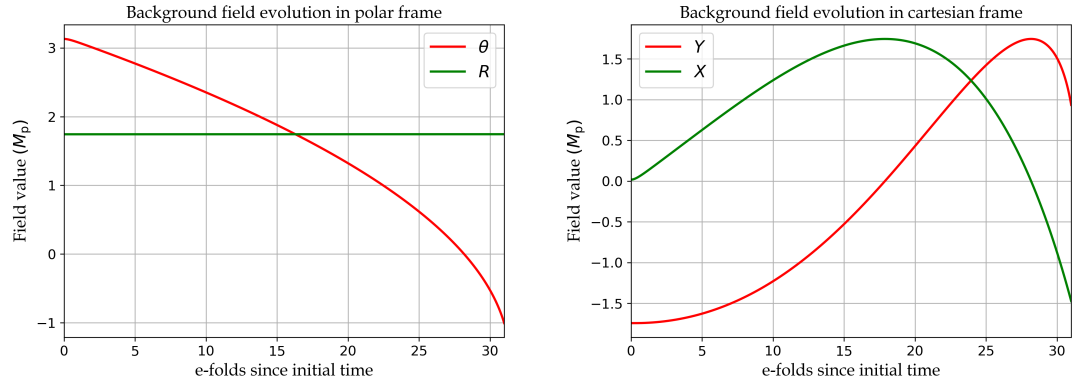

(a) **(b)**

Figure 6.2.: *The time evolution of the polar coordinate fields θ and R with metric (6.2) on the left, and the Cartesian coordinates, X and Y on the right.*

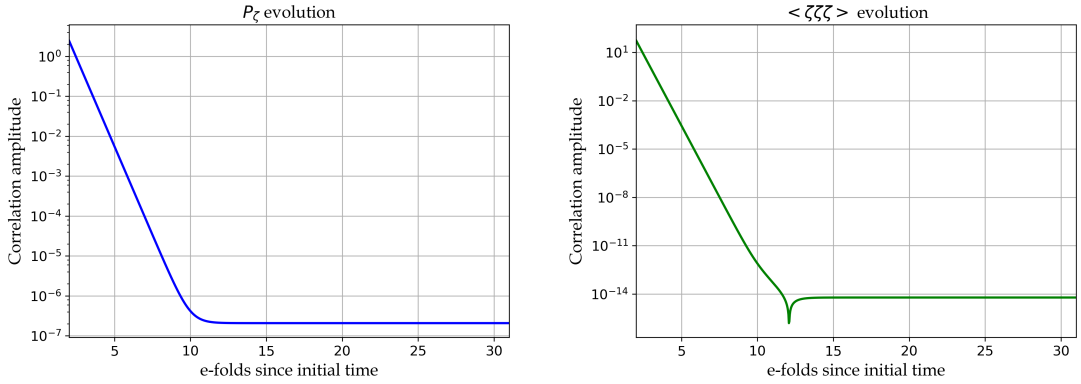

(a) **(b)**

Figure 6.3.: *The time evolution of correlation functions. On the left the time evolution of the two-point function of the curvature perturbation, ζ, and on the right the evolution of the three-point function for an equilateral configuration. Both were taken for modes exiting the horizon 21 e-folds before the end of inflation.*

6.3. PyTransport 2.0: Examples

6.3.1. Model with a Continuous Curved Trajectory

Ref. [78] attempted to construct a model in which the field-space trajectory was curved in such a way as to exhibit Gelaton [132] or QSFI [136] behaviour. For reasons presented there, this behaviour was difficult to achieve, but the model presented there is still a useful example, and in the present context provides a useful check of our code.

The model is defined by the action for two fields R and θ as

$$S = -\frac{1}{2}\int d^4x\sqrt{-g}\left[(\partial R)^2 + R^2(\partial\theta)^2 + 2V(R,\theta)\right] , \tag{6.1}$$

where the potential (defined below in Eqn. (6.3)) represents a circular valley at a

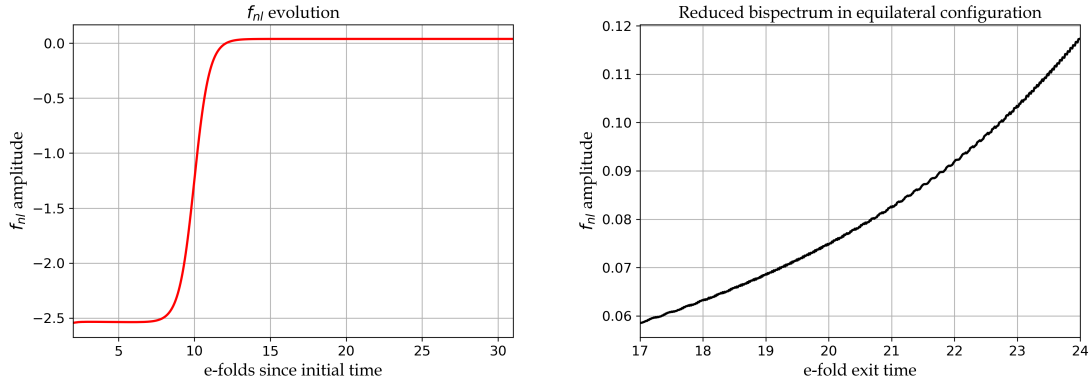

(a) **(b)**

Figure 6.4.: *The reduced bispectrum $f_{nl}(k_1, k_2, k_3)$ for equilateral configurations. On the left the evolution of f_{nl} versus time for an equilateral configuration with modes leaving the horizon 21 e-folds prior to the end of inflation. On the right the bispectrum over a range of equilateral configurations as a function of exit time of the scale $k_s/3$.*

fixed value of R – and hence is naturally written in terms of these 'polar coordinate' fields. However, as the codes developed for Ref. [78] only dealt with canonical kinetic terms, in that work it was necessary to perform a field redefinition to Cartesian coordinates X and Y. Here we evolve the statistics directly for the fields R and θ and compare results, using this as a test case to benchmark our code against its canonical precursor.

The field-space metric of the model can be read off from Eqn. (6.1), and is

$$G_{IJ} = \begin{pmatrix} 1 & 0 \\ 0 & R^2 \end{pmatrix} . \tag{6.2}$$

The potential is

$$V = V_0 \left(1 + \frac{29\pi}{120}\theta + \frac{1}{2}\frac{\eta_{\rm R}}{M_{\rm p}^2}(R-R_0)^2 + \frac{1}{3!}\frac{g_{\rm R}}{M_{\rm p}^3}(R-R_0)^3 + \frac{1}{4!}\frac{\lambda_{\rm R}}{M_{\rm p}^3}(R-R_0)^4 \right) , \tag{6.3}$$

and we choose parameters $V_0 = 10^{-10}M_{\rm p}^4$, $\eta_{\rm R} = 1/\sqrt{3}$, $g_{\rm R} = M_{\rm p}^2 V_0^{-1/2}$, $\omega = \pi/30$, $\lambda_{\rm R} = 0.5 M_{\rm p}^3 \omega^{-1/2} V_0^{-3/4}$ and $R_0 = \frac{30\sqrt{10^{-10}/3}}{\pi\sqrt{10^{-9}}}$. With these choices, the radial direction represents a heavy mode confining the inflationary trajectory to the valley, with a light angular direction. We further choose initial conditions

$$R_{\rm ini} = \sqrt{R_0^2 + (10^{-2}R_0)^2} \quad \text{and} \quad \theta_{\rm ini} = \arctan\left(\frac{10^{-2}R_0}{R_0}\right) . \tag{6.4}$$

Generating results using our new code for the field evolution and correlations in the

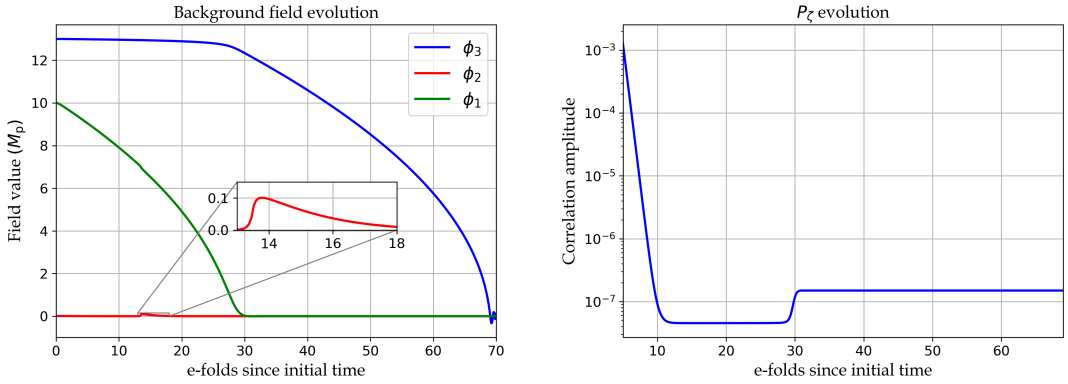

(a) **(b)**

Figure 6.5.: *The time evolution of the fields ϕ_1, ϕ_2 and ϕ_3 on the left, and the time evolution of the two-point function of ζ for a k-mode exiting the horizon 60 e-folds before the end of inflation on the right. The turn in field-space occurs 13 e-folds into inflation when the field ϕ_2 experiences excitations from its coupling to the lighter field ϕ_1 via the field-space metric. After roughly 30-e-folds the ϕ_1 field reaches the minimum and the amplitude of the power spectrum increases at this time.*

$\{R, \theta\}$ basis, and then subsequently using a coordinate transformation to translate the results to the $\{X, Y\}$ basis, we can compare our results to the output of the canonical code. We find excellent agreement. The evolution of correlation functions of the curvature perturbation, ζ, are coordinate invariant, and also match that generated using the canonical code. In Fig. (6.2a) the background field evolution in the non-canonical case is plotted. Under the coordinate transformation to the canonical fields X and Y we get the evolution in Fig. (6.2b). In Fig. (6.3a) & (6.3b) one can clearly see that after horizon crossing the curvature perturbation freezes in, becoming constant on large scales as expected. The evolution of the reduced Bispectrum (Eqn. (2.147)) f_{nl} for one equilateral triangle is shown in Fig. (6.4a). The reduced bispectrum in the equilateral configuration as a function of horizon crossing time is given in Fig. (6.4b), and can be compared with Fig. 11 of Ref. [78].

6.3.2. Quasi-Two-Field Inflation

Next we consider the quasi-two field model introduced in Ref. [118] where the power spectrum was calculated. In this model there are two light scalar fields which drive inflation and one heavy field which interacts with the light ones through a coupling in the kinetic terms. This leads to a fast turn in the plane of the lighter two fields resulting in the well known feature of oscillations in the power spectrum and bispectrum (see for example [133–135, 174–178]). In this section we reproduce the power spectrum presented in Ref. [118] as a test of our code and then calculate the bispectrum for the first time. The three fields are labelled ϕ_1, ϕ_2 and ϕ_3, and

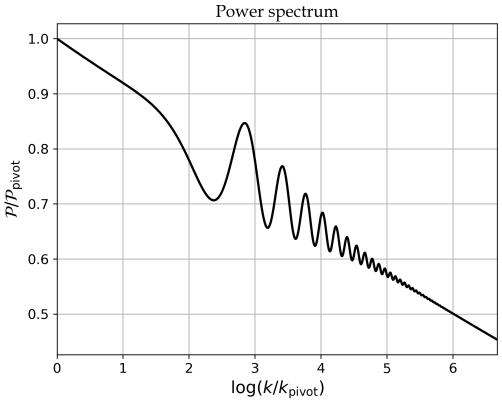

Figure 6.6.: *The power-spectrum of the curvature perturbation for a range of modes which exit the horizon over a window of 7 e-folds. The scale k_{pivot} is taken to be when the mode leaves the horizon at 58 e-folds prior to the end of inflation. Both the scales and amplitudes are normalised to the spectrum at the pivot scale.*

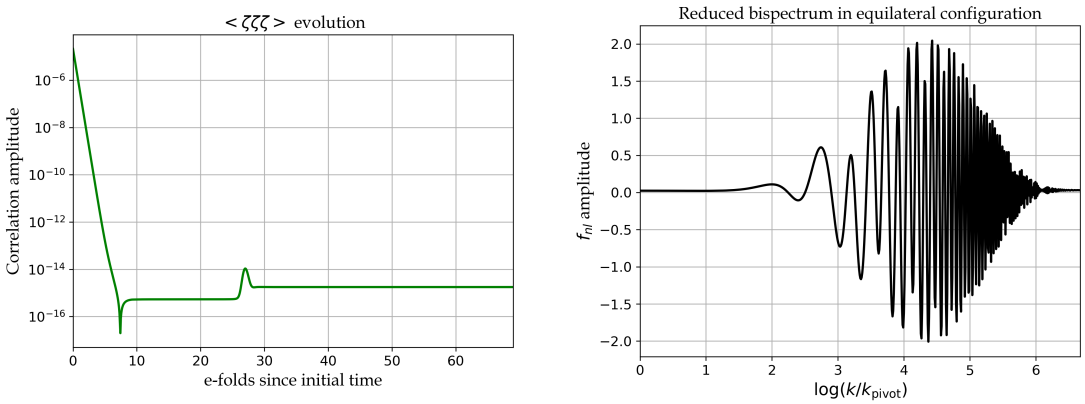

(a) **(b)**

Figure 6.7.: *The evolution of the three-point function for one equilateral configuration, and the reduced bispectrum, f_{nl}, for equilateral configurations over a range k_s. The reduced bispectrum is plotted for modes leaving the horizon between 59 and 51 e-folds before the end of inflation. The highly oscillatory behaviour is a result of the excitations to the heavy field around horizon crossing.*

model has a metric which takes the form

$$G_{IJ} = \begin{pmatrix} 1 & \Gamma(\phi_1) & 0 \\ \Gamma(\phi_1) & 1 & 0 \\ 0 & 0 & 1 \end{pmatrix} . \tag{6.5}$$

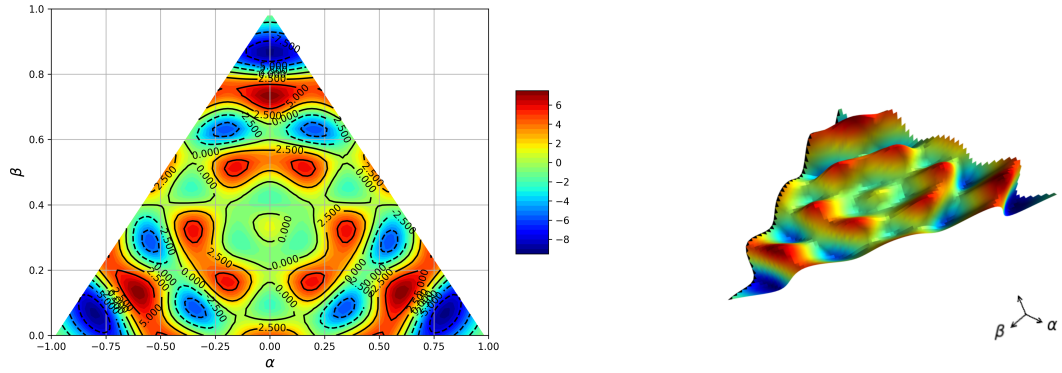

Figure 6.8.: *Amplitude over shape configurations of the reduced bispectrum* $f_{nl}(\alpha, \beta)$ *at a fixed* k_t *53 e-folds before the end of inflation, corresponding to* $\log(k/k_{pivot}) = 4.79$.

The function $\Gamma(\phi_1)$ has the following ϕ_1 dependence [127],

$$\Gamma(\phi_1) = \frac{\Gamma_0}{\cosh^2\left(2\left(\frac{\phi_1 - \phi_{1(0)}}{\Delta\phi_1}\right)\right)}\,, \tag{6.6}$$

with $\Gamma_0 = 0.9$ the maximum value attained by $\Gamma(\phi_1)$. $\phi_{1(0)} = 7M_{\rm p}$ is the value of ϕ_1 at the apex of the turn in field-space and $\Delta\phi_1 = 0.12$ is the range of ϕ_1 over which the turn occurs. The potential is defined as

$$V = \frac{1}{2}g_1 m^2\phi_1 + \frac{1}{2}g_2 m^2\phi_2 + \frac{1}{2}g_3 m^2\phi_3\,, \tag{6.7}$$

with parameters $g_1 = 30$, $g_2 = 300$, $g_3 = 30/81$ and $m = 10^{-6}$. The initial conditions of the fields are

$$\phi_1 = 10.0M_{\rm p} \quad \phi_2 = 0.01M_{\rm p} \quad \phi_3 = 13.0M_{\rm p}\,. \tag{6.8}$$

In Fig. (6.5a) the background field evolution is plotted. At 13 e-folds into the evolution the turn in the inflationary trajectory occurs, as can be seen by the increase in the amplitude of the heaviest field. In Figs. (6.5b) & (6.7a) the evolution of both the two and three-point correlation functions of curvature perturbations are plotted. The power spectrum obtained in Fig. (6.6) matches that seen in Ref. [118] illustrating that the code is in good agreement with this earlier implementation. We produce the reduced bispectrum over equilateral configurations in Fig. (6.7b), the structure of which is defined by a pulse of large and rapidly oscillating values of the three-point function. Finally, for a fixed scale k_t we plot the reduced bispectrum in Fig. (6.8) as a function of the α and β parameters discussed in (2.6.2) for a fixed k_t.

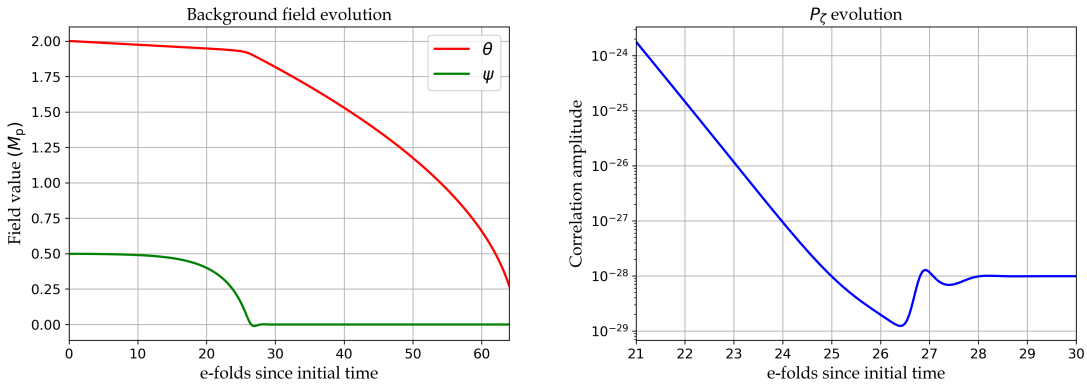

(a) **(b)**

Figure 6.9.: *The evolution of the fields θ and ψ on the left and the evolution two-point function of the curvature perturbation on the right for a mode leaving the horizon 50 e-folds prior to the end of inflation. From 30 e-folds into inflation until the end there is no further evolution of the two-point function.*

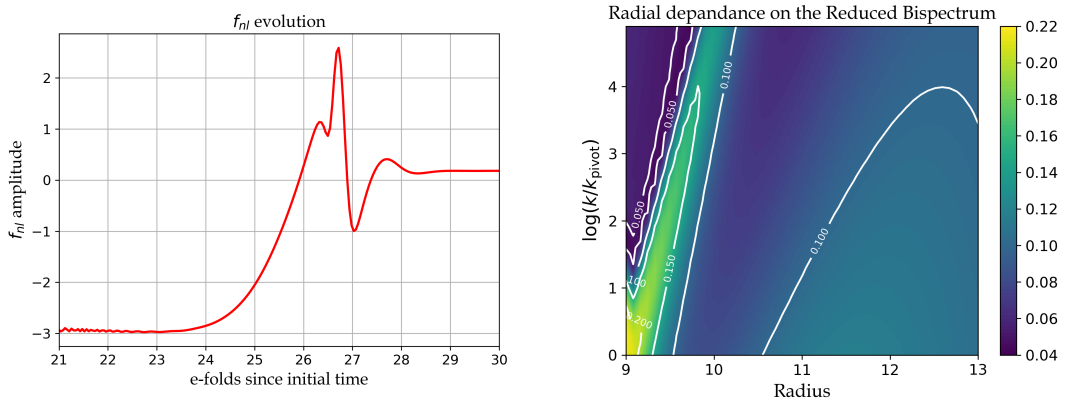

(a) **(b)**

Figure 6.10.: *Evolution of the reduced bispectrum in an equilateral configuration on the left and the reduced bispectrum for an equilateral configuration versus the radius of the metric sphere on the right. From 30 e-folds into inflation until the end there is no further evolution of f_{nl}. The evolution of f_{nl} was taken for a mode leaving the horizon at 26 e-folds from the beginning of inflation. The bispectrum on the right is taken for a range of modes in the window between 25 and 30 e-folds and for a radius between 9 and 11.5. It illustrates a large amplitude correlation over scales for a small radius (or rather large field-space curvature).*

6.3.3. Inflation on a 2-Sphere Metric

In the models considered above the field-space metrics were non-trival, but flat. As a further test of our code, therefore, we now introduce a model with a constant non-zero Ricci curvature.

We construct a toy model containing two fields θ and ψ, where the action is defined as

$$S = -\frac{1}{2}\int d^4x\sqrt{-g}\left[r_0^2(\partial\theta)^2 + r_0^2\sin^2\theta(\partial\psi)^2 + 2V(\theta,\psi)\right] , \tag{6.9}$$

where r_0 is the radius of the surface of the sphere which the field trajectory is confined to. The curvature of the field-space, defined by the Ricci Scalar, is related to the radius, $R = \frac{2}{r_0^2}$. The field-space metric which describes the line element along the surface of a sphere is therefore

$$G_{IJ} = \begin{pmatrix} r_0^2 & 0 \\ 0 & r_0^2\sin^2\theta \end{pmatrix} . \tag{6.10}$$

For the potential we use the same potential given for the axion-quartic model studied in Ref. [78]. The potential is of the form,

$$V = \frac{1}{4}g_\theta\theta^4 + \Lambda^2\left(1 - \cos\left(\frac{2\pi\psi}{f}\right)\right) , \tag{6.11}$$

where the field ψ is our "2-sphere-axion" and our parameters are $g_\theta = 10^{-10}$, $\Lambda^4 = (25/2\pi)^2 g M_{\rm p}^4$, $\omega = 30/\pi$ and $f = M_{\rm p}$. The initial conditions of the fields are set to

$$\theta_{\rm ini} = 2.0M_{\rm p} \quad and \quad \phi_{\rm ini} = f/2 - 10^{-3}M_{\rm p}, \tag{6.12}$$

which is sufficient for inflation for 64 e-folds. The background evolution of the fields are plotted in Fig. (6.9a), with the corresponding evolution of correlations of the curvature perturbations for two-point (Fig. (6.9b)) and three-point (Fig. (6.10a)) functions. We study the effects of curvature on quantities like the bispectrum by varying the radius r_0. Figure (6.10b) is a contour graph of the bispectrum as a function of r_0. We see that for a radius $r_0 > 11.0$ the bispectrum is small, but for $r_0 < 11.0$ the bispectrum begins to increase. This indicates a correlation between large curvature and a value of large f_{nl} in this model.

6.3.4. Inflation on a Conifold Metric

Finally we consider a more realistic case inspired by models of D-brane inflation. Such models have recently been the subject of considerable interest, with a number

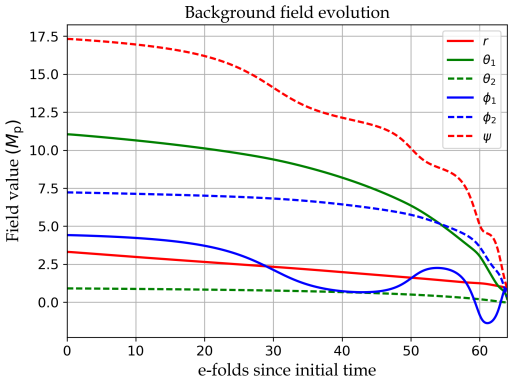

Figure 6.11.: *The evolution of the 6 moduli fields during inflation. Rich dynamics exist owing to the couplings in the conifold metric. Inflation ends when the branes collide at a value of* $r = 0$.

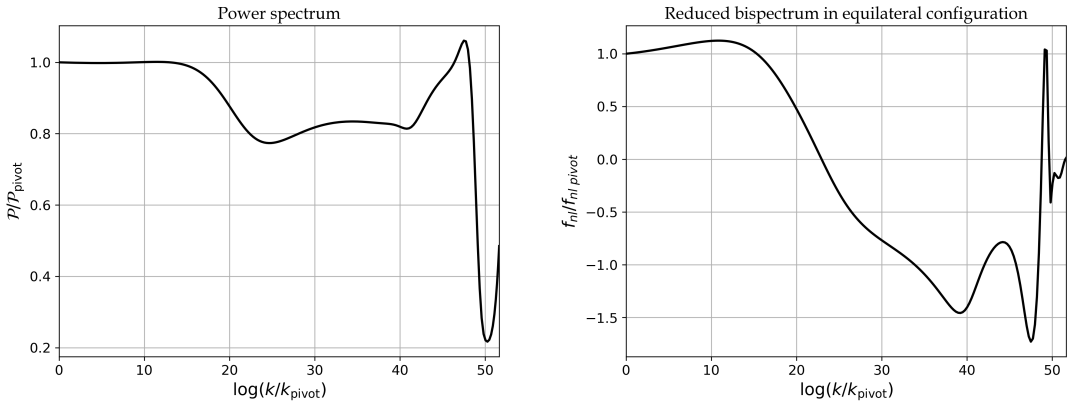

(a) **(b)**

Figure 6.12.: *On the left, the power spectrum of curvature perturbation and on the right the bispectrum of curvature perturbations over an equilateral configuration for modes exiting the horizon after a large range of times between 12 and 64 e-folds.*

of groups statistically probing their realisations [179–181]. In one such scenario two D3-branes are attracted by a Coulomb force. Compactification induces a warping of the 6-D manifold where the D3-brane sits, resulting in a non-trivial field-space metric in the Lagrangian of the system. Both the geometry of the metric and structure of the potential affect the inflationary dynamics. Initial work [179] looked at the background dynamics of this system, while more recent studies looked into the distribution of 2-point statistics [180, 181]. Here we illustrate how our new code could be used to obtain information about the bispectrum, though we defer realistic studies to future work.

We consider the Lagrangian of D3-brane inflation as

$$S = -\frac{1}{2}\int d^4x\sqrt{-g}\left(G_{IJ}d\phi^I d\phi^J + 2V(\phi_1,\ldots\phi_6)\right), \tag{6.13}$$

where a is the scale factor. The scalar fields represent the 6 brane coordinates, one

radial r and five angular dimensions $\theta_1, \theta_2, \phi_1, \phi_2$ and ψ. The field-space metric G_{IJ} corresponds to the Klebanov-Witten conifold geometry [182]. The metric is of the form,

$$G_{IJ}d\phi^I d\phi^J = dr^2 + r^2 d\Omega^2 \,, \tag{6.14}$$

with the metric of the cone $d\Omega$ [183] is given by

$$d\Omega^2 = \frac{1}{6}\sum_{i=1}^{2}\left(d\theta_i^2 + \sin^2\theta_i d\phi_i^2\right) + \frac{1}{9}\left(d\psi + \sum_{i=1}^{2}\cos\theta_i d\phi_i\right)^2 \,, \tag{6.15}$$

which is a non-compact geometry built over the five-dimensional $(SU(2)\times SU(2))/U(1)$ coset space $T^{1,1}$. As a toy example we do not generate a realistic potential (motivated by any attractive forces between branes or contribution from either the homogeneous or the inhomogeneous bulk), instead, for simplicity, we take a quadratic potential for the 6 fields

$$V(\phi) = \sum_{i=1}^{6} m_i^2\phi_i^2 \,, \tag{6.16}$$

where m_i are the randomised masses of the fields. A randomised set of masses and initial conditions are selected with the criteria that 64 e-folds of inflation occur. With these parameters the evolution of the dynamics and statistics can be run and the background trajectory for each of the six fields is plotted in Fig. (6.11). The power spectrum is plotted in Fig. (6.12a) and the bispectrum in the equilateral configuration is plotted in Fig. (6.12b). It would be interesting to run a more realistic analysis including the full potential of the system but this is beyond the scope of our work. We have, however, demonstrated that this is possible using the transport method and its implementation in code via `PyTransport`.

6.4. Performance

In this section we will examine the performance of `PyTransport 2.0` by conducting convergence test and comparing the computation time with its predecessor `PyTransport`. To illustrate this we will use the model in Sec. (6.3.3) with a double quadratic and 2-sphere metric. The double quadratic potential has been used extensively as a proving ground for many numerical methods [78, 121, 123, 169, 172, 184–187]. As the potential is sum-separable the analytical expressions can be calculated using the slow-roll approximation [124], however, we wish to test our code with the field-space metric implementation we make a departure from this standardized testing and lose the analytical results that come with it.

6.4.1. Convergence Tests

Number of massless sub-horizon e-folds

As we discussed in Ch. (4) the initial conditions, derived from the quantum calculations, are valid when $k^2/a^2 \gg m^2$ where m^2 is the largest eigenvalue of the mass matrix which is model and typically time dependent. Typically this is a few e-folds before horizon crossing $k^2/a^2 = H^2$ in the required massless regime where we can start our evolution numerically for a particular wavelength. In the case of the bispectrum we choose the earliest massless time which is associated to the set of wavenumbers in the configuration (for example in the squeezed configuration this corresponds to when the smallest mode satisfies the above condition). The number of e-folds of massless evolution is a factor in the accuracy of our result, therefore we wish to spend as long as possible in this regime. There is, however, a trade off between amount of massless evolution and computation time as integrating is expensive in this phase. Therefore it is important to know when our result converges.

In `PyTransport` there are automated scripts that allow the user to set the initial time for each configuration a number of e-folds prior to its massless time. The convergence plot, in Fig. (6.13), shows the reduced bispectrum in both equilateral and squeezed configurations as a function of the number of e-folds of massless evolution.

Integration tolerance

The evolution of the three point function can be a numerically intensive task, requiring high numerical accuracy. The question arises how low (the lower the higher the accuracy) do we need to set numerical tolerances. This question can't be answered absolutely, and must be dealt with on a model by model basis. Models with finer features in the potential, or in which the excitation of the two and three point function occurs on sub-horizon scales will require lower tolerances (high accuracy). Models which produce a small signature may also need higher accuracy to resolve the true answer from noise than models which produce a large bispectrum. As the values are lowered, the code takes longer to run and eventually will fail. Therefore, there is significant benefit for picking a required accuracy which is sufficient for the task, but not one which is too stringent. Convergence is the key criterion in selecting tolerances.

In `PyTransport` (as in most packages involving numerical integrators) there are two tolerances to set; the relative and the absolute tolerance. In Fig. (6.14) we show the value of the reduced bispectrum in both equilateral and squeezed configurations as a function of the integration tolerances.

6.4.2. Comparative Performance

In `PyTransport 2.0`, one can opt to specify explicitly a field space metric. If this option is not selected the code defaults to assuming that the metric is Euclidean and

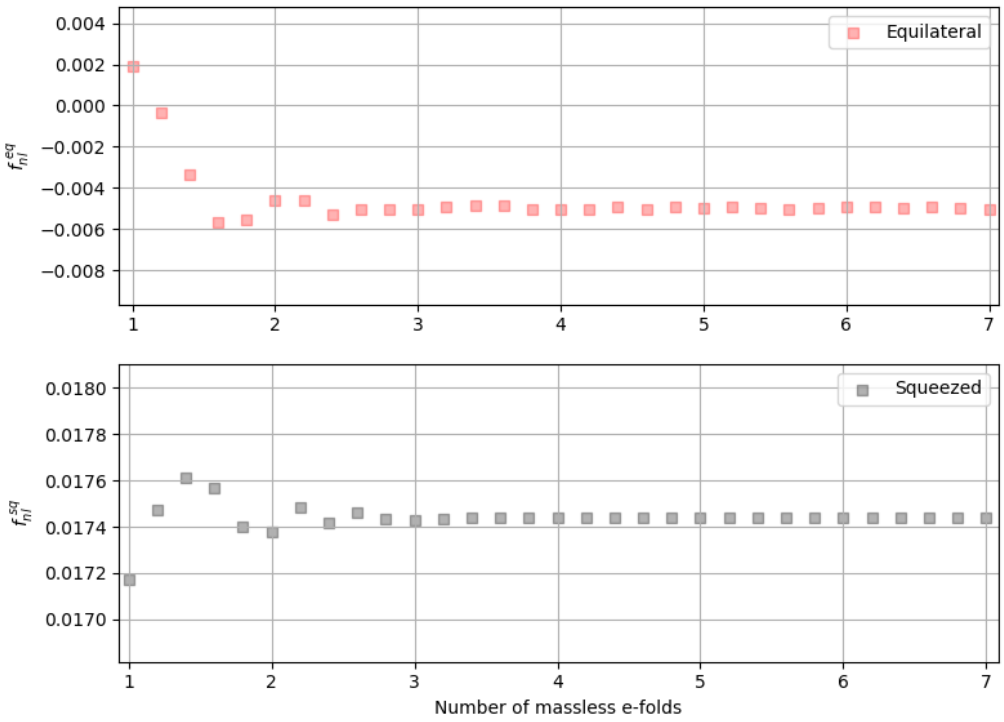

Figure 6.13.: *Top panel: Convergence of f_{nl}^{eq} with increasing number of massless (or sub-horizon) e-folds (using relative and absolute tolerances of 10^{-8}) for an equilateral triangle of the bispectrum. Bottom panel: Convergence of f_{nl}^{sq} with increasing number of massless (or sub-horizon) e-folds (using relative and absolute tolerances of 10^{-8}) for a squeezed triangle ($\alpha = 0$, $\beta = 0.99$). The double quadratic model with a 2-sphere field-space metric from Sec. (6.3.3) was used for the purpose of this test.*

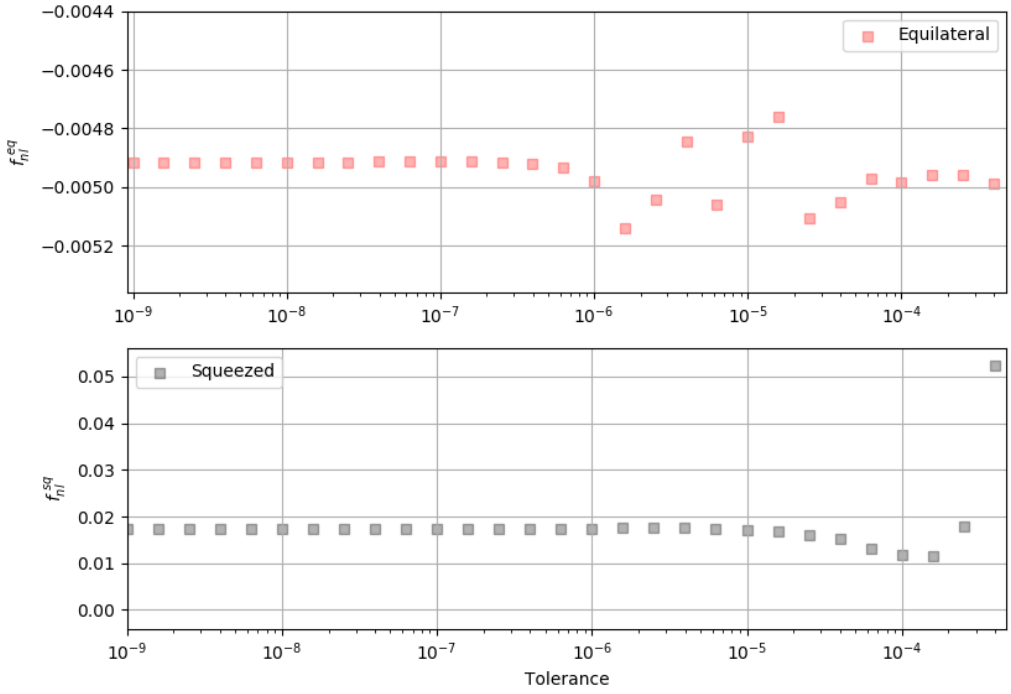

Figure 6.14.: *Top panel: Convergence of f_{nl}^{eq} with decreasing relative and absolute tolerances (using 5 e-folds of massless evolution) for an equilateral triangle of the bispectrum. Bottom panel: Convergence of f_{nl}^{sq} with decreasing relative and absolute tolerances (using 5 e-folds of massless evolution) for a squeezed triangle ($\alpha = 0$, $\beta = 0.99$). The double quadratic model with a 2-sphere field-space metric from Sec. (6.3.3) was used for the purpose of this test.*

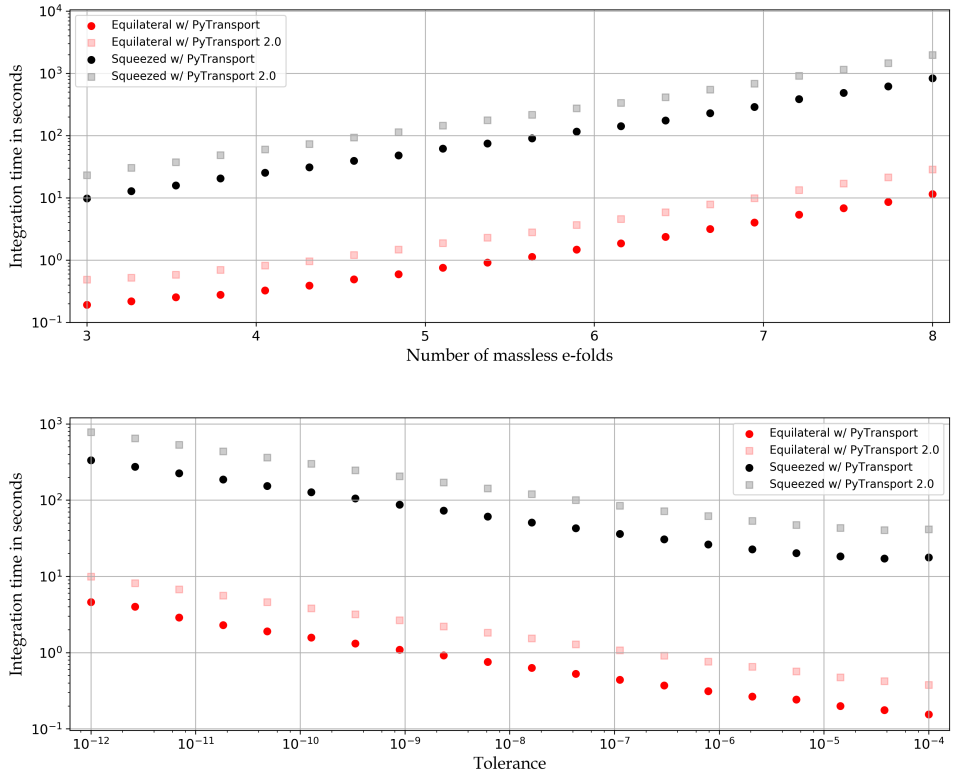

Figure 6.15.: *Top panel: scaling of integration time with increasing number of massless (or sub-horizon) e-folds (using relative and absolute tolerances of* 10^{-8}*) for an equilateral triangle of the bispectrum and a squeezed triangle* ($\alpha = 0$, $\beta = 0.99$)*. Timings were performed using the canonical code and the new non-canonical code setting a Euclidean metric explicitly. Bottom panel: scaling of integration time with integration tolerance with 5 e-folds of massless evolution. The double quadratic model used to analysis performance in Ref. [78] is timed using the canonical* `PyTransport` *package and compared to the same model using* `PyTransport 2.0`*. The computer used for timings contained an 3.1 GHz Intel i7-4810MQ processor.*

the code reverts back to the previous canonical code. The simplicity of a Euclidean metric means that a number of internal loops do not need to be performed, and hence the canonical code is expected to be faster than when a metric is specified explicitly (even if the metric is the Euclidean one). To demonstrate this effect and also to benchmark the speed of the new code in Fig. (6.15) we show how the speed of the new code compares with that of the canonical one. We also show how the speed of the code is sensitive to the number of e-folds before horizon crossing (of the shortest scale in the triangle being evaluated) at which initial conditions are fixed, and to different tolerances which fix the accuracy of the code. For this purpose we use the double quadratic potential used to calculate performance data in Ref. [78]. As can be seen, the new code is roughly a factor of 2 slower for this two field model. We find that introducing a simple field space metric, such as the 2-sphere metric used in Sec. (6.3.3), leads to very similar timing data to the Euclidean metric (though more complicated metrics will inevitably slow down the code as the terms in the metric need to be evaluated at each time step). A more significant effect comes from increasing the number of fields. The size of the arrays which store information about the Riemann tensor and its derivative scale as $\mathcal{N}^4$ and $\mathcal{N}^5$ respectively (for the canonical code the largest arrays scale as $\mathcal{N}^3$), and therefore memory issues and overheads resulting form accessing and looping over these arrays grow rapidly as field number increases.

In this chapter we constructed a numerical code from the transport method. Now we can use it examine more realistic situations where we may wish to extract some interesting physics.

7. Attractor Behaviour in Multifield Inflation

In this chapter we study multifield inflation in scenarios where the fields are coupled non-minimally to gravity. We illustrate that gravity formulation plays an important role: in the case of metric gravity the coupling means that multifield models approach the single-field α-attractor limit, whereas in the Palatini case the attractor behaviour is lost in the case of multifield inflation, as has previously been observed in the single-field case. In Sec. (7.1) we present a summary of attractors in inflationary observables. We then present the multifield models we are considering and perform the conformal transformation to the Einstein frame where the non-minimal couplings vanish in Sec. (7.2), and numerical set-up in Sec. (7.3). Finally we present the results in Sec. (7.4), discussing observational ramifications and demonstrating why the curved field-space metric in the Einstein frame has no influence on the inflationary dynamics.

7.1. Attractor Models of Inflation

In 1980 Starobinsky proposed that quantum corrections to general relativity could have some cosmological consequences in the early universe, particularly for inflation [20]. Originally, these quantum corrections were formulated in the language of 'semi-classical' gravity [59] (which relates the Einstein tensor to the expectation value of the energy-momentum tensor under the assumption that the quantum effects are dominated by the more numerous matter fields). It was later formalized so that the standard Ricci scalar in the Einstein-Hilbert Lagrangian is replaced by a function of the Ricci Scalar. The action for Starobinsky inflation (sometimes refered to as R^2 inflation) is

$$S = \frac{1}{2}\int d^4x\sqrt{-g}\left(R + \frac{R^2}{6M^2}\right), \tag{7.1}$$

where M is some mass scale smaller than $M_{\rm pl}$. This model propagates a spin-2 graviton and a scalar degree of freedom which manifests itself under a conformal

transformation of the metric,

$$\bar{g}_{\mu\nu} = \left(1 + \frac{\phi}{3M^2}\right) g_{\mu\nu} \,. \tag{7.2}$$

We then impose a field redefinition of ϕ,

$$\bar{\phi} = \sqrt{\frac{3}{2}} \ln\left(1 + \frac{\phi}{3M^2}\right) \,, \tag{7.3}$$

so that our kinetic terms are canonical to obtain the action,

$$S = \frac{1}{2}\int d^4x\sqrt{-\bar{g}}\left[\bar{R} - \partial_\mu\bar{\phi}\partial^\mu\bar{\phi} - \frac{3}{2}M^2\left(1 - e^{-\sqrt{\frac{2}{3}}\bar{\phi}}\right)\right] \,. \tag{7.4}$$

In this frame the additional degree of freedom in the action of Eqn. (7.1) due to the R^2 term is now manifest as a scalar field minimally coupled to gravity. Moreover the observational predictions from this model are $(n_s\,, r) = (1 - 2/N\,, 12/N^2)$ (with $(n_s\,, r) = (0.967\,, 0.003)$ for $N = 60$). Coincidentally this result also fits neatly in observational data [103].

Recently it has emerged that many, seemingly unrelated, inflationary models converge on this same result (up to some uncertainty on the effect of reheating). This has appeared in Higgs-type inflationary models with the non-minimal couplings to gravity [188] $\xi\phi^2 R$ with $\xi < 0$, in chaotic inflation with non-minimal coupling to gravity [189, 190] with $\xi > 0$ and in the context of supersymmetric extensions involving kähler potential [191–195] the study of which later evolved into the field of generalised α-attractors. A typical feature of α-attractor models is a pole that appears in the Laurent expansion of the kinetic term in the Einstein Frame. This is a similar property in a related family of models, the ξ-attractor models. It is this common pole which underlines the attractor properties of these models [194].

7.2. Non-Minimal Coupling to Gravity

In scalar-tensor theories the Jordan frame is referred to as the frame where the Lagrangian contains a coupling between the scalar field and the scalar curvature. The frame where the expressions for observations take the usual form is the Einstein frame, where there is no coupling to gravity and where the weak energy condition is not violated [196]. The action in the Jordan frame takes the form,

$$S_J = \frac{1}{2}\int d^4x\sqrt{-g}\left[(M_{\rm pl}^2 + f(\phi^I))g_{\mu\nu}R^{\mu\nu} - \delta_{IJ}\partial_\mu\phi^I\partial^\mu\phi^J - U(\phi^I)\right] \,, \tag{7.5}$$

where the $U(\phi)$ is the potential in the Jordan frame and the non-minimal coupling function, $f(\phi^I)$, will, in the following, take the form

$$f(\phi^I) = \sum_I \xi_I^{(n)} \left(\frac{\phi^I}{M_{\rm pl}}\right)^n , \tag{7.6}$$

with $\xi_I^{(n)}$, the dimensionless non-minimal coupling parameters. Any physical answer should not depend on the frame you are working in (in the same way as coordinate invariance) and the ones we choose to calculate in is more a matter of convenience. At the end of inflation (when scalar field stops evolving) the ζ in the two frames should be conserved and equivalent under a certain frame-covariant transformation [197, 198]. The transformation from the Jordan Frame to the Einstein frame is by means of a conformal transformation. A conformal transformation is a rescaling of the space-time metric $g_{\mu\nu} \to \bar{g}_{\mu\nu}$, and as we have seen above this is often accompanied by a rescaling of the scalar field $\phi \to \bar{\phi}$. Under the conformal transformation,

$$g_{\mu\nu} \to \Omega^{-1}(\phi^I) g_{\mu\nu}, \quad \Omega(\phi^I) = 1 + f(\phi^I) , \tag{7.7}$$

we obtain the action in the Einstein frame

$$S_E = \frac{1}{2}\int d^4x\sqrt{-g}\left[\frac{1}{2}M_{\rm pl}^2 R - \frac{1}{2}G_{IJ}(\phi^I)\partial_\mu\phi^I\partial^\mu\phi^J - U(\phi^I)\Omega^{-2}(\phi^I)\right] . \tag{7.8}$$

In the case of more than one scalar field minimally attached to gravity it is not possible to canonicalize the model, so we are inevitably left with a field-space metric. In the case of a single-field one could redefine the scalar field so that the kinetic terms become canonical and only the potential is modified. For multiple fields this is in general not possible however using the transport method and code we can these calculate directly with Eqn. (7.8).
If we take the single-field example, Eqn. (7.8) becomes,

$$S_E = \frac{1}{2}\int d^4x\sqrt{-g}\left[\frac{1}{2}M_{\rm pl}^2 R - \frac{1}{2}\partial_\mu\phi\partial^\mu\phi - U(\phi)\Omega^{-2}(\phi)\right] . \tag{7.9}$$

In slow-roll, the inflationary dynamics are parameterized just by the potential, and by transforming to the Einstein frame from the Jordan frame we recover this parameterization.

In addition, the larger the size of the coupling parameter ξ the flatter the potential in the Einstein frame becomes and the closer the potential become to resembling the potential in Eqn. (7.4). This is what is called attractor behaviour. Essentially what we believed to be a large collection of different models in the Jordan frame gets mapped into a smaller subset of models in the Einstein Frame with a narrow range of dynamics.

7.2.1. The Palatini Formalism

Recently, however, in Ref. [84] it was shown that α-attractors are in fact not universal but depend on the underlying theory of gravity in a subtle way. The non-minimal couplings of the type $\xi_I(\phi^I)^n g^{\mu\nu} R_{\mu\nu}$ contain freedom to choose the space-time connection: one can either study the usual metric case where $R_{\mu\nu} = R_{\mu\nu}(g_{\mu\nu})$, or choose an alternative approach, the so-called *Palatini* formulation of gravity, where the connection Γ and hence also $R_{\mu\nu} = R_{\mu\nu}(\Gamma)$ are independent variables. In the metric formulation of gravity, the connection Γ is determined uniquely as a function of the metric tensor, i.e. it is $\bar{\Gamma} = \bar{\Gamma}(g_{\mu\nu})$ with

$$\bar{\Gamma}^{\lambda}_{\alpha\beta} = \frac{1}{2} g^{\lambda\rho} (\partial_\alpha g_{\beta\rho} + \partial_\beta g_{\rho\alpha} - \partial_\rho g_{\alpha\beta}) \,, \tag{7.10}$$

the Levi-Civita connection. The application of the variational principle then gives rise to an extra equation for the connection, in addition to the one for the metric. For the Einstein-Hilbert action, the extra equation forces the connection to have the usual Levi-Civita form, but in more general theories of gravity, such as $f(R)$ theories, or in the presence of non-minimal couplings, this is no longer true in the Jordan frame. In the context of general theory of relativity, the metric formalism coincides with the one of Palatini, as minimizing the Einstein-Hilbert action with respect to the connection uniquely fixes it to be of the Levi-Civita form, $\Gamma = \Gamma(g_{\mu\nu})$. In more general models, however, especially in the ones involving matter fields that are non-minimally coupled to gravity, these two formalisms lead to two inherently different gravitational theories [10, 85, 199]. This means that inflationary models with non-minimal couplings to gravity cannot be characterized just by the inflaton field potential, but that the connection must also be specified. This was originally studied in [200–202], and has recently gained increasing attention, see [52, 84, 203–209]. A non-minimally coupled scalar field model in the Jordan frame with Palatini gravity, when mapped to the Einstein frame, can be written as Einstein gravity where the fields are uncoupled from the Ricci scalar. This means instead of studying Einstein of Palatini with non-minimally coupled fields in the Jordan frame, we can study uncoupled fields in the Einstein frame. The field-space metric in the action in Eqn. (7.8) can be written for both theories as

$$G_{IJ} = \Omega^{-1} \delta_{IJ} + \frac{3}{2} \nu M_{\rm pl}^2 \Omega^{-2} \frac{d\Omega}{d\phi^I} \frac{d\Omega}{d\phi^J} \,, \tag{7.11}$$

with $\nu = 1$ in the metric case and $\nu = 0$ in the Palatini case. With this conformal transformation, we have therefore transferred the dependence on the choice of gravitational theory (choice of gravitational degrees of freedom) from the connection to the field-space metric.

7.3. Multifield Attractors

In previous studies, [84], comparing the consequences of inflation in both the metric and the Palatini case, it was shown that the attractor behaviour is not recovered when the underlying theory of gravity is Palatini. At large values of ξ_I the results for the metric case asymptote to those of Starobinsky inflation [20]

$$\begin{aligned} n_s^{\rm M} &\simeq 1 - \frac{2}{N}, \\ r^{\rm M} &\simeq \frac{12}{N^2}, \end{aligned} \tag{7.12}$$

while those for Palatini do not. The Palatini case approaches vanishing r at strong coupling and observable quantities asymptote to,

$$\begin{aligned} n_s^{\rm P} &\simeq 1 - \left(1 + \frac{n}{2}\right) \frac{1}{N}\,, \\ r^{\rm P} &\simeq 0\,. \end{aligned} \tag{7.13}$$

We wish to generalize the analysis of non-minimally coupled models in both of the above formulations of gravity to the case of multifield inflation, where there is more than one field taking part in inflationary dynamics, and to study attractor behaviour in this case.

In the following, we will analyse inflation in both cases, metric and Palatini. For simplicity, we start by studying two-field models with the potential

$$U(\phi,\sigma) = \lambda_\phi^{(2n)} M_{\rm P}^{4-2n} \phi^{2n} + \lambda_\sigma^{(2n)} M_{\rm P}^{4-2n} \sigma^{2n}, \tag{7.14}$$

where $n > 0$, $\lambda_\phi^{(2n)}$ and $\lambda_\sigma^{(2n)}$ are dimensionless coupling constants, and $M_{\rm P}^{4-2n}$ has been introduced to have a scalar potential with a mass dimension equal to four. Later on, in Sec. (7.4.2), we will also discuss the case where more than two fields take part in inflationary dynamics. In metric gravity, the above models are cosmological attractors, i.e., their predictions for observables asymptote to those of R^2 or Starobinsky inflation in the limit of strong non-minimal coupling ξ, see Eqn. (7.12). This is, however, known not to be true for the single-field case in the Palatini scenario [84], and here we will test it also in a multifield case.

For the potential (7.14), the Einstein frame potential is

$$V(\phi,\sigma) = \Omega(\phi,\sigma)^{-2} U(\phi,\sigma) = \frac{\lambda_\phi^{(2n)} M_{\rm P}^{4-2n} \phi^{2n} + \lambda_\sigma^{(2n)} M_{\rm P}^{4-2n} \sigma^{2n}}{\left(1 + \xi_\phi^{(n)} \left(\frac{\phi}{M_{\rm P}}\right)^n + \xi_\sigma^{(n)} \left(\frac{\sigma}{M_{\rm P}}\right)^n\right)^2}\,. \tag{7.15}$$

For this and all other models in this formulation, the potential V is the same for both metric and Palatini gravity. The major difference between the two is the Einstein frame field-space metric, G_{IJ}, in Eqn. (7.11). We will therefore focus

mostly on the parameters appearing in G_{IJ} in our analysis, namely the non-minimal couplings, $\xi_I^{(n)}$.

7.3.1. Numerical Set-up

For a given sets of model parameters, we explore the initial condition space by first calculating an approximate position in field-space corresponding to 73 e-folds before the end of inflation[1]. Before sampling, we transform our fields to polar form. Then we sample an angle from a uniform distribution. Following that we incrementally increase the radial distance from the minimum until a coordinate in field space is found for which inflation lasts 73 e-folds. Sampling over the full distribution of angles would reveal an approximate 73 e-folds surface in the field space. Next we transform our fields back to their Cartesian form and numerically evolve the background equations forward in time until the end of inflation. This provides a set of evolutions of roughly 73 e-folds. For each set of model parameters the process is repeated with a new random angle. Finally, we evaluate the observables of interest – n_s, r and $f_{\rm NL}$ as defined in Eqs. (2.144)–(2.147) – at the scale which left the horizon 60 e-folds before the end of inflation. We repeat this procedure for a representative set of values of the model parameters focusing mostly on the effect of the non-minimal couplings, ξ_I.

Already at the background level, the evolution is different between metric and Palatini gravity. We can clearly see this in Fig. (7.1), which shows the initial conditions corresponding to 73 e-folds of inflation for both metric and Palatini gravity, with varying strengths of the non-minimal couplings. For Palatini gravity, the initial condition surface is independent of the value of the non-minimal coupling for nearly all cases, while for metric gravity the distance from the origin decreases with ξ_I regardless of the value of n.

One can understand this by using the slow-roll approximation where inflation is sustained while the slow-roll parameter ϵ from Eqn. (2.34) and it's time derivative η from Eqn. (2.35) are small for a sufficiently long period. We also assume that the background trajectories are approximately radial. Writing the fields in polar coordinates as

$$\phi = \rho\cos\psi\,, \quad \sigma = \rho\sin\psi\,, \tag{7.16}$$

the number of e-folds can be approximated by

$$N \approx \int_{\rho_e}^{\rho_i} \frac{V}{V_{,\rho}} G_{\rho\rho}\mathrm{d}\rho\,, \tag{7.17}$$

in which we use the notation $V_{,\rho}$ for a derivative in the direction of the radial coordinate ρ. All of the quantities in the integrand above can be calculated straight-

[1]The number $N = 73$ is chosen to start the evolution so that the modes which cross the horizon 60 e-folds before the end of inflation are accurately evolved in the sub-horizon stage.

forwardly, given the field-space metric and the Einstein frame potential. To further simplify the notation, we also write the non-minimal couplings in polar coordinates as

$$\xi_\phi = \xi \cos\theta\,, \quad \xi_\sigma = \xi \sin\theta\,. \tag{7.18}$$

For Palatini gravity where $G_{\rho,\rho} = \Omega^{-1}(\rho,\psi)$, due to a cancelation of ξ depdendent terms in the denominator of Eqn. (7.17), the result is independent of ξ and given by

$$N \approx \frac{\rho_{\rm i}^2 - \rho_{\rm e}^2}{4nM_{\rm P}^2}\,, \tag{7.19}$$

in which $\rho_{\rm i}$ is the value of ρ when the mode of interest exists the horizon and $\rho_{\rm e}$ is the value at the end of inflation. Interestingly, this is exactly the same result as for $\xi = 0$, which is why the initial conditions for the Palatini case coincide with those for the metric case at low ξ. For metric gravity and large values of ξ, the leading order term in the expansion in ξ^{-1} is

$$N \approx \xi F_n(\psi,\theta)\frac{\rho_{\rm i}^n - \rho_{\rm e}^n}{M_{\rm P}^n}\,, \tag{7.20}$$

which shows that to keep the number of e-folds constant, one requires smaller $\rho_{\rm i}$ for larger ξ, as indeed is the case in Fig. (7.1). The function $F_n(\psi,\theta)$ simplifies to the single-field result when $\psi = \theta = 0$ or $\psi = \theta = \pi/2$, which, for $n = 2$, is $F_2(0,0) = 3/4$, matching the result in Ref. [200].

We see that this approximation works generically very well, except when the parameter ratio is large in certain directions in the field-space. This is because the approximation of radial trajectories fails in those cases, rendering the above approximate result inapplicable. This emphasizes the importance of accurate numerical analysis of multifield models, to which we now turn.

7.4. Monte Carlo Method Results

We study the cases for which $n = (1/2, 1, 3/2, 2)$ in Eqs. (7.6) and (7.14). We show the results for n_s and r in Fig. (7.2) using `PyTransport 2.0`. We see here a clear difference between the formulations of gravity at large values of ξ_I asymptoting to the single-field case [84]. However, we find that in the Palatini case the results converge to a non-zero value of $f_{\rm NL}$, is different from that of the metric case. The results are shown in Figs. (7.3) and (7.4) along with lines corresponding to the Maldacena's consistency relation from Eqn. (4.40) [106] for the single-field case[2].

[2] One expects Maldacena's relation to hold for squeezed configurations of the reduced bispectrum, while here we are plotting the reduced bispectrum in the equilateral limit. However, in canonical single-field models in which $\epsilon \ll \eta$, which is the case for the single-field limit here, the bispectrum is very close to local and the reduced bispectrum is almost the same in all configurations. This

We see that the values of $f_{\rm NL}$ converge to the single-field result at strong coupling for both Palatini and metric gravity, confirming the general trend that the multifield results mimic those of the single-field case in the strong coupling limit.

We see that all multifield models considered reduce to an effective single-field model at the limit of strong coupling. In the metric case this generalizes the earlier findings in the literature[3], whereas in the Palatini case the results are entirely new. We elaborate on the reason for this behaviour in the next subsection. However, we stress that the scenario was not constructed to obtain an α-attractor model but it emerges naturally from the Jordan frame action (7.5), which is our starting point.

Also, note that if one considered a scenario in which the Jordan frame action included non-canonical kinetic terms of a specific kind, one would get the same result as in the present case where the kinetic terms are canonical in the Jordan frame but where the conformal transformation and the resulting kinetic terms in the Einstein frame depend upon the assumed gravitational degrees of freedom. For example, the models that we consider in the Palatini formalism are equivalent to non-canonical scalar-tensor theories in the metric formalism [211]. However, non-minimal couplings to gravity should be seen not as an *ad-hoc* addition to inflationary models but as a generic ingredient of coherent model frameworks, generated by quantum corrections in a curved space-time. It is by this notion that one can say that the differences observed between the cases which we call 'metric' and 'Palatini' are indeed in the underlying theory of gravity, i.e., whether the space-time connection was determined by the metric only, or both the metric and the inflaton field(s). Our study therefore reveals an interesting subtlety in a broad class of models where the scalar potential is multidimensional and the fields are non-minimally coupled to gravity.

Alternatively, one can view this work as a more detailed way to answer the question 'What are the predictions of a given model of inflation?'. As shown, they clearly depend on the choice of the gravitational degrees of freedom, even though usually such a choice is not considered to be part of models of inflation. It is therefore important to investigate all possibilities concerning the physics at high energies, as one cannot distinguish between the metric and Palatini formalisms at late times. Detailed studies of non-minimally coupled models are therefore interesting not only from the inflationary point of view, but also because they may provide for a way to distinguish between different formulations of gravity.

7.4.1. Multifield Effects

Having discussed the general trends in the previous sections, we now discuss some of the effects of having multiple fields. The first effect we study is the dependence

is why our plot for $f_{\rm NL}$ against n_s follows so closely the Maldacena relation.

[3] Outside the context of inflation, similar single-field behaviour has been found in other scenarios with non-minimally coupled multifield models [210].

on the hierarchy between the values for the non-minimal couplings. In order to do that, we use the polar coordinates in parameter space introduced in Eqn. (7.18) and test the evolution of the observables depending on θ.

We see in Fig. (7.5) that the results depend crucially on the ratio of the parameters in the potential, λ_I. When the parameters for both fields are similar, the observables quickly approach a single limiting value corresponding to the single-field case, while for the larger λ_I ratio the predictions are substantially broadened throughout the entire ξ range, with a clear dependence on the angular parameter θ. The trajectories in (n_s, r) space as a function of ξ are also broadened, as is also clear in Fig. (7.2). The predictions are thus somewhat different from the single-field case for low and intermediate values of ξ, but converge to the same limit for sufficiently large ξ.

Having now analysed the dependence on both ξ and θ, we confirm that the results resemble the single-field case for both metric and Palatini gravity. The differences between single-field and multifield that do arise are apparent in the spread in the results for low values of ξ. This spread is due to a larger dependence on the initial conditions of the fields and on the direction in ξ_I parameter space. At strong coupling, all the results found asymptote to the single-field ones. This similarity may be somewhat surprising, given that in the multifield case the field-space can be curved. We now show the reasons why this additional multifield effect is not affecting the results at strong coupling.

We first note that field-space curvature does not directly affect the evolution of the field fluctuations in the inflationary direction. This is because the field-space Riemann tensor appears in the effective mass matrix of the fluctuations, m_L^I, in the following term

$$m_L^I \supset R^I_{JKL}\dot{\phi^J}\dot{\phi^K}\,. \tag{7.21}$$

To obtain the term relevant for the fluctuations in the inflationary direction, one must multiply m_L^I with $\dot{\phi^L}$, which always results in zero for the term shown above, given the symmetries of the Riemann tensor.

We specify to the case of a two-dimensional field space, although the analysis can in principle be generalized to arbitrarily many fields. As mentioned above, we introduce the adiabatic and entropic fluctuations, respectively defined by $Q_\sigma \equiv e_{\sigma I}Q^I$ and $Q_s \equiv e_{sI}Q^I$. On super-Hubble scales, one can deduce from extracting the equation of motion for the linear fluctuations from Eqn. (3.24) (in Fourier space),

$$D_t^2 Q^I + 3HD_tQ^I + \frac{k^2}{a^2}Q^I + m_{IJ}Q^J = 0\,, \tag{7.22}$$

(see section (8.4.2) for details) that Q_s satisfies the following equation of motion,

$$\ddot{Q}_s + 3H\dot{Q}_s + m^2_{s\,(\mathrm{eff})}Q_s \approx 0\,, \tag{7.23}$$

where $m^2_{s\,(\mathrm{eff})}$ is a super-Hubble effective mass for entropic fluctuations such that

$$\frac{m^2_{s(eff)}}{H^2} = \frac{V_{;ss}}{H^2} + 3\eta_\perp^2 + \epsilon R_{\mathrm{fs}} M^2_{\mathrm{pl}}\,, \tag{7.24}$$

in which

$$\eta_\perp = V_{,s}/H\dot{\phi}\,. \tag{7.25}$$

Here $V_{;ss} \equiv e^I_s e^J_s V_{;IJ}$ is the projection of the Hessian matrix along the entropic direction, $\eta_\perp$ has been defined in Eqn. (7.25) and is a measure of the bending of the trajectory, $\dot{\phi} = \sqrt{G_{IJ}\dot{\phi}^I\dot{\phi}^J}$, s is the field coordinate in the entropic direction — the direction perpendicular to $\dot{\phi}^I$ — and R_{fs} is the Ricci scalar of the field-space manifold. There is, however, an effect on the entropy perturbations, as they are sensitive to the perpendicular projection of the effective mass matrix.
The effect of the curvature is somewhat less relevant if R_{fs} is positive, as it simply contributes to a smaller amplitude of the entropy perturbations. If it is negative, however, it reduces the effective mass and may even render it tachyonic should it be large enough [212], thus dangerously enhancing the entropy fluctuations. Our numerical results seem to indicate that this never occurs, given their similarity with the single-field results, for which the curvature is not present. We can verify this by checking whether the condition $m_s^2 > 0$ is always verified in our numerical results. We can see this in Fig. (7.6), in which we show that the effective mass is always positive for all values of n studied above. When ξ is large, the effective mass is also large, with the dominant contribution coming from the first term on the right hand side of Eqn. (7.24), the Hessian of the potential. Specifically, the effective mass values calculated in the metric and Palatini cases are equivalent for small ξ and consequently the resulting observables (n_s, r and f_{NL}) are affected in similar ways in both cases. Where the observables deviate between the two cases, i.e. for large ξ, the effective masses also deviate with an overall larger effective mass in the metric case.

The evolution of the entropy modes is independent of the adiabatic modes on large scales, and thus only depends on the effective mass. They can, however, source curvature perturbations via the bending parameter $\eta_\perp$ in the equation [38, 113, 213]

$$\dot{\zeta} \approx \sqrt{2} H \eta_\perp \frac{H}{M_{\mathrm{P}}\sqrt{\epsilon}} \frac{Q_s}{H}\,, \tag{7.26}$$

with Q_s the fluctuations in the entropic direction. Thus, we can recover the single-field results if $\eta_\perp$ is sufficiently small. We can estimate the entropy fluctuations via their variance $Q_s \sim H^2/m_s$. Furthermore, we note that $H/\left(M_{\mathrm{P}}\sqrt{\epsilon}\right)$ is approximately the value of ζ at horizon crossing, ζ_*, and that the typical time scale associated to its variation is H, making $H\zeta_*$ the natural size of $\dot{\zeta}$, should it vary considerably.

Given these arguments, we can rewrite Eqn. (7.26) as

$$\frac{\dot{\zeta}}{H\zeta_*} \sim \frac{\eta_\perp H}{m_s}\,, \tag{7.27}$$

and conclude that if the the right-hand-side of Eqn. (7.27) is much smaller than 1, the evolution of ζ is negligible. Therefore, to determine the importance of entropy fluctuations in the evolution of adiabatic ones, we must only calculate $\eta_\perp H/m_s$. In the right panel of Fig. (7.6), we show the size of $\eta_\perp^2$ during inflation. Comparison with the effective mass shown in the left panel demonstrates that the bending parameter is sub-dominant relative to the effective mass. For example, for the $n = 1$ metric case the ratio $\eta_\perp^2 H^2/m_s^2 \sim 10^{-3}$ when ξ is small and for large ξ, $\eta_\perp^2 H^2/m_s^2 \sim 10^{-8}$, demonstrating that the entropy fluctuations are negligible at strong coupling. Comparing the metric and Palatini case for small ξ we see that the results for the evolution of $\eta_\perp$ are the same. For large ξ, the evolutions diverge and $\eta_\perp$ in the metric case decays, while it grows in the Palatini case.

7.4.2. Extension to Scenarios with Higher Number of Fields

We have also extended our calculations to the three-field case for n_s and r. We found that the results resemble those for the two-field case, converging to the same limit in the strong coupling approximation for both metric and Palatini gravity. This can be seen in Fig. (7.7). The main difference is the spread in observable space, which is substantially larger than in the two-field case. This is a consequence of the increased number of possible background field trajectories that result in successful inflation in higher field-space dimensions as well as the larger number of free parameters. This can affect the ability of distinguishing between different models, with some results for the Palatini model giving the same observables as those for the metric case, even at strong coupling for the latter. The strongly coupled Palatini case is still distinctive, given its very low tensor-to-scalar ratio prediction.

With an even larger number of fields, these predictions are expected to broaden further, but may ultimately converge again, in a statistical sense, as such a behaviour has been demonstrated in other scenarios with random potentials and very large numbers of fields [72, 214–218].

7.5. Discussion

In this chapter we studied the multifield models of inflation non-minimally coupled to gravity, for Einstein's metric gravity and Palatini gravity. We primarily examined two field models. By examining the evolution of the entropic modes, we have shown that the multifield effects, sourced by the bending term $\eta_\perp$, diminishes with large couplings ξ. This mean we effectively recovered the single-field results for n_s and r

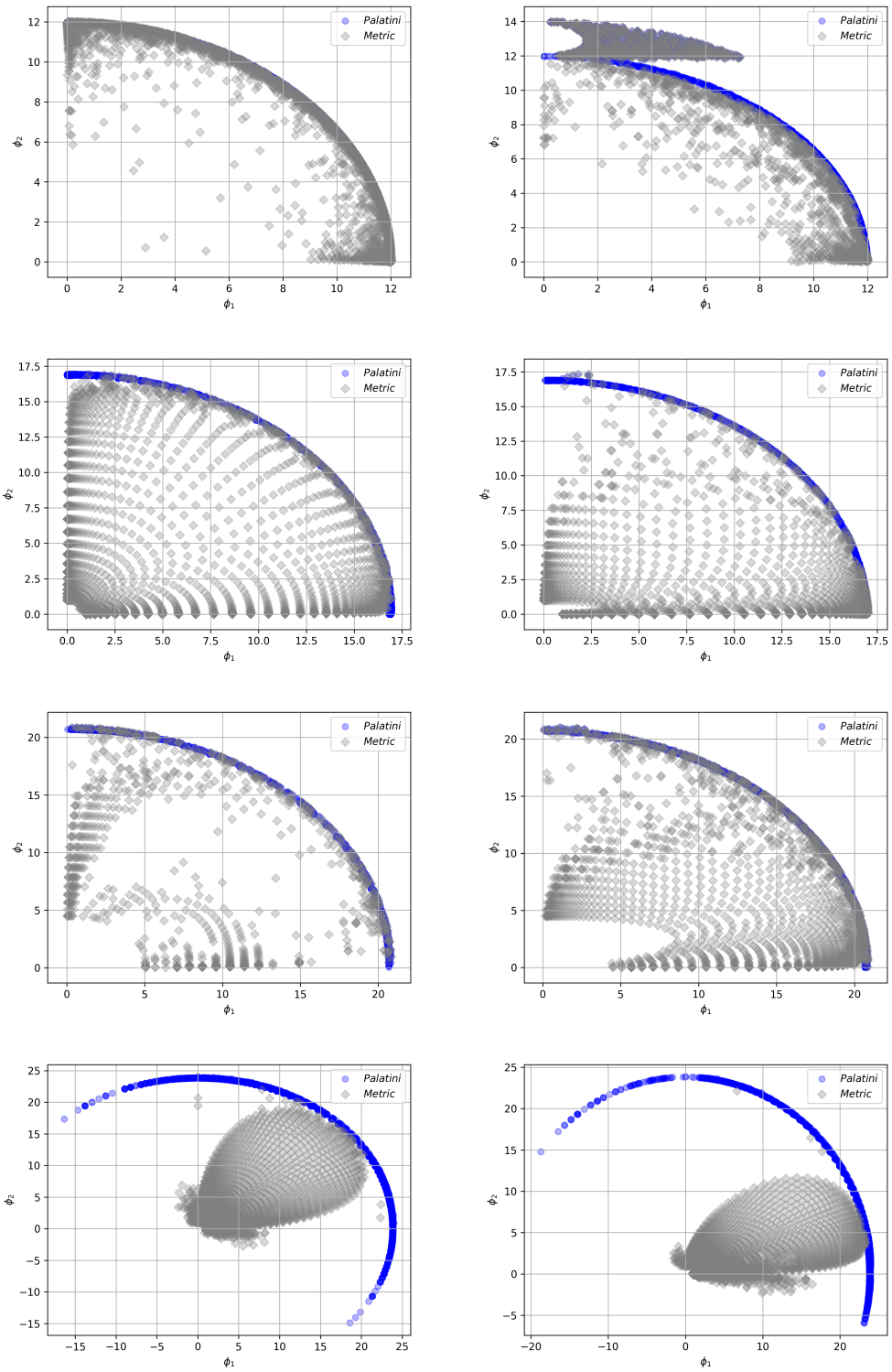

Figure 7.1.: *Sampling of initial conditions for metric (grey) and Palatini gravity (blue),* $n = (1/2, 1, 3/2, 2)$ *from top to bottom. The left and right panels show the scenarios for different parameter ratios:* $\lambda_\sigma/\lambda_\phi = 19/14$ *(left) and* $\lambda_\sigma/\lambda_\phi = 95/14$ *(right). In all cases* ξ *is varied between* $(10^{-3}, 10)$.

in the limit of large ξ and the observe the same attractor behaviour for each case of the gravity formulation. We extended this to three field models and have observed the same convergence on single-field results.

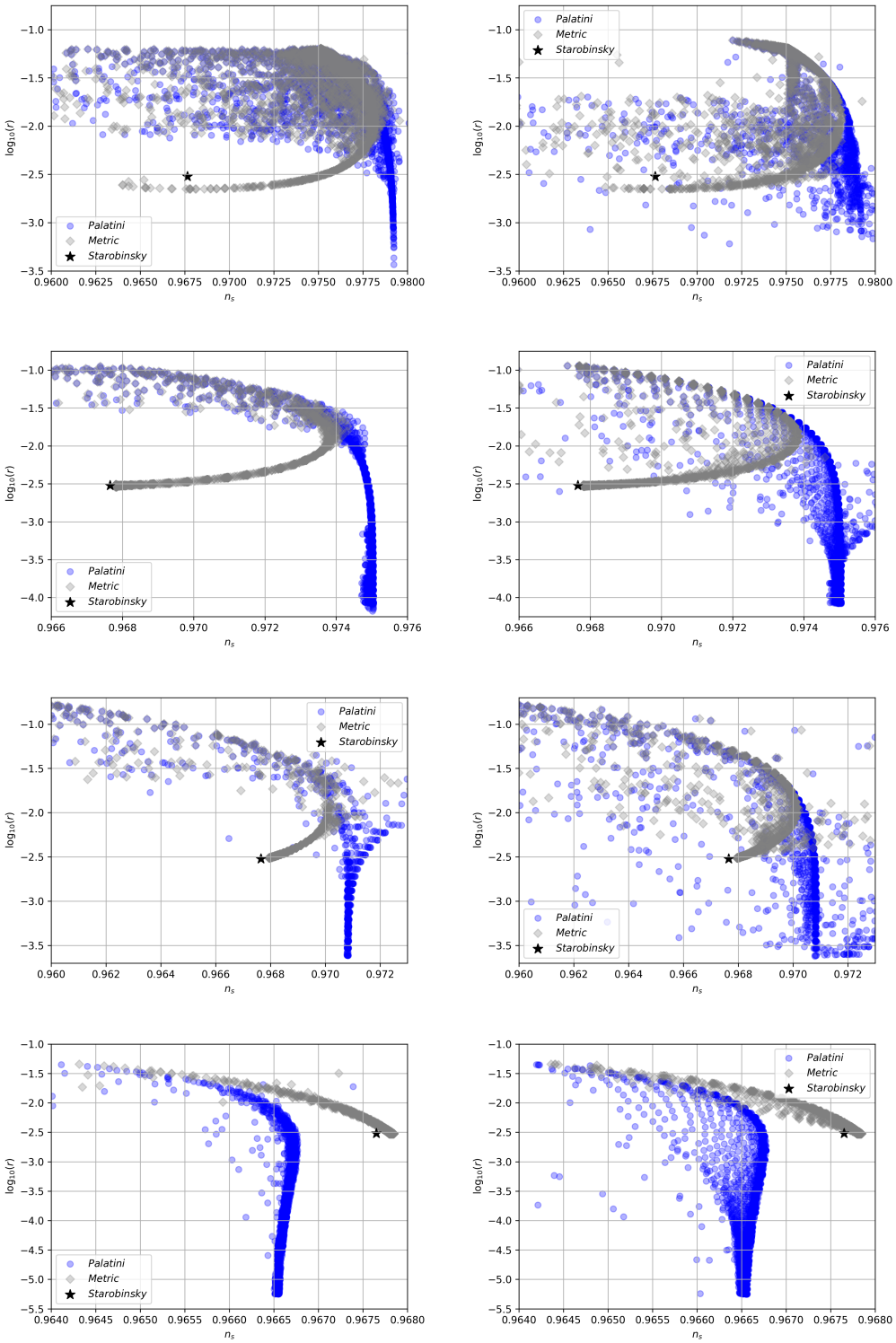

Figure 7.2.: *Predictions for n_s and r in metric (grey) and Palatini gravity (blue). The panels are the same as in Fig.* (7.1).

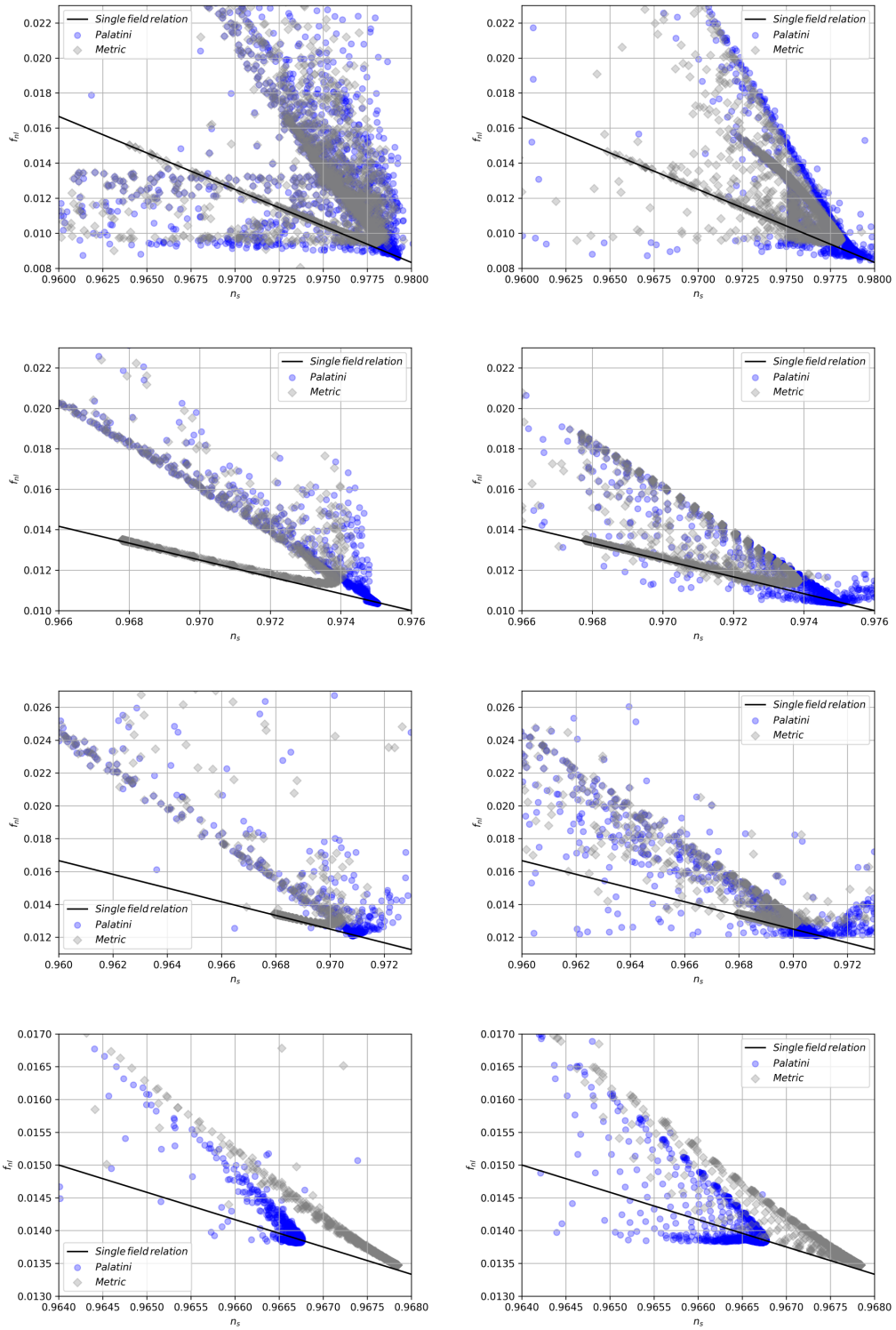

Figure 7.3.: *Predictions for n_s and $f_{\rm NL}$ in metric (grey) and Palatini gravity (blue). The panels are the same as in Fig.* (7.1).

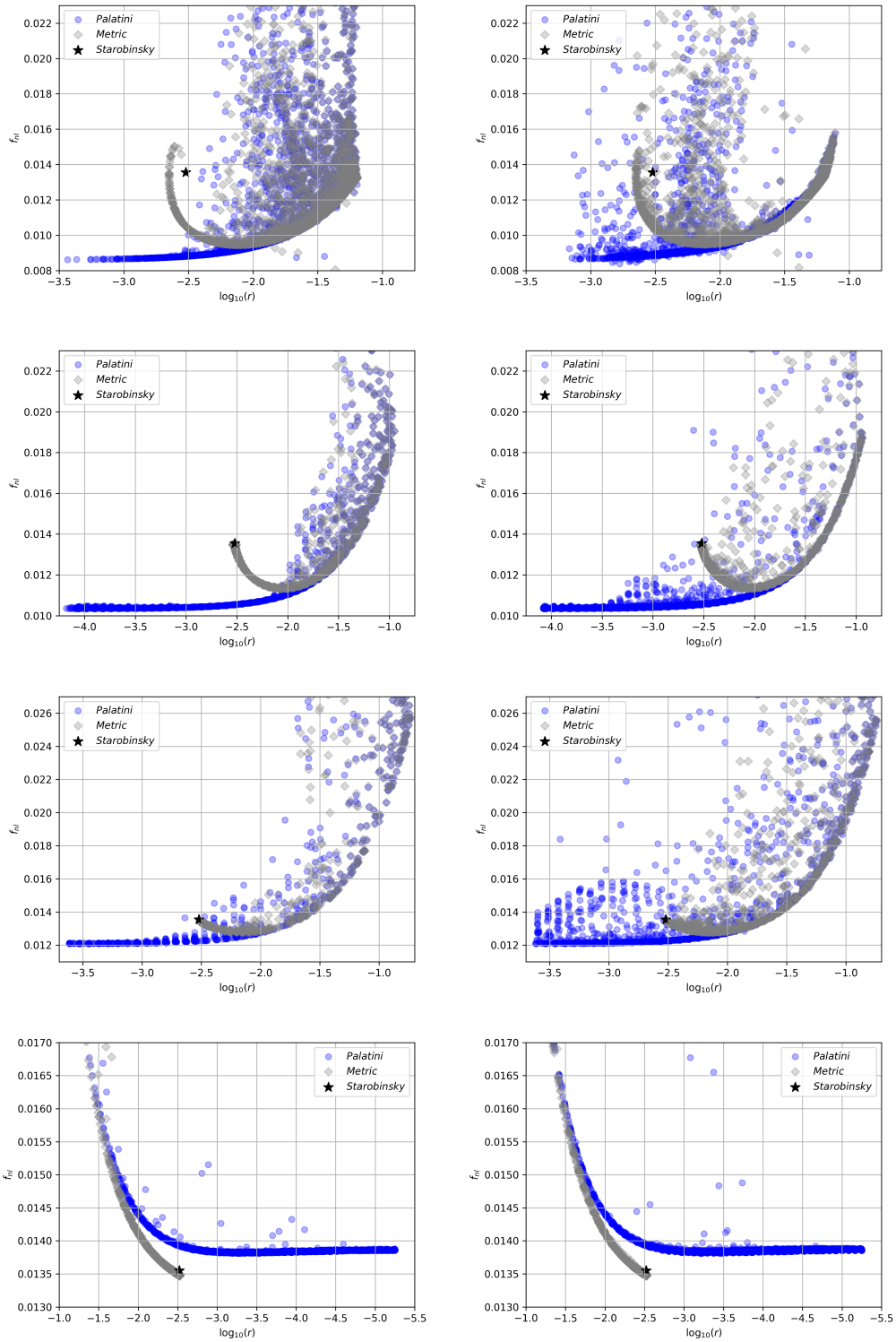

Figure 7.4.: *Predictions for r and $f_{\rm NL}$ in metric (grey) and Palatini gravity (blue). The panels are the same as in Fig.* (7.1).

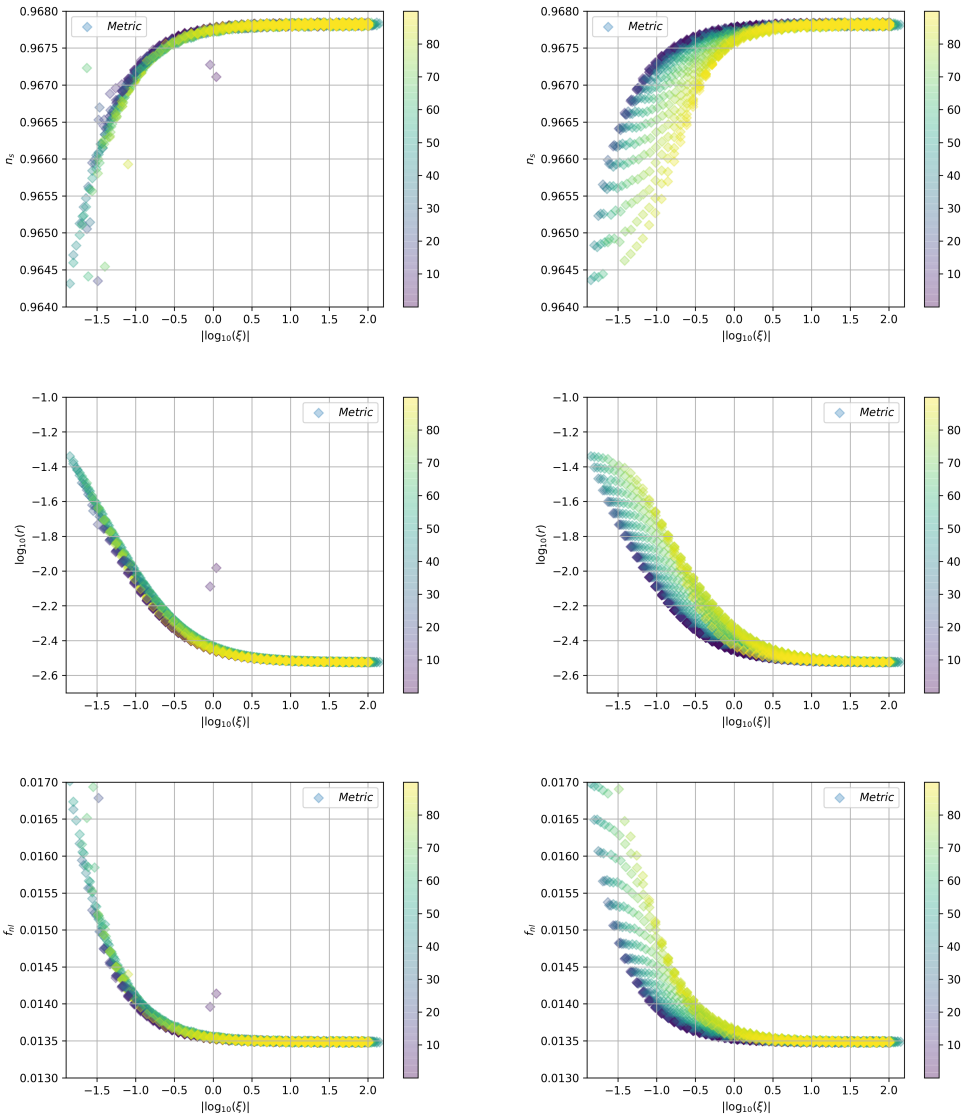

Figure 7.5.: *Predictions for n_s (top) r (middle) and $f_{\rm NL}$ (bottom) as a function of ξ along the x-axis and $\theta = \tan^{-1}(\xi_\sigma/\xi_\phi)$ (illustrated by the color gradient in degrees) in metric gravity for $n = 2$ and for the same $\lambda_\sigma/\lambda_\phi$ ratios as in Fig. (7.1).*

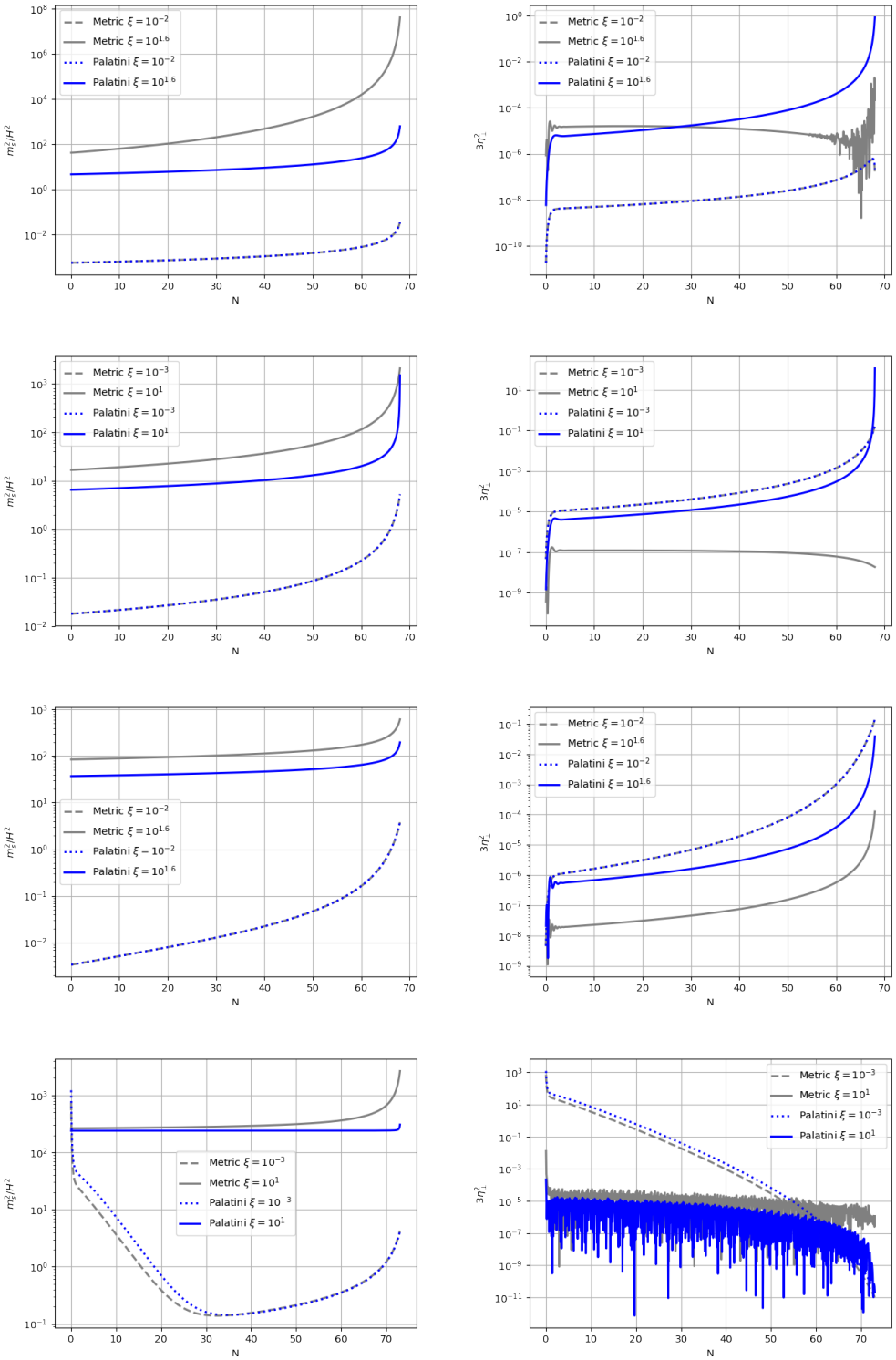

Figure 7.6.: *Evolution of the effective mass normalized to H and bending parameter $\eta_\perp^2$ for metric (grey) and Palatini gravity (blue), $n = (1/2, 1, 3/2, 2)$ from top to bottom. The dashed lines represent a sample with a small magnitude of the coupling parameters ξ whereas the solid lines represents one with a large coupling.*

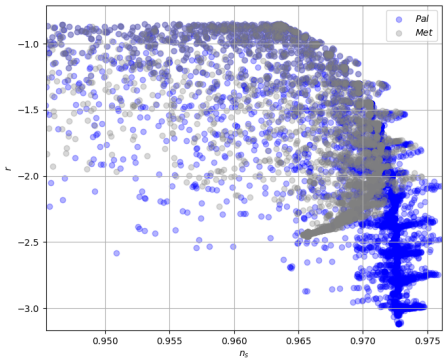

Figure 7.7.: *Predictions for n_s and r in metric (grey) and Palatini gravity (blue) for three fields.*

8. Sidetracked Inflation

In this chapter we study a class of models where the inflaton is coupled to a heavy scalar field and can initially undergo geometrical destabilization [212] and then drive a second phase of inflation dubbed sidetracked inflation. These models have the common feature of a negative field-space curvature. In Sec. (8.2) we explain our implementation of the sidetracked inflation scenario, including the way we reach this attractor phase from a heuristic modeling of the geometrical destabilization that precedes the second inflationary phase. We study in Sec. (8.3) the background dynamics of the sidetracked phase, before devoting Sec. (8.4) to a detailed study of the properties of linear cosmological fluctuations. We show how single-field effective theories for the fluctuations can reproduce with a good accuracy the exact results from numerical computations in the full two-field system, and give results for the tensor-to-scalar ratio r and spectral index n_s of the curvature power spectrum computed for each model. Similarly in Sec. (8.5) we give numerical results from the full two-field picture concerning the primordial bispectrum. Finally discuss the relationship between the class of models that we analyze and the models of α-attractors in Sec. (8.7).

8.1. Introduction

Multifield inflation provides an extension of the minimal single-field inflationary paradigm that is most natural from a theoretical point of view. Multiple scalars are generically present in most top-down scenarios of the very early universe, including constructions in the contexts of string theory [219], supergravity [220], and other theories beyond the Standard Model [221]. Nevertheless, in view of the spectacular agreement of the predictions of slow-roll single-field inflation with experimental data [46], it is commonly argued that the additional fields must be very heavy, with masses parametrically larger than the inflationary Hubble scale H, and should therefore play no important role in the cosmological dynamics. A more precise statement is that these "spectator" fields can be integrated out to yield an effectively single-field description that is valid throughout the epoch of inflation [127, 132, 222], and hence one may expect the heavy scalars to affect inflation only indirectly through

the renormalization of operators controlling the dynamics of the inflaton.

Recently, however, it has been shown that heavy scalar fields with bare masses $m_h^2 \gg H^2$ can undergo, under very general conditions, a tachyonic-like instability induced by kinetic couplings with the inflaton, as one generically has in nonlinear sigma models. This has been named *the geometrical destabilization* of inflation [212]. It is akin to the instability that arises in models of hybrid inflation [223] where the heavy scalars become tachyonic as a result of their coupling to the inflaton at the level of the potential. The geometrical destabilization on the other hand is triggered by the rolling of the inflaton in a negatively curved internal field space, and may take place well before any potential-driven "waterfalls" along the inflationary trajectory.

If the geometrical destabilization does occur, its outcome is quite uncertain. Standard perturbation theory breaks down at the onset of the instability and the vacuum state that describes inflation can no longer be trusted. Nevertheless, on physical grounds we may expect either of two things to happen depending on the interactions and the scales involved. The first possibility is that the universe becomes dominated by inhomogeneities and that inflation ends prematurely, that is at a time much before the end of the slow-roll phase as it would have happened in the absence of any instability. The consequence is that cosmological modes that are observable through cosmic microwave background (CMB) and large scale structure data probe a different part of the inflaton potential, leading to modifications to their correlation functions and the corresponding predictions for the cosmological parameters of interest. This scenario was analyzed in reference [224] for a large class of inflationary models using Bayesian techniques, and it was quantified how such a premature end of inflation results in sizable changes to the constraints on theoretical models from experimental data.

The second possible outcome is that the exponential growth of the unstable fields drives the system to a new inflationary vacuum. Thus, in this set-up, the universe undergoes a second phase of inflation in which one (or more) of the heavy scalars evolves along a path away from its ground state. We dub this scenario *sidetracked inflation*, owing to the way the geometric destabilization causes the field-space trajectory to divert from its original, effectively single-field path (see fig. (8.1)). It is our objective to perform an analysis of the dynamics and properties of sidetracked inflation, with a focus on its peculiar multifield effects on the power spectrum and primordial non-Gaussianities.

This picture obviously glosses over the details related to the physics of the instability, which as explained lie beyond the reach of perturbative field theory. It is motivated however by the fact that, at least in a large number of cases, the equations of motion indeed admit a nontrivial time-dependent attractor away from the inflationary valley of the potential, as we have investigated with a broad class of two-field models. Thus, provided inflation does not abruptly end as described above in the

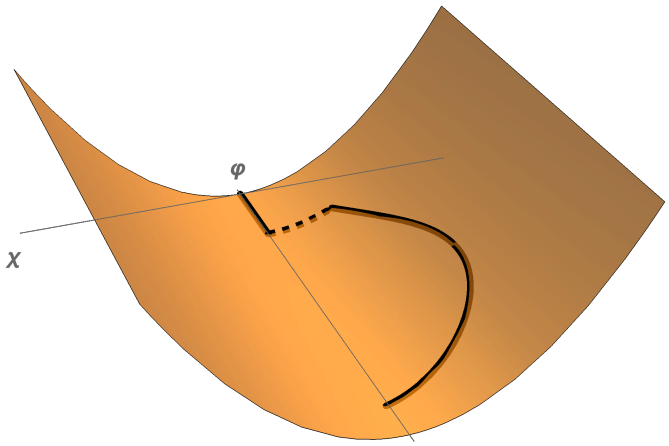

Figure 8.1.: *Schematic plot of the field-space trajectory in sidetracked inflation. The field φ corresponds to the inflaton and χ is the heavy field that becomes unstable. The dashed line represents the instability phase where the classical field picture is lost. The orange surface represents the potential. The information on the field space geometry is not represented.*

first scenario, it is natural to expect that the unstable system will eventually settle into this attractor and give rise to another phase of inflation. We will see that this second phase features some very interesting dynamics: it can last extremely long, as the increase in the value of the non-canonical kinetic term of the inflaton translates into an effective flattening of the potential; its path in the internal field space can deviate very strongly from a geodesic; and multifield effects are very important.

In particular, we show that the dynamics of linear cosmological fluctuations can be effectively described by a single-field effective theory, that is characterized, depending on the field space manifold and the potential that is considered, by a modified dispersion relation, a reduced speed of sound, or an imaginary one, describing a transient tachyonic instability. The bispectrum is generically large in these models, with shapes that can be of equilateral but also of orthogonal type, in particular in models with hyperbolic field spaces and that feature an effective imaginary speed of sound.

Hyperbolic field space geometry is an essential aspect of so-called cosmological attractors—inflationary models whose predictions are insensitive to the form of the inflaton potential [190, 192, 225]. It has been explained that this universality stems from the presence of a pole in the kinetic term of the inflaton [194, 226], which translates into an exponential flattening of the potential upon canonical normalization. It is thus natural to ask whether the geometrical destabilization and sidetracked inflation could be relevant for such theories and possibly hinder some of their successful features. We will show however that, on closer inspection, our models present a subtle but crucial difference with cosmological attractors, to do with the fact that in our case it is both the kinetic term *and* the potential that exhibit a pole (in a

suitable parametrization). This possibility appears to have been overlooked perhaps because it doesn't arise in the single-field context where a singular potential would be unnatural, but we will argue that it can be perfectly generic within multifield scenarios.

We consider nonlinear sigma models for a set of scalar fields ϕ^I minimally coupled to gravity,

$$S = \int d^4x\sqrt{-g}\left[\frac{1}{2}R(g) - \frac{1}{2}G_{IJ}(\phi)\nabla^\mu\phi^I\nabla_\mu\phi^J - V(\phi)\right]. \tag{8.1}$$

8.2. Formalism and Setup

8.2.1. Geometrical Destabilization and Sidetracked Inflation

We now review the mechanism behind the geometrical destabilization uncovered in [212], and our implementation of the sidetracked inflation scenario that we described qualitatively in section (8.1). The crucial observation is that $m^2_{s\,(\mathrm{eff})}$ from Eqn. (7.24) can become negative, for realistic values of the scales involved, whenever the field space manifold is negatively curved.

This can be made more explicit by considering the following scenario, which is the one we will focus on in the remainder of the chapter. Assume a model with two scalar fields: an inflaton φ that initially drives inflation in a standard slow-roll fashion, and a spectator field χ with a large bare mass m_h sitting at the bottom of the potential valley at $\chi = 0$, corresponding to a field space geodesic. Thus, at this stage, we have $V_{;ss} = m_h^2$ and $\eta_\perp = 0$. We define the curvature scale M of the field space manifold in such a way that $R_{\mathrm{fs}} = -4/M^2$ when restricted to the $\chi = 0$ line (or exactly if the space has constant curvature).[1] During this "primary" inflationary phase Eqn. (7.24) becomes

$$\frac{m^2_{s\,(\mathrm{eff})}}{H^2} = \frac{m_h^2}{H^2} - 4\epsilon\,\frac{M_{\mathrm{Pl}}^2}{M^2}\,, \tag{8.2}$$

which implies that the super-Hubble entropic perturbation Q_s becomes tachyonic, and therefore the instability of the background, at a critical time $N = N_c$ when the slow-roll parameter ϵ reaches the value

$$\epsilon_c = \frac{M^2}{4M_{\mathrm{Pl}}^2}\,\frac{m_h^2}{H_c^2}\,, \tag{8.3}$$

and with $H_c = H(N_c)$. Notice that even though H decreases during inflation, ϵ typically grows at a faster rate during a slow-roll regime,[2] and therefore the insta-

[1] This assumes, as we will do, that the internal metric depends only on χ. We will further comment on this point later.

[2] More precisely, a necessary condition for the geometrical destabilization to occur in this setup

bility can be quite generic for reasonable values of m_h and M. Taking for instance $m_h \sim 10H \sim 10H_c$ and $M \sim M_{\rm GUT} \sim 10^{-3}\, M_P$ one has $\epsilon_c \ll 1$, and hence the instability can take place well before the end of inflation as it would occur in a single-field context.

As explained in [212] and above in section (8.1), what happens after the geometrical destabilization is so far highly uncertain, and very likely model-dependent anyway. It therefore makes sense, as a first step towards a more thorough understanding of the physics involved, to adopt a specific outcome as a working assumption and study its consequences for a broad and generic class of models. This is what we do in this work for the situation where inflation doesn't end as a result of the instability (the case studied in [224]), but instead continues along a "sidetracked" trajectory away from the bottom of the potential valley at $\chi = 0$.

Our modeling of the sidetracked inflation scenario will be as a two-step process (see fig. (8.1)). The system is assumed to start in the standard inflationary vacuum, with $\chi = 0$ and a slowly rolling inflaton φ. At the critical time of the instability, defined by Eqn. (8.3), we displace the heavy field by an amount $\chi_c \equiv H_c/2\pi$, which is a typical value for the amplitude of quantum fluctuations in a massless field. Together with the inflaton field's amplitude φ_c (and its derivative) at the time N_c, this provides the initial conditions for the second phase of inflation. The latter then ends in a standard manner through slow-roll violation defined by the condition $\epsilon = 1$.

This is admittedly a very blurry picture of the dynamics involved, but it is motivated by the fact that the second inflationary trajectory corresponds to an attractor of the equations of motion, at least in the models we have analyzed. Indeed, we have checked numerically that varying the initial conditions described in the previous paragraph, even by a large amount, doesn't affect any of the conclusions, as the system is inevitably driven towards the sidetracked attractor where the heavy field slowly evolves with a typical amplitude $\chi \sim M$, as might be expected on dimensional grounds[3]. The evolution then ends as both χ and the inflaton φ fall into the stable minimum of the potential (or in any case by slow-roll violation when the potential chosen to model the inflationary phase solely does not admit a stable minimum).

The existence of this attractor solution may be heuristically understood as arising from an interplay between the repulsive force of the negatively curved field manifold and the stabilizing force of the χ potential, so that one can expect a regime where the two effects compensate each other allowing for a stable inflationary phase — this intuitive picture will be confirmed analytically and numerically in section (8.3). It is worth emphasizing that, as we will see below, the field trajectory in this set-up is typically very different from a geodesic, which is a central feature of the sidetracked

is that the quantity ϵH^2 be an increasing function of time. This translates into the inequality $\epsilon'/\epsilon > 2\epsilon$, which holds for concave potentials and even some convex ones [212].

[3] This heuristic picture will be refined in section (8.3).

scenario that we are putting forth.

8.2.2. Geometries and Potentials

We will study two classes of nonlinear sigma models with scalar fields $\phi^I = (\varphi, \chi)$, characterized by different field space metrics G_{IJ}. For each class, we will consider several choices of the potential V that are theoretically motivated and extensively studied in the context of single-field inflation [227].

The first internal metric we scrutinize is

$$G_{IJ}d\phi^I d\phi^J = \left(1 + \frac{2\chi^2}{M^2}\right) d\varphi^2 + d\chi^2 \,. \tag{8.4}$$

We will refer to this as the "minimal" model, as it amounts to the addition of a single dimension-6 operator to the standard scalar field action; it is also the minimal sample realization of the geometrical destabilization used in reference [212]. The corresponding scalar curvature is

$$R_{\rm fs} = -\frac{4}{M^2(1 + 2\chi^2/M^2)^2} \,, \tag{8.5}$$

and so indeed $R_{\rm fs} \simeq -4/M^2$ before the time of the geometrical destabilization when $\chi \simeq 0$; see the previous subsection.

The second case is the metric of the hyperbolic plane,

$$G_{IJ}d\phi^I d\phi^J = \left(1 + \frac{2\chi^2}{M^2}\right) d\varphi^2 + \frac{2\sqrt{2}\,\chi}{M}\, d\varphi d\chi + d\chi^2 \,, \tag{8.6}$$

which has a *constant* scalar curvature $R_{\rm fs} = -4/M^2$. We have chosen this particular parametrization for the reason that it gives a seemingly "small" deformation of the above minimal model (although in fact the extra operator is less irrelevant as it is dimension-5), and hence may allow us to better understand the physical effects due to changes in the field space manifold. We remark that (8.6) can be obtained from the dilatonic-type metric $d\varphi^2 + e^{-2\sqrt{2}\,\varphi/M} d\psi^2$ upon letting $e^{-\sqrt{2}\,\varphi/M}\psi \equiv \chi$. The two theories are of course inequivalent, however, as a field redefinition will have the effect of changing the form of the potential. We will further elaborate on this point in section (8.7) where we comment on the relation between our set-up and the models of cosmological attractors.

The potentials we will consider are all of the form

$$V = \Lambda^4 \mathcal{V}(\varphi) + \frac{1}{2} m_h^2 \chi^2 \,, \tag{8.7}$$

where $\mathcal{V}(\varphi)$ is a dimensionless function of φ. Similarly to [212, 224], we choose

$m_h = 10H_c$, so that, according to Eqn. (8.3), one has $\epsilon_c = 25(M/M_P)^2$. As usual the energy scale Λ will determine the overall scale of the power spectrum and can therefore be fixed a posteriori to match the observed amplitude of the curvature power spectrum.

The four specific models we have studied are shown in table (8.1). We refer the reader to [224, 227] for details about these models and their relevant parameter spaces, but in the following we give a brief rationale for our choices.

The first case we investigate is the Starobinsky potential (SI) [20, 228], a prototypical example of plateau models. It is an interesting case study because it has no free parameter and, in its single-field realization, is in excellent agreement with experimental constraints. Then we consider three characteristic hilltop models: natural inflation (NI) [62], quadratic small-field inflation SFI_2, and quartic small-field inflation SFI_4. The case of SFI_2 can be regarded as truncation of NI if we take the scale $\mu = 2f$, and hence the comparison between the two models gives a way to study the effects of the nonlinearities of the potential. We use $f = 1, 10, 100$, which are the orders of values commonly assumed in order to have agreement with data. On the other hand SFI_4 has a vanishing mass at the hilltop, $V''(\varphi = 0) = 0$, and is therefore a priori in a different class. To enable comparison, we choose for it the same values of the scale μ as in SFI_2.

Eventually, to study the influence of the results on the curvature scale M, we consider the three values $M = (10^{-2}, 10^{-2.5}, 10^{-3})\, M_{\mathrm{Pl}}$, although for NI, SFI_2 and SFI_4, we did that only for the central values of the parameters $f = 10$ and $\mu = 20$.

Although we studied all these models (36 with the various parameters' choice), and we will indeed give results for the observables for each of them, when we display detailed results and comparison with analytical formulae in the central part of the chapter, we decided to use two representative examples: Starobinsky inflation and Natural Inflation with $f = 10$, each with $M = 10^{-3}$ (which is the value by default, if not otherwise specified), as they exhibit both characteristic features and varied properties.

Model	Acronym	Inflaton potential $\mathcal{V}(\varphi)$	Parameter values
Starobinsky inflation	SI	$\left(1 - e^{-\sqrt{2/3}\,\varphi}\right)^2$	—
Natural inflation	NI	$1 + \cos\left(\frac{\varphi}{f}\right)$	$f = \{1, 10, 100\}$
Quadratic small field	SFI_2	$1 - \left(\frac{\varphi}{\mu}\right)^2$	$\mu = \{2, 20, 200\}$
Quartic small field	SFI_4	$1 - \left(\frac{\varphi}{\mu}\right)^4$	$\mu = \{2, 20, 200\}$

Table 8.1.: *List of inflationary models and values considered for the free parameters. The dimensionless potential function $\mathcal{V}(\varphi)$ is introduced in Eqn. (8.7).*

8.3. Background Dynamics of Sidetracked Inflation

In this section, we describe in more details the physics of sidetracked inflation at the level of the background. In a conventional phase of inflation driven by multiple scalar fields all slowly rolling down the potential, the acceleration term $\mathcal{D}_t\dot{\phi}^I$ in Eqn. (3.2) is negligible compared to the Hubble friction and to the effect of the potential, so that all fields approximately follow $\dot{\phi}^I \simeq -V^{,I}/(3H)$. The sidetracked phase is markedly different, as we will see, as a central ingredient of it is that some acceleration terms are large. This is not in conflict with the existence of a phase of inflation, as the latter only requires ϵ (Eqn. (2.34))as well as its time derivative η (Eqn. (2.35)) to be small, for inflation to occur and to last long enough. Given that $\epsilon = \frac{1}{2}\dot{\sigma}^2/H^2$, this readily implies that $\ddot{\sigma} \ll 3H\dot{\sigma}$, in other words that the acceleration of the fields tangential to the background trajectory be small. The perpendicular acceleration, quantified by the parameter $\eta_\perp$, need not be small in general, and indeed it will be large in sidetracked inflation.

8.3.1. Background Trajectories and Qualitative Understanding

To gain a qualitative understanding of the second phase of inflation following the geometrical destabilization, we begin by displaying some representative field space trajectories. We show these for the SI and NI potentials in fig. (8.2) (taking the NI scale $f = 10$). We have displayed each curve as divided into three portions: (1) the first part starts at the time of the instability and ends at time $N = N_*$ when perturbations of the CMB pivot scale size exit the Hubble radius; (2) the second is the phase of inflation that goes from N_* to the time at which inflation ends at $N = N_{\rm end}$ by slow-roll violation (i.e. when $\epsilon = 1$), and corresponds roughly to the range of field values, and hence the part of the potential, that can be probed via cosmological and astrophysical observations; (3) the third phase shows how the curve continues for a few more e-folds after the end of inflation. The curve of phase (1) is of course uncertain in its initial part as a field trajectory cannot be defined immediately following the geometrical destabilization. Similarly phase (3) is simply a qualitative representation of how the fields settle down into the stable minimum of the potential, as we expect other physical effects to become important after inflation ends.

One important observation is that, for each inflaton potential, the trajectories obtained with the minimal and hyperbolic field spaces are very nearly the same. Although we only display two cases, we have checked that the same conclusion applies for all the models we have studied, and we will prove this feature analytically below. Another important feature, not visible in fig. (8.2), is that the sidetracked

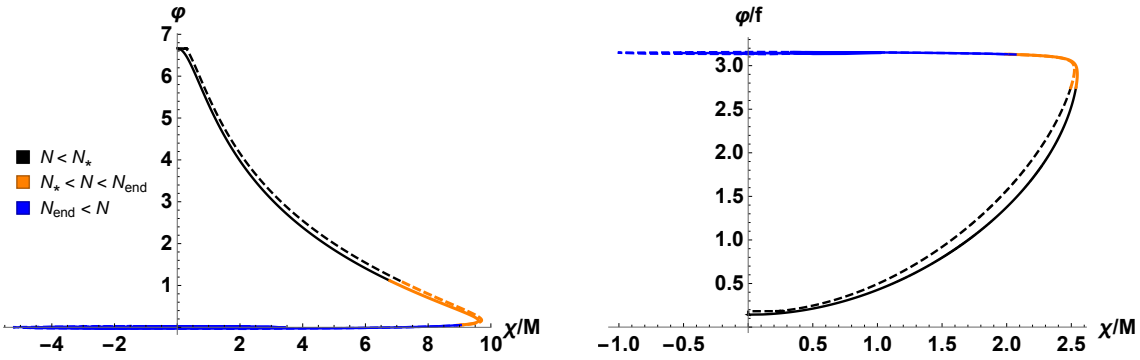

(a) *Starobinsky inflation* **(b)** *Natural inflation* ($f = 10$)

Figure 8.2.: *Field space trajectories for the SI and NI potentials (with* $f = 10$*), for both the minimal (solid line) and hyperbolic (dashed line) field space geometries. The three portions of the curve indicated in the legend correspond to the phase from the time of the instability to the Hubble crossing at* $N = N_*$ *of the CMB pivot scale; the phase of inflation from* N_* *to the time at which inflation ends at* $N = N_{\rm end}$*; and the phase after this instant obtained by continuing the integration for a few more e-folds, ignoring any other physical effects. We use the representative value* $\Delta N_{\rm pivot} \equiv N_{\rm end} - N_* = 55$*.*

phase of inflation last in general very long, comparatively much longer than along the (unstable) single-field trajectory lying at $\chi = 0$: taking the minimal model for concreteness, while there are 170 e-folds of inflation (respectively 531) left along $\chi = 0$ starting from the critical point in SI (respectively in NI), the corresponding sidetracked phase lasts about 770 e-folds (respectively about 2630). Eventually, the velocity of χ is negligible compared to the one of ϕ (see fig. (8.3)), and with χ of order M, it is straightforward to see that χ gives a negligible contribution to the total potential energy. The turing of the trajectory in Fig. (8.2) occurs after the cancellation between the repulsive force originating from the field space geometry and the one from the potential. The simple intuitive picture that emerges from these observations is that the sidetracked phase of inflation is supported by a slowly-varying inflaton field φ, slowed down on its potential due its non-canonical normalization provided by the almost constant non-zero value of χ.

8.3.2. Minimal Geometry

Let us determine the conditions under which this can be realized, considering first the minimal model. With the field space metric (8.4), the scalar fields' equations of motion (3.2) then take the form:

$$\ddot{\varphi} + 3H\dot{\varphi} + \frac{4\chi}{M^2\left(1+\frac{2\chi^2}{M^2}\right)}\dot{\chi}\dot{\varphi} + \frac{V_{,\varphi}}{1+\frac{2\chi^2}{M^2}} = 0\,, \tag{8.8}$$

$$\ddot{\chi} + 3H\dot{\chi} - 2\frac{\dot{\varphi}^2}{M^2}\chi + V_{,\chi} = 0\,, \tag{8.9}$$

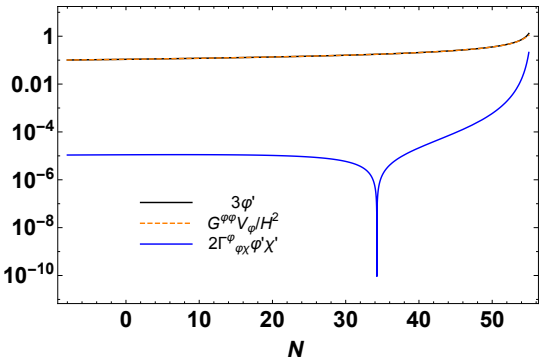

(a) *Terms in the equation of motion for φ in the minimal geometry.*

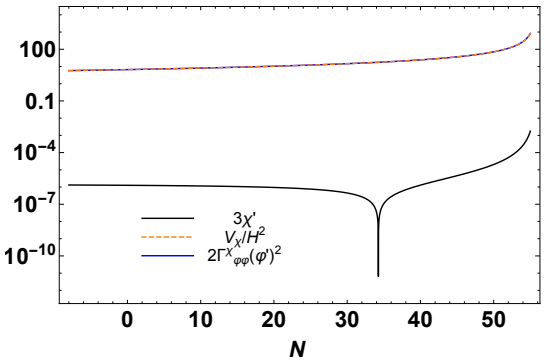

(b) *Terms in the equation of motion for χ in the minimal geometry.*

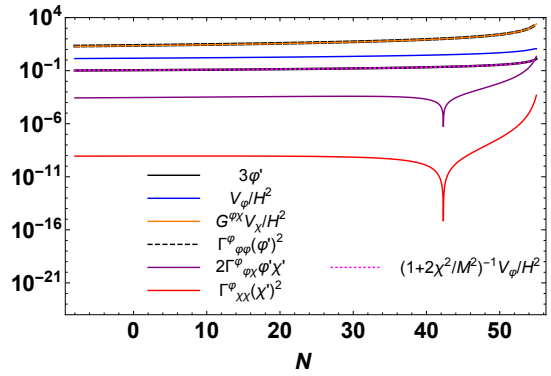

(c) *Terms in the equation of motion for φ in the hyperbolic geometry.*

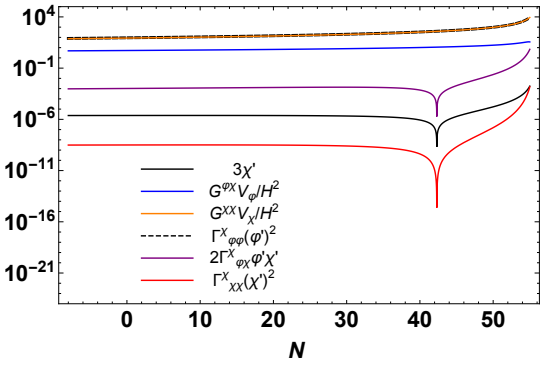

(d) *Terms in the equation of motion for χ in the hyperbolic geometry.*

Figure 8.3.: *Relative contributions of the absolute values of the different terms in the equations of motion for the scalar fields φ (left) and χ (right), for the minimal geometry (top) and the hyperbolic geometry (bottom). The model is Natural Inflation with $f = 10$ and $M = 10^{-3}$, and the plots show the last 63 e-folds of inflation. One can explicitly check that the terms dominating the dynamics are the ones described in the main text. We made use of derivatives with respect to the number of e-folds, denoted by a prime. The spike observed in some of these plots occurs from the sign of χ' flipping to negative at the turning point observed in Fig. (8.2).*

where remember that we make use of the potential (8.7), so that $V_{,\chi} = m_h^2\chi$. A non-zero approximately constant χ can only be a solution of Eqn. (8.9) provided that

$$2\frac{\dot{\varphi}^2}{M^2} \simeq m_h^2, \tag{8.10}$$

expressing the almost cancellation between the repulsive force originating from the field space geometry and the one from the potential. The fact that this relation holds, and that the last two terms in (8.9) completely dominate the equation of motion of χ, can be seen in Fig. (8.3b) for the representative example of NI with $f = 10$. As we previously said, this is in sharp contrast with a field slowly rolling down its potential, for which the dominating terms would be the Hubble friction term and the gradient of the potential. This standard situation is at play however for the inflaton φ, as can be checked in Fig. (8.3a), where the third term in (8.8), originating from the non-standard field space metric, and suppressed by the velocity of χ, is shown to be negligible in the dynamics. The inflaton field therefore approximately verifies

$$3H\dot{\varphi} \simeq -\frac{V_{,\varphi}}{1+\frac{2\chi^2}{M^2}}\,, \tag{8.11}$$

showing clearly how the non-standard normalization of φ generates an effective flattened potential compared to the single-field case. Obviously, the agreement between the two expressions (8.10) and (8.11) determines the yet unknown value of the field χ that enables to support the sidetracked phase, such that

$$1+\frac{2\chi^2}{M^2} \simeq \sqrt{\frac{2}{3}}\frac{M_{\rm Pl}|V_{,\varphi}|}{m_h M\sqrt{V(\varphi)}}\,. \tag{8.12}$$

Here, we used that $3H^2M_{\rm Pl}^2 \simeq \Lambda^4\mathcal{V}(\varphi) \equiv V(\varphi)$ to explicitly express that Eqn. (8.12) fixes χ as a function of φ. As all the approximate relations given in this section, one can check that the above relation is verified to a very good accuracy, determining χ to a few 0.1% in NI with $f = 10$ for instance. To have a better understanding of the order of magnitude of χ along sidetracked inflation, one can rewrite Eqn. (8.12) as

$$1+\frac{2\chi^2}{M^2} \simeq \sqrt{2}\left(M_{\rm Pl}\frac{|V_{,\varphi}|}{V(\varphi)}\right)\left(\frac{1}{m_h/H}\right)\left(\frac{M_{\rm Pl}}{M}\right)\,, \tag{8.13}$$

where the first two terms in parentheses are small, due to the flatness of the inflaton potential and the heavy bare mass of χ, while the last term is enhanced by the hierarchy between the curvature and the Planck scale. It is hard therefore to conclude in general about the amplitude of χ. As a very rough estimate though, one can assume that the first two terms have a similar order of magnitude than at the critical time, despite the very long duration of the sidetracked phase[4]. Together with Eqn. (8.3),

[4]This holds for the potentials we have studied, but it would not necessarily be true for potentials whose shape is vastly different in the sidetracked phase and around the critical time. The values

and the slow-roll expression $\epsilon_c \simeq M_{\rm Pl}^2/2\,(V_{,\varphi}/V)_c^2$, one therefore concludes that the left hand side of Eqn. (8.12) is of order one, *i.e.* that χ is stabilized in the sidetracked phase at χ of order M, as announced. Now that χ is known as a function of φ, one can of course check the consistency of the approximations that we have performed. In particular, one can determine the velocity of χ as

$$\frac{\dot\chi}{\dot\varphi} \simeq \frac{\mathrm{sign}(V_{,\varphi})}{2\sqrt{2}}\frac{H}{m_h}\frac{M}{\chi}\left[M_{\rm Pl}^2\frac{V_{,\varphi\varphi}}{V} - \frac{M_{\rm Pl}^2}{2}\left(\frac{V_{,\varphi}}{V}\right)^2\right], \tag{8.14}$$

which shows that it is indeed suppressed compared to the one of φ, by $H/m_h \ll 1$, and by the flatness of the inflaton potential.

8.3.3. Hyperbolic Geometry

We now turn to the hyperbolic field space, whose scalar fields' equations of motion can be out in the form:

$$\ddot\varphi + 3H\dot\varphi + \frac{4\chi}{M^2}\dot\chi\dot\varphi + \frac{\sqrt{2}}{M}\dot\chi^2 + \sqrt{2}\frac{\chi}{M}\left[2\frac{\dot\varphi^2}{M^2}\chi - V_{,\chi}\right] + V_{,\varphi} = 0 \tag{8.15}$$

$$\ddot\chi + 3H\dot\chi - \frac{2\chi}{M^2}\dot\chi^2 - 4\sqrt{2}\frac{\chi^2}{M^3}\dot\varphi\dot\chi + \left(1+2\frac{\chi^2}{M^2}\right)\left[-2\frac{\dot\varphi^2}{M^2}\chi + V_{,\chi}\right] - \sqrt{2}\frac{\chi}{M}V_{,\varphi} = 0\,. \tag{8.16}$$

As the field space metric (8.6) is non-diagonal, Eqns. (8.15)-(8.16) are more complicated than their minimal counterparts (8.8)-(8.9). However, we will show that all the approximate relations we have derived above for the minimal model still hold in this seemingly more intricate case, and that the two dynamics are similar, something we have already noted by looking at the field space trajectories in fig. (8.2).

We start again by looking for an approximately constant χ providing a non-trivial solution of Eqn. (8.16). It can exist provided now that

$$2\frac{\dot\varphi^2}{M^2} \simeq m_h^2 - \sqrt{2}V_{,\varphi}/M\left(1+\frac{2\chi^2}{M^2}\right)^{-1}, \tag{8.17}$$

where the last term is new compared to the minimal case. One can check that it is subdominant compared to the first term on the right hand side, although not always negligible. In NI with $f = 10$ for instance, its value diminishes from about 15 % of the first term in the bulk of the sidetracked phase to a few percent of it in the last 60 e-folds. The fact that it is subdominant can be understood using the same back of

at which χ is stabilized could then differ from M by a large amount, but our analysis and our analytical estimates would still apply in that case.

the envelope estimates as we have used below Eqn. (8.12), showing that it is smaller than the first term by at least the ratio H/m_h. In fig. (8.3d), we display the relative contributions of the various terms in Eqn. (8.16), showing that the latter is indeed dominated by the cancellation between the two terms in brackets in (8.16), so that Eqn. (8.10) approximately holds, like in the minimal case. For simplicity, we do not display the even more precise cancellation between the last three 'forces', which gives the relation (8.17). However, this refined estimate is important to understand the dynamics of the inflaton. Indeed, by using it in the equation of motion for φ, one can see that the last three terms in Eqn. (8.15) sum up to $\simeq V_{,\varphi}/\left(1+\frac{2\chi^2}{M^2}\right)$. As the third and fourth terms, involving the velocity of χ, are consistently negligible (see fig. (8.3c)), one deduces that the inflaton field verifies, like in the minimal case, the simple equation (Eqn. (8.11)), as shown in fig. (8.3c) by the superposition of the black and dotted magenta lines.

Like in the minimal case, the agreement between the two expressions (8.17) and (8.11) of $\dot{\varphi}$ determine χ as a function of φ. Because of the subdominant second term in (8.17), $1+\frac{2\chi^2}{M^2}$ now verifies a quadratic equation, whose solution is straightforward to write down, but that we will not need in the following, and that is not particularly illuminating. At leading order, one can thus simply employ expressions (8.12)-(8.13).

8.3.4. Summary and Effective Single-Field Theory for the Background

Let us summarize the main findings above. Despite small and understood differences, the background dynamics of sidetracked inflation in the minimal and in the hyperbolic field spaces are similar, and can be summarized at leading order by the simple equations (Eqns.(8.11) and (8.12)), expressing: 1) the rolling of the inflaton φ on its potential, further slowed-down through its interactions with the accompanying scalar field χ, giving it more inertia. 2) the fact that the dynamics of the latter is being completely fixed by the inflaton, as a result of the competition between the force originating from the field space geometry and the one from the quadratic potential of χ. The background dynamics can therefore be reformulated in terms of φ uniquely, which sheds an interesting light on sidetracked inflation. In table (8.2), we collect a number of useful relations that derive easily from the equations above, that we compare to their counterparts in standard single-field slow-roll inflation.

One can see that the dynamics and the functional dependences of the various inflationary parameters on the shape of the potential are very different between standard slow-roll inflation and sidetracked inflation. For the latter, we give each time two equivalent expressions, the first one in terms of the various mass scales $M_{\rm Pl}, M, m_h$ and the potential, and the second one that make appear the ratio $m_h/H(\varphi)$ by using $3H(\varphi)^2M_{\rm Pl}^2 \simeq V(\varphi)$. Strictly speaking, one could envisage situations in which m_h has no relationship with the Hubble scale. However, this is not the case in realistic

Functions	Sidetracked inflation	Slow-roll inflation
$\frac{\mathrm{d}\varphi}{\mathrm{d}N} \simeq$	$\begin{cases} -\sqrt{\frac{3}{2}} M_{\rm Pl} M m_h / \sqrt{V}\, \mathrm{sign}(V_{,\varphi}) \\ -\frac{M}{\sqrt{2}} \frac{m_h}{H(\varphi)}\, \mathrm{sign}(V_{,\varphi}) \end{cases}$	$-M_{\rm Pl}^2 \frac{V_{,\varphi}}{V}$
$\epsilon \simeq$	$\begin{cases} \frac{1}{2}\sqrt{\frac{3}{2}} M_{\rm Pl} M m_h |V_{,\varphi}|/V^{3/2} \\ \frac{1}{2\sqrt{2}} M \frac{|V_{,\varphi}|}{V} \frac{m_h}{H(\varphi)} \end{cases}$	$\frac{M_{\rm Pl}^2}{2}\left(\frac{V_{,\varphi}}{V}\right)^2$
$\eta = \frac{\mathrm{d}\ln\epsilon}{\mathrm{d}N} \simeq$	$\begin{cases} 3\epsilon - \sqrt{\frac{3}{2}} M_{\rm Pl} M m_h \frac{V_{,\varphi\varphi}}{|V_{,\varphi}| V^{1/2}} \\ 3\epsilon - \frac{M}{\sqrt{2}} \frac{V_{,\varphi\varphi}}{|V_{,\varphi}|} \frac{m_h}{H(\varphi)} \end{cases}$	$4\epsilon - 2M_{\rm Pl}^2 \frac{V_{,\varphi\varphi}}{V}$
$N - N_{\rm ini} \simeq$	$\begin{cases} -\sqrt{\frac{2}{3}} \frac{1}{M_{\rm Pl} M m_h} \int_{\varphi_{\rm ini}}^{\varphi} \mathrm{sign}(V_{,\varphi'}) \sqrt{V(\varphi')} \mathrm{d}\varphi' \\ -\frac{\sqrt{2}}{M} \int_{\varphi_{\rm ini}}^{\varphi} \mathrm{sign}(V_{,\varphi'}) \frac{H(\varphi')}{m_h} \mathrm{d}\varphi' \end{cases}$	$-\frac{1}{M_{\rm Pl}^2} \int_{\varphi_{\rm ini}}^{\varphi} \frac{V(\varphi')}{V_{,\varphi'}} \mathrm{d}\varphi'$

Table 8.2.: *Comparison between sidetracked inflation and slow-roll inflation.*

situations, and in our approach and our numerical examples, we took $m_h = 10 H_c$. The ratio $m_h/H(\varphi)$ is a dynamical quantity and is larger in sidetracked inflation than at the critical time because of the decrease of the Hubble scale, however, for qualitative estimates, one can think of it as an $\mathcal{O}(10)$ quantity. The second expressions of ϵ and η make it clear therefore that the overall scale Λ of the potential (see Eqn. (8.7)) is irrelevant for the dynamics, and that only its shape $\mathcal{V}(\varphi)$ matters, like in slow-roll inflation. In the latter case, the expressions of ϵ and η indicate the well known fact that the (log) potential should be flat in Planck units. In sidetracked inflation, the corresponding expressions rather indicate that the potential should be flat with respect to the curvature scale M, with the requirements:

$$M \frac{V_{,\varphi}}{V} \ll 1\,, \quad M \frac{V_{,\varphi\varphi}}{V_{,\varphi}} \ll 1\,. \tag{8.18}$$

Concretely, this implies that one can have a prolonged phase of inflation supported by potentials that would be too steep to allow standard slow-roll inflation. This is clearly visible in fig. (8.2) for instance, where inflation arises on the Starobinsky potential with $\varphi \sim M_{\rm Pl}$, and on the natural inflation potential with $\varphi \sim f$.[5] Additionally, the second criteria in Eqn. (8.18) does not involve $M_{\rm Pl}^2 V_{,\varphi\varphi}/V$ in the standard way, but rather $M V_{,\varphi\varphi}/V_{,\varphi}$. In NI near the top of the hill for instance, this translates into $M \ll \varphi \ll f$ rather than the standard requirement that $f \gg M_{\rm Pl}$. More generally, it is interesting that inflation can occur in the presence of steep potentials, both for the inflaton φ and its parter χ. This amusing feature of sidetracked

[5] Note that in the last 55 e-folds in NI, inflation does not arise near the top of the hill, but rather near the minimum of the potential, so that it is approximately quadratic.

inflation thus offers an interesting playground for future work, notably with respect to the eta problem. Note however that it comes at the expense of the appearance of the sub-Planckian curvature scale M, and is likely that a proper treatment of naturalness issues in quantum field theory renders the situation more intricate.

8.4. Cosmological Fluctuations and Power Spectrum

8.4.1. Numerical Methods

To determine the properties of the linear cosmological fluctuations generated in sidetracked inflation, we solve the coupled equations (Eqns. (7.22)) in the natural coordinate basis (φ, χ), choosing Bunch-Davies initial conditions. We follow a by now standard procedure to implement numerically the quantization of the system (see *e.g.* references [127, 172, 181, 229–234]): we identify two variables (as we are dealing with two fields) that are independent deep inside the Hubble radius, each corresponding to an independent set of creation and annihilation operators whose effects add incoherently, and solve the system of equations (Eqn. (7.22)) two times, each time imposing the Bunch-Davies initial conditions for only one of the independent variables, while setting the other variables to zero initially. One then extracts power spectra by summing the relevant quantities over the two runs. Deep inside the Hubble radius, one can neglect the mass matrix in the action (3.24), so that identifying a set of independent variables is equivalent to identifying a set of vielbeins for the field space metric G_{IJ}, which is straightforward. In practice, we impose initial conditions eight e-folds before Hubble crossing. This is larger than what is sufficient in more conventional circumstances but, as we will see, the strong bending of the trajectory entails a non-trivial evolution of the fluctuations inside the Hubble radius, and starting the evolution at a later time would give inaccurate results.

As we encountered a highly non-trivial behaviour of the fluctuations, we also used the completely independent so-called transport approach to determine their properties, finding excellent agreement between the two methods. In this work, we make use of the `PyTransport 2.0` code from Ch.(5).

Contrary to the study of the premature end of inflation possibly triggered by the geometrical destabilization [224], in which it was important to take into account the uncertainties of the reheating phase, and given the exploratory nature of our study here, we do not attempt to model reheating and simply assume throughout the representative value $\Delta N_{\rm pivot} = 55$ for the number of e-folds between Hubble crossing of the CMB pivot scale and the end of inflation, the latter defined by the instant at which $\epsilon = 1$.

8.4.2. Adiabatic and Entropic Fluctuations

With the two approaches described above, it is relatively straightforward to determine the power spectra of the curvature and entropic perturbations for any scale, and therefore the scalar spectral index n_s as well as the tensor-to-scalar ratio r[6]. However, to gain more insight into the physics of the fluctuations, it is instructive to formulate it in terms of the instantaneous adiabatic/entropic splitting. In particular, from Eqn. (7.22), one can deduce the coupled adiabatic and entropic equations of motion as

$$\ddot{Q}_\sigma + 3H\dot{Q}_\sigma + \left(\frac{k^2}{a^2} + m_\sigma^2\right) Q_\sigma = (2H\eta_\perp Q_s)^{\cdot} - \left(\frac{\dot{H}}{H} + \frac{V_{,\sigma}}{\dot{\sigma}}\right) 2H\eta_\perp\, Q_s\,, \tag{8.19}$$

$$\ddot{Q}_s + 3H\dot{Q}_s + \left(\frac{k^2}{a^2} + m_s^2\right) Q_s = -2\dot{\sigma}\eta_\perp\dot{\zeta}\,, \tag{8.20}$$

where the adiabatic mass (squared) m_σ^2 is given by

$$\frac{m_\sigma^2}{H^2} \equiv -\frac{3}{2}\eta - \frac{1}{4}\eta^2 - \frac{1}{2}\epsilon\eta - \frac{1}{2}\dot{\eta}/H\,, \tag{8.21}$$

the entropic mass (squared) m_s^2 is given by

$$\frac{m_s^2}{H^2} \equiv \frac{V_{;ss}}{H^2} + \epsilon R_{\rm fs} M_{\rm pl}^2 - \eta_\perp^2\,, \tag{8.22}$$

and in Eqn. (8.20), we employed in the right hand side the comoving curvature perturbation ζ, directly proportional to the adiabatic fluctuation, such that

$$\zeta = \frac{H}{\dot{\sigma}} Q_\sigma\,. \tag{8.23}$$

In a symmetric way, note that it is also useful to introduce the rescaled entropic perturbation

$$\mathcal{S} = \frac{H}{\dot{\sigma}} Q_s\,. \tag{8.24}$$

As in Eqn. (7.26), on super-Hubble scales such that $k \ll aH$, there exists a first integral for Q_σ, which can be conveniently rewritten in terms of ζ and $\mathcal{S}$ as

$$\dot{\zeta} \approx 2H\eta_\perp\, \mathcal{S} \tag{8.25}$$

where $\dot{\sigma} = H\sqrt{2\epsilon}$, (one can check indeed that the large-scale limit of (Eqn. (8.19)) is a consequence of Eqn. (8.25)). Inserting the latter result into Eqn. (8.20), one

[6] As usual, the tensor fluctuations are decoupled from the scalar sector, and the standard result $\mathcal{P}_{\rm t}(k) = 2/\pi^2 H^2_{k=aH}/M^2_{\rm pl}$ holds.

finds that on super-Hubble scales,

$$\ddot{Q}_s + 3H\dot{Q}_s + \left(m_s^2 + 4H^2\eta_\perp^2\right) Q_s \approx 0\,, \tag{8.26}$$

which is in agreement with the already given result (7.24), with $m^2_{s\,(\mathrm{eff})} = m_s^2 + 4H^2\eta_\perp^2$. One can see that the two notions of entropic masses coincide in the case of a geodesic motion with $\eta_\perp = 0$, but that they differ in general, a feature that plays a central role in sidetracked inflation, as we will see.

Complementary to the super-Hubble limit discussed above, it is useful to recast the equations of motion (Eqns. (8.19)-(8.20)) in a form that is more adapted to understand the physics on sub-Hubble scales. By introducing the canonically normalized fields in conformal time τ (such that $\mathrm{d}t = a\,\mathrm{d}\tau$), $v_\sigma = a\,Q_\sigma$ and $v_s = a\,Q_s$, for the adiabatic and entropic fluctuations respectively, the equations can be put in the compact form, derived in reference [235] in a more general context:

$$v_\sigma'' - \xi v_s' + \left(k^2 - \frac{z''}{z}\right) v_\sigma - \frac{(z\xi)'}{z} v_s = 0\,, \tag{8.27}$$

$$v_s'' + \xi v_\sigma' + \left(k^2 - \frac{a''}{a} + a^2 m_s^2\right) v_s - \frac{z'}{z}\xi v_\sigma = 0\,, \quad {}' = \mathrm{d}/\mathrm{d}\tau\,. \tag{8.28}$$

In these two equations only, in order not to clutter the text with two many notations, we used primes to denote derivatives with respect to conformal time, whereas other instances in the rest of the text do denote derivatives with respect to the number of e-folds. These equations render it clear that in addition to the scale factor, the only other background quantities affecting the dynamics of fluctuations are

$$z \equiv \frac{a\dot{\sigma}}{H} = a\sqrt{2\epsilon}\,, \tag{8.29}$$

such that $v_\sigma = z\zeta$, the entropic mass (8.22), and the time-dependent coupling between the adiabatic and entropic fluctuation

$$\xi \equiv 2aH\eta_\perp\,. \tag{8.30}$$

Although detailed predictions of the cosmological fluctuations, even in a single-field context, depend on the precise time evolution of z, when the background evolution is close to de Sitter, with ϵ, η and $\dot{\eta}/(H\eta)$ all much smaller than unity, one can consider at leading order that time derivatives of z are dominated by the variation of the scale factor, *i.e.* $\frac{1}{z}\frac{\mathrm{d}z}{\mathrm{d}\tau} \simeq \frac{1}{a}\frac{\mathrm{d}a}{\mathrm{d}\tau} \simeq -\frac{1}{\tau}$ and $\frac{1}{z}\frac{\mathrm{d}^2z}{\mathrm{d}\tau^2} \simeq \frac{1}{a}\frac{\mathrm{d}a}{\mathrm{d}\tau^2} \simeq \frac{2}{\tau^2}$. This corresponds to situations in which the adiabatic mass (8.21) is negligible compared to the Hubble scale, which applies in all the cases we have considered. Were the effect of the bending trajectory, *i.e* of the coupling ξ, negligible in the dynamics of the fluctuations, this would lead to the well known slow-roll single-field like result $v_{\sigma\,k} \simeq \frac{1}{\sqrt{2k}} e^{-ik\tau}\left(1 - \frac{i}{k\tau}\right)$, and hence to the standard result $\mathcal{P}_{\zeta_k} = \left(H^2/(8\pi^2\epsilon)\right)_{k=aH}$ for the dimensionless power spectrum

$\mathcal{P}_{\zeta_k} = k^3/(2\pi^2)P_{\zeta_k}$, where $\langle\zeta_{\boldsymbol{k}_1}\zeta_{\boldsymbol{k}_2}\rangle \equiv (2\pi)^3\delta(\boldsymbol{k}_1+\boldsymbol{k}_2)P_{\zeta_k}$ with $k = |\boldsymbol{k}_1| = |\boldsymbol{k}_2|$. On the contrary, as we have mentioned in section (8.3), the trajectory of sidetracked inflation differs strongly from a geodesic, so that it is important to take into account the coupled dynamics between the adiabatic and entropic degrees of freedom. For this, we need to understand the behaviour of the various (related) mass scales $m_s^2, H^2\eta_\perp^2$ and $m^2_{s\,(\mathrm{eff})}$ compared to the Hubble scale. This is what we do in the following, building on our understanding of the background dynamics in section (8.3).

8.4.3. Analytical Understanding of Relevant Mass Scales

We have explained in section (8.3) that $\dot\chi \ll \dot\varphi$ in the sidetracked phase of inflation (see Eqn. (8.14) for instance). To a very good approximation, one can then consider that the adiabatic vector points in the direction of φ only, *i.e.* that $e^I_\sigma \propto (\dot\varphi, 0)$ in the natural coordinate basis. With the expressions (8.4) and (8.6) of the field space metrics, this leads to

$$e^I_\sigma = \left(\left(1+\frac{2\chi^2}{M^2}\right)^{-1/2}, 0\right) . \tag{8.31}$$

From this, it is straightforward to deduce the form of the entropic unit vector as

$$e^I_s = \begin{cases} (0,1) & \text{minimal} \\ \left(-\sqrt{2}\,\frac{\chi}{M}\left(1+\frac{2\chi^2}{M^2}\right)^{-1/2}, \left(1+\frac{2\chi^2}{M^2}\right)^{1/2}\right) & \text{hyperbolic} \end{cases} \tag{8.32}$$

where here the two results differ in the minimal and in the hyperbolic model. Contrary to the background properties, the estimation of the various parameters, and the resulting dynamics of the fluctuations, will be rather different for the two geometries, so we treat them separately in what follows. Before that, let us just note the common formal expression of $\eta_\perp$ that we will use. From its definition in Eqn. (7.25), and the fact that the adiabatic acceleration $\ddot\sigma$ (derived from the standard Klein-Gordon equation for the scalar field, as in Eqn. (2.195)) is negligible during inflation, we deduce that

$$\eta_\perp \simeq 3\frac{V_{,s}}{V_{,\sigma}} \tag{8.33}$$

to a very good approximation.

Minimal Geometry

From the expression (8.33) of $\eta_\perp$, together with (8.31)-(8.32), one finds $\eta_\perp \simeq 3V_{,\chi}/V_{,\varphi} \times \left(1+\frac{2\chi^2}{M^2}\right)^{1/2}$. Using Eqn. (8.11) to express $V_{,\varphi}$ in terms of $\dot\varphi$, and the

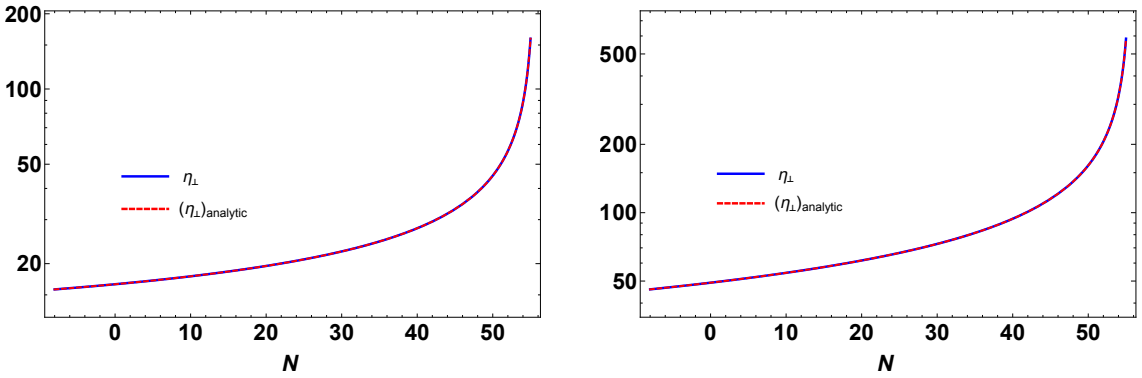

(a) *Starobinsky inflation* **(b)** *Natural inflation* ($f = 10$)

Figure 8.4.: *Fully numerical and analytical result* (8.34) *for the absolute value of* $\eta_\perp$ *in the last 63 e-folds of sidetracked inflation in the minimal geometry, for the potentials of SI (left) and NI,* $f = 10$ *(right).*

simple form (8.11) of the latter, one then finds

$$\eta_\perp \simeq \frac{m_h}{H} \frac{\frac{\sqrt{2}\chi}{M}}{\left(1+\frac{2\chi^2}{M^2}\right)^{1/2}} \times \text{sign}(V_{,\varphi})\,. \tag{8.34}$$

One can of course express this result in terms of φ only, by using Eqn. (8.12). However, Eqn. (8.34) is more instructive: as $\chi = \mathcal{O}(M)$, the second multiplicative factor in (8.34) is of order one. Let us also recall that, as a consequence of the decrease of the Hubble scale, $m_h/H > m_h/H_c = 10$. One therefore reaches the conclusion that, as announced, the bending of the background trajectory, as measured by $\eta_\perp$, is large in sidetracked inflation in the minimal geometry. Intuitively, one can understand this result: as the sidetracked phase stems from the competition (and neutralization) of the effects from the geometry and from the potential, it is not surprising that 1) the resulting trajectory deviates from a geodesic, and 2) that it does so by an amount related to how massive the field χ is. The fully numerical result for $\eta_\perp$, as well as the analytical estimate (8.34), are shown in Fig. (8.4) for the two examples of SI and NI with $f = 10$. Note that in each case the agreement is excellent, with a relative accuracy of order 10^{-5} and 10^{-7} (not visible in the figures).

We now determine expressions for the two entropic masses. With (8.32), it is straightforward to find that $V_{;ss} \simeq m_h^2$. For the geometrical contribution, we use Eqn. (8.10) to find that $\epsilon \simeq \left(1+\frac{2\chi^2}{M^2}\right)\frac{m_h^2}{H^2}\frac{M^2}{4M_{\rm pl}^2}$, and hence, with the expression (8.5) of the field space curvature, that $\epsilon R_{\rm fs} M_{\rm pl}^2 \simeq -\frac{m_h^2}{H^2}\left(1+\frac{2\chi^2}{M^2}\right)^{-1}$. The three contributions — the Hessian, the bending, and the geometrical ones — to $m^2_{s\,(\text{eff})}/H^2$ (Eqn. (7.24)) and m_s^2/H^2 (Eqn. (8.22)) are therefore individually large, each of order

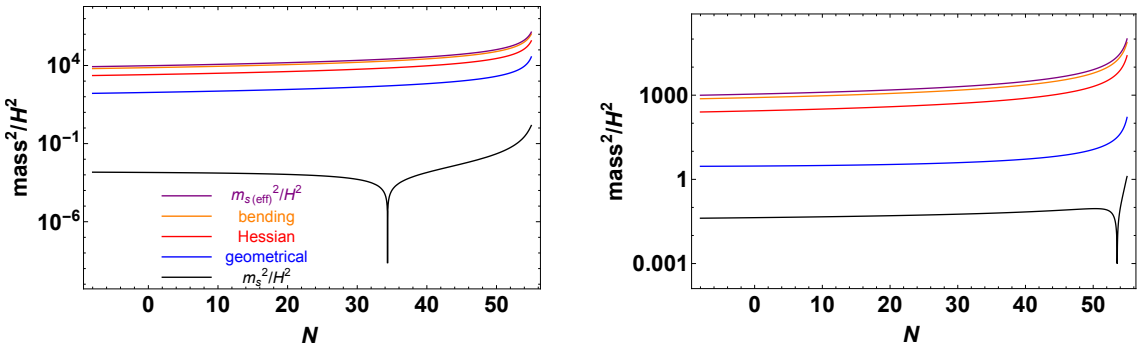

(a) *Natural inflation ($f = 10$)* **(b)** *Starobinsky inflation*

Figure 8.5.: *Absolute values of $m^2_{s\,(\mathrm{eff})}/H^2$, its three contributions (see Eqn. (7.24)), as well as m_s^2/H^2, for our two representative examples of SI and NI with $f = 10$, in the minimal geometry. The plots show the last 63 e-folds of inflation. One can check that $m_s^2/H^2 \ll 1$, and one actually has $m_s^2/H^2 < 0$ around Hubble crossing.*

of the large mass m_h^2/H^2. However, by summing them, we find

$$\frac{m^2_{s\,(\mathrm{eff})}}{H^2} \simeq \frac{4m_h^2}{H^2}\frac{\frac{2\chi^2}{M^2}}{\left(1+\frac{2\chi^2}{M^2}\right)} \gg 1 \tag{8.35}$$

$$\frac{m_s^2}{H^2} \simeq 0\,. \tag{8.36}$$

In other words, while the effective mass $m^2_{s\,(\mathrm{eff})}$, which dictates the evolution of the entropic fluctuations on super-Hubble scales according to Eqn. (7.23), is much larger than the Hubble rate, the various large contributions to the entropic mass m_s^2, which is important for the sub-Hubble dynamics (see Eqn. (8.28)), cancel, at least in our analytical treatment. This is confirmed numerically, as we can see in Fig. (8.5), where we plot (the absolute values of) $m^2_{s\,(\mathrm{eff})}/H^2$, its three contributions, as well as m_s^2/H^2, for the two representative examples of SI and NI with $f = 10$. In both cases, we indeed find that $m_s^2 \ll H^2$, and we also observe that m_s^2 is negative. Naturally, we could keep track of subleading terms in our analytical treatment, beginning with the correction to e_σ^I induced by the non-zero velocity of χ, that is suppressed by 10^{-5} compared to the one of χ in these two examples (see Fig. (8.3) and Eqn. (8.14)). Although we did not attempt it, we expect it would reproduce the small value of m_s^2, that is indeed suppressed by 10^{-5} compared to $m^2_{s\,(\mathrm{eff})}$.

Hyperbolic Geometry

As for the hyperbolic geometry, we can follow the same steps as in the minimal one, which used the estimate (8.10) for $\dot\varphi$ in particular, finding again large individual contributions to $m^2_{s\,(\mathrm{eff})}/H^2$, of order m_h^2/H^2, and a vanishing m_s^2/H^2. While these results are indeed quantitatively correct for each of the various contributions, and for $m^2_{s\,(\mathrm{eff})}$, this result is misleading for m_s^2, the reason being that the subleading correction to $\dot\varphi$ in the refined expression (8.17) has to be taken into account when

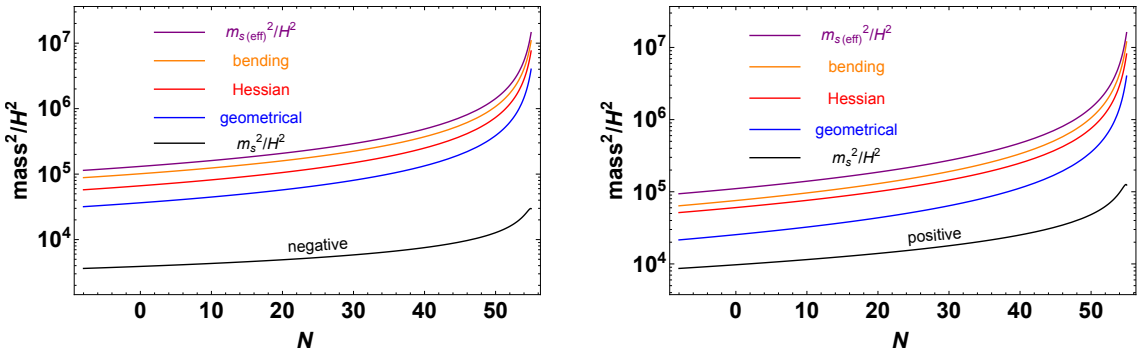

(a) *Natural inflation ($f = 10$)* **(b)** *Starobinsky inflation*

Figure 8.6.: *Absolute values of $m^2_{s\,(\mathrm{eff})}/H^2$, its three contributions (see Eqn. (7.24)), as well as m_s^2/H^2, for our two representative examples of SI and NI with $f = 10$, in the hyperbolic geometry. The plots show the last 63 e-folds of inflation. Contrary to the minimal geometry, one has $|m_s^2|/H^2 \gg 1$ in that case. In addition, note that m_s^2 is positive in SI, and negative in NI.*

the leading order result vanishes. In what follows, we give both the leading-order expressions of the various quantities involved, making use of (8.10), as well as refined ones, making use of (8.17)-(8.11). We do this in particular because the magnitude of these parameters is most easily understood with the leading-order estimates.

For $\eta_\perp$, starting from (8.33), one then finds[7]

$$\eta_\perp \simeq \begin{cases} \frac{\sqrt{2}\chi}{M}\,\frac{m_h}{H}\,\mathrm{sign}(V_{,\varphi}) & \mathrm{leading-order} \\ \frac{2\frac{\chi}{M}}{1+\frac{2\chi^2}{M^2}}\,\frac{V_{,\varphi}}{3H^2M} & \mathrm{refined} \end{cases} \tag{8.37}$$

where the leading-order (respectively the refined) estimate is accurate to the level 10^{-2} (respectively 10^{-4}) for the NI potential with $f = 10$ for instance. As announced, one finds a large bending, like in the minimal model, and the same remarks as in that case apply regarding an intuitive picture of its origin.

By using (8.32), one can straightforwardly compute $V_{;ss}$, finding

$$V_{;ss} \simeq \left(1+\frac{4\chi^2}{M^2}\right) m_h^2 - \sqrt{2}\frac{V_{,\varphi}}{M}\left(1+\frac{2\chi^2}{M^2}\right)^{-1} + \frac{\frac{2\chi^2}{M^2}}{\left(1+\frac{2\chi^2}{M^2}\right)} V_{,\varphi\varphi}\,, \tag{8.38}$$

where one would keep the first term at leading-order, the second term in the refined estimate, and the last term can always be neglected for practical purposes. Eventually, using $\epsilon \simeq \left(1+\frac{2\chi^2}{M^2}\right)\dot\varphi^2/(2H^2M_{\mathrm{pl}}^2)$, together with $R_{\mathrm{fs}} = -4/M^2$, one deduces

[7] The complete leading-order result has an additional contribution $-3\sqrt{2}\chi/M$, which however exceeds the accuracy of this calculation.

that

$$\epsilon R_{\rm fs} M_{\rm pl}^2 \simeq \begin{cases} -\left(1+\frac{2\chi^2}{M^2}\right)\frac{m_h^2}{H^2} & {\rm leading-order} \\ -\frac{2}{1+\frac{2\chi^2}{M^2}}\left(\frac{V_{,\varphi}}{3H^2M}\right)^2 & {\rm refined}\,. \end{cases} \tag{8.39}$$

Summing these contributions, one deduces that

$$\frac{m_{s\,({\rm eff})}^2}{H^2} \simeq 8\frac{m_h^2}{H^2}\frac{\chi^2}{M^2} \gg 1 \qquad {\rm leading-order} \tag{8.40}$$

$$\frac{m_s^2}{H^2} \simeq 2\sqrt{2}\frac{\frac{2\chi^2}{M^2}}{\left(1+\frac{2\chi^2}{M^2}\right)}\frac{V_{,\varphi}}{H^2M} \qquad {\rm refined}\,, \tag{8.41}$$

where it is sufficient to give the leading-order form of the super-Hubble entropic mass for our purpose. Now that a non-zero result for m_s^2 is found, one can use Eqn. (8.11) and the simple leading-order estimate (8.10) to find the simple, more intuitive form

$$\frac{m_s^2}{H^2} \simeq 12\frac{m_h}{H}\frac{\chi^2}{M^2}\,{\rm sign}(V_{,\varphi})\,. \tag{8.42}$$

This shows that, contrary to the minimal case, $|m_s^2/H^2| \gg 1$, and that it is smaller than $m_{s\,({\rm eff})}^2/H^2$ only by a factor m_h/H. In addition to its amplitude, a crucial feature of the result (8.41)-(8.42) is that the sign of the entropic mass squared m_s^2 can be positive or negative — with important observational consequences — depending on whether the slope of the potential is positive or negative respectively. It is rather unusual in inflationary models to find a physical quantity that depends on the sign of the slope of the potential. In standard single-field inflationary models in particular, one can arbitrarily change the definition of φ into $-\varphi$, and hence the sign of $V_{,\varphi}$, without physical consequences. One can do so because the standard kinetic term $(\partial\varphi)^2$ is trivially $\mathbb{Z}_2$ symmetric. However, while this feature is still true for the minimal field space metric (8.4), this is not the case for the hyperbolic metric (8.6). Hence, it is not surprising that a physical quantity can depend on the choice of labelling the field φ or $-\varphi$, and hence on the sign of $V_{,\varphi}$, simply because the starting point Lagrangian does depend on this choice in our hyperbolic model.

Similarly to the minimal model, all our analytical estimates above have been checked to agree with very high accuracy with the fully numerical results. For instance, the non-trivial result (8.41) for m_s^2 is accurate to the level 10^{-5} for our two representative examples of SI and NI with $f = 10$. We show in Fig. (8.6) (the absolute values of) $m_{s\,({\rm eff})}^2/H^2$, its three contributions, as well as m_s^2/H^2, for these two examples.

Summary

Let us summarize the important features for the dynamics of the fluctuations that we learned in sections (8.4.3)-(8.4.3), and describe their consequences.

• The deviation of sidetracked inflation's trajectory from a geodesic, and hence the coupling between the adiabatic and entropic fluctuations, is very large, as measured by the parameter $\eta_\perp \gg 1$.

• The super-Hubble effective mass $m^2_{s\,(\mathrm{eff})}$, governing the dynamics of entropic fluctuations once they exit the Hubble radius (see (7.23)), is positive and much larger than the Hubble rate. Hence entropic fluctuations decay extremely fast outside the Hubble radius and the curvature perturbation is expected to be conserved on super-Hubble scales. An adiabatic limit is therefore reached by the end of inflation, rendering the multifield scenario of sidetracked inflation predictive without the need to describe the reheating stage.

• The entropic mass squared m_s^2, which dictates the evolution of the entropic fluctuations inside the Hubble radius — together with its coupling to the adiabatic degree of freedom — has different behaviours in the two field space geometries that we consider: it is much smaller than the Hubble rate in the minimal model (and negative), and much larger in the hyperbolic one. In that case, its sign depends on whether inflation proceeds along increasing or decreasing φ, and hence on the choice of the potential and the branch on which inflation occurs.

Let us stress that a negative entropic mass squared m_s^2 does not by no means imply that the background is unstable. A direct measure of the stability of the latter is provided by the sign of $m^2_{s\,(\mathrm{eff})} = m_s^2 + 4H^2\eta_\perp^2$, which is the mass of the fluctuations orthogonal to the background trajectory in the $k \to 0$ limit. While this quantity becomes negative along $\chi = 0$ after the critical time, signaling the instability of this inflationary solution, and hence the geometrical destabilization, the large positive value of $m^2_{s\,(\mathrm{eff})}/H^2$ in sidetracked inflation was expected, as the latter corresponds by definition to the stable attractor trajectory in these models.

In addition, we saw in section (8.3.4) that one can achieve an effective description of this attractor in terms of one degree of freedom only, in which case the curvature perturbation ζ is conserved on super-Hubble scales [38]. Using the expression of $N(\varphi_{\mathrm{ini}})$ given in table (8.2), and the δN-separate universe picture, one then obtains $\zeta = N_{,\varphi} Q_\varphi$[8], where the right-hand side is evaluated at Hubble crossing such that $k = aH$, and hence

$$\mathcal{P}_{\zeta_k} = \left(\frac{2V}{3(M_{\mathrm{pl}} M m_h)^2} \mathcal{P}_{Q_\varphi} \right)_{k=aH} . \tag{8.43}$$

[8]Note that in table (8.2), the number of e-folds of inflation as a function of initial conditions is evaluated on the sidetracked attractor, in particular with χ determined as a function of φ. This is different from the quantity $N(\varphi_{\mathrm{ini}}, \chi_{\mathrm{ini}})$ one should compute in the δN formalism, but it is legitimate to do so given the strong attractor solution, and hence the negligible dependence of N on χ_{ini}

Taking into account the fact that

$$Q_\sigma = \begin{cases} \left(1+\frac{2\chi^2}{M^2}\right)^{1/2} Q_\varphi & \text{minimal} \\ \left(1+\frac{2\chi^2}{M^2}\right)^{1/2} Q_\varphi + \sqrt{2}\chi/M \left(1+\frac{2\chi^2}{M^2}\right)^{-1/2} Q_\chi & \text{hyperbolic} \end{cases} , \tag{8.44}$$

Eqn. (8.43) consistently coincides with evaluating $\mathcal{P}_{\zeta_k} = (H/\dot\sigma)^2 \mathcal{P}_{Q_\sigma}$ at Hubble crossing (let us recall Eqn. (8.23)), when neglecting Q_χ fluctuations in the hyperbolic model. This is indeed a good approximation, as

$$Q_s = \begin{cases} Q_\chi & \text{minimal} \\ \left(1+\frac{2\chi^2}{M^2}\right)^{-1/2} Q_\chi & \text{hyperbolic} \end{cases} , \tag{8.45}$$

and, as we will see, entropic fluctuations are already negligible compared to adiabatic ones at Hubble crossing. However, note that contrary to standard situations, Eqn. (8.43) is of little practical use without further input, as the non-trivial sub-Hubble dynamics caused by the bending trajectory renders $\left(\mathcal{P}_{Q_\varphi}\right)_{k=aH}$ unknown, or more precisely, it can substantially differ from the purely adiabatic result $\left(\frac{H}{2\pi}\right)^2_{k=aH}$.

Some analytical understanding can however be achieved. In the hyperbolic geometry in particular, we have seen that the entropic mass m_s^2 is much larger than the Hubble rate. This type of framework has been extensively studied (see *e.g.* [127, 132, 222, 236–246]), and it has been shown that the heavy entropic fluctuation can then be integrated out, resulting in a single-field effective theory for the adiabatic fluctuation, with a non-trivial speed of sound different from unity. More surprisingly at first sight, when the entropic mass is much smaller than the Hubble scale, one can still integrate out the entropic fluctuation in the presence of a large bending, as is relevant in the minimal geometry, obtaining then a single-field effective theory with a modified dispersion relation [222, 236, 242, 246]. We make use of these tools in the following section, treating each of the two situations in turn.

8.4.4. Effective Single-Field Theory for the Fluctuations

When the entropic mass of the entropic fluctuation m_s^2 is large compared to the Hubble scale, as it is relevant in the hyperbolic geometry, one can integrate it out: neglecting the first two terms in its equation of motion (Eqn. (8.20)), one can express Q_s in terms of the curvature perturbation ζ, plug it back into the second-order action and deduce

$$S_{(2)\,(\mathrm{EFT})} = \int dt\, d^3k\, \frac{a^3\,\epsilon\, M_{\mathrm{Pl}}^2}{c_s^2(k)} \left[\dot\zeta_k^2 + c_s^2(k) k^2 \frac{\zeta_k^2}{a^2}\right] , \tag{8.46}$$

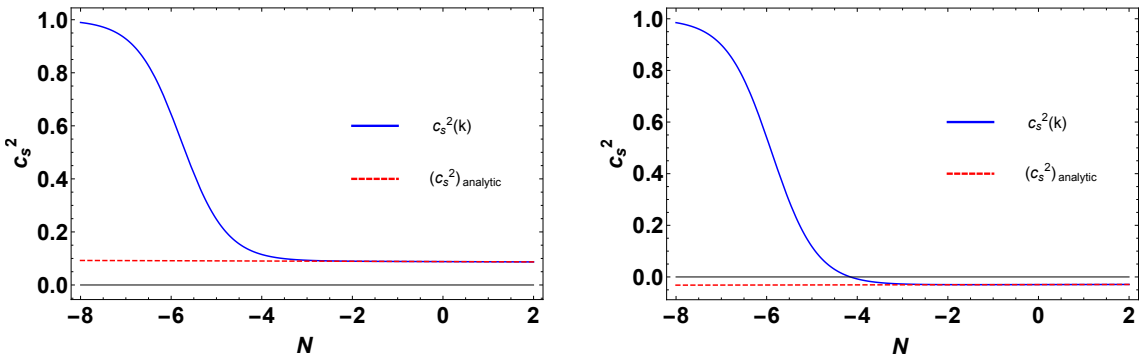

(a) *Starobinsky inflation* **(b)** *Natural inflation* ($f = 10$)

Figure 8.7.: *Fully numerical* $c_s^2(k)$ (8.47) *and analytical result* (8.50) *for its 'late time' behaviour when* $k^2/a^2 \ll m_s^2$*, for the potentials of SI (left) and NI,* $f = 10$ *(right). The corresponding scale crosses the Hubble radius 55 e-folds before the end of inflation, at* $N = 0$ *in the plots.*

where

$$\frac{1}{c_s^2(k)} \equiv 1 + \frac{4H^2\eta_\perp^2}{k^2/a^2 + m_s^2}\,. \tag{8.47}$$

We will discuss below the conditions determining the validity of such an effective field theory (EFT), a subject which has been extensively studied (see *e.g.* [127, 132, 222, 236–246]). Note already that in addition to the condition of a heavy entropic field, $m_s^2 \gg H^2$, one should also verify the generalized adiabaticity condition [238]

$$|\dot{\eta}_\perp/(m_s\eta_\perp)| \ll 1\,, \tag{8.48}$$

expressing the fact that the rate of change of the bending should be smaller than the large entropic mass, so as not to excite high-frequency modes that are not captured by the low-energy effective field theory (8.46). There is no restriction on the amplitude of the bending however, which can consistently be large, as in sidetracked inflation. From the expression (8.37) of $\eta_\perp$ (see also the numerical results in Fig. (8.5)), it is easy to see that the stronger condition $|\dot{\eta}_\perp/(H\eta_\perp)| \ll 1$ holds in sidetracked inflation in the hyperbolic geometry, so that the condition (8.48) is safely verified.

Note that deep on sub-Hubble scales, when $k^2/a^2 \gg (m_s^2, H^2\eta_\perp^2)$, the speed of sound equals unity and one recovers the Bunch-Davies behaviour of the full two-field situation, as it should be. One can not integrate out the entropic field in this regime, but the adiabatic and entropic fluctuations behave as uncoupled free fields, and including the gradient terms in (8.47) can be seen as an effective way to treat in a unified manner this regime and the subsequent one, with good results as we will see. As soon as k^2/a^2 drops below m_s^2, the speed of sound becomes k-independent,

and approximately reads, using (8.37)-(8.42)

$$\frac{1}{c_s^2}-1\simeq 4H^2\eta_\perp^2/m_s^2\simeq\begin{cases}\frac{2}{3}\frac{m_h}{H}\,\mathrm{sign}(V_{,\varphi}) & \mathrm{leading-order}\\ \\ \frac{1}{1+\frac{2\chi^2}{M^2}}\frac{4V_{,\varphi}}{9\sqrt{2}H^2M} & \mathrm{refined}\end{cases} \tag{8.49}$$

where, as before, the refined estimate is very accurate (to the level 5×10^{-3} in SI for instance), while the leading-order one is less accurate (to the level 8×10^{-2} for the same model), but easier to grasp the physics: as $m_h\gg H$, one has $|1/c_s^2-1|\gg1$, and therefore a low speed of sound determined by the hierarchy between the heavy mass m_h and the Hubble scale, given by

$$c_s^2\simeq\frac{3H}{2m_h}\,\mathrm{sign}(V_{,\varphi})\,. \tag{8.50}$$

We show in Fig. (8.7) the fully numerical result (8.47) for $c_s^2(k)$ and the analytical result (8.50) for its 'late time' behaviour when $k^2/a^2\ll m_s^2$, for the scale k_{55} that crosses the Hubble radius 55 e-folds before the end of inflation, at $N=0$ in the plot, and for the potentials of SI (left) and NI, $f=10$ (right). Note that c_s^2 is moderately small in the first case, but the agreement is nonetheless excellent.

As the reader should have noticed, we treated in a unified manner the situations in which the large entropic mass squared m_s^2/H^2 is positive, like in SI, or in which it is negative, like in NI. Although the latter situation is unusual, as it corresponds to a negative speed of sound squared, it does not violate the conditions under which the effective field theory (8.46) has been derived, and its predictive power is equally applicable here. The physical consequences are however very different and we treat each of them separately, beginning with the more conventional situation.

Positive Speed of Sound

When the entropic mass m_s^2 is positive, $c_s^2(k)$ is always positive, and the action (8.46) for $k^2/a^2\ll m_s^2$ describes a standard set-up with a reduced speed of sound c_s given by (8.49)-(8.50). One then finds that ζ_k becomes constant soon after sound Hubble crossing such that $kc_s=aH$, with the usual result [79]

$$\mathcal{P}_{\zeta_k}\simeq\left(\frac{H^2}{8\pi^2\epsilon c_s}\right)_\star\,, \tag{8.51}$$

where here $\star$ denotes evaluation at $kc_s=aH$ (In the three different situations studied respectively in sections (8.4.4), (8.4.4), (8.4.4), the subscript $\star$ indicates an evaluation at different times. This is summarized in table (8.3)). In SI, and for the scale k_{55} that crosses the Hubble radius 55 e-folds before the end of inflation, this predicts a value of the enhancement of the curvature power spectrum compared

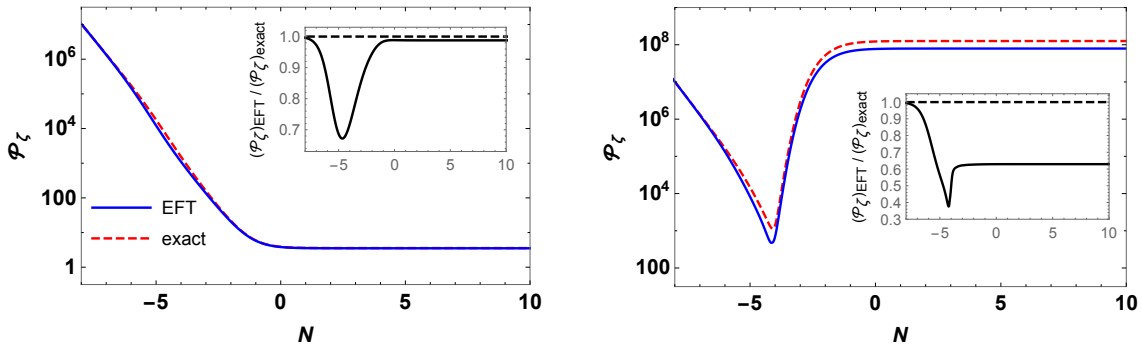

(a) *Starobinsky inflation* **(b)** *Natural inflation* ($f = 10$)

Figure 8.8.: *Power spectra of the curvature perturbation as functions of the number of e-folds, computed numerically in the full two-field model (exact, in dashed red), and from the effective field theory* (8.46) *using* (8.55)*, for SI (left) and NI with* $f = 10$ *(right) in the hyperbolic geometry. The spectra are evaluated for the scale that crosses the Hubble radius 55 e-folds before the end of inflation, at* $N = 0$ *in the plots, and are normalized by the adiabatic result* (8.52)*. The insets show the ratios between the EFT and the exact results.*

to the adiabatic result $\mathcal{P}_\zeta/\mathcal{P}_{\rm ad} \simeq 3.50$ (respectively 3.56 for the two-field numerical result). In Fig. (8.8a) one can also see the very good agreement between the full two-field numerical result and the numerical result corresponding to the effective theory (8.46) (see below for the detailed procedure of the computation). Additionally, one can see in Fig. (8.10a) how the entropic power spectrum decreases as $1/a^3$ as soon as $k^2/(a^2 m_s^2)$ drops below one. Note that all quantities in the various plots of the power spectra in this section are for the scale k_{55}, and are normalized by

$$\mathcal{P}_{\rm ad} = \left(H^2/(8\pi^2\epsilon)\right)_{k=aH} , \tag{8.52}$$

which, as we have explained in section (8.4.2), is the prediction for the curvature power spectrum if the effects of the bending were negligible, which we call the adiabatic result. Thus, the deviation from one of the final value observed for $\mathcal{P}_\zeta$ in these plots is a measure of the non-trivial multifield effects, that occur on sub-Hubble scales in sidetracked inflation. Note also that deep inside the Hubble radius, the Bunch-Davies behaviour implies that all plotted quantities behave as $\simeq k^2/(a^2H^2)$.

From the result (8.51) for the power spectrum, one deduces the familiar expression of the scalar spectral index $n_s - 1 \simeq -2\epsilon_\star - \eta_\star - s_\star$, where $s \equiv c_s'/c_s$. For the scale k_{55}, this gives $n_s \simeq 0.969$, whereas the full two-field numerical result gives $n_s = 0.970$, and the adiabatic result would give $n_s = 0.965$; the agreement between the effective field theory and the full result is thus very good. Note eventually that with the expression (8.50) for c_s^2, one obtains $2s \simeq -\epsilon$, and hence the simplified form of the result $n_s - 1 \simeq -\frac{3}{2}\epsilon_\star - \eta_\star$.

Imaginary Speed of Sound

We now discuss situations in which the effective speed of sound squared is negative (situations in which m_s^2 is negative but c_s^2 is still positive do not arise in our framework, but results of the previous section would apply in that case). Let us first give a few details about how we calculate the EFT prediction. From the action (8.46), one deduces the equation of motion for the complex mode function

$$\ddot{\zeta}_k + H(3+\eta-2s)\dot{\zeta}_k + \frac{c_s^2(k)k^2}{a^2}\zeta_k = 0\,, \tag{8.53}$$

and the quantization condition, which states that

$$\zeta_k\dot{\zeta}_k^* - \dot{\zeta}_k\zeta_k^* = \frac{ic_s^2(k)}{2\epsilon a^3} \tag{8.54}$$

holds at all time. Following [247, 248], one can then easily deduce a non-linear evolution equation for the power spectrum $\mathcal{P}_{\zeta_k} \equiv k^3/(2\pi^2)|\zeta_k|^2$ itself, which reads, in e-fold time:

$$\mathcal{P}''_{\zeta_k} + (3-\epsilon+\eta-2s)\mathcal{P}'_{\zeta_k} + \frac{2c_s^2(k)k^2}{a^2H^2}\mathcal{P}_{\zeta_k} = \frac{1}{2\mathcal{P}_{\zeta_k}}\left(\mathcal{P}'^2_{\zeta_k} + \left(\frac{k^3c_s^2(k)}{4\pi^2\epsilon Ha^3}\right)^2\right)\,. \tag{8.55}$$

One can then easily solve this equation numerically, with initial conditions $\mathcal{P}_{\zeta_k} = \frac{1}{8\pi^2\epsilon}\frac{k^2}{a^2}\left(1+\mathcal{O}((aH)^2/k^2)\right)$ deep inside the Hubble radius, where we took into account that c_s equals unity in this regime. Note that in Eqs. (8.53)-(8.55), $2s \equiv c_s^{2\prime}(k)/c_s^2(k)$. An important subtlety in models with $m_s^2 < 0$, and hence in which $c_s^2(k)$ crosses 0 around $k^2/a^2 \simeq |m_s^2|$, is that s, which multiplies $\mathcal{P}'_{\zeta_k}$ in (8.55), blows up at that time. We then solve Eqn. (8.55) in two steps, before this jump, and afterwards, imposing continuity and the regularity condition $\mathcal{P}'_{\zeta_k} = 0$ as an initial condition for the second phase. In this respect, note that the artifact of c_s^2 crossing zero comes from our will to have a single EFT that captures both the Bunch-Davies regime $k^2/a^2 \gg |m_s^2|$, and the subsequent period. Contrary to what the action (8.46) might suggest, there is no ghost or strong coupling problem in the full two-field theory, and $c_s^2(k)$ becoming negative around $k^2/a^2 \simeq |m_s^2|$ simply signals the tachyonic growth of the entropic fluctuation, which in turns feeds the curvature perturbation. Our matching procedure can thus be physically motivated as interpolating between the Bunch-Davies behaviour, in which $\mathcal{P}_{\zeta_k}$ decreases as $1/a^2$, and the subsequent phase in which $\mathcal{P}_{\zeta_k}$ grows, hence having $\mathcal{P}'_{\zeta_k} = 0$ at the transition.

We show in Fig. (8.8b) the result of this procedure for the model of NI with $f = 10$, together with the numerical result of the full two-field theory. The agreement between the exact result and the one derived from our effective field theory treatment is impressive: the two differ only by a factor of 2 despite the unusually large growth of the power spectrum on sub-Hubble scales, by five orders of magnitude. In addition,

we show in what follows that one can derive an analytical understanding of this large growth, as well as the final result for the power spectrum and its running, building on the matching procedure described above.

Let us consider the action (8.46) in the regime where k^2/a^2 has dropped below $|m_s^2|$, so that c_s^2 is k-independent and negative. The canonically normalized field $v_k = z\zeta_k$ with $z = a\sqrt{2\epsilon}/|c_s|$ verifies the standard equation, of k-inflationary type, $\frac{\mathrm{d}^2 v_k}{\mathrm{d}\tau^2} + \left(c_s^2 k^2 - \frac{1}{z}\frac{\mathrm{d}^2 z}{\mathrm{d}\tau^2}\right) v_k = 0$. As we discussed below Eqn. (8.30), we assume that ϵ and c_s evolve much less rapidly than the Hubble scale, which is well verified in our setup, so that one approximately obtains, with $a \simeq -1/(H\tau)$:

$$\frac{\mathrm{d}^2 v_k}{\mathrm{d}\tau^2} + \left(c_s^2\, k^2 - \frac{2}{\tau^2}\right) v_k \simeq 0\,. \tag{8.56}$$

For practical purposes, we can take c_s^2 to be constant, and the general solution of (8.56) is simply obtained from the usual situation, in which $c_s^2 > 0$, by changing c_s into $i|c_s|$, where we use the notation $|c_s| \equiv \sqrt{|c_s^2|}$ (and similarly for analogous quantities). It reads

$$v_k = A_k e^{k|c_s|\tau}\left(1 - \frac{1}{k|c_s|\tau}\right) + B_k e^{-k|c_s|\tau}\left(1 + \frac{1}{k|c_s|\tau}\right)\,, \tag{8.57}$$

where the standard oscillatory behaviour is now turned into increasing and decreasing exponential ones, and where A_k and B_k are two constants to determined. As explained above, we determine them by requiring that $\zeta_k' = 0$ (implying $\mathcal{P}_k' = 0$) at the matching time such that $k^2 = a^2|m_s^2|$, denoted by a $\star$, and the continuity with the standard Bunch-Davies result $v_k \sim \frac{1}{\sqrt{2k}} e^{-ik\tau}$. This readily gives

$$B_k = A_k e^{2k|c_s|\tau_\star}\,, \tag{8.58}$$

and then

$$A_k = \frac{1}{2\sqrt{2k}} e^{-k|c_s|\tau_\star}\,, \tag{8.59}$$

where we omitted an irrelevant phase factor. The time dependent power spectrum then reads

$$\mathcal{P}_{\zeta_k}(\tau) = \frac{H^2}{32\pi^2\epsilon}\left[e^{x-x_\star}(x-1) + e^{-(x-x_\star)}(x+1)\right]^2\,, \tag{8.60}$$

where $x = k|c_s|\tau \simeq -k|c_s|/(aH)$ is negative and grows with time, from $x_\star$ such that $x_\star^2 \gg 1$, towards zero on super-Hubble scales. Eqn. (8.60), which rightly reproduces the time-dependence of the power spectrum seen in Fig. (8.8b), shows that the two modes are equally important at the transition time, although it is dominated very rapidly by the exponentially growing mode. With $|x_\star| \simeq (|c_s||m_s|/H)_\star$, this gives

the final result for the power spectrum

$$\mathcal{P}_{\zeta_k} = \left(\frac{H^2}{8\pi^2\epsilon} \frac{1}{4} e^{2|c_s| \frac{|m_s|}{H}} \right)_\star = \left(\frac{H^2}{8\pi^2\epsilon} \frac{1}{4} e^{|\frac{m_s^2}{H^2\eta_\perp}|} \right)_\star , \tag{8.61}$$

where we should consistently take for the values of the slowly-varying quantities the ones at the matching time $\star$, *i.e* at entropic mass crossing such that $k^2 = a^2|m_s^2|$. Let us stress that $|c_s|_\star$ here is evaluated using the k-independent limit (8.49) and not (8.47), which would give a vanishing value. Note also that the result (8.61) is expressed in terms of general quantities and holds beyond our particular framework of sidetracked inflation.

Now specifying the general result (8.61) to this setup, and using Eqs. (8.37)-(8.41)-(8.50), one finds that the exponential enhancement simply reads $e^{6\sqrt{2}\chi_\star/M}$, so that the scalar spectral index reads

$$n_s - 1 = -2\epsilon_\star - \eta_\star + 6\sqrt{2}\chi_\star'/M \, . \tag{8.62}$$

For NI with $f = 10$, these results predict a value of the enhancement of the power spectrum compared to the adiabatic result $\mathcal{P}_\zeta/\mathcal{P}_{\rm ad} \simeq 4.4 \times 10^8$ (respectively 1.26×10^8 for the two-field numerical result), as well as $n_s = 0.973$ (respectively 0.974). Given the highly non-trivial and very large growth of the power spectrum, and the degree of arbitrariness in our matching procedure, we find this order one agreement very good for the first result, and rather remarkable for n_s. In addition, although we concentrated here on our representative example, we will comment in section (8.4.5) how our analytical formula enable one to reproduce and understand the full numerical results for a variety of models and parameters.

Before closing this section, let us note that a similar sub-Hubble growth of the curvature perturbation induced by a transient tachyonic instability has already been observed in the literature in reference [222], although it has not been studied in detail. More recently, a two-field model with hyperbolic geometry and that features the same type of behaviour has also been studied [249, 250]. The authors there used a full two-field description, but we note that our description in terms of an effective single-field theory with an imaginary speed of sound seems equally applicable there.

Modified Dispersion Relation

We now discuss the single-field effective field theory behind sidetracked inflation in the minimal geometry. As we have seen, we have $|m_s^2|/H^2 \ll 1$ in that case, and one would usually not expect to be able to integrate out a light field around Hubble crossing. However, this picture can be modified when the background trajectory does not follow a geodesic, as this introduces the new mass scale $H^2\eta_\perp^2$. When it is much larger than the Hubble scale, like in sidetracked inflation, a non-trivial

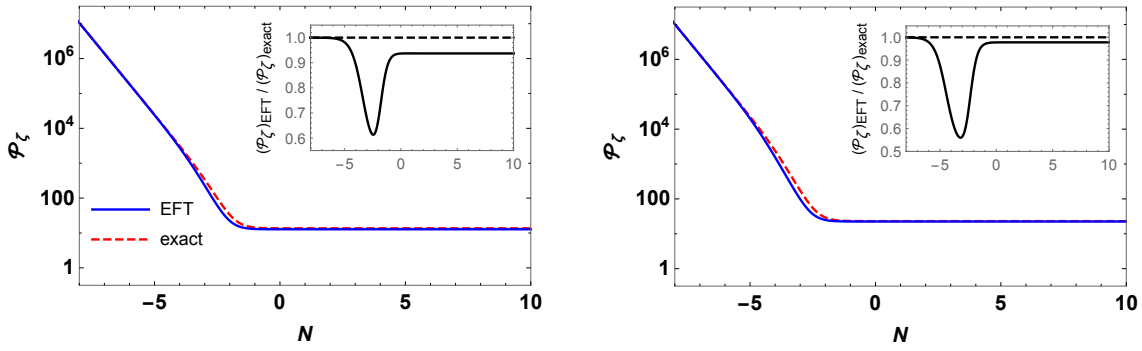

(a) *Starobinsky inflation* **(b)** *Natural inflation* ($f = 10$)

Figure 8.9.: *Power spectra of the curvature perturbation as functions of the number of e-folds, computed numerically in the full two-field model (exact, in dashed red), and from the effective field theory* (8.46) *using* (8.55)*, for SI (left) and NI with* $f = 10$ *(right) in the minimal geometry. The spectra are evaluated for the scale that crosses the Hubble radius 55 e-folds before the end of inflation, at* $N = 0$ *in the plots, and are normalized by the adiabatic result* (8.52)*. The insets show the ratios between the EFT and the exact results.*

dynamics is arising on sub-Hubble scales, and it is then legitimate to integrate out the entropic field. This situation has been studied in references [222, 236, 242, 246], to which we refer the reader for more details. The resulting effective action for the curvature perturbation is still formally given by (8.46), but the relevant energy scale of applicability and phenomenology are markedly different from what we discussed previously.

On sub-Hubble scales, one can now neglect m_s^2 with respect to k^2/a^2 in the expression of the effective speed of sound (8.47). And while the dynamics is naturally of Bunch-Davies type deep on sub-Hubble scales, with $c_s^2(k) \simeq 1$ for $k^2/a^2 \gg H^2\eta_\perp^2$, one obtains $c_s^2(k) \simeq k^2/(4a^2H^2\eta_\perp^2)$ in the relevant intermediate regime $4H^2\eta_\perp^2 \gg k^2/a^2 \gg m_s^2$. The dynamics of the cosmological fluctuations is hence characterized by a non-linear dispersion relation $\omega(k) \propto k^2$, similarly to what arises in ghost inflation [251]. It is distinct however, contrary to what the familiar form of the evolution equation (8.53) might suggest. In that case, indeed, the speed of sound is not slowly evolving compared to the scale factor, and the friction term $-2sH\dot{\zeta}_k$ is not a small correction to the Hubble friction. With $s \simeq -1$ and with $\eta \ll 1$, Eqn. (8.53) indeed reads

$$\ddot{\zeta}_k + 5H\dot{\zeta}_k + \frac{1}{4H^2\eta_\perp^2}\frac{k^4}{a^4}\zeta_k \simeq 0\,, \tag{8.63}$$

which displays both a quadratic dispersion relation and an unusual friction term. Upon quantization and the choice of the Bunch-Davies vacuum, the relevant solution reads [236]

$$\zeta_k = \frac{H}{k^{3/2}}\sqrt{\frac{\pi}{2\epsilon}}\eta_\perp^{1/4}y^{5/2}H^{(1)}_{5/4}(y^2) \tag{8.64}$$

where $y \equiv -k\tau/(2\sqrt{\eta_\perp})$, and all slowly evolving parameters have taken to be con-

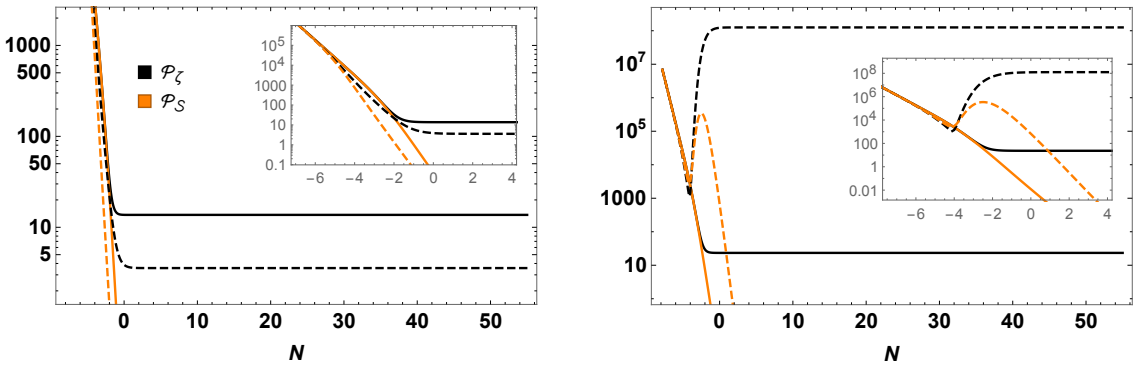

(a) *Starobinsky inflation* **(b)** *Natural inflation* ($f = 10$)

Figure 8.10.: *Adiabatic* ($\mathcal{P}_\zeta$) *and entropic* ($\mathcal{P}_\mathcal{S}$) *power spectra as functions of the number of e-folds, for both the minimal (solid lines) and hyperbolic (dashed lines) internal metrics. The spectra are evaluated for the scale crosses the Hubble radius 55 e-folds before the end of inflation, at* $N = 0$ *in the plots, and are normalized by the adiabatic result* (8.52)*. The insets are details of the same curves around the time of Hubble crossing.*

stants here to obtain an analytical solution. With $y^{5/2}H^{(1)}_{5/4}(y^2) \underset{y\sim 0}{\sim} -i\frac{2^{5/4}}{\pi}\Gamma(\frac{5}{4})$, one finds that the curvature perturbation becomes constant soon after $y \sim 1$, with an almost scale-invariant power spectrum

$$\mathcal{P}_{\zeta_k} = \frac{\sqrt{2}\Gamma(5/4)^2}{\pi^3}\left(\frac{H^2}{\epsilon}\sqrt{\eta_\perp}\right)_\star \tag{8.65}$$

(note that the enhancement of the power spectrum by $\sqrt{\eta_\perp}$ in this kind of setup was first given in [222]). Determining at which time $\tau_\star$ exactly should slowly evolving parameters be evaluated exceeds the accuracy of the calculation here, but it is natural to choose it such that $y_\star = 1$, at the transition between the two asymptotic regimes of the solution (8.64). From (8.65), one then finds

$$n_s - 1 = -2\epsilon_\star - \eta_\star + \frac{1}{2}\left(\frac{\eta_\perp'}{\eta_\perp}\right)_\star , \tag{8.66}$$

where the new last term is small, as we explained below Eqn. (8.48). With the explicit expression (8.34) of $\eta_\perp$, one finds $\frac{\eta_\perp'}{\eta_\perp} \simeq \epsilon + \frac{\chi'}{\chi}\left(1 + \frac{2\chi^2}{M^2}\right)^{-1}$, where it can easily be checked that the second term is negligible compared to the first, simplifying the general result (8.66) to

$$n_s - 1 = -\frac{3}{2}\epsilon_\star - \eta_\star. \tag{8.67}$$

In Fig. (8.9), we show the curvature perturbation power spectrum computed numerically in the full two-field model, and from the effective field theory (8.46) using (8.55), for SI (left) and NI with $f = 10$ (right) in the minimal geometry. The two results are in very good agreement, as well as with the analytical solution (8.64). In SI, the latter predict a value of the enhancement of the power spectrum compared

to the adiabatic result $\mathcal{P}_\zeta/\mathcal{P}_{\rm ad} \simeq 12.9$ (respectively 13.6 for the two-field numerical result), as well as $n_s = 0.969$ (respectively 0.968). In NI, one predicts $\mathcal{P}_\zeta/\mathcal{P}_{\rm ad} \simeq 22.5$ (respectively 23.0 for the two-field numerical result), as well as $n_s = 0.969$ (respectively 0.969).

Summary

Here, we simply collect and present in a unified manner in table (8.3) the characteristic features and analytical results for the observables n_s and r, for the three different types of sidetracked inflationary scenarios that we encountered. We give expressions for the observables that are expressed in terms of general quantities, applicable to other multifield scenarios with the same characteristics, as well as specific results that take into account the particular background of sidetracked inflation. Note that the factor $\left(\frac{H_{k=aH}}{H_\star}\right)^2$ appearing in the expression of r comes from the different time around which the curvature power spectrum and the tensor one become constant.

8.4.5. Numerical Results for all Potentials

In this section, we give the results for the observables r and n_s for the four type of potentials that we have studied, and the various lists of parameters indicated in table (8.1), both for the minimal and the hyperbolic geometry. It is interesting to compare our results with the values of r and n_s of single-field inflation, that is the results in the absence of any geometrical destabilization. The difference between the two outcomes is therefore a measure of the overall observable consequences of the instability and the second sidetracked phase. To better quantify how the predictions are affected by the non-trivial multifield effects, we further do another comparison by displaying the power spectrum parameters calculated on the sidetracked trajectory using the adiabatic description, *i.e.* by completely neglecting entropic perturbations. As the evolution of the scale factor is close to the de-Sitter one, in the sense made precise in section (8.4.2), the adiabatic power spectrum is given to a very good approximation by Eqn. (8.52), which hence gives

$$r_{\rm ad} = 16\,\epsilon\,, \qquad n_{s\,\rm ad} = 1 - 2\epsilon - \eta\,, \tag{8.68}$$

where all quantities are evaluated at Hubble crossing such that $k = aH$.

We present the results in the (n_s, r) plane in Figs. (8.11) and (8.12), while precise values are also listed in the section (8.6). The different markers used in the plots relate to the three descriptions above: the results labeled "exact" correspond to the numerical results in the full sidetracked inflation set-up; the ones labeled "without GD" mean those obtained along $\chi = 0$, *i.e.* when the geometrical destabilization is overlooked; and the description called "adiabatic" is the one where we use Eqn. (8.68) to compute the results of the sidetracked phase.

	Minimal geometry
Entropic mass	$\lvert m_s^2\rvert \ll H^2$
Single-field EFT	Quadratic dispersion relation
Relevant time $\star$	$k/a = 2H\sqrt{\lvert\eta_\perp\rvert}$
r	$\frac{\sqrt{2}\pi}{(\Gamma(5/4))^2}\frac{\epsilon_\star}{\sqrt{\eta_{\perp\star}}}\left(\frac{H_{k=aH}}{H_\star}\right)^2$
$n_s - 1$	$-2\epsilon_\star - \eta_\star + \frac{1}{2}\left(\frac{\eta_\perp'}{\eta_\perp}\right)_\star \simeq -\frac{3}{2}\epsilon_\star - \eta_\star$

	Hyperbolic geometry and $V_{,\varphi} > 0$	Hyperbolic geometry and $V_{,\varphi} < 0$
Entropic mass	$m_s^2 \gg H^2$, $m_s^2 > 0$	$\lvert m_s^2\rvert \gg H^2$, $m_s^2 < 0$
Single-field EFT	Reduced speed of sound $0 < c_s^2 \ll 1$	Imaginary speed of sound $c_s^2 < 0$
Relevant time $\star$	$k/a = H/c_s$	$k/a = \lvert m_s\rvert$
r	$16\,\epsilon_\star c_{s\star}\left(\frac{H_{k=aH}}{H_\star}\right)^2$	$64\,\epsilon_\star e^{-\lvert\frac{m_s^2}{H^2\eta_\perp}\rvert}\left(\frac{H_{k=aH}}{H_\star}\right)^2$ $\simeq 64\,\epsilon_\star e^{-6\sqrt{2}\chi_\star/M}\left(\frac{H_{k=aH}}{H_\star}\right)^2$
$n_s - 1$	$-2\epsilon_\star - \eta_\star - s_\star \simeq -\frac{3}{2}\epsilon_\star - \eta_\star$	$-2\epsilon_\star - \eta_\star + \lvert\frac{m_s^2}{H^2\eta_\perp}\rvert'$ $\simeq -2\epsilon_\star - \eta_\star + 6\sqrt{2}\chi_\star'/M$

Table 8.3.: *Comparison between the three different sidetracked inflationary scenarios.*

All the results that we obtained are in very good agreement with the predictions of the single-field effective theories that we have derived in section (8.4.4), and although it will be tedious to make a detailed account of all the 36 models, we will comment on how the EFT results, summarized in table (8.3), enable one to explain the different behaviours and parameters' dependences that we observe.

Minimal Geometry

We show in fig. (8.11) the results in the minimal geometry (8.4) for the ten models under study, at the fixed curvature scale $M = 10^{-3}M_{\rm Pl}$. One of the first thing to notice is that the exact tensor-to-scalar ratio r is always smaller than its adiabatic counterpart (8.68). This is well understood using the analytical result for r in table

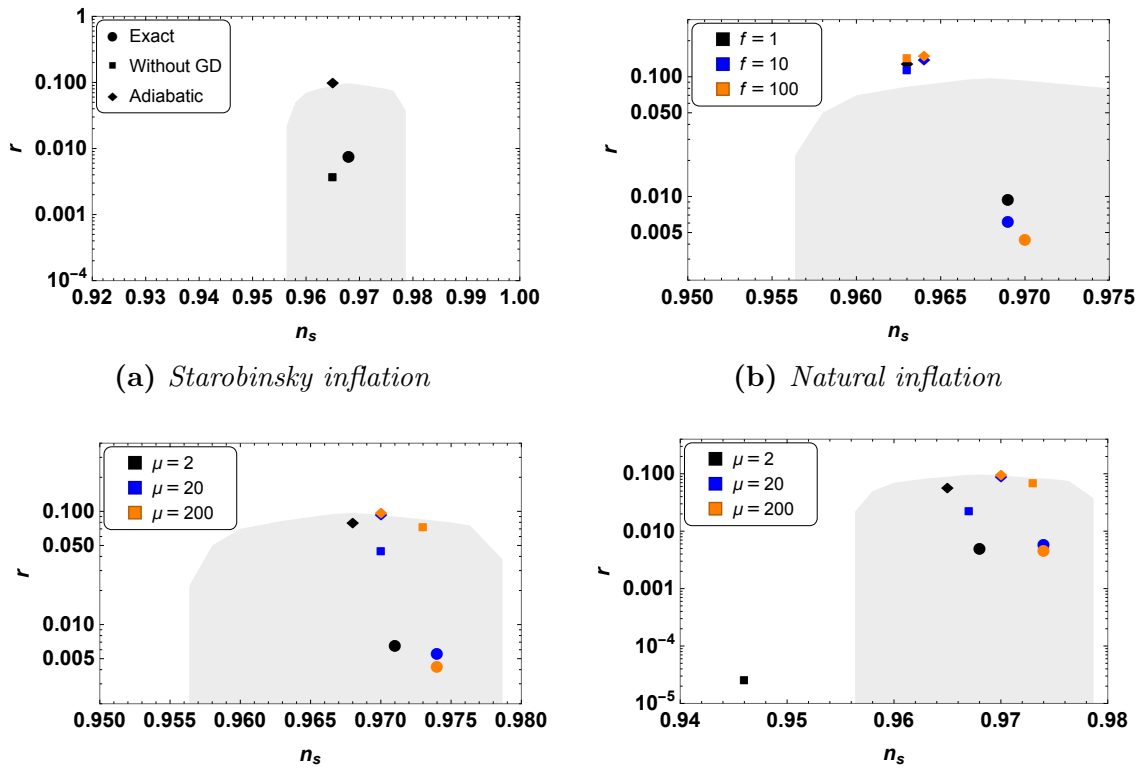

(a) *Starobinsky inflation* **(b)** *Natural inflation*

(c) *Quadratic small field inflation* **(d)** *Quartic small field inflation*

Figure 8.11.: *Results for the power spectrum parameters n_s and r in the minimal field space geometry defined by the metric (8.4). The shaded region represents approximately the experimental bounds of Planck 2015 [46]. As indicated in the legends, different colors label different models, while the marker shapes correspond to the three descriptions we consider, as explained in the main text.*

(8.3), which gives

$$\frac{r}{r_{\rm ad}} \simeq 0.34 \frac{\epsilon_\star}{\epsilon_{k=aH}} \left(\frac{H_{k=aH}}{H_\star}\right)^2 \frac{1}{\sqrt{|\eta_{\perp\star}|}} \,. \tag{8.69}$$

Because ϵ grows in time in these models, the time $\star$ is earlier than the one of Hubble crossing, and more importantly because of the large bending, all the factors in (8.69) are indeed smaller than unity. Note that, since the adiabatic result can be greater than without geometrical destabilization (and is often so), the exact r can also be bigger, like in SI and SFI_4. Concerning the scalar spectral index, one can observe that in all models, $n_s > n_{s\,\rm ad}$. This can also be easily understood, as the result of two effects: first, as ϵ and η are increasing functions of time in these models, one has $(-2\epsilon - \eta)_{k=aH} < (-2\epsilon - \eta)_\star$. Moreover, compared to the adiabatic result, n_s in Eqn. (8.67) has the additional positive contribution $+\frac{1}{2}\left(\frac{\eta_\perp'}{\eta_\perp}\right)_\star \simeq \frac{1}{2}\epsilon_\star$.

One can also observe that for a given model, the bigger the scale f or μ in its potential, and the larger the decrease of r compared to the adiabatic result. One should be careful in the comparison, because the various trajectories are different then. One can nonetheless explain this trend using our analytical formulae. For this, note that the suppression in Eqn. (8.69) is dominated by the large bending, with $\eta_\perp$ given in (8.34) which depends on m_h/H, and χ/M. The bigger the scale f or μ in its potential, and the flatter it is. As the potential gets flatter, the duration of the sidetracked phase increases. And as we used the same initial condition $m_h/H_c = 10$ at the critical time preceding the sidetracked phase, this gives a larger m_h/H when evaluated $\simeq 55$ e-folds before Hubble crossing. Using (8.13), this effect, combined with a flatter potential, generates smaller values of χ/M. This effect is however numerically milder than the growth of m_h/H. This explains why the bending is larger for flatter potentials, and hence why the suppression of r by multifield effects is more important.

Let us also briefly comment on the dependence on the observables on the curvature scale M, with results listed in table (8.7). While the dependence of n_s on M is mild, we observe for all models (except SI) that a smaller M comes with a smaller r. Again, one should be careful in comparing different models, but this result can be understood intuitively: as the field space curvature increases, one expects the sidetracked phase to display more bending, and hence more multifield effects. Indeed, one can check more quantitatively that both χ/M and $\eta_\perp$ increase as M decrease, hence the smaller tensor-to-scalar ratio.

Hyperbolic Geometry

Continuing with the hyperbolic field space geometry (8.6), we present in fig. (8.12) the results of r and n_s for the ten models under study, at the fixed curvature scale $M = 10^{-3} M_{\rm Pl}$. The most striking fact lies in the very small values of r obtained in all models except SI, with a decrease with respect to the adiabatic result by several

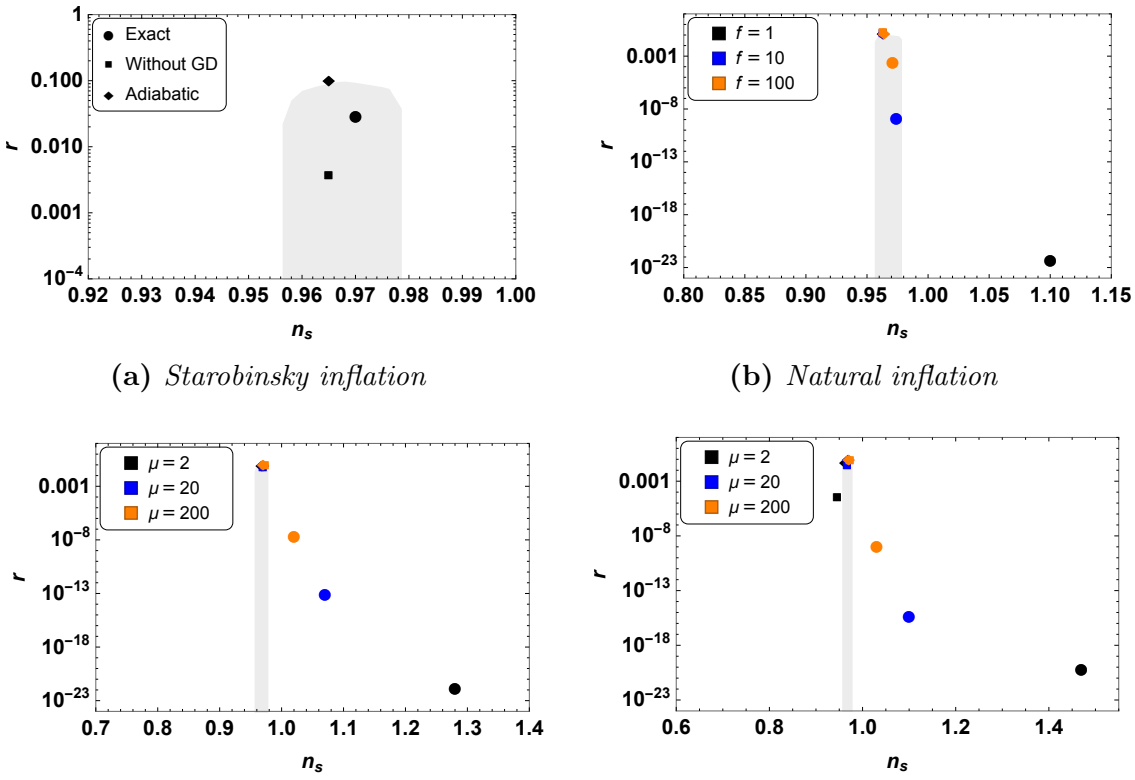

(a) *Starobinsky inflation*

(b) *Natural inflation*

(c) *Quadratic small field inflation*

(d) *Quartic small field inflation*

Figure 8.12.: *Results for the power spectrum parameters n_s and r in the hyperbolic field space geometry defined by the metric (8.6). The shaded region represents approximately the experimental bounds of Planck 2015 [46]. As indicated in the legends, different colors label different models, while the marker shapes correspond to the three descriptions we consider, as explained in the main text. Note the logarithmic scale used to represent the very large spread of values of r.*

orders of magnitude. This is in perfect agreement with the understanding gained in section (8.4.4): like NI, SFI_2 and SFI_4 have a negative slope, hence they fall in the category studied in (8.4.4) of models with a transient tachyonic instability, and that can be described by an effective single-fied theory with an imaginary speed of sound around Hubble crossing. This leads to a very large enhancement of the power spectrum compared to the adiabatic result, and hence a decreased r, following

$$\frac{r}{r_{\mathrm{ad}}} \simeq 4\frac{\epsilon_\star}{\epsilon_{k=aH}}\left(\frac{H_{k=aH}}{H_\star}\right)^2 e^{-6\sqrt{2}\chi_\star/M}\,. \tag{8.70}$$

Like in the minimal case, all the factors on the right hand are smaller than unity, but with $\chi_\star = \mathcal{O}(M)$, the effect is largely dominated by the exponential factor.

Another observation is that n_s in these models can deviate rather strongly from scale invariance, notably with a blue spectrum in SFI_2 and SFI_4. This can be understood using our estimate (8.62): $n_s - 1 = -2\epsilon_\star - \eta_\star + 6\sqrt{2}\chi_\star'/M$. With the approximate expressions (8.14)-(8.10), one can find indeed

$$\frac{\chi'}{M} \simeq \frac{1}{4}\frac{M}{\chi}\left[\frac{M_{\mathrm{Pl}}^2}{2}\left(\frac{V_{,\varphi}}{V}\right)^2 - M_{\mathrm{Pl}}^2\frac{V_{,\varphi\varphi}}{V}\right]\,, \tag{8.71}$$

where all the terms are positive for the concave potentials of SFI_2 and SFI_4 (and the net result is also positive for NI), so that the last contribution to $n_s - 1$ is positive.

Using these formulae, one can also understand the dependence of the observables on the parameter (f and μ) controlling the steepness of the potential. We have seen in section (8.4.5) that the smaller this scale, the bigger the value of $\chi_\star/M$ (remember that the background in the minimal and the hyperbolic geometry are the same to a good approximation). As r depends exponentially on $\chi_\star/M$, this well explains the huge decrease of r as this scale gets lower. As μ say, decreases, two competing effects arise for χ'/M in Eqn. (8.71): M/χ decreases, but $(V_{,\varphi}/V)^2$ and $V_{,\varphi\varphi}/V$ decrease. The latter effect, as $1/\mu^2$, is however more important than the decrease of M/χ, which roughly scales as $\mu^{1/2}$. As a result, $\chi_\star'/M$ increases when lowering μ or f, and so does its large positive contribution to $n_s - 1$, in plain agreement with the results visible in fig. (8.12). Eventually, one can see in table (8.7) that for all models with negative slope, r decreases exponentially as M decreases. We have indeed indicated that χ/M increases as M decrease, so this result is well understood as a result of the exponential dependence of $r \propto e^{-6\sqrt{2}\chi_\star/M}$.

8.5. Primordial Non-Gaussianities

In the preceding section, we have seen that the curvature power spectrum generated in sidetracked inflation can be understood by an effective single-field description of the fluctuations with, depending on the type of scenarios, an imaginary speed

of sound, a reduced speed of sound, or a modified dispersion relation. It is well understood in the framework of the effective field theory of fluctuations that the two latter situations come along with large primordial non-Gaussianities of the curvature perturbation [252]. Hence it is a natural question to investigate the non-Gaussian signal generated in sidetracked inflation (see *e.g.* [48, 253–255] for reviews about primordial non-Gaussianities). For this purpose, we make a preliminary analysis by numerically calculating the bispectrum for the various models under study. It is a non-trivial task, both theoretically and numerically, to calculate the bispectrum from generic nonlinear sigma models of inflation with curved field spaces, and it is only recently that the powerful transport approach has been numerically implemented to calculate the bispectrum in this framework, with the code `PyTransport 2.0`.

8.5.1. Numerical Results

We now discuss our numerical results for the bispectrum, which can all be found in a tabulated form in the Sec. (8.6). In particular, for the minimal geometry (respectively the hyperbolic one), we list in table (8.4) (respectively (8.5)) our numerical results for f_{nl} in the equilateral configuration for the pivot scale k_{55}, for the 10 models under study, and at the fixed curvature scale $M = 10^{-3} M_{\rm pl}$. In table (8.6) (respectively (8.7)), similar results are shown when varying the curvature scale. Eventually, in table (8.8) (respectively (8.9)) we give for all the models the correlations between the shape of the bispectrum and the equilateral and orthogonal templates, as well as the corresponding amplitudes $f_{nl}^{\rm eq}$ and $f_{nl}^{\rm orth}$.

Minimal Geometry

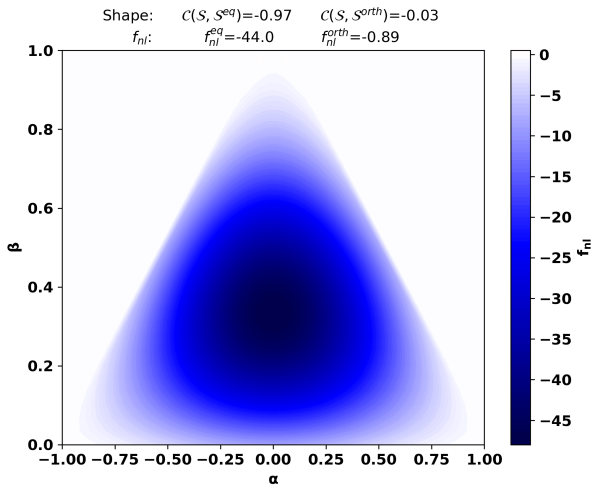

Figure 8.13.: *Shape dependence $f_{nl}(\alpha, \beta)$ generated for NI with $f = 10$ and $M = 10^{-3}$ in the minimal geometry. We used $k_s = 3\,k_{55}$. The shape has a very large correlation with the equilateral template and a very small one with the orthogonal template.*

The first thing to notice is that a large non-Gaussian signal is generated in the minimal geometry for all type of potentials, parameters in the potential and curvature scales, as indicated by the consistently large (negative) values of f_{nl} in the equilateral limit that we find, typically of a few tens, ranging from -7 to -98. The second striking result is that the non-Gaussian shape has a very large (anti) correlation with the equilateral template — we find an overlap of -0.97 for all models — and a negligible correlation with the orthogonal one — with an overlap always less than 0.03 (see table (8.8)). The fact that the shape is almost indistinguishable from the equilateral one is illustrated in fig. (8.13) for the representative example of NI with $f = 10$. More quantitatively, the fact that the shape is faithfully represented by the equilateral template implies a very low value of $f_{nl}^{\rm orth} \lesssim 1$, and a value of $f_{nl}^{\rm eq}$ almost identical to the reduced bispectrum (2.147) in the equilateral limit (only lowered by few percents). Eventually, we observe a very clear correlation between the curvature scale and the parameter controlling the steepness of the potential on the one hand, and the value of $f_{nl}^{\rm eq}$ on the other hand: the latter grows as M decreases, or the steepness parameter f or μ increases, in the same way as the bending parameter $\eta_\perp$ does. More quantitatively, we find that all the results are in very good agreement with the simple behaviour

$$f_{nl}^{\rm eq} \simeq \eta_{\perp\star}\,, \tag{8.72}$$

up to an order one coefficient. Similar results for the shape and the amplitude of the bispectrum have been found in related contexts in references [236, 242, 246] by using the effective field theory of fluctuations. There, however, only the quadratic action for the entropic field was taken into account in the unitary gauge. The fact that our full numerical results agree with this picture hints at the fact that the interactions taken into account there are dominant, and it would be interesting to study this further. Note also that although one obtains large negative values for $f_{nl}^{\rm eq}$, they lie within the Planck constraints (2.199) for all the models we have studied, with the only exception of NI with $f = 100$ and $M = 10^{-3}$.

Eventually, we display in figure (8.14) the time evolution of the reduced bispectrum in the equilateral configuration for the scale k_{55}, for the representative model of NI with the five different combinations of parameters that we studied. We can see that the bispectrum starts to differ from the Bunch-Davies regime a few e-folds before Hubble crossing (arising at $N = 10$ e-folds in the plot), and one can check that this arises when $2H\sqrt{|\eta_\perp|}$ becomes non-negligible compared to k/a, in agreement with the identification in section (8.4.4) of this relevant timescale for the physics of the fluctuations. After a rapid growth, the bispectrum then stabilizes at its final value soon after Hubble crossing.

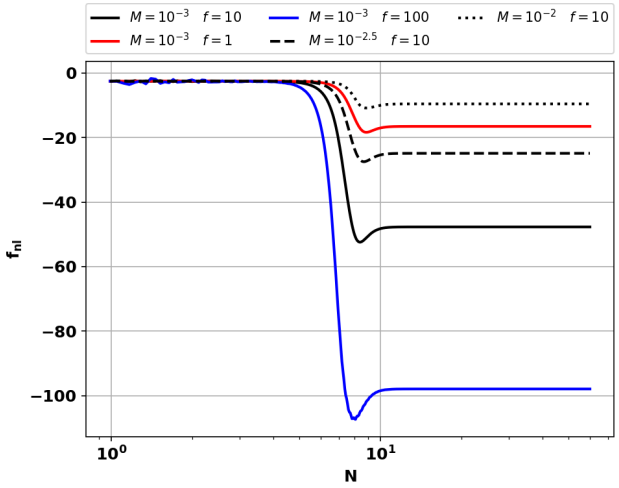

Figure 8.14.: *Time evolution of the reduced bispectrum (2.147), evaluated on the equilateral triangle for the pivot scale k_{55}, for NI in the minimal geometry, and different parameters for the curvature scale M and steepness parameter f. Note that that we use of a logarithmic scale for the number of e-folds, and that Hubble crossing arises at $N = 10$ e-folds.*

Hyperbolic Geometry

As far as the hyperbolic geometry is concerned, based on the understanding of the linear fluctuations in section (8.4.4), one can expect two qualitatively different results, respectively for models with $V_{,\varphi} > 0$, which are characterized by a reduced speed of sound, and for the ones with $V_{,\varphi} < 0$, that feature a transient tachyonic instability induced by an effective imaginary speed of sound. In our models, only Starobinsky inflation belong to the first class. Unfortunately, we have not been able to reliably compute the bispectrum numerically for this model. As the effective field theory of fluctuations indicate though [252], a reduced sound speed implies the appearance of boosted cubic interactions leading to an equilateral-type contribution to the bispectrum of amplitude $f_{nl}^{\rm eq} \sim 1/c_s^2$. Additional cubic interactions can however be present, and we leave for future work a more in-depth study of this setup, both numerically and analytically.

Concentrating on the other class of models, with NI, SFI_2 and SFI_4, we find again, for all models with curvature scale $M = 10^{-3}$, a large negative reduced bispectrum of a few tens in the equilateral limit, with values ranging from -16 to -57. The same qualitatively holds true when varying the curvature scale, but the value of f_{nl} can sometimes be reduced to $\simeq 1$, as we find for NI ($f = 10$) and SFI_2 ($\mu = 20$) with $M = 10^{-2}$. However, the striking difference compared to the minimal geometry concerns the shape of the bispectrum: although the values of the two correlations depend on the precise model, we find across all of them a small overlap with the equilateral template (typically $\simeq -0.1$, ranging from -0.01 to -0.47), and a very significant one with the orthogonal shape (typically $\simeq -0.78$, ranging from -0.66 to

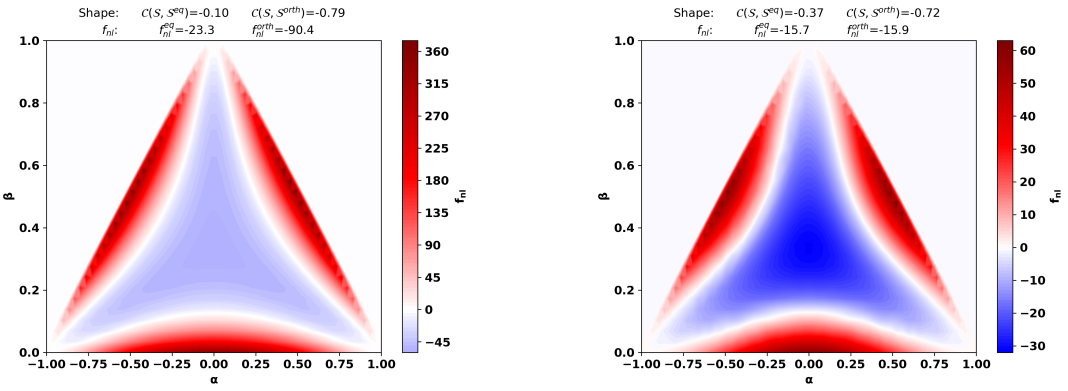

(a) *Natural inflation ($f = 10$)* **(b)** *Natural inflation ($f = 100$)*

Figure 8.15.: *Shape dependence $f_{nl}(\alpha, \beta)$ generated for NI with $f = 10$ (left) and $f = 100$ (right), in the hyperbolic geometry for $M = 10^{-3}$. We used $k_s = 3\,k_{55}$. We see for both of them a modest anti-correlation with the equilateral shape template and a large anti-correlation with the orthogonal shape template.*

-0.80). It is rather unusual to generate orthogonal non-Gaussianities. Let us recall indeed that the orthogonal shape has been designed in the context of the effective field theory of inflation by carefully choosing a linear combinations of otherwise equilateral-type shapes [53], so as to fully cover the space of possible shapes in the simplest singe-field extensions of slow-roll inflation. As a result, in the past it is only for rather fine-tuned parameters that this shape of the bispectrum has been shown to be generated in explicit models (see *e.g.* [47, 256, 257]).

We show in fig. (8.15) the shapes of the bispectra obtained for NI with $M = 10^{-3}$, for the two parameters $f = 10$ and $f = 100$, as they are representative of the other models. The main difference with the shape obtained in the minimal geometry in fig. (8.13) is readily apparent: the bispectrum is still negative in the equilateral limit, but it changes sign and becomes positive for squashed, and more generally, for flattened triangles, a distinctive feature of the orthogonal shape (with negative $f_{nl}^{\rm orth}$). In both cases, the amplitude of the signal is even more important in the squashed configuration than in the equilateral limit. The difference between the amplitudes in the two configurations is comparatively less pronounced for $f = 100$ however, which explains why the correlation with the equilateral shape is larger in that case than for $f = 10$.

Similarly to the minimal geometry, we show in fig. (8.16) the time evolution of the reduced bispectrum in the equilateral configuration for the scale k_{55}, for the representative model of NI with the five different combinations of parameters that we studied. We can check that the bispectrum starts to differ from the Bunch-Davies regime when $|m_s^2|$ becomes non-negligible compared to k^2/a^2, and that the bispectrum has become constant already at Hubble crossing. The time-dependence however is more complicated than in the minimal geometry, especially for $M = 10^{-3}$ with an oscillatory behaviour of the bispectrum for $f = 10$ and $f = 1$, and in that

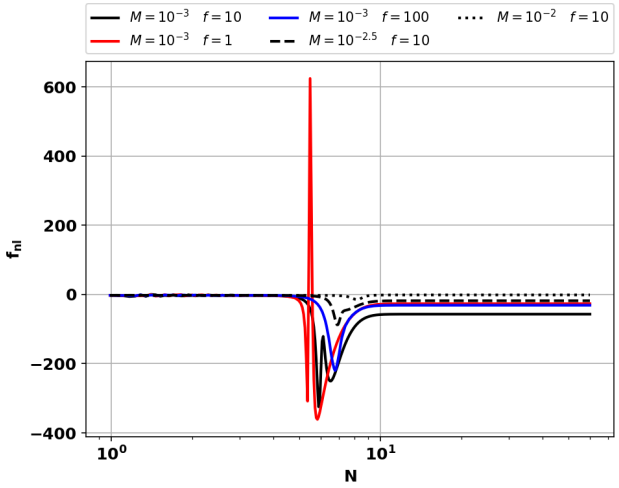

Figure 8.16.: *Time evolution of the reduced bispectrum (2.147), evaluated on the equilateral triangle for the pivot scale k_{55}, for NI in the hyperbolic geometry, and different parameters for the curvature scale M and steepness parameter f. Note that that we use of a logarithmic scale for the number of e-folds, and that Hubble crossing arises at $N = 10$ e-folds.*

case, with even a brief spike of f_{nl} to large positive values before returning to negative values.

As far as the parameters' dependence is concerned, one globally observes the same trends as in the minimal geometry: decreasing the curvature scale, or the steepness parameter of the potential, comes with an increase of the bispectrum in the equilateral configuration. The latter monotonous behaviour is broken for NI though, which generates f_{nl} in this limit smaller for $f = 100$ than for $f = 10$. More importantly, as the shape differs strongly from the equilateral one, the reduced bispectrum in the equilateral configuration, although instructive, does not faithfully represent the overall amplitude of the bispectrum. This can be easily seen in fig. (8.15) where, as we have noticed, the bispectrum is larger in the squashed configuration than in the equilateral one. A more robust measure of the non-Gaussianities is provided by the amplitude of the orthogonal signal f_{nl}^{orth}. The latter is always found to be roughly minus a quarter of the reduced bispectrum in the squashed configuration, and contrary to the signal in the equilateral limit, the global trend is that f_{nl}^{orth} decreases as the steepness parameter increases (see table (8.9)). This is at least what we observe for NI and SFI_2, with SFI_4 breaking this monotonous behaviour in that case. Thus there is no obvious universal relationship that we can observe between values of background quantities and f_{nl}^{orth}, although for NI and SFI_2, one has the rough behaviour $f_{nl}^{\text{orth}} \sim \mathcal{O}\left(6\sqrt{2}\chi_\star/M\right)$. It would of course be interesting to understand analytically the appearance of the orthogonal shape as well as its amplitude, which we leave for future work.[9]

Note eventually that the values one obtains for f_{nl}^{orth} often lie beyond the Planck

[9]It has later been shown in reference [258] how an orthogonal-type shape originates on general grounds from an imaginary speed of sound.

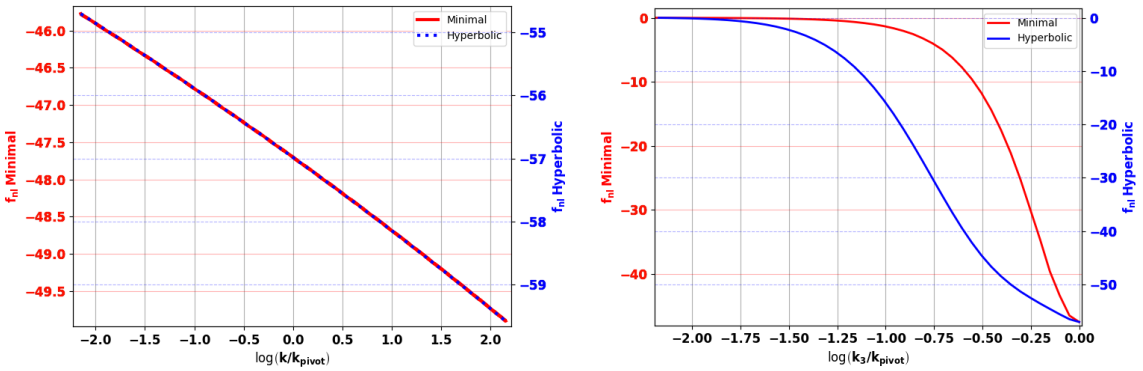

Figure 8.17.: *Left: scale dependence of the reduced equilateral bispectrum over a range of scales exiting the Hubble radius between* 60 *and* 50 *e-folds before the end of inflation, for NI with* $f = 10$ *and* $M = 10^{-3}$*, in the minimal geometry (red) and the hyperbolic one (blue). Right: for the same models and color coding, reduced bispectrum* $f_{nl}(k_1, k_2, k_3)$ *for* $k_1 = k_2 = k_{\rm pivot} = k_{55}$ *and* $k_3 \to 0$*, showing how the single-clock consistency relation is verified in the squeezed limit. Note each time the two different scales for the vertical axes.*

observational bound (2.199), contrary to the equilateral bispectrum generated in the minimal geometry. Moreover, when $f_{nl}^{\rm orth}$ is within the observational bound, it is the spectral index that is often too blue compared to the observations, leaving only, within the models we have studied, NI with $f = 100$ and $M = 10^{-3}$ as a viable model (and marginally NI with $f = 10$ and $M = 10^{-2.5}$).

Squeezed Limit and Scale Dependence of the Bispectrum

Eventually, as the reader might have noticed from figs. (8.13) and (8.15), all the bispectra that we have computed have a small amplitude in the squeezed limit. This is expected theoretically, as we have seen that one can derive an effective single-field theory for the fluctuations, so that all models should verify the single-clock consistency relation from Eqn. (4.40) [106, 119]. This relation is indeed satisfied, as one shows in fig. (8.17) (right) for the two models of NI with $f = 10$ and $M = 10^{-3}$, in the minimal and in the hyperbolic geometry. There, we plot $f_{nl}(k_1, k_2, k_3)$, keeping two modes the same ($k_1 = k_2 = k_{\rm pivot} = k_{55}$), and letting $k_3 \to 0$, i.e. approaching the squeezed limit, finding that the single-clock consistency relation $f_{nl}^{\rm squeezed} = \frac{5}{12}(1 - n_s)(k_{\rm pivot})$ is well verified as soon as $k_3 \ll k_{\rm pivot}$.

Eventually, while we concentrated our efforts on studying the shape of the bispectrum generated in sidetracked inflation, it is useful to comment on its scale dependence. For this, we show in fig. (8.17) (left) the reduced bispectrum in the equilateral configuration over a range of scales exiting the Hubble radius between 60 and 50 e-folds before the end of inflation, for the same models of NI with $f = 10$ and $M = 10^{-3}$ in the two geometries. We have chosen to overlap the two cases for better comparison (note therefore the two different scales for the vertical axis). It is

clear they both have very small scale dependencies with $d\log|f_{nl}|/d\log(k) \sim 0.02$.

8.6. Tabulated Results

Acronym	Parameter	r	n_s	f_{nl}	$r_{\rm ad}$	$n_{s\,\rm ad}$
SI	-	0.0075	0.968	-16.31	0.10	0.965
NI	$f = 1$	0.0095	0.968	-16.54	0.13	0.963
	$f = 10$	0.0063	0.969	-47.71	0.14	0.964
	$f = 100$	0.0046	0.970	-97.95	0.15	0.964
SFI_2	$\mu = 2$	0.0065	0.971	-12.85	0.079	0.968
	$\mu = 20$	0.0056	0.973	-25.32	0.094	0.970
	$\mu = 200$	0.0043	0.974	-46.63	0.097	0.970
SFI_4	$\mu = 2$	0.0049	0.967	-11.40	0.057	0.965
	$\mu = 20$	0.0059	0.973	-20.63	0.090	0.970
	$\mu = 200$	0.0046	0.974	-39.14	0.096	0.970

Table 8.4.: *Results of sidetracked inflation in the minimal geometry with* $M = 10^{-3}M_{\rm pl}$. f_{nl} *is the reduced bispectrum* (2.147) *evaluated on the equilateral triangle for the pivot scale* k_{55}.

8.7. Comparisons with Cosmological Attractors

In this section we would like to address the question of whether the geometrical destabilization, and sidetracked inflation in particular, could play a relevant role in cosmological attractors. A recent work [259] has established that the predictions for the power spectrum parameters in α-attractors remain universal even when the multifield dynamics is important (see also the recent work [260] in which similar conclusions are reached in multifield ξ attractors). Sidetracked inflation has some interesting similarities with the axion-dilaton model of [259]—in both scenarios the second field evolves away from the minimum of the potential trough—and yet the predictions are markedly different. We have seen that the results of sidetracked inflation are typically highly sensitive to multifield effects, while the opposite appears to happen in the α-attractor set-up.

One reason for this discrepancy can be easily understood if we express our hyperbolic metric model, Eqn. (8.6), in Poincaré disk coordinates. It is simpler to first go

Acronym	Parameter	r	n_s	f_{nl}	$r_{\rm ad}$	$n_{s\,\rm ad}$
SI	-	0.029	0.969	*	0.10	0.965
NI	$f = 1$	4.5×10^{-23}	1.10	-26.77	0.13	0.963
	$f = 10$	1.2×10^{-9}	0.974	-56.98	0.15	0.963
	$f = 100$	5.9×10^{-4}	0.970	-31.24	0.15	0.964
SFI_2	$\mu = 2$	1.5×10^{-22}	1.282	-19.00	0.079	0.968
	$\mu = 20$	8.0×10^{-14}	1.066	-31.33	0.095	0.970
	$\mu = 200$	2.0×10^{-8}	1.019	-51.50	0.097	0.970
SFI_4	$\mu = 2$	5.4×10^{-21}	1.476	–15.92	0.055	0.963
	$\mu = 20$	4.0×10^{-16}	1.105	-25.21	0.091	0.969
	$\mu = 200$	1.1×10^{-9}	1.030	-46.69	0.097	0.970

Table 8.5.: *Results of sidetracked inflation in the hyperbolic geometry with* $M = 10^{-3} M_{\rm pl}$. f_{nl} *is the reduced bispectrum* (2.147) *evaluated on the equilateral triangle for the pivot scale* k_{55}. * *for SI indicates that we have not been able to reliably compute the bispectrum, as we explain in the main text.*

to half-plane coordinates (X, Y) with

$$\varphi = \frac{M}{\sqrt{2}} \log Y \,, \qquad \chi = \frac{M}{\sqrt{2}} \frac{X}{Y} \,, \tag{8.73}$$

so that the field space metric takes the form

$$ds^2_{\rm fs} = 2M^2 \, \frac{dX^2 + dY^2}{4Y^2} \qquad (-\infty < X < \infty \,,\, 0 < Y) \,. \tag{8.74}$$

The transformation to disk coordinates (ρ, θ) is given by the standard formulae

$$X = \frac{2\rho \sin\theta}{1 + \rho^2 - 2\rho\cos\theta} \,, \qquad Y = \frac{1 - \rho^2}{1 + \rho^2 - 2\rho\cos\theta} \,, \tag{8.75}$$

and

$$ds^2_{\rm fs} = 2M^2 \, \frac{d\rho^2 + \rho^2 d\theta^2}{(1-\rho^2)^2} \qquad (0 \leqslant \rho < 1 \,,\, 0 \leqslant \theta < 2\pi) \,. \tag{8.76}$$

The contours of constant φ and χ in the Poincaré disk are shown in fig. (8.18). The φ contours are given by circles of radius $(1 + e^{\sqrt{2}\,\varphi/M})^{-1}$ and centered at the Cartesian point $(x_\varphi, 0)$ with $x_\varphi = (1 + e^{-\sqrt{2}\,\varphi/M})^{-1}$. The χ contours are also part of circles of radius $\sqrt{1 + M^2/2\chi^2}$ with center at the Cartesian point $(0, y_\chi)$, with $y_\chi = -M/(\sqrt{2}\,\chi)$. Since during most of the sidetracked inflationary phase, $\varphi/M \gg 1$ for the models we have investigated, we observe that inflation is spent very near

Acronym	Parameter	r	n_s	f_{nl}
SI	$M = 10^{-2}$	NA	NA	NA
	$M = 10^{-2.5}$	0.0057	0.965	-11.31
	$M = 10^{-3}$	0.0075	0.968	-16.31
$NI\ f = 10$	$M = 10^{-2}$	0.0131	0.969	-9.56
	$M = 10^{-2.5}$	0.0085	0.969	-24.89
	$M = 10^{-3}$	0.0063	0.969	-47.71
$SFI_2\ \mu = 20$	$M = 10^{-2}$	0.0088	0.975	-7.62
	$M = 10^{-2.5}$	0.0067	0.973	-16.52
	$M = 10^{-3}$	0.0056	0.973	-25.32
$SFI_4\ \mu = 20$	$M = 10^{-2}$	0.0070	0.976	-6.53
	$M = 10^{-2.5}$	0.0064	0.972	-13.99
	$M = 10^{-3}$	0.0059	0.973	-20.63

Table 8.6.: *Results of sidetracked inflation in the minimal geometry, here with varying M. f_{nl} is the reduced bispectrum (2.147) evaluated on the equilateral triangle for the pivot scale k_{55}. NA indicates that the sidetracked phase lasts less than 55 e-folds.*

the rightmost corner of the disk, i.e. near the edge of the Poincaré disk at $\rho = 1$.

The single-field inflationary path $\chi = 0$, which is potentially unstable because of the geometrical destabilization, corresponds to the lines $\theta = 0, \pi$, on which

$$\rho = \tanh\left(\pm\varphi/\sqrt{2}M\right) , \tag{8.77}$$

where the $+$ sign (respectively $-$) correspond to $\varphi > 0$, $\theta = 0$ (respectively $\varphi < 0$, $\theta = \pi$). This is the familiar relation that gives rise to the stretching of the potential in α-attractors. The origin of this property can be traced to the presence of a pole at $\rho = 1$ in the kinetic term of the inflaton before canonical normalization, and the universality of the predictions of cosmological attractors stems from the fact that inflationary parameters depend, to leading order in the number of e-folds, only on the characteristics of the pole [194].

However, a crucial assumption behind this is that the potential must be regular at $\rho = 1$. This is hardly restrictive when only the inflaton potential is concerned, since in α-attractors the potential is usually analytic at the pole's location. But things get more intricate in the two-field scenario and the choice of parametrization

Acronym	Parameter	r	n_s	f_{nl}
SI	$M = 10^{-2}$	NA	NA	NA
	$M = 10^{-2.5}$	NA	NA	NA
	$M = 10^{-3}$	0.029	0.969	*
$NI\ f = 10$	$M = 10^{-2}$	0.0024	0.991	-1.40
	$M = 10^{-2.5}$	6.875×10^{-6}	0.977	-18.19
	$M = 10^{-3}$	1.2×10^{-9}	0.974	-56.98
$SFI_2\ \mu = 20$	$M = 10^{-2}$	0.0020	1.038	-1.03
	$M = 10^{-2.5}$	4.3×10^{-7}	1.027	-15.78
	$M = 10^{-3}$	8.0×10^{-14}	1.066	-31.33
$SFI_4\ \mu = 20$	$M = 10^{-2}$	NA	NA	NA
	$M = 10^{-2.5}$	9.0×10^{-8}	1.054	-14.74
	$M = 10^{-3}$	4.0×10^{-16}	1.105	-25.21

Table 8.7.: *Results of sidetracked inflation in the hyperbolic geometry, here with varying M. f_{nl} is the reduced bispectrum (2.147) evaluated on the equilateral triangle for the pivot scale k_{55}. NA indicates that the sidetracked phase lasts less than 55 e-folds. * for SI with $M = 10^{-3}$ indicates that we have not been able to reliably compute the bispectrum, as we explain in the main text.*

becomes important. Indeed, from (8.73) and (8.75) we see that

$$\chi = \frac{M}{\sqrt{2}} \frac{2\rho \sin\theta}{1-\rho^2}\,, \tag{8.78}$$

and so any pedestrian polynomial function of the heavy field χ will have a pole at $\rho = 1$ when expressed in disk coordinates. In particular the simple mass term $m_h^2\,\chi^2/2$ that we have used in our models has a pole of order two, just like the kinetic term.

The conclusion is that the existence of a pole shared by both the kinetic and potential terms in a hyperbolic nonlinear sigma model action can invalidate the universal predictions of cosmological attractors. Our results of sections (8.4) and (8.5) are clear evidence that this is the case, as we have seen that the predictions of the sidetracked inflation scenario are quite sensitive to the form of the potential and the scales involved. We therefore expect that our findings may be useful to better understand the constrains that the potentials must satisfy for instance in α-attractors,

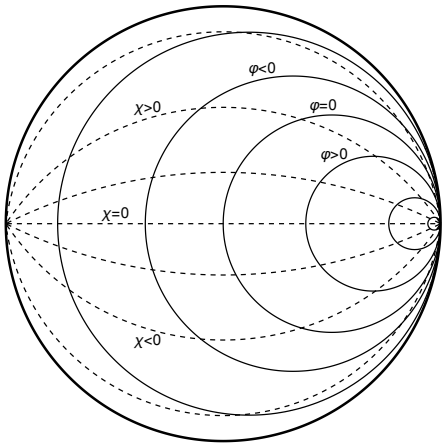

Figure 8.18.: *Constant φ (solid curves) and χ (dashed curves) contours in the Poincaré disk.*

but also more generally.[10] Indeed, although above we focused on the hyperbolic manifold, similar conclusions regarding the presence of coordinate singularities are likely to apply for more general field space metrics.

8.8. Discussion

We observed that the background dynamics of the sidetracked phase is very similar for the two types of geometries, which we have examined analytically. In each model, the heavy field is adiabatically following the inflaton, stabilized by the competition between the force originating from the field space geometry and the one from its potential, like in the gelaton model [132]. This field in turn modifies the dynamics of the inflaton, slowing it down by giving it more inertia. The background dynamics can hence be described by an effective single-field model with unusual properties. In particular it allows inflation on potentials that would otherwise be too steep for standard slow-roll inflation, with the weaker requirement that the potential be flat with respect, not to the Planck scale, but to the curvature scale of the field space manifold.

Equipped with our analytical understanding of the background, we were able to explain the very different behaviours exhibited by the cosmological fluctuations in the two geometries, despite the very similar background dynamics. In both cases, the deviation of sidetracked inflation's trajectory from a geodesic, and hence the coupling between the adiabatic and entropic fluctuations, is very large. However, in the minimal geometry, the mass of the entropic fluctuation is small compared to the Hubble scale, whereas it is large in the hyperbolic geometry. Moreover, in this case, the entropic mass squared can be positive or negative, depending on whether the slope of the inflaton potential being positive or negative. Building on previous

[10] We also remark that in the models we have considered the potential is clearly not a monotonic function of ρ, which was one of the assumptions made in [259].

studies, we showed that the resulting dynamics of the curvature perturbation can be described by an effective single-field theory, in which the entropic fluctuations have been integrated out, albeit with very different properties in each case: a modified dispersion relation when the entropic field is light in the minimal geometry, and a reduced speed of sound or an imaginary one, depending on the potential, in the hyperbolic geometry. In each of these three qualitatively different scenarios, we gave analytical formulae for the tensor-to-scalar-ratio r and the spectral index n_s, showing how they enable to reproduce and understand the full numerical results and their parameter dependencies.

Scenarios described by a single-field effective theory with an imaginary speed of sound around the time of Hubble crossing arise in the presence of a large and tachyonic mass of the entropic fluctuation. While this generates a transient tachyonic growth of the fluctuations, we stress that these situations do not present any fundamental pathology. In particular, they can be perfectly compatible with a stable background, as it is here, in the presence of a trajectory deviating strongly from a field space geodesic that render the *super-Hubble* entropic mass squared, the true indicator of the stability or not of the background, indeed positive.

We also made a preliminary numerical study of the bispectrum generated in sidetracked inflation, finding for almost all models large non-Gaussianities, but characterized by different shapes: equilateral in the minimal geometry, and orthogonal in scenarios featuring an imaginary speed of sound in the hyperbolic geometry.[11] While models of the first type are typically in agreement with observational bounds on non-Gaussianities, for the second type we find large negative values of $f_{nl}^{\rm orth}$ that often exceed the Planck constraints, together with marked deviations from scale invariance, although some models are observationally viable.

Lastly we made a brief comparison between sidetracked inflation and the two-field cosmological attractor models that arise in supergravity implementations of inflation. We pointed out that beyond the single-field case the choice of field parametrization becomes subtle—a simple quadratic potential for our heavy field was seen to exhibit a pole at the edge of the Poincaré disk. We argued that such a singularity evades the assumptions that lead to the universality of the predictions of cosmological attractors, and indeed our results were seen to depend strongly on the details of the potential. It would hence be interesting to gain further insight into the role of the pole structure of the potential beyond the simple case we have considered as well as for more general field space manifolds.

In the future it would be interesting to study if a fully non-linear single-field effective description of sidetracked inflation can be made, that would enable to unify the effective single-field dynamics that we derived separately for the background and the fluctuations. Such a description is known in related frameworks like the

[11] The link between an imaginary speed of sound and orthogonal and flattened non-Gaussianities has later been made in reference [258].

gelaton model, giving rise to effective k-inflationary models. However, preliminary investigations indicate that the two setup differ, as one can anticipate by noting that sidetracked inflation can exhibit modified dispersion relations that are not present in k-inflationary models.

We should note as well that the nonlinear sigma models we have examined are phenomenological and don't have an obvious theoretical justification, since our goal for now has been to gain insight into the physics of sidetracked inflation rather than to provide a top-down motivation for it. The hyperbolic plane metric is perhaps the most interesting case study because of its maximal isometries and its relation to α-attractor models, but the class of potentials we considered is of course restricted. Similarly, our focus on the minimal geometry was motivated by its simplicity. It cannot be regarded as a consistent truncation of an effective field theory for the reason that the heavy scalar field probes values of order M during the sidetracked inflationary phase, and this is precisely the scale at which the putative effective theory is expected to break down (although as usual the true cutoff may be actually even lower).

Acronym	Parameter	M	$\mathcal{C}(S, S^{\rm eq})$	$\mathcal{C}(S, S^{\rm orth})$	$f_{nl}^{\rm eq}$	$f_{nl}^{\rm orth}$
SI		10^{-2}	NA	NA	NA	NA
		$10^{-2.5}$	-0.97	-0.03	-10.4	-0.2
		10^{-3}	-0.97	-0.03	-15.0	-0.3
NI	$f = 1$	10^{-3}	-0.97	-0.03	-15.2	-0.3
	$f = 10$	10^{-2}	-0.97	-0.01	-8.99	-0.07
	$f = 10$	$10^{-2.5}$	-0.97	-0.03	-23.0	-0.43
	$f = 10$	10^{-3}	-0.97	-0.03	-44.0	-0.89
	$f = 100$	10^{-3}	-0.97	-0.02	-91.1	-1.30
SFI_2	$\mu = 2$	10^{-3}	-0.97	-0.03	-11.8	-0.23
	$\mu = 20$	10^{-2}	-0.97	-0.01	-7.19	-0.05
	$\mu = 20$	$10^{-2.5}$	-0.97	-0.03	-15.2	-0.28
	$\mu = 20$	10^{-3}	-0.97	-0.03	-23.3	-0.46
	$\mu = 200$	10^{-3}	-0.97	-0.03	-43.0	-0.84
SFI_4	$\mu = 2$	10^{-3}	-0.97	-0.03	-10.5	-0.20
	$\mu = 20$	10^{-2}	-0.97	-0.01	-6.21	-0.01
	$\mu = 20$	$10^{-2.5}$	-0.97	-0.03	-12.9	-0.24
	$\mu = 20$	10^{-3}	-0.97	-0.03	-19.0	-0.37
	$\mu = 200$	10^{-3}	-0.97	-0.03	-36.1	-0.71

Table 8.8.: *Results for the bispectrum generated in sidetracked inflation in the minimal geometry, indicating the correlation of the shape with the equilateral and orthogonal templates, as well as the corresponding amplitudes. NA indicates that the sidetracked phase lasts less than 55 e-folds.*

Acronym	Parameter	M	$\mathcal{C}(S, S^{\rm eq})$	$\mathcal{C}(S, S^{\rm orth})$	$f_{nl}^{\rm eq}$	$f_{nl}^{\rm orth}$
SI		10^{-2}	NA	NA	NA	NA
		$10^{-2.5}$	NA	NA	NA	NA
		10^{-3}	*	*	*	*
NI	$f = 1$	10^{-3}	-0.03	-0.77	-13.9	-176.0
	$f = 10$	10^{-2}	-0.31	-0.71	-0.66	-0.78
	$f = 10$	$10^{-2.5}$	-0.22	-0.77	-7.73	-13.6
	$f = 10$	10^{-3}	-0.10	-0.79	-23.3	-90.4
	$f = 100$	10^{-3}	-0.37	-0.72	-15.7	-15.9
SFI_2	$\mu = 2$	10^{-3}	-0.01	-0.78	-3.98	-136.0
	$\mu = 20$	10^{-2}	-0.47	-0.66	-0.62	-0.46
	$\mu = 20$	$10^{-2.5}$	-0.18	-0.78	-6.67	-14.5
	$\mu = 20$	10^{-3}	-0.02	-0.79	-6.57	-105.0
	$\mu = 200$	10^{-3}	-0.15	-0.78	-22.9	-59.6
SFI_4	$\mu = 2$	10^{-3}	-0.01	-0.79	-1.49	-106.0
	$\mu = 20$	10^{-2}	NA	NA	NA	NA
	$\mu = 20$	$10^{-2.5}$	-0.15	-0.79	-6.04	-15.7
	$\mu = 20$	10^{-3}	-0.01	-0.80	-0.69	-123.0
	$\mu = 200$	10^{-3}	-0.11	-0.79	-19.5	-71.8

Table 8.9.: *Results for the bispectrum generated in sidetracked inflation in the hyperbolic geometry, indicating the correlation of the shape with the equilateral and orthogonal templates, as well as the corresponding amplitudes. NA indicates that the sidetracked phase lasts less than 55 e-folds. * for SI with $M = 10^{-3}$ indicates that we have not been able to reliably compute the bispectrum, as we explain in the main text.*

9. Conclusions

In this thesis we have described the background to and the work that has gone into the development of the transport method to calculate the statistics of non-canonical inflation. Specifically we began in Ch. 2 by giving an introductory overview of the success of ΛCDM and highlighted it's major shortcomings which can be rectified by inflation. We reviewed tools, such as cosmological perturbation theory, necessary to construct observable quantities such as the power spectrum and bispectrum of curvature perturbations that can be then compared to data.

In Ch. 3 the equations of motion and the evolution equations for perturbations were derived for a multifield system. We reviewed how the system of equations can be written with a non-trivial field-space metric as an autonomous system for a set of covariant "field" perturbations. In terms of the covariant field-space perturbations we then determined the curvature perturbation ζ. A neat result we found is that our expressions for these quantities take the form of the covariant versions of the expressions presented in Ref. [78], with no additional Riemann curvature terms appearing (except through the new terms that appear in the a, b and c tensors of Eqns. (3.32)–(3.34) which define the equations of motion).

To use the transport system in practice we also needed to calculate initial conditions. In Ch. 4 we find the initial conditions for the two- and three-point function and showed that they also take the form of covariant versions of the canonical expressions.

In the next chapter, Ch. 5 we reviewed methods for calculating inflationary statistics and how the transport method is applied in combination with these equations to give equations for the evolution of the correlations of the covariant perturbations during inflation. Together with the work of the previous chapters, this provided an extension to the method of calculating the power spectrum and bispectrum developed in Ref. [78] for canonical multifield inflation to include models which contain a non-trivial field-space metric.

In Ch. 6 we demonstrated explicitly that our method is successful in evaluating the observable statistics of inflationary models with many fields and a curved field-space metric. The code we have developed to do this is the second iteration of the `PyTransport` package, `PyTransport 2.0`, and agrees with its predecessor in the case of models which can be written in Euclidean and non-Euclidean coordinates (as discussed in Sec. 6.3.1). Moreover, we have shown that for simple 2-field models that the speed of the new code compares well with that of the canonical model. It should

be noted, however, that the new code has not been tested for models exceeding more than six fields, and that we expect time taken to scale poorly with the number of fields. Our hope is that this new code will be useful to the inflationary cosmology community.

In Ch. 7 we studied multifield inflation in scenarios where the fields are coupled non-minimally to gravity via $\xi_I(\phi^I)^n g^{\mu\nu}R_{\mu\nu}$. We concentrated on the so-called α-attractor models with the potential $U = \lambda_I^{(2n)} M_{\rm P}^{4-2n}(\phi^I)^{2n}$ in two formulations of gravity: in the usual metric case where $R_{\mu\nu} = R_{\mu\nu}(g_{\mu\nu})$, and in the Palatini formulation where also the connection Γ and hence also $R_{\mu\nu} = R_{\mu\nu}(\Gamma)$ are independent variables.

As the main result, we showed that the curvature of the field-space in the Einstein frame has no influence on the inflationary dynamics at the limit of large ξ_I, and one effectively retains the single-field case regardless of the underlying theory of gravity. In the metric case this means that multifield models approach the single-field α-attractor limit, whereas in the Palatini case the attractor behaviour is lost also in the case of multifield inflation.

In Ch. 8 we studied the sidetracked inflation model where the inflationary trajectory deviates from its initial effectively single-field path as a result of the geometrical destabilization. We explore two types of models; ones with hyperbolic geometries and ones with minimal geometries. We find that their background evolutions are similar in the sidetracked phase and both can be described by an effective single-field trajectory. We then study the evolution of the cosmological perturbations, in particular, the two-point function. We construct an effective single-field model where entropic fluctuations are integrated out. The effective field theory may have the property of a modified dispersion relation when the entropic field is light in the minimal geometry, and a reduced speed of sound or an imaginary one, depending on the potential, in the hyperbolic geometry. This allows us to construct analytical results for n_s and r which we compare to our numerical results. We then study the bispectrum that these models generate using our code. We find large non-Gaussianities are produced in all models, particularly in the equilateral and orthogonal shapes. Finally we conclude on a brief comparison between the sidetracked inflation and cosmological attractors.

We see the interesting phenomenological consequences of sidetracked inflationary scenarios as motivations to consider more realistic setups in the future. Eventually, we have seen that several important features of sidetracked inflation are tied to the heavy mass of the additional scalar field and it would be interesting to see how observables may be modified when this field has an intermediate mass of order the Hubble scale. We hope to come back to these questions in future works.

A. Appendices

A.1. Background Geometry

The background FLRW line element in Eqn. (2.6) has the following non-vanishing Chistoffel symbols,

$$\begin{aligned}\Gamma^0_{00} &= \mathcal{H}\,,\\ \Gamma^0_{ij} &= \mathcal{H}\gamma_{ij}\,,\\ \Gamma^j_{0i} &= \mathcal{H}\delta^j_i\,,\\ \Gamma^j_{ij} &= \gamma^i_{jk}\,.\end{aligned} \tag{A.1}$$

where γ^i_{jk} is the Chistoffel symbols of the 3 dimensional spatial metric γ_{ij}. The non-vanishing components components of the Riemann tensors are,

$$\begin{aligned}R^0_{i0j} &= \mathcal{H}'\gamma_{ij}\,,\\ R^i_{00j} &= \mathcal{H}'\delta^i_j\,,\\ R^i_{jml} &= (\mathcal{H}'+\kappa)\left(\delta^i_m\gamma_{jl}-\delta^i_l\gamma_{jm}\right)\,.\end{aligned} \tag{A.2}$$

From these we construct the Ricci tensors,

$$\begin{aligned}R_{00} &= -3\mathcal{H}'\,,\\ R_{ij} &= (2\mathcal{H}^2+\mathcal{H}'+2\kappa)\gamma_{ij}\,.\end{aligned} \tag{A.3}$$

The Ricci scalar is then calculated as,

$$R = \frac{6}{a^2}\left(\mathcal{H}^2+\mathcal{H}'+\kappa\right)\,, \tag{A.4}$$

and the spatial curvature is,

$$^{(3)}R = 6\kappa \tag{A.5}$$

We can then calculate the Einstein tensor using Eqn. (2.3),

$$\begin{aligned}G_{00} &= 3(\mathcal{H}^2+\kappa)\,,\\ G_{ij} &= -(\mathcal{H}^2+2\mathcal{H}'\kappa)\gamma_{ij}\,.\end{aligned} \tag{A.6}$$

A.2. Perturbed Geometry

We will now derive the perturbations to the geometric quantities necessary to obtain the perturbations to the Einstein equations. We first fully expand out the perturbed metric in Eqn. (2.43) by apply SVT decomposition as in Eqn. (2.44). Then by substitution of the perturbations to the metric into the connection coefficients we get the six non-vanishing quantities,

$$\begin{aligned}
\delta\Gamma^0_{00} &= \phi_1{}' & \delta\Gamma^0_{ij} &= -2\mathcal{H}\phi_1\delta_{ij} + 2\mathcal{H}C_{ij} + C'_{ij} - B_{,(ji)} - B^{vec}_{(j,i))} \\
\delta\Gamma^0_{0i} &= \partial_i(\phi_1 + \mathcal{H}B) + \mathcal{H}B^{vec}_i & \delta\Gamma^i_{00} &= \partial^i(\phi_1 + B' + \mathcal{H}B) + B^{i\prime}_{vec} + \mathcal{H}B^i_{vec} \\
\delta\Gamma^i_{j0} &= C^{i\prime}_j + \delta^{il}B^{vec}_{[l,j]} & \delta\Gamma^i_{jk} &= -\mathcal{H}(\partial^i B + B^i_{vec})\delta_{jk} + 2C^i_{(k,j)} - \partial^i C_{jk}.
\end{aligned} \tag{A.7}$$

Next we calculate the Ricci tensor,

$$R_{\mu\nu} = \partial_\lambda\Gamma^\lambda_{\mu\nu} - \partial_\nu\Gamma^\lambda_{\mu\lambda} + \Gamma^\lambda_{\lambda\rho}\Gamma^\rho_{\mu\nu} - \Gamma^\rho_{\mu\lambda}\Gamma^\lambda_{\nu\rho}. \tag{A.8}$$

Into this we then substitute equation (A.7) and determine the components as,

$$\begin{aligned}
\delta R_{00} =& 3\mathcal{H}\phi_1{}' + \nabla^2\phi_1 + \nabla^2(B' + \mathcal{H}B) - (C'' + \mathcal{H}C'), \\
\delta R_{0i} =& 2\mathcal{H}\partial_i\phi_1 + (\mathcal{H}' + 2\mathcal{H}^2)B^{vec}_i + \partial^k\partial_{[i}B^{vec}_{k]} + (C'^k_{i,k} - C'_{,i}), \\
\delta R_{ij} =& -\left[2(2\mathcal{H}^2 + \mathcal{H}')\phi_1 + \mathcal{H}\phi_1{}' + \mathcal{H}\nabla^2 B\right]\delta_{ij} - \partial_i\partial_j\phi_1 - \partial_{(i}[B'^{vec}_{j)} + \mathcal{H}B_{j)}] \\
&+ 2(2\mathcal{H}^2 + \mathcal{H}')C_{ij} + 2\mathcal{H}C'_{ij} + \mathcal{H}C'\delta_{ij} + C''_{ij} \\
&+ 2C^k_{(j|,k|i)} - \nabla^2 C_{ij} - C_{ij}.
\end{aligned} \tag{A.9}$$

The Ricci scalar is then the trace of the Ricci tensor components which at linear order becomes,

$$\delta R = a^{-2}\left[2C'' + 6\mathcal{H}C' - 4\nabla^2\psi - 2\nabla^2\phi_1 - 12(\mathcal{H}' + \mathcal{H}^2)\psi - 6\mathcal{H}\phi_1{}' - 2\nabla^2\left(B' + 3\mathcal{H}B\right)\right], \tag{A.10}$$

where C is the trace of C_{ij}. To compute the Einstein tensor we need to take the results from the perturbed Ricci scalar and Ricci tensors in the form $\delta G_{ij} = \delta R_{ij} -$

$\frac{1}{2}g_{ij}\delta R$ with components,

$$\begin{aligned}
\delta G^0_0 =& 2a^{-2}\left[3\mathcal{H}^2\boldsymbol{\phi} - 3\mathcal{H}\psi' + \nabla^2(\psi + \mathcal{H}B - \mathcal{H}E')\right] , \\
\delta G^0_i =& a^{-2}\left[-2\partial_i[\mathcal{H}\phi_1 - \psi'] - \frac{1}{2}\nabla^2(F'_i - B^{vec}_i)\right] , \\
\delta G^i_j =& a^{-2}[\partial^i\partial_j\left[(E' - B)' + 2\mathcal{H}(E^i - B) - (\psi + \phi_1)\right] \\
&+ \delta^i_j[-\nabla^2(E' - B)' - 2\mathcal{H}\nabla^2(E' - B) - 2\psi'' - 4\mathcal{H}\psi' + \nabla^2\psi \\
&+ 2\mathcal{H}\psi' + \nabla\psi + 2(2\mathcal{H}' + \mathcal{H}^2)\psi] \\
&+ \delta^{ik}\partial_{(k}\left[(F'_{j)} - B^{vec}_{j)})' + 2\mathcal{H}(F'_{j)} - B^{vec}_{j)})\right] \\
&+ F''^i_j + 2\mathcal{H}F'^i_j - \nabla^2 F^i_j].
\end{aligned} \tag{A.11}$$

A.3. Perturbed Matter

We will now derive the perturbations to the energy–momentum tensor for a fluid and for scalar fields.

Using Eqn. (2.53) and Eqn. (2.51) for a fluid we get,

$$\begin{aligned}
\delta T_{00} &= \rho_0 a^2\left(\frac{\delta\rho}{\rho_0} + 2\phi_1\right) , \\
\delta T_{0i} &= -\rho_0 a^2[(1 + \frac{P_0}{\rho_0})(v_{,i} + \bar{v}^{vec}_i) + B_{,i} + \bar{B}^{vec}_i] , \\
\delta T_{ij} &= Pa^2\left(C_{ij} + \frac{\delta P}{P}\delta_{ij} + a^{-2}\pi_{ij}\right) .
\end{aligned} \tag{A.12}$$

Using Eqn. (2.62) we get the perturbed energy–momentum tensors,

$$\begin{aligned}
\delta T_{00} &= \phi'_0\delta\phi' + 2a^2V\phi_1 + a^2V_{,\phi}\delta\phi , \\
\delta T_{0i} &= \phi'_0\delta\phi_{,i} + \left(\frac{\phi'^2_0}{2} - a^2V\right)(B_{,i} + \bar{B}^{vec}_i) , \\
\delta T_{ij} &= \left(\phi'_0\delta\phi' - \phi'^2_0\phi_1 - a^2V_{,\phi}\delta\phi\right)\gamma_{ij} + \left(\frac{\phi'^2_0}{2} - a^2V\right)h_{ij} .
\end{aligned} \tag{A.13}$$

Bibliography

[1] Peter P. and Uzan J.P., *Primordial Cosmology*. Oxford Graduate Texts. Oxford University Press, 2013.

[2] Ellis G., Maartens R., and MacCallum M., *Relativistic cosmology*. Cambridge University Press, United Kingdom, 2012.

[3] Planck Collaboration, Aghanim N. *et al.*, "Planck 2018 results. VI. Cosmological parameters," arXiv:1807.06209 [astro-ph.CO].

[4] Lyth D.H. and Liddle A.R., "The primordial density perturbation: Cosmology, inflation and the origin of structure,".

[5] Planck Collaboration, Ade P.A.R. *et al.*, "Planck 2013 results. XXII. Constraints on inflation," *Astron. Astrophys.* **571** (2014) A22, arXiv:1303.5082 [astro-ph.CO].

[6] 2DFGRS Collaboration, Colless M. *et al.*, "The 2dF Galaxy Redshift Survey: Spectra and redshifts," *Mon. Not. Roy. Astron. Soc.* **328** (2001) 1039, arXiv:astro-ph/0106498 [astro-ph].

[7] Colless M. *et al.*, "The 2dF Galaxy Redshift Survey: Final data release," arXiv:astro-ph/0306581 [astro-ph].

[8] SDSS Collaboration, Pris I. *et al.*, "The Sloan Digital Sky Survey Quasar Catalog: Fourteenth data release," *Astron. Astrophys.* **613** (2018) A51, arXiv:1712.05029 [astro-ph.GA].

[9] Joyce M., Anderson P.W., Montuori M., Pietronero L., and Sylos Labini F., "Fractal cosmology in an open universe," *Europhys. Lett.* **50** (2000) 416–422, arXiv:astro-ph/0002504 [astro-ph]. [Europhys. Lett.49,416(2000)].

[10] Clifton T., Ferreira P.G., Padilla A., and Skordis C., "Modified Gravity and Cosmology," *Phys. Rept.* **513** (2012) 1–189, arXiv:1106.2476 [astro-ph.CO].

[11] Will C.M., "The Confrontation between general relativity and experiment," *Living Rev. Rel.* **9** (2006) 3, arXiv:gr-qc/0510072 [gr-qc].

[12] Supernova Cosmology Project Collaboration, Perlmutter S. *et al.*, "Discovery of a supernova explosion at half the age of the Universe and its cosmological implications," *Nature* **391** (1998) 51–54, arXiv:astro-ph/9712212 [astro-ph].

[13] Supernova Search Team Collaboration, Riess A.G. *et al.*, "Observational evidence from supernovae for an accelerating universe and a cosmological constant," *Astron. J.* **116** (1998) 1009–1038, arXiv:astro-ph/9805201 [astro-ph].

[14] Wald R.M., *General Relativity*. Chicago Univ. Pr., Chicago, USA, 1984.

[15] Lyth D.H., "Non-gaussianity and cosmic uncertainty in curvaton-type models," *JCAP* **0606** (2006) 015, arXiv:astro-ph/0602285 [astro-ph].

[16] Caldwell R.R., Battye R.A., and Shellard E.P.S., "Relic gravitational waves from cosmic strings: Updated constraints and opportunities for detection," *Phys. Rev.* **D54** (1996) 7146–7152, arXiv:astro-ph/9607130 [astro-ph].

[17] Basu R. and Vilenkin A., "Evolution of topological defects during inflation," *Phys. Rev.* **D50** (1994) 7150–7153, arXiv:gr-qc/9402040 [gr-qc].

[18] 't Hooft G., "Magnetic Monopoles in Unified Gauge Theories," *Nucl. Phys.* **B79** (1974) 276–284. [,291(1974)].

[19] Guth A.H., "The Inflationary Universe: A Possible Solution to the Horizon and Flatness Problems," *Phys.Rev.* **D23** (1981) 347–356.

[20] Starobinsky A.A., "A New Type of Isotropic Cosmological Models Without Singularity," *Phys.Lett.* **B91** (1980) 99–102.

[21] Baumann D., "Inflation," in *Physics of the large and the small, TASI 09, proceedings of the Theoretical Advanced Study Institute in Elementary Particle Physics, Boulder, Colorado, USA, 1-26 June 2009*, pp. 523–686. 2011. arXiv:0907.5424 [hep-th]. https://inspirehep.net/record/827549/files/arXiv:0907.5424.pdf.

[22] Vilenkin A., "The Birth of Inflationary Universes," *Phys. Rev.* **D27** (1983) 2848.

[23] Guth A.H., "Eternal inflation and its implications," *J. Phys.* **A40** (2007) 6811–6826, arXiv:hep-th/0702178 [HEP-TH].

[24] Malik K.A. and Wands D., "Cosmological perturbations," *Phys. Rept.* **475** (2009) 1–51, arXiv:0809.4944 [astro-ph].

[25] Mukhanov V.F., Feldman H., and Brandenberger R.H., "Theory of cosmological perturbations. Part 1. Classical perturbations. Part 2. Quantum theory of perturbations. Part 3. Extensions," *Phys.Rept.* **215** (1992) 203–333.

[26] Liddle A.R. and Lyth D., "Cosmological inflation and large scale structure,".

[27] Acquaviva V., Bartolo N., Matarrese S., and Riotto A., "Second order cosmological perturbations from inflation," *Nucl. Phys.* **B667** (2003) 119–148, arXiv:astro-ph/0209156 [astro-ph].

[28] Malik K.A., "Gauge-invariant perturbations at second order: Multiple scalar fields on large scales," *JCAP* **0511** (2005) 005, arXiv:astro-ph/0506532 [astro-ph].

[29] Nakamura K., "Second-order Gauge-Invariant Cosmological Perturbation Theory: Current Status," *Adv. Astron.* **2010** (2010) 576273, arXiv:1001.2621 [gr-qc].

[30] Malik K.A. and Matravers D.R., "A Concise Introduction to Perturbation Theory in Cosmology," *Class.Quant.Grav.* **25** (2008) 193001, arXiv:0804.3276 [astro-ph].

[31] Malik K.A. and Matravers D.R., "Comments on gauge-invariance in cosmology," *Gen. Rel. Grav.* **45** (2013) 1989–2001, arXiv:1206.1478 [astro-ph.CO].

[32] Mukhanov V.F., Abramo L.R.W., and Brandenberger R.H., "On the Back reaction problem for gravitational perturbations," *Phys. Rev. Lett.* **78** (1997) 1624–1627, arXiv:gr-qc/9609026 [gr-qc].

[33] Bardeen J.M., "Gauge Invariant Cosmological Perturbations," *Phys. Rev.* **D22** (1980) 1882–1905.

[34] Kodama H. and Sasaki M., "Cosmological perturbation theory," *Progress of Theoretical Physics Supplement* **78** (1984) 1–166, /oup/backfile/content$_p$*ublic/journal/ptps/*78/10.1143/*ptps*.78.1/2/78 – 1.*pdf*. http://dx.doi.org/10.1143/PTPS.78.1.

[35] Bertschinger E., "Cosmological dynamics: Course 1," in *Proceedings, Les Houches Summer School on Cosmology and Large Scale Structure (Session 60): Les Houches, France, August 1-28, 1993*, pp. 273–348. 1993. arXiv:astro-ph/9503125 [astro-ph].

[36] Ma C.P. and Bertschinger E., "Cosmological perturbation theory in the synchronous and conformal Newtonian gauges," *Astrophys. J.* **455** (1995) 7–25, arXiv:astro-ph/9506072 [astro-ph].

[37] Bruni M., Matarrese S., Mollerach S., and Sonego S., "Perturbations of space-time: Gauge transformations and gauge invariance at second order and beyond," *Class. Quant. Grav.* **14** (1997) 2585–2606, arXiv:gr-qc/9609040 [gr-qc].

[38] Wands D., Malik K.A., Lyth D.H., and Liddle A.R., "A new approach to the evolution of cosmological perturbations on large scales," *Phys. Rev.* **D62** (2000) 043527, arXiv:astro-ph/0003278.

[39] Lyth D.H., Malik K.A., and Sasaki M., "A General proof of the conservation of the curvature perturbation," *JCAP* **0505** (2005) 004, arXiv:astro-ph/0411220 [astro-ph].

[40] Malik K.A. and Wands D., "Adiabatic and entropy perturbations with interacting fluids and fields," *JCAP* **0502** (2005) 007, arXiv:astro-ph/0411703 [astro-ph].

[41] Christopherson A.J. and Malik K.A., "The non-adiabatic pressure in general scalar field systems," *Phys.Lett.* **B675** (2009) 159–163, arXiv:0809.3518 [astro-ph].

[42] Brown I.A., Christopherson A.J., and Malik K.A., "The magnitude of the non-adiabatic pressure in the cosmic fluid," *Mon. Not. Roy. Astron. Soc.* **423** (2012) 1411–1415, arXiv:1108.0639 [astro-ph.CO].

[43] Weinberg S., "Adiabatic modes in cosmology," *Phys. Rev.* **D67** (2003) 123504, arXiv:astro-ph/0302326.

[44] Lopez-Monsalvo C.S. and Andersson N., "Thermal Dynamics in General Relativity," *Proc. Roy. Soc. Lond.* **A467** (2010) 738–759, arXiv:1006.2978 [gr-qc].

[45] Liddle A.R., Lyth D.H., Malik K.A., and Wands D., "Superhorizon perturbations and preheating," *Phys. Rev.* **D61** (2000) 103509, arXiv:hep-ph/9912473 [hep-ph].

[46] Planck Collaboration, Ade P.A.R. *et al.*, "Planck 2015 results. XX. Constraints on inflation," *Astron. Astrophys.* **594** (2016) A20, arXiv:1502.02114 [astro-ph.CO].

[47] Renaux-Petel S., Mizuno S., and Koyama K., "Primordial fluctuations and non-Gaussianities from multifield DBI Galileon inflation," *JCAP* **1111** (2011) 042, arXiv:1108.0305 [astro-ph.CO].

[48] Chen X., "Primordial Non-Gaussianities from Inflation Models," *Adv. Astron.* **2010** (2010) 638979, arXiv:1002.1416 [astro-ph.CO].

[49] Creminelli P., Nicolis A., Senatore L., Tegmark M., and Zaldarriaga M., "Limits on non-gaussianities from wmap data," *JCAP* **0605** (2006) 004, arXiv:astro-ph/0509029 [astro-ph].

[50] Chen X., Huang M.x., Kachru S., and Shiu G., "Observational signatures and non-Gaussianities of general single field inflation," *JCAP* **0701** (2007) 002, arXiv:hep-th/0605045 [hep-th].

[51] Koyama K., Pettinari G.W., Mizuno S., and Fidler C., "Orthogonal non-Gaussianity in DBI galileon: prospect for Planck polarization and post-Planck experiments," *Class. Quant. Grav.* **31** (2014) 125003, arXiv:1303.2125 [astro-ph.CO].

[52] Garcia-Saenz S., Renaux-Petel S., and Ronayne J., "Primordial fluctuations and non-Gaussianities in sidetracked inflation," arXiv:1804.11279 [astro-ph.CO].

[53] Senatore L., Smith K.M., and Zaldarriaga M., "Non-Gaussianities in Single Field Inflation and their Optimal Limits from the WMAP 5-year Data," *JCAP* **1001** (2010) 028, arXiv:0905.3746 [astro-ph.CO].

[54] Seery D. and Lidsey J.E., "Primordial non-Gaussianities from multiple-field inflation," *JCAP* **0509** (2005) .

[55] Lyth D.H. and Zaballa I., "A Bound concerning primordial non-Gaussianity," *JCAP* **0510** (2005) 005, arXiv:astro-ph/0507608 [astro-ph].

[56] Hawking S. and Ellis G., *The Large scale structure of space-time.* Cambridge University Press, 1973.

[57] Spradlin M., Strominger A., and Volovich A., "Les Houches lectures on de Sitter space," in *Unity from duality: Gravity, gauge theory and strings. Proceedings, NATO Advanced Study Institute, Euro Summer School, 76th*

session, Les Houches, France, July 30-August 31, 2001, pp. 423–453. 2001. arXiv:hep-th/0110007 [hep-th].

[58] Bunch T.S. and Davies P.C.W., "Quantum Field Theory in de Sitter Space: Renormalization by Point Splitting," *Proc. Roy. Soc. Lond.* **A360** (1978) 117–134.

[59] Birrell N.D. and Davies P.C.W., *Quantum Fields in Curved Space*. Cambridge Monographs on Mathematical Physics. Cambridge Univ. Press, Cambridge, UK, 1984. http://www.cambridge.org/mw/academic/subjects/physics/theoretical-physics-and-mathematical-physics/quantum-fields-curved-space?format=PB.

[60] Linde A.D., "Chaotic Inflation," *Phys.Lett.* **B129** (1983) 177–181.

[61] Liddle A.R., "Power Law Inflation With Exponential Potentials," *Phys. Lett.* **B220** (1989) 502–508.

[62] Freese K., Frieman J.A., and Olinto A.V., "Natural inflation with pseudo - Nambu-Goldstone bosons," *Phys. Rev. Lett.* **65** (1990) 3233–3236.

[63] Kim J.E., Nilles H.P., and Peloso M., "Completing natural inflation," *JCAP* **0501** (2005) 005, arXiv:hep-ph/0409138 [hep-ph].

[64] Lyth D.H., "What would we learn by detecting a gravitational wave signal in the cosmic microwave background anisotropy?," *Phys. Rev. Lett.* **78** (1997) 1861–1863, arXiv:hep-ph/9606387 [hep-ph].

[65] German G., Ross G.G., and Sarkar S., "Low scale inflation," *Nucl. Phys.* **B608** (2001) 423–450, arXiv:hep-ph/0103243 [hep-ph].

[66] Adams J.A., Cresswell B., and Easther R., "Inflationary perturbations from a potential with a step," *Phys. Rev.* **D64** (2001) 123514, arXiv:astro-ph/0102236 [astro-ph].

[67] Adshead P., Dvorkin C., Hu W., and Lim E.A., "Non-Gaussianity from Step Features in the Inflationary Potential," *Phys. Rev.* **D85** (2012) 023531, arXiv:1110.3050 [astro-ph.CO].

[68] Wess J. and Zumino B., "Supergauge Transformations in Four-Dimensions," *Nucl. Phys.* **B70** (1974) 39–50. [,24(1974)].

[69] Nilles H.P., "Supersymmetry, Supergravity and Particle Physics," *Phys. Rept.* **110** (1984) 1–162.

[70] Liddle A.R., Mazumdar A., and Schunck F.E., "Assisted inflation," *Phys. Rev.* **D58** (1998) 061301, arXiv:astro-ph/9804177.

[71] Malik K.A. and Wands D., "Dynamics of assisted inflation," *Phys. Rev.* **D59** (1999) 123501, arXiv:astro-ph/9812204 [astro-ph].

[72] Easther R., Frazer J., Peiris H.V., and Price L.C., "Simple predictions from multifield inflationary models," *Phys. Rev. Lett.* **112** (2014) 161302, arXiv:1312.4035 [astro-ph.CO].

[73] Dimopoulos S., Kachru S., McGreevy J., and Wacker J.G., "N-flation," *JCAP* **0808** (2008) 003, arXiv:hep-th/0507205 [hep-th].

[74] Elliston J., Alabidi L., Huston I., Mulryne D., and Tavakol R., "Large trispectrum in two-field slow-roll inflation," *JCAP* **1209** (2012) 001, arXiv:1203.6844 [astro-ph.CO].

[75] Kim S.A., Liddle A.R., and Seery D., "Non-gaussianity in axion N-flation models: detailed predictions and mass spectra," *Phys.Rev.* **D85** (2012) 023532, arXiv:1108.2944 [astro-ph.CO].

[76] Kim S.A., Liddle A.R., and Seery D., "Non-gaussianity in axion Nflation models," *Phys.Rev.Lett.* **105** (2010) 181302, arXiv:1005.4410 [astro-ph.CO].

[77] Lyth D.H. and Wands D., "Generating the curvature perturbation without an inflaton," *Phys.Lett.* **B524** (2002) 5–14, arXiv:hep-ph/0110002 [hep-ph].

[78] Dias M., Frazer J., Mulryne D.J., and Seery D., "Numerical evaluation of the bispectrum in multiple field inflationthe transport approach with code," *JCAP* **1612** (2016) no. 12, 033, arXiv:1609.00379 [astro-ph.CO].

[79] Garriga J. and Mukhanov V.F., "Perturbations in k-inflation," *Phys.Lett.* **B458** (1999) 219–225, arXiv:hep-th/9904176 [hep-th].

[80] Armendariz-Picon C., Damour T., and Mukhanov V.F., "k - inflation," *Phys.Lett.* **B458** (1999) 209–218, arXiv:hep-th/9904075 [hep-th]. s

[81] Silverstein E. and Tong D., "Scalar speed limits and cosmology: Acceleration from D-cceleration," *Phys.Rev.* **D70** (2004) 103505, arXiv:hep-th/0310221 [hep-th].

[82] Arroja F., Mizuno S., and Koyama K., "Non-gaussianity from the bispectrum in general multiple field inflation," *JCAP* **0808** (2008) 015, arXiv:0806.0619 [astro-ph].

[83] Dvali G.R. and Tye S.H.H., "Brane inflation," *Phys. Lett.* **B450** (1999) 72–82, arXiv:hep-ph/9812483 [hep-ph].

[84] Jrv L., Racioppi A., and Tenkanen T., "Palatini side of inflationary attractors," *Phys. Rev.* **D97** (2018) no. 8, 083513, arXiv:1712.08471 [gr-qc].

[85] Sotiriou T.P. and Faraoni V., "f(R) Theories Of Gravity," *Rev. Mod. Phys.* **82** (2010) 451–497, arXiv:0805.1726 [gr-qc].

[86] De Felice A. and Tsujikawa S., "f(R) theories," *Living Rev. Rel.* **13** (2010) 3, arXiv:1002.4928 [gr-qc].

[87] Kofman L., Linde A.D., and Starobinsky A.A., "Reheating after inflation," *Phys. Rev. Lett.* **73** (1994) 3195–3198, arXiv:hep-th/9405187 [hep-th].

[88] Kofman L., Linde A.D., and Starobinsky A.A., "Towards the theory of reheating after inflation," *Phys. Rev.* **D56** (1997) 3258–3295, arXiv:hep-ph/9704452 [hep-ph].

[89] Huston I. and Christopherson A.J., "Isocurvature Perturbations and Reheating in Multi-Field Inflation," arXiv:1302.4298 [astro-ph.CO].

[90] Bassett B.A., Tsujikawa S., and Wands D., "Inflation dynamics and reheating," *Rev. Mod. Phys.* **78** (2006) 537–589, arXiv:astro-ph/0507632 [astro-ph].

[91] Tashiro H., Chiba T., and Sasaki M., "Reheating after quintessential inflation and gravitational waves," *Class. Quant. Grav.* **21** (2004) 1761–1772, arXiv:gr-qc/0307068 [gr-qc].

[92] Felder G.N., Garcia-Bellido J., Greene P.B., Kofman L., Linde A.D., and Tkachev I., "Dynamics of symmetry breaking and tachyonic preheating," *Phys. Rev. Lett.* **87** (2001) 011601, arXiv:hep-ph/0012142 [hep-ph].

[93] Mason B.S. *et al.*, "The Anisotropy of the microwave background to l = 3500: Deep field observations with the Cosmic Background Imager," *Astrophys. J.* **591** (2003) 540–555, arXiv:astro-ph/0205384 [astro-ph].

[94] Dickinson C. *et al.*, "High sensitivity measurements of the CMB power spectrum with the extended Very Small Array," *Mon. Not. Roy. Astron. Soc.* **353** (2004) 732, arXiv:astro-ph/0402498 [astro-ph].

[95] ACBAR Collaboration, Kuo C.l. *et al.*, "High resolution observations of the CMB power spectrum with ACBAR," *Astrophys. J.* **600** (2004) 32–51, arXiv:astro-ph/0212289 [astro-ph].

[96] Montroy T.E. *et al.*, "A Measurement of the CMB ¡ EE ¿ spectrum from the 2003 flight of BOOMERANG," *Astrophys. J.* **647** (2006) 813–822, arXiv:astro-ph/0507514 [astro-ph].

[97] Filippini J.P. *et al.*, "SPIDER: a balloon-borne CMB polarimeter for large angular scales," *Proc. SPIE Int. Soc. Opt. Eng.* **7741** (2010) 77411N, arXiv:1106.2158 [astro-ph.CO].

[98] Bennett C.L. *et al.*, "Cosmic temperature fluctuations from two years of COBE differential microwave radiometers observations," *Astrophys. J.* **436** (1994) 423–442, arXiv:astro-ph/9401012.

[99] WMAP Collaboration, Komatsu E. *et al.*, "Five-Year Wilkinson Microwave Anisotropy Probe (WMAP) Observations: Cosmological Interpretation," *Astrophys. J. Suppl.* **180** (2009) 330–376, arXiv:0803.0547 [astro-ph].

[100] Lamarre J.M. *et al.*, "The planck high frequency instrument, a 3rd generation cmb experiment, and a full sky submillimeter survey," *New Astron. Rev.* **47** (2003) 1017, arXiv:astro-ph/0308075 [astro-ph].

[101] Planck Collaboration Collaboration, Ade P. *et al.*, "Planck Early Results: The Planck mission," arXiv:1101.2022 [astro-ph.IM].

[102] Planck Collaboration Collaboration, "The scientific programme of Planck." 2006.

[103] Planck Collaboration, Akrami Y. *et al.*, "Planck 2018 results. X. Constraints on inflation," arXiv:1807.06211 [astro-ph.CO].

[104] Elliston J., Seery D., and Tavakol R., "The inflationary bispectrum with curved field-space," *JCAP* **1211** (2012) 060, arXiv:1208.6011 [astro-ph.CO].

[105] Arnowitt R.L., Deser S., and Misner C.W., "The Dynamics of general relativity," *Gen. Rel. Grav.* **40** (2008) 1997–2027, arXiv:gr-qc/0405109 [gr-qc].

[106] Maldacena J.M., "Non-Gaussian features of primordial fluctuations in single field inflationary models," *JHEP* **05** (2003) 013, arXiv:astro-ph/0210603 [astro-ph].

[107] Seery D. and Lidsey J.E., "Primordial non-Gaussianities in single field inflation," *JCAP* **0506** (2005) 003, arXiv:astro-ph/0503692 [astro-ph].

[108] Park I.Y., "Hypersurface foliation approach to renormalization of ADM formulation of gravity," *Eur. Phys. J.* **C75** (2015) no. 9, 459, arXiv:1404.5066 [hep-th].

[109] Gong J.O. and Tanaka T., "A covariant approach to general field space metric in multi-field inflation," *JCAP* **1103** (2011) 015, arXiv:1101.4809 [astro-ph.CO]. [Erratum: JCAP1202,E01(2012)].

[110] Langlois D., "Hamiltonian formalism and gauge invariance for linear perturbations in inflation," *Class. Quant. Grav.* **11** (1994) 389–407.

[111] Dias M., Elliston J., Frazer J., Mulryne D., and Seery D., "The curvature perturbation at second order," *JCAP* **1502** (2015) no. 02, 040, arXiv:1410.3491 [gr-qc].

[112] Christopherson A.J., Nalson E., and Malik K.A., "A short note on the curvature perturbation at second order," *Class. Quant. Grav.* **32** (2015) 075005, arXiv:1409.5106 [astro-ph.CO].

[113] Carrilho P. and Malik K.A., "Vector and tensor contributions to the curvature perturbation at second order," *JCAP* **1602** (2016) no. 02, 021, arXiv:1507.06922 [astro-ph.CO].

[114] Weinberg S., "Quantum contributions to cosmological correlations," *Phys. Rev.* **D72** (2005) 043514, arXiv:hep-th/0506236 [hep-th].

[115] Koyama K., "Non-Gaussianity of quantum fields during inflation," *Class. Quant. Grav.* **27** (2010) 124001, arXiv:1002.0600 [hep-th].

[116] Chen X., Easther R., and Lim E.A., "Generation and Characterization of Large Non-Gaussianities in Single Field Inflation," *JCAP* **0804** (2008) 010, arXiv:0801.3295 [astro-ph].

[117] Sasaki M. and Stewart E.D., "A General analytic formula for the spectral index of the density perturbations produced during inflation," *Prog.Theor.Phys.* **95** (1996) 71–78, arXiv:astro-ph/9507001.

[118] Dias M., Frazer J., and Seery D., "Computing observables in curved multifield models of inflationA guide (with code) to the transport method," *JCAP* **1512** (2015) no. 12, 030, arXiv:1502.03125 [astro-ph.CO].

[119] Creminelli P. and Zaldarriaga M., "Single field consistency relation for the 3-point function," *JCAP* **0410** (2004) 006, arXiv:astro-ph/0407059 [astro-ph].

[120] Lyth D.H. and Rodríguez Y., "The inflationary prediction for primordial non-gaussianity," *Phys.Rev.Lett.* **95** (2005) 121302, arXiv:astro-ph/0504045.

[121] Mulryne D.J., Seery D., and Wesley D., "Moment transport equations for non-Gaussianity," *JCAP* **1001** (2010) 024, arXiv:0909.2256 [astro-ph.CO].

[122] Mulryne D.J., "Transporting non-Gaussianity from sub to super-horizon scales," *JCAP* **1309** (2013) 010, arXiv:1302.3842 [astro-ph.CO].

[123] Mulryne D.J., Seery D., and Wesley D., "Moment transport equations for the primordial curvature perturbation," *JCAP* **1104** (2011) 030, arXiv:1008.3159 [astro-ph.CO].

[124] Vernizzi F. and Wands D., "Non-gaussianities in two-field inflation," *JCAP* **0605** (2006) 019, arXiv:astro-ph/0603799 [astro-ph].

[125] Chen X., Easther R., and Lim E.A., "Large Non-Gaussianities in Single Field Inflation," *JCAP* **0706** (2007) 023, arXiv:astro-ph/0611645 [astro-ph].

[126] Avgoustidis A., Cremonini S., Davis A.C., Ribeiro R.H., Turzyński K., *et al.*, "The Importance of Slow-roll Corrections During Multi-field Inflation," *JCAP* **1202** (2012) 038, arXiv:1110.4081 [astro-ph.CO].

[127] Achucarro A., Gong J.O., Hardeman S., Palma G.A., and Patil S.P., "Features of heavy physics in the CMB power spectrum," *JCAP* **1101** (2011) 030, arXiv:1010.3693 [hep-ph].

[128] Appelquist T. and Carazzone J., "Infrared Singularities and Massive Fields," *Phys. Rev.* **D11** (1975) 2856.

[129] Ball R.D. and Thorne R.S., "The Decoupling theorem in effective scalar field theory," *Annals Phys.* **241** (1995) 368–393, arXiv:hep-th/9404156 [hep-th].

[130] Hetz A. and Palma G.A., "Sound Speed of Primordial Fluctuations in Supergravity Inflation," *Phys. Rev. Lett.* **117** (2016) no. 10, 101301, arXiv:1601.05457 [hep-th].

[131] Kidani T. and Koyama K., "Non-Gaussianities in DBI inflation with angular motion," *Phys. Rev.* **D90** (2014) no. 2, 023515, arXiv:1403.6687 [hep-th].

[132] Tolley A.J. and Wyman M., "The Gelaton Scenario: Equilateral non-Gaussianity from multi-field dynamics," *Phys. Rev.* **D81** (2010) 043502, arXiv:0910.1853 [hep-th].

[133] Gao X., Langlois D., and Mizuno S., "Influence of heavy modes on perturbations in multiple field inflation," *JCAP* **1210** (2012) 040, arXiv:1205.5275 [hep-th].

[134] Gao X., Langlois D., and Mizuno S., "Oscillatory features in the curvature power spectrum after a sudden turn of the inflationary trajectory," *JCAP* **1310** (2013) 023, arXiv:1306.5680 [hep-th].

[135] Flauger R., Mirbabayi M., Senatore L., and Silverstein E., "Productive Interactions: heavy particles and non-Gaussianity," arXiv:1606.00513 [hep-th].

[136] Chen X. and Wang Y., "Large non-Gaussianities with Intermediate Shapes from Quasi-Single Field Inflation," *Phys. Rev.* **D81** (2010) 063511, arXiv:0909.0496 [astro-ph.CO].

[137] Chen X. and Wang Y., "Quasi-Single Field Inflation and Non-Gaussianities," *JCAP* **1004** (2010) 027, arXiv:0911.3380 [hep-th].

[138] Dias M. and Seery D., "Transport equations for the inflationary spectral index," *Phys.Rev.* **D85** (2012) 043519, arXiv:1111.6544 [astro-ph.CO].

[139] Anderson G.J., Mulryne D.J., and Seery D., "Transport equations for the inflationary trispectrum," *JCAP* **1210** (2012) 019, arXiv:1205.0024 [astro-ph.CO].

[140] Hazra D.K., Sriramkumar L., and Martin J., "BINGO: A code for the efficient computation of the scalar bi-spectrum," *JCAP* **1305** (2013) 026, arXiv:1201.0926 [astro-ph.CO].

[141] Mulryne D.J. and Ronayne J.W., "PyTransport: A Python package for the calculation of inflationary correlation functions," *JOSS* **3** (2016) no. 23, 494, arXiv:1609.00381 [astro-ph.CO].

[142] Seery D., "CppTransport: a platform to automate calculation of inflationary correlation functions," arXiv:1609.00380 [astro-ph.CO].

[143] Ronayne J.W. and Mulryne D.J., "Numerically evaluating the bispectrum in curved field-space with PyTransport 2.0," *JCAP* **1801** (2018) no. 01, 023, arXiv:1708.07130 [astro-ph.CO].

[144] Butchers S. and Seery D., "Numerical evaluation of inflationary 3-point functions on curved field space," arXiv:1803.10563 [astro-ph.CO].

[145] Corcella G., Knowles I.G., Marchesini G., Moretti S., Odagiri K., Richardson P., Seymour M.H., and Webber B.R., "HERWIG 6: An Event generator for hadron emission reactions with interfering gluons (including supersymmetric processes)," *JHEP* **01** (2001) 010, arXiv:hep-ph/0011363 [hep-ph].

[146] CompHEP Collaboration, Boos E., Bunichev V., Dubinin M., Dudko L., Ilyin V., Kryukov A., Edneral V., Savrin V., Semenov A., and Sherstnev A., "CompHEP 4.4: Automatic computations from Lagrangians to events," *Nucl. Instrum. Meth.* **A534** (2004) 250–259, arXiv:hep-ph/0403113 [hep-ph].

[147] Pukhov A., "CalcHEP 2.3: MSSM, structure functions, event generation, batchs, and generation of matrix elements for other packages," arXiv:hep-ph/0412191 [hep-ph].

[148] Alwall J., Frederix R., Frixione S., Hirschi V., Maltoni F., Mattelaer O., Shao H.S., Stelzer T., Torrielli P., and Zaro M., "The automated computation of tree-level and next-to-leading order differential cross sections, and their matching to parton shower simulations," *JHEP* **07** (2014) 079, arXiv:1405.0301 [hep-ph].

[149] Stelzer T. and Long W.F., "Automatic generation of tree level helicity amplitudes," *Comput. Phys. Commun.* **81** (1994) 357–371, arXiv:hep-ph/9401258 [hep-ph].

[150] Maltoni F. and Stelzer T., "MadEvent: Automatic event generation with MadGraph," *JHEP* **02** (2003) 027, arXiv:hep-ph/0208156 [hep-ph].

[151] Alwall J., Artoisenet P., de Visscher S., Duhr C., Frederix R., Herquet M., and Mattelaer O., "New Developments in MadGraph/MadEvent," *AIP Conf. Proc.* **1078** (2009) 84–89, arXiv:0809.2410 [hep-ph].

[152] Alwall J., Herquet M., Maltoni F., Mattelaer O., and Stelzer T., "MadGraph 5 : Going Beyond," *JHEP* **06** (2011) 128, arXiv:1106.0522 [hep-ph].

[153] Gleisberg T., Hoeche S., Krauss F., Schalicke A., Schumann S., and Winter J.C., "SHERPA 1. alpha: A Proof of concept version," *JHEP* **02** (2004) 056, arXiv:hep-ph/0311263 [hep-ph].

[154] Gleisberg T., Hoeche S., Krauss F., Schonherr M., Schumann S., Siegert F., and Winter J., "Event generation with SHERPA 1.1," *JHEP* **02** (2009) 007, arXiv:0811.4622 [hep-ph].

[155] Kilian W., Ohl T., and Reuter J., "WHIZARD: Simulating Multi-Particle Processes at LHC and ILC," *Eur. Phys. J.* **C71** (2011) 1742, arXiv:0708.4233 [hep-ph].

[156] Hahn T. and Perez-Victoria M., "Automatized one loop calculations in four-dimensions and D-dimensions," *Comput. Phys. Commun.* **118** (1999) 153–165, arXiv:hep-ph/9807565 [hep-ph].

[157] Hahn T. and Rauch M., "News from FormCalc and LoopTools," *Nucl. Phys. Proc. Suppl.* **157** (2006) 236–240, arXiv:hep-ph/0601248 [hep-ph]. [,236(2006)].

[158] Christensen N.D. and Duhr C., "FeynRules - Feynman rules made easy," *Comput. Phys. Commun.* **180** (2009) 1614–1641, arXiv:0806.4194 [hep-ph].

[159] Christensen N.D., de Aquino P., Degrande C., Duhr C., Fuks B., Herquet M., Maltoni F., and Schumann S., "A Comprehensive approach to new physics simulations," *Eur. Phys. J.* **C71** (2011) 1541, arXiv:0906.2474 [hep-ph].

[160] Semenov A.V., "LanHEP: A Package for automatic generation of Feynman rules in gauge models," arXiv:hep-ph/9608488 [hep-ph].

[161] Semenov A., "LanHEP: A Package for the automatic generation of Feynman rules in field theory. Version 3.0," *Comput. Phys. Commun.* **180** (2009) 431–454, arXiv:0805.0555 [hep-ph].

[162] Ringeval C., Brax P., van de Bruck C., and Davis A.C., "Boundary inflation and the WMAP data," *Phys.Rev.* **D73** (2006) 064035, arXiv:astro-ph/0509727 [astro-ph].

[163] Martin J. and Ringeval C., "Inflation after WMAP3: Confronting the Slow-Roll and Exact Power Spectra to CMB Data," *JCAP* **0608** (2006) 009, arXiv:astro-ph/0605367 [astro-ph].

[164] Ringeval C., "The exact numerical treatment of inflationary models," *Lect.Notes Phys.* **738** (2008) 243–273, arXiv:astro-ph/0703486 [astro-ph].

[165] Mortonson M.J., Peiris H.V., and Easther R., "Bayesian Analysis of Inflation: Parameter Estimation for Single Field Models," *Phys.Rev.* **D83** (2011) 043505, arXiv:1007.4205 [astro-ph.CO].

[166] Easther R. and Peiris H.V., "Bayesian Analysis of Inflation II: Model Selection and Constraints on Reheating," *Phys.Rev.* **D85** (2012) 103533, arXiv:1112.0326 [astro-ph.CO].

[167] Norena J., Wagner C., Verde L., Peiris H.V., and Easther R., "Bayesian Analysis of Inflation III: Slow Roll Reconstruction Using Model Selection," *Phys.Rev.* **D86** (2012) 023505, arXiv:1202.0304 [astro-ph.CO].

[168] Price L.C., Peiris H.V., Frazer J., and Easther R., "Gravitational wave consistency relations for multifield inflation," *Phys. Rev. Lett.* **114** (2015) no. 3, 031301, arXiv:1409.2498 [astro-ph.CO].

[169] Price L.C., Frazer J., Xu J., Peiris H.V., and Easther R., "MultiModeCode: An efficient numerical solver for multifield inflation," *JCAP* **03** (2015) 005, arXiv:1410.0685 [astro-ph.CO].

[170] Huston I. and Malik K.A., "Numerical calculation of second order perturbations," *JCAP* **0909** (2009) 019, arXiv:0907.2917 [astro-ph.CO].

[171] Huston I. and Malik K.A., "Second Order Perturbations During Inflation Beyond Slow-roll," *JCAP* **1110** (2011) 029, arXiv:1103.0912 [astro-ph.CO].

[172] Huston I. and Christopherson A.J., "Calculating Non-adiabatic Pressure Perturbations during Multi-field Inflation," *Phys.Rev.* **D85** (2012) 063507, arXiv:1111.6919 [astro-ph.CO].

[173] Sreenath V., Hazra D.K., and Sriramkumar L., "On the scalar consistency relation away from slow roll," *JCAP* **1502** (2015) no. 02, 029, arXiv:1410.0252 [astro-ph.CO].

[174] Achúcarro A., Atal V., Ortiz P., and Torrado J., "Localized correlated features in the CMB power spectrum and primordial bispectrum from a transient reduction in the speed of sound," *Phys. Rev.* **D89** (2014) no. 10, 103006, arXiv:1311.2552 [astro-ph.CO].

[175] Achúcarro A., Atal V., Hu B., Ortiz P., and Torrado J., "Inflation with moderately sharp features in the speed of sound: Generalized slow roll and in–in formalism for power spectrum and bispectrum," *Phys. Rev.* **D90** (2014) no. 2, 023511, arXiv:1404.7522 [astro-ph.CO].

[176] Adshead P., Hu W., and Miranda V., "Bispectrum in Single-Field Inflation Beyond Slow-Roll," *Phys. Rev.* **D88** (2013) no. 2, 023507, arXiv:1303.7004 [astro-ph.CO].

[177] Palma G.A., "Untangling features in the primordial spectra," *JCAP* **1504** (2015) no. 04, 035, arXiv:1412.5615 [hep-th].

[178] Mooij S., Palma G.A., Panotopoulos G., and Soto A., "Consistency relations for sharp features in the primordial spectra," *JCAP* **1510** (2015) no. 10, 062, arXiv:1507.08481 [astro-ph.CO]. [Erratum: JCAP1602,no.02,E01(2016)].

[179] Agarwal N., Bean R., McAllister L., and Xu G., "Universality in D-brane Inflation," *JCAP* **1109** (2011) 002, arXiv:1103.2775 [astro-ph.CO].

[180] Dias M., Frazer J., and Liddle A.R., "Multifield consequences for D-brane inflation," *JCAP* **1206** (2012) 020, arXiv:1203.3792 [astro-ph.CO]. [Erratum: JCAP1303,E01(2013)].

[181] McAllister L., Renaux-Petel S., and Xu G., "A Statistical Approach to Multifield Inflation: Many-field Perturbations Beyond Slow Roll," *JCAP* **1210** (2012) 046, arXiv:1207.0317 [astro-ph.CO].

[182] Klebanov I.R. and Witten E., "AdS / CFT correspondence and symmetry breaking," *Nucl. Phys.* **B556** (1999) 89–114, arXiv:hep-th/9905104 [hep-th].

[183] Candelas P. and de la Ossa X.C., "Comments on Conifolds," *Nucl. Phys.* **B342** (1990) 246–268.

[184] Rigopoulos G.I., Shellard E.P.S., and van Tent B.J.W., "Non-linear perturbations in multiple-field inflation," *Phys.Rev.* **D73** (2006) 083521, arXiv:astro-ph/0504508.

[185] Rigopoulos G., Shellard E., and van Tent B., "Quantitative bispectra from multifield inflation," *Phys.Rev.* **D76** (2007) 083512, arXiv:astro-ph/0511041 [astro-ph].

[186] Peterson C.M. and Tegmark M., "Testing Two-Field Inflation," *Phys.Rev.* **D83** (2011) 023522, arXiv:1005.4056 [astro-ph.CO].

[187] Alvarez M. *et al.*, "Testing Inflation with Large Scale Structure: Connecting Hopes with Reality," arXiv:1412.4671 [astro-ph.CO].

[188] Linde A., Noorbala M., and Westphal A., "Observational consequences of chaotic inflation with nonminimal coupling to gravity," *JCAP* **1103** (2011) 013, arXiv:1101.2652 [hep-th].

[189] Kallosh R. and Linde A., "Superconformal generalization of the chaotic inflation model $\frac{\lambda}{4}\phi^4 - \frac{\xi}{2}\phi^2 R$," *JCAP* **1306** (2013) 027, arXiv:1306.3211 [hep-th].

[190] Kallosh R., Linde A., and Roest D., "Universal Attractor for Inflation at Strong Coupling," *Phys. Rev. Lett.* **112** (2014) no. 1, 011303, arXiv:1310.3950 [hep-th].

[191] Kallosh R. and Linde A., "Superconformal generalizations of the Starobinsky model," *JCAP* **1306** (2013) 028, arXiv:1306.3214 [hep-th].

[192] Kallosh R. and Linde A., "Universality Class in Conformal Inflation," *JCAP* **1307** (2013) 002, arXiv:1306.5220 [hep-th].

[193] Ferrara S., Kallosh R., Linde A., and Porrati M., "Minimal Supergravity Models of Inflation," *Phys. Rev.* **D88** (2013) no. 8, 085038, arXiv:1307.7696 [hep-th].

[194] Galante M., Kallosh R., Linde A., and Roest D., "Unity of Cosmological Inflation Attractors," *Phys. Rev. Lett.* **114** (2015) no. 14, 141302, arXiv:1412.3797 [hep-th].

[195] Linde A., "Random Potentials and Cosmological Attractors," *JCAP* **1702** (2017) no. 02, 028, arXiv:1612.04505 [hep-th].

[196] Faraoni V. and Gunzig E., "Einstein frame or Jordan frame?," *Int. J. Theor. Phys.* **38** (1999) 217–225, arXiv:astro-ph/9910176 [astro-ph].

[197] Karamitsos S. and Pilaftsis A., "Frame Covariant Nonminimal Multifield Inflation," *Nucl. Phys.* **B927** (2018) 219–254, arXiv:1706.07011 [hep-ph].

[198] Karamitsos S. and Pilaftsis A., "On the Cosmological Frame Problem," *PoS* **CORFU2017** (2018) 036, arXiv:1801.07151 [hep-th].

[199] Nojiri S., Odintsov S.D., and Oikonomou V.K., "Modified Gravity Theories on a Nutshell: Inflation, Bounce and Late-time Evolution," *Phys. Rept.* **692** (2017) 1–104, arXiv:1705.11098 [gr-qc].

[200] Bauer F. and Demir D.A., "Inflation with Non-Minimal Coupling: Metric versus Palatini Formulations," *Phys. Lett.* **B665** (2008) 222–226, arXiv:0803.2664 [hep-ph].

[201] Tamanini N. and Contaldi C.R., "Inflationary Perturbations in Palatini Generalised Gravity," *Phys. Rev.* **D83** (2011) 044018, arXiv:1010.0689 [gr-qc].

[202] Bauer F. and Demir D.A., "Higgs-Palatini Inflation and Unitarity," *Phys. Lett.* **B698** (2011) 425–429, arXiv:1012.2900 [hep-ph].

[203] Rasanen S. and Wahlman P., "Higgs inflation with loop corrections in the Palatini formulation," *JCAP* **1711** (2017) no. 11, 047, arXiv:1709.07853 [astro-ph.CO].

[204] Tenkanen T., "Resurrecting Quadratic Inflation with a non-minimal coupling to gravity," *JCAP* **1712** (2017) no. 12, 001, arXiv:1710.02758 [astro-ph.CO].

[205] Fu C., Wu P., and Yu H., "Inflationary dynamics and preheating of the nonminimally coupled inflaton field in the metric and Palatini formalisms," *Phys. Rev.* **D96** (2017) no. 10, 103542, arXiv:1801.04089 [gr-qc].

[206] Racioppi A., "Coleman-Weinberg linear inflation: metric vs. Palatini formulation," *JCAP* **1712** (2017) no. 12, 041, arXiv:1710.04853 [astro-ph.CO].

[207] Markkanen T., Tenkanen T., Vaskonen V., and Veerme H., "Quantum corrections to quartic inflation with a non-minimal coupling: metric vs. Palatini," *JCAP* **1803** (2018) no. 03, 029, arXiv:1712.04874 [gr-qc].

[208] Racioppi A., "A new universal attractor: linear inflation," arXiv:1801.08810 [astro-ph.CO].

[209] Enckell V.M., Enqvist K., Rasanen S., and Tomberg E., "Higgs inflation at the hilltop," arXiv:1802.09299 [hep-ph].

[210] Hohmann M., Jarv L., Kuusk P., Randla E., and Vilson O., "Post-Newtonian parameter γ for multiscalar-tensor gravity with a general potential," *Phys. Rev.* **D94** (2016) no. 12, 124015, arXiv:1607.02356 [gr-qc].

[211] Sotiriou T.P., "f(R) gravity and scalar-tensor theory," *Class. Quant. Grav.* **23** (2006) 5117–5128, arXiv:gr-qc/0604028 [gr-qc].

[212] Renaux-Petel S. and Turzyski K., "Geometrical Destabilization of Inflation," *Phys. Rev. Lett.* **117** (2016) no. 14, 141301, arXiv:1510.01281 [astro-ph.CO].

[213] Renaux-Petel S. and Turzynski K., "On reaching the adiabatic limit in multi-field inflation," *JCAP* **1506** (2015) no. 06, 010, arXiv:1405.6195 [astro-ph.CO].

[214] Aazami A. and Easther R., "Cosmology from random multifield potentials," *JCAP* **0603** (2006) 013, arXiv:hep-th/0512050 [hep-th].

[215] Easther R. and McAllister L., "Random matrices and the spectrum of N-flation," *JCAP* **0605** (2006) 018, arXiv:hep-th/0512102 [hep-th].

[216] Dias M., Frazer J., and Marsh M.C.D., "Simple emergent power spectra from complex inflationary physics," *Phys. Rev. Lett.* **117** (2016) no. 14, 141303, arXiv:1604.05970 [astro-ph.CO].

[217] Dias M., Frazer J., and Marsh M.c.D., "Seven Lessons from Manyfield Inflation in Random Potentials," *JCAP* **1801** (2018) no. 01, 036, arXiv:1706.03774 [astro-ph.CO].

[218] Bjorkmo T. and Marsh M.C.D., "Manyfield Inflation in Random Potentials," *JCAP* **1802** (2018) no. 02, 037, arXiv:1709.10076 [astro-ph.CO].

[219] Baumann D. and McAllister L., *Inflation and String Theory*. Cambridge Monographs on Mathematical Physics. Cambridge University Press, 2015. arXiv:1404.2601 [hep-th]. http://www.cambridge.org/mw/academic/subjects/physics/theoretical-physics-and-mathematical-physics/inflation-and-string-theory?format=HB.

[220] Yamaguchi M., "Supergravity based inflation models: a review," *Class. Quant. Grav.* **28** (2011) 103001, arXiv:1101.2488 [astro-ph.CO].

[221] Linde A.D., "Particle physics and inflationary cosmology," *Contemp. Concepts Phys.* **5** (1990) 1–362, arXiv:hep-th/0503203 [hep-th].

[222] Cremonini S., Lalak Z., and Turzynski K., "Strongly Coupled Perturbations in Two-Field Inflationary Models," *JCAP* **1103** (2011) 016, arXiv:1010.3021 [hep-th].

[223] Linde A.D., "Hybrid inflation," *Phys. Rev.* **D49** (1994) 748–754, arXiv:astro-ph/9307002 [astro-ph].

[224] Renaux-Petel S., Turzyski K., and Vennin V., "Geometrical destabilization, premature end of inflation and Bayesian model selection," *JCAP* **1711** (2017) no. 11, 006, arXiv:1706.01835 [astro-ph.CO].

[225] Kallosh R., Linde A., and Roest D., "Superconformal Inflationary α-Attractors," *JHEP* **11** (2013) 198, arXiv:1311.0472 [hep-th].

[226] Kallosh R. and Linde A., "Escher in the Sky," *Comptes Rendus Physique* **16** (2015) 914–927, arXiv:1503.06785 [hep-th].

[227] Martin J., Ringeval C., and Vennin V., "Encyclopdia Inflationaris," *Phys. Dark Univ.* **5-6** (2014) 75–235, arXiv:1303.3787 [astro-ph.CO].

[228] Bezrukov F.L. and Shaposhnikov M., "The Standard Model Higgs boson as the inflaton," *Phys. Lett.* **B659** (2008) 703–706, arXiv:0710.3755 [hep-th].

[229] Salopek D., Bond J., and Bardeen J.M., "Designing Density Fluctuation Spectra in Inflation," *Phys.Rev.* **D40** (1989) 1753.

[230] van Tent B.J.W., *Cosmological Inflation with Multiple Fields and the Theory of Density Fluctuations*. PhD thesis, Utrecht U., 2002. http://igitur-archive.library.uu.nl/dissertations/2002-1004-084000/inhoud.htm.

[231] Groot Nibbelink S. and van Tent B., "Scalar perturbations during multiple field slow-roll inflation," *Class.Quant.Grav.* **19** (2002) 613–640, arXiv:hep-ph/0107272 [hep-ph].

[232] Tsujikawa S., Parkinson D., and Bassett B.A., "Correlation - consistency cartography of the double inflation landscape," *Phys. Rev.* **D67** (2003) 083516, arXiv:astro-ph/0210322 [astro-ph].

[233] Weinberg S., *Cosmology*. 2008. http://www.oup.com/uk/catalogue/?ci=9780198526827.

[234] Amin M.A., Hertzberg M.P., Kaiser D.I., and Karouby J., "Nonperturbative Dynamics Of Reheating After Inflation: A Review," *Int. J. Mod. Phys.* **D24** (2014) 1530003, arXiv:1410.3808 [hep-ph].

[235] Langlois D. and Renaux-Petel S., "Perturbations in generalized multi-field inflation," *JCAP* **0804** (2008) 017, arXiv:0801.1085 [hep-th].

[236] Baumann D. and Green D., "Equilateral Non-Gaussianity and New Physics on the Horizon," *JCAP* **1109** (2011) 014, arXiv:1102.5343 [hep-th].

[237] Shiu G. and Xu J., "Effective Field Theory and Decoupling in Multi-field Inflation: An Illustrative Case Study," *Phys. Rev.* **D84** (2011) 103509, arXiv:1108.0981 [hep-th].

[238] Cespedes S., Atal V., and Palma G.A., "On the importance of heavy fields during inflation," *JCAP* **1205** (2012) 008, arXiv:1201.4848 [hep-th].

[239] Achúcarro A., Gong J.O., Hardeman S., Palma G.A., and Patil S.P., "Effective theories of single field inflation when heavy fields matter," *JHEP* **05** (2012) 066, arXiv:1201.6342 [hep-th].

[240] Avgoustidis A., Cremonini S., Davis A.C., Ribeiro R.H., Turzynski K., and Watson S., "Decoupling Survives Inflation: A Critical Look at Effective Field Theory Violations During Inflation," *JCAP* **1206** (2012) 025, arXiv:1203.0016 [hep-th].

[241] Achúcarro A., Atal V., Cespedes S., Gong J.O., Palma G.A., and Patil S.P., "Heavy fields, reduced speeds of sound and decoupling during inflation," *Phys. Rev.* **D86** (2012) 121301, arXiv:1205.0710 [hep-th].

[242] Gwyn R., Palma G.A., Sakellariadou M., and Sypsas S., "Effective field theory of weakly coupled inflationary models," *JCAP* **1304** (2013) 004, arXiv:1210.3020 [hep-th].

[243] Gong J.O., Pi S., and Sasaki M., "Equilateral non-Gaussianity from heavy fields," *JCAP* **1311** (2013) 043, arXiv:1306.3691 [hep-th].

[244] Cspedes S. and Palma G.A., "Cosmic inflation in a landscape of heavy-fields," *JCAP* **1310** (2013) 051, arXiv:1303.4703 [hep-th].

[245] Gong J.O., Seo M.S., and Sypsas S., "Higher derivatives and power spectrum in effective single field inflation," *JCAP* **1503** (2015) no. 03, 009, arXiv:1407.8268 [hep-th].

[246] Gwyn R., Palma G.A., Sakellariadou M., and Sypsas S., "On degenerate models of cosmic inflation," *JCAP* **1410** (2014) no. 10, 005, arXiv:1406.1947 [hep-th].

[247] Romania M.G., Tsamis N.C., and Woodard R.P., "Primordial Gravitational Waves Enhancement," *Class. Quant. Grav.* **30** (2013) 025004, arXiv:1108.1696 [gr-qc].

[248] Romania M.G., Tsamis N.C., and Woodard R.P., "Computing the Primordial Power Spectra Directly," *JCAP* **1208** (2012) 029, arXiv:1207.3227 [astro-ph.CO].

[249] Brown A.R., "Hyperinflation," arXiv:1705.03023 [hep-th].

[250] Mizuno S. and Mukohyama S., "Primordial perturbations from inflation with a hyperbolic field-space," *Phys. Rev.* **D96** (2017) no. 10, 103533, arXiv:1707.05125 [hep-th].

[251] Arkani-Hamed N., Creminelli P., Mukohyama S., and Zaldarriaga M., "Ghost inflation," *JCAP* **0404** (2004) 001, arXiv:hep-th/0312100 [hep-th].

[252] Cheung C., Creminelli P., Fitzpatrick A.L., Kaplan J., and Senatore L., "The Effective Field Theory of Inflation," *JHEP* **03** (2008) 014, arXiv:0709.0293 [hep-th].

[253] Wands D., "Local non-Gaussianity from inflation," *Class. Quant. Grav.* **27** (2010) 124002, arXiv:1004.0818 [astro-ph.CO].

[254] Wang Y., "Inflation, Cosmic Perturbations and Non-Gaussianities," *Commun. Theor. Phys.* **62** (2014) 109–166, arXiv:1303.1523 [hep-th].

[255] Renaux-Petel S., "Primordial non-Gaussianities after Planck 2015: an introductory review," *Comptes Rendus Physique* **16** (2015) 969–985, arXiv:1508.06740 [astro-ph.CO].

[256] Renaux-Petel S., "Orthogonal non-Gaussianities from Dirac-Born-Infeld Galileon inflation," *Class. Quant. Grav.* **28** (2011) 182001, arXiv:1105.6366 [astro-ph.CO]. [Erratum: Class. Quant. Grav.28,249601(2011)].

[257] Green D., Lewandowski M., Senatore L., Silverstein E., and Zaldarriaga M., "Anomalous Dimensions and Non-Gaussianity," *JHEP* **10** (2013) 171, arXiv:1301.2630 [hep-th].

[258] Garcia-Saenz S. and Renaux-Petel S., "Flattened non-Gaussianities from the effective field theory of inflation with imaginary speed of sound," arXiv:1805.12563 [hep-th].

[259] Achcarro A., Kallosh R., Linde A., Wang D.G., and Welling Y., "Universality of multi-field α-attractors," arXiv:1711.09478 [hep-th].

[260] Carrilho P., Mulryne D., Ronayne J., and Tenkanen T., "Attractor Behaviour in Multifield Inflation," *JCAP* **1806** (2018) no. 06, 032, arXiv:1804.10489 [astro-ph.CO].

List of Figures

List of Tables